Copper maturation of nitrous oxide reductase in *Paracoccus denitrificans*

Manuel J. Soriano Laguna

A Thesis submitted to the University of East Anglia in accordance with the requirements of the degree of Doctor of Philosophy

School of Biological Sciences

August, 2018

This copy of the thesis has been supplied on condition that anyone who consults it is understood to recognise that its copyright rests with the author and that use of any information derived there from must be in accordance with current UK Copyright Law. In addition, any quotation or extract must include full attribution.

Abstract

Nitrous oxide (N_2O) is an important greenhouse gas that is also responsible for stratospheric ozone depletion [1, 2]. Human activity is the main source of N_2O due to the use of fertilisers in agriculture. Nitrous oxide reductase (N_2OR) is the only enzyme to destroy N_2O as part of a biological process termed denitrification. This enzyme has a unique catalytic Cu_Z centre, an electron transfer Cu_A centre and a high demand for Cu with 12 atoms required per functional dimer. A previous transcriptomic study revealed that two putative Cu chaperones, ScoB and PCuC were upregulated under Cu limiting conditions [3]. Here we demonstrate that ScoB/PCuC is a high-affinity Cu system essential for N_2O respiration.

Deletion of *scoB* causes N_2O accumulation under anoxic and Cu-limited growth. N_2O respiration could be restored complementation *in trans* with recombinant full-length, or soluble, periplasmic ScoB proteins ($ScoB_{FL}$ and $ScoB_{sol}$, respectively). $ScoB_{sol}$ was biochemically characterised and found to be a monomeric protein of $\sim$25 kDa that can bind Cu^{1+} or Cu^{2+} with an apparent K_D value within the subfemtomolar range. In contrast, PCuC is a multidomain protein with a Ycn-like N-terminal domain [4], and a PCu_AC-like C-terminal domain [5]. Recombinant periplasmic proteins for each individual domain and full-length protein were generated (i.e., $PCuC_{Nt}$, $PCuC_{Ct}$ and $PCuC_{FL}$). The *pcuC* deletion strain has an N_2O-genic phenotype. Only complementation *in trans* with $PCuC_{FL}$ restored N_2O reduction under anaerobic and Cu-limited conditions.

In addition, the crystallographic structure of Cu-bound $PCuC_{Nt}$ was solved to a resolution of 1.5 Å revealing a trimeric protein of ∼56 kDa with a novel *histidine brace* metal binding site. $PCuC_{Nt}$ can bind $^{1+}$ or $^{2+}$ and competition assays with $^{1+}$ chelators revealed that metallation occurs with femtomolar affinity. Analysis of YcnI-type proteins revealed the presence of two defined families. Family A contains a $HX_{22}HX_{101}W$ consensus Cu-binding motif and was principally found among alphaproteobacteria, while Family B contain a $HX_{22}DX_{90}WX_{13}H$ motif and are distributed in actinobacteria and firmicutes. The Cu-bound structure of $PCuC_{Ct}$ was also solved to a resolution of 1.6 Å and reveals a ∼18 kDa monomer that contains a defined $H(M)X_{10}MX_{21}HXM$ Cu-binding site that can bind Cu^{1+} with subfemtomolar affinity. Further biochemical studies of native PCuC confirmed that the full-length protein forms a ∼100 kDa homotrimer in solution regardless of metallation state, with the N-terminal domain driving oligomerization exposing individual C-terminal domains to bulk solution through a flexible linker region. Each trimer can bind up to 6 Cu atoms with binding affinities within the subfemtomolar range.

Finally, the maturation of the Cu centres of N_2OR was studied in *P. denitrificans* WT, *scoB* and *pcuC* deletion strains. A periplasmic and readily isolatable affinity-tagged N_2OR protein was expressed *in cis* under two different Cu regimes in *P. denitrificans*. N_2OR purified from WT cells grown under anaerobic and Cu-limited conditions only contained a recognisable Cu_A centre. However, N_2OR from *scoB* and *pcuC* mutants lacked both Cu-centres, had significantly lower Cu content and impaired enzymatic activity. A model for the metallation process of the Cu_A centre of N_2OR by the high affinity Cu-maturation system ScoB/PCuC has been proposed.

Contents

Abstract iv

Contents iv

List of Figures ix

List of Tables xiii

Abbreviations xv

Acknowledgements xxiv

1 Introduction 1

1.1 Biogeochemical nitrogen cycle 1

1.2 Heme-copper oxidases from *Paracoccus denitrificans* 5

1.2.1 Eukaryotic cytochrome *c* oxidase Cu_A centre maturation . . 8

1.2.2 Prokaryotic cytochrome *c* oxidase Cu_A centre maturation . . 10

1.3 Copper and microbiology 10

1.3.1 Bacterial cuproenzymes 11

1.3.2 Copper import mechanisms 12

1.3.3 Cu export systems 14

1.3.3.1 Cu-transporting P-type ATPases 14

1.3.3.2 Cus system 14

1.3.3.3 CopCD/PcoCD system 15

1.4 Nitrous oxide reductase 15

1.4.1 Patterns in *nos* gene clusters 16

1.4.1.1 Typical *nos* gene clusters 16

1.4.1.2 Atypical *nos* gene clusters 17

1.4.2 Mechanism of action of N_2OR 17

1.4.2.1 The Cu_A electron transfer centre of N_2OR 21

1.4.2.2 The Cu_Z catalytic centre of N_2OR 21

1.4.2.3 N_2O binding at the Cu_Z centre of N_2OR 24
1.4.3 Regulation of *nos* genes 25
1.4.3.1 FNR transcriptional factor 26
1.4.3.2 NosR and NosX 26
1.4.3.3 NasS-NasT 28
1.4.3.4 Copper regulation 29
1.5 Experimental Aims 30

2 Materials and Methods **33**
2.1 Media and conditions for bacterial growth 33
2.1.1 Complete medium 33
2.1.2 Minimal medium 35
2.2 Analytical Methods 38
2.2.1 Measurement of nitrate and nitrite in cultures 38
2.2.2 Measurement of nitrous oxide in cultures 38
2.2.3 Analysis of metal content in protein samples 39
2.2.4 Determination of protein concentration 39
2.2.5 Enzymatic assay for nitrous oxide reductase activity 41
2.3 Preparation of nucleic acids 42
2.3.1 Isolation of genomic DNA 42
2.3.2 Preparation of plasmid DNA 42
2.3.3 Restriction enzyme digestion 42
2.3.4 Ligation of DNA fragments 43
2.3.5 Agarose gel electrophoresis 43
2.3.6 Recovery of DNA from agarose gels 44
2.3.7 DNA sequencing 44
2.4 Amplification of DNA using the polymerase chain reaction (PCR) . 45
2.4.1 Oligonucleotide design 45
2.4.2 PCR of DNA using High-Fidelity Phusion Polymerase 46
2.4.3 Diagnostic PCR of DNA using *Taq* DNA polymerase 46
2.4.4 Colony PCR 46
2.4.5 Purification of DNA PCR products 48
2.5 Transformation of *E. coli* with plasmid DNA 48
2.5.1 Preparation of competent cells 48
2.5.2 Transformation of competent cells 49
2.6 *in vivo* genetic manipulations 49
2.6.1 Conjugation via patch crosses 49
2.6.2 Conjugation via filter crosses 50
2.7 Polyacrylamide gel electrophoresis 50
2.7.1 Resolution of proteins by SDS-PAGE 50
2.7.2 Western-Blot analysis 51
2.8 Mass Spectrometry of proteins 53
2.9 Protein structure prediction 54
2.10 Synthesis of pLMB510 and pLMB511 plasmid vectors 54

2.11 Construction of knock-in mutants . . . 56
2.12 Protein overexpression and purification . . . 60
2.12.1 Purification of $ScoB_{sol}$-6His and $PCuC_{WT}$ . . . 61
2.12.2 Purification of recombinant PCuC proteins . . . 62
2.12.3 Purification of recombinant N_2OR . . . 63
2.13 N-terminal sequencing of PCuC . . . 64
2.13.1 Edman degradation . . . 64
2.13.2 Protein sequencing by in source decay MALDI-TOF . . . 64
2.14 Addition of Cu ions to Cu-binding proteins . . . 64
2.15 Analytical ultracentrifugation . . . 66
2.16 Analytical size exclusion chromatography . . . 67
2.17 Estimation of metal dissociation constants using copper chelators . . . 67
2.18 Small-angle X-ray scattering . . . 71
2.19 Protein crystallography . . . 71
2.19.1 Crystal formation . . . 72
2.19.2 Data collection . . . 72
2.19.2.1 $PCuC_{Nt}$ . . . 73
2.19.2.2 $PCuC_{Ct}$ . . . 73

3 Biochemical characterisation of $ScoB_{sol}$ 77
3.1 Introduction . . . 77
3.2 A Sco protein from *P. denitrificans* necessary for N_2O reduction . . . 81
3.3 Phenotypical characterisation of *scoB* . . . 83
3.4 Soluble $ScoB_{sol}$-6His purification . . . 87
3.5 UV-visible absorbance and fluorescence spectroscopy characterisation of copper binding to $ScoB_{sol}$ . . . 90
3.6 Investigating the solution state of $ScoB_{sol}$ . . . 94
3.7 Small-Angle X-ray scattering of $ScoB_{sol}$ . . . 97
3.8 Discussion . . . 99

4 Biochemical characterisation of PCuC 107
4.1 Introduction . . . 107
4.1.1 The novel two-domain fusion protein PCuC . . . 108
4.1.2 The N-terminal YcnI domain of PCuC . . . 116
4.1.3 The C-terminal PCu_AC-like domain of PCuC . . . 121
4.2 Generation of the tools for the study of PCuC from *P. denitrificans* 124
4.3 Characterisation of *pcuC*$^-$ deletion strains . . . 125
4.4 Production of PCuC proteins for biochemical analyses . . . 129
4.4.1 Purification of recombinant $PCuC_{FL}$-6His protein . . . 129
4.4.2 Purification of recombinant $PCuC_{Nt}$-6His protein . . . 130
4.4.3 Purification of recombinant $PCuC_{Ct}$-6His protein . . . 132
4.5 Investigating Cu-binding by PCuC . . . 136
4.5.1 Cu-binding to wild-type PCuC . . . 136
4.5.2 Cu-binding to $PCuC_{Nt}$ . . . 137

4.5.3 Cu-binding to $PCuC_{Ct}$ . . . 142
4.6 Cu^{1+} binding affinity of PCuC proteins . . . 144
4.6.1 Cu^{1+} binding affinity of wild-type PCuC . . . 145
4.6.2 Cu^{1+} binding affinity of $PCuC_{Nt}$ . . . 145
4.6.3 Cu^{1+} binding affinity of $PCuC_{Ct}$ . . . 150
4.7 Discussion . . . 150
4.7.1 The native full-length PCuC protein . . . 151
4.7.2 PCuC N-terminal domain variant . . . 152
4.7.3 PCuC C-terminal domain variant . . . 154

5 Solution properties and structural resolution of PCuC 159
5.1 Introduction . . . 159
5.1.1 PCuC N-terminal domain . . . 160
5.1.2 PCuC C-terminal domain . . . 162
5.2 Solution state characterisation of PCuC proteins . . . 162
5.2.1 Investigating the solution state of $PCuC_{Nt}$ . . . 164
5.2.2 Investigating the solution state of $PCuC_{Ct}$ . . . 164
5.2.3 Investigating the solution state of $PCuC_{WT}$ . . . 169
5.3 Structural determination of PCuC proteins . . . 172
5.3.1 Crystallographic structure of $PCuC_{Nt}$ . . . 172
5.3.2 Crystallographic structure of $PCuC_{Ct}$ . . . 181
5.3.3 Small-Angle X-ray scattering, SAXS . . . 189
5.4 Discussion . . . 193

6 Purification and characterisation of N_2OR from *pcuC* and *scoB* deficient strains 207
6.1 Introduction . . . 207
6.1.1 Assembly of copper centres in N_2OR . . . 207
6.1.1.1 Maturation of the Cu_Z centre of N_2OR . . . 208
6.1.1.2 Maturation of the Cu_A centre of N_2OR . . . 209
6.2 Nitrous oxide reductase purification and characterisation . . . 212
6.3 Discussion . . . 220

7 Conclusions and future perspectives 227

A Supplementary information 237
A.1 Antibiotics and supplements . . . 237
A.2 Sequences of DNA synthesized . . . 237
A.3 Clustal X Colour Scheme . . . 239
A.4 Structures used as templates for homology ScoB model . . . 240
A.5 Signal peptide prediction . . . 240
A.6 Dynafit script: Competition with proteins that bind one ligand . . . 241
A.7 Dynafit script: Competition with proteins that bind two ligands . . . 242

Bibliography 245

List of Figures

1.1 Schematic illustration of the microbial nitrogen cycle 2
1.2 Schematic illustration of denitrification enzymes and their cellular location in *Paracoccus denitrificans* 3
1.3 Copper dependent terminal reductases from *Paracoccus denitrificans* 6
1.4 Pathway of copper insertion into the Cu_A centre of cytochrome *c* oxidase 9
1.5 Summary of characterised prokaryotic cuproenzymes responsible for copper homeostasis of the cell 13
1.6 Comparison of the organisation of typical *nos* gene clusters. 18
1.7 Comparison of the organisation of atypical *nos* gene clusters. 19
1.8 Schematic diagram of the copper centres of N_2OR 22
1.9 Cartoon representation of nitrous oxide reductase from *Pseudomonas stutzeri* 23
1.10 UV-visible spectra of *P. stutzeri* N_2OR. 25
1.11 NosR topology model 27
1.12 Heat map representing the gene expression profile of *P. denitrificans* PD1222 under copper sufficient and limited regimes 30

2.1 The impact of Vishniac and Santer trace element solution on bacterial growth 37
2.2 Representative standard curves. 40
2.3 The taurine inducible expression vectors for *Alphaproteobacteria*. . . 55
2.4 Map of the mobilizable multi-purpose cloning vector pK18*mobsacB* used for construction of insertion mutants. 58
2.5 Schematic representation of the genetic events leading to generation of knock-in mutants 59
2.6 UV-visible spectra of CuCl and $CuSO_4$ 65
2.7 Analytical size exclusion chromatography standards 68

3.1 Schematic representation of the general fold topology of a bacterial Sco protein 79

3.2 Sequence alignment and cartoon representation copper binding site of Sco proteins . . . 80
3.3 Properties of *scoA* and *scoB* genes from *P. denitrificans* . . . 82
3.4 Aerobic growth characteristics of *P. denitrificans* WT, Δ*scoB* deletion mutant and complemented strains in batch culture conditions . 84
3.5 Anaerobic growth characteristics of *P. denitrificans* WT, Δ*scoB* deletion mutant and complemented strains in batch culture conditions in the absence of taurine . . . 85
3.6 Anaerobic growth characteristics of *P. denitrificans* WT, Δ*scoB* deletion mutant and complemented strains in batch culture conditions in the presence of 1 mM taurine . . . 86
3.7 Steps for the purification of $ScoB_{sol}$-6His . . . 88
3.8 Cleavage of affinity tag and apo-$ScoB_{sol}$ generation . . . 89
3.9 Absorbance and fluorescence studies of Cu^{1+} binding by reduced apo-$ScoB_{sol}$. . . . 92
3.10 Absorbance and fluorescence studies of Cu^{2+} binding by reduced apo-$ScoB_{sol}$. . . . 93
3.11 Copper binding solvatochromic effect of $ScoB_{sol}$. . . . 94
3.12 Effect of copper on the sedimentation equilibrium of $ScoB_{sol}$ . . . 95
3.13 Analytical size exclusion chromatography of $ScoB_{sol}$ . . . 96
3.14 Solution characterization of $ScoB_{sol}$ by SAXS . . . 98
3.15 Estimation of Cu^{1+} binding affinity of $ScoB_{sol}$ . . . 102
3.16 Cartoon representation of apo-$ScoB_{sol}$ . . . 104

4.1 Representation of the domain configuration of YcnI and PCu_AC proteins. . . . 108
4.2 Cladogram of PCuC proteins. . . . 109
4.3 Overview of the gene neighbourhood of *pcuC* genes in bacteria . . . 111
4.4 Multiple sequence alignment of hypothetical gene products homologous to Pden_4445 . . . 112
4.5 Multiple sequence alignment of PCuC proteins . . . 113
4.6 Properties of YcnI and PCu_AC domain containing proteins from *P. denitrificans* . . . 115
4.7 Proposed mechanism of action of YcnLKJI in *Bacillus subtilis* . . . 117
4.8 Overview of the gene neighbourhood of *ycnI* genes in bacteria . . . 118
4.9 Multiple sequence alignment of YcnI proteins . . . 119
4.10 Overview of the gene neighbourhood of *pcu$_A$C* genes in bacteria . . . 122
4.11 Multiple sequence alignment of PCu_AC proteins . . . 123
4.12 Representation of recombinant $PCuC_{FL}$, $PCuC_{Nt}$ and $PCuC_{Ct}$ . . . 124
4.13 Aerobic growth characteristics of *P. denitrificans* WT and *pcuC*$^-$ complemented strains in batch culture conditions . . . 126
4.14 Anaerobic growth characteristics of *P. denitrificans* WT and *pcuC*$^-$ complemented strains in batch culture conditions in the absence of taurine . . . 127

4.15 Anaerobic growth characteristics of *P. denitrificans* WT and *pcuC*⁻ complemented strains in batch culture conditions in the presence of 1 mM taurine . . . 128
4.16 Purification of $PCuC_{FL}$-6His from *P. denitrificans pcuC*⁻ mutant . 131
4.17 Purification of $PCuC_{Nt}$-6His from *P. denitrificans pcuC*⁻ mutant . . 133
4.18 Purification of $PCuC_{Ct}$-6His from *P. denitrificans pcuC*⁻ mutant . . 135
4.19 Absorbance and fluorescence spectroscopy studies of Cu^{1+} binding to reduced apo-$PCuC_{WT}$. . . 138
4.20 Absorbance and fluorescence spectroscopy studies of Cu^{2+} binding to reduced apo-$PCuC_{WT}$. . . 139
4.21 Absorbance and fluorescence spectroscopy studies of Cu^{1+} binding to reduced apo-$PCuC_{Nt}$. . . 140
4.22 Absorbance and fluorescence spectroscopy studies of Cu^{2+} binding to reduced apo-$PCuC_{Nt}$. . . 141
4.23 Absorbance and fluorescence spectroscopy studies of Cu^{1+} binding to apo-$PCuC_{Ct}$. . . 143
4.24 Estimation of Cu^{1+} binding affinity of $PCuC_{WT}$ . . . 146
4.25 Estimation of Cu^{1+} binding affinity of $PCuC_{Nt}$ . . . 147
4.26 Estimation of Cu^{1+} binding affinity of $PCuC_{Ct}$ . . . 148
4.27 Summary of the Cu-binding properties of *P. denitrificans* PCuC and its constituent domains . . . 156

5.1 Structural representation of YcnI from *Nocardia farcinica* . . . 161
5.2 Structural representation of PCu_AC from *Thermus thermophilus* . . 163
5.3 Effect of Cu^{1+} and Cu^{2+} on the sedimentation equilibrium of $PCuC_{Nt}$ 165
5.4 Analytical size exclusion chromatography of $PCuC_{Nt}$ . . . 166
5.5 Effect of Cu^{1+} on the sedimentation equilibrium of $PCuC_{Ct}$ . . . 167
5.6 Analytical size exclusion chromatography of $PCuC_{Ct}$ . . . 168
5.7 Effect of Cu^{1+} and Cu^{2+} on the sedimentation equilibrium of $PCuC_{WT}$ 170
5.8 Analytical size exclusion chromatography of $PCuC_{WT}$ . . . 171
5.9 Protein crystals of $PCuC_{Nt}$ . . . 173
5.10 Ramachandran plot generated from a $PCuC_{Nt}$ monomer . . . 176
5.11 Cartoon and transparent surface representation of the crystallographic structure of a Cu-bound $PCuC_{Nt}$ trimer . . . 177
5.12 Crystallographic structure of $PCuC_{Nt}$ . . . 178
5.13 Schematic diagram of $PCuC_{Nt}$ *histidine brace* . . . 179
5.14 Example of polygonal crystals obtained for $PCuC_{Ct}$ . . . 181
5.15 Schematic diagram of $PCuC_{Ct}$ Cu^{1+} binding site . . . 183
5.16 Ramachandran plot generated for a $PCuC_{Ct}$ monomer . . . 184
5.17 Crystallographic structure of $PCuC_{Ct}$ . . . 185
5.18 Symmetry axis of $PCuC_{Ct}$ . . . 186
5.19 Schematic diagram of the residues involved in the coordination of the special position Cu ion of $PCuC_{Ct}$ . . . 187
5.20 Solution characterisation of native full-length PCuC by SAXS . . . 190
5.21 PCuC full length structural model . . . 191

5.22 Purification of $PCuC_{Nt}$-6His from wild-type *P. denitrificans* 194
5.23 Structural aspects of *histidine brace* copper-binding proteins 196
5.24 Superposition of $PCuC_{Nt}$ from *P. denitrificans* and YcnI from *N. farcinica* 199
5.25 Phylogenetic tree of YcnI proteins. 201
5.26 Multiple sequence alignment of YcnI proteins belonging to family A. 202
5.27 Multiple sequence alignment of YcnI proteins belonging to family B. 203
5.28 Structural aspects of PCu_AC proteins 205

6.1 Schematic illustration of the components involved in N_2OR biogenesis and their cellular location in *P. denitrificans* 211
6.2 Anaerobic growth characteristics of *P. denitrificans* WT and $NosZ_{WT}$ mutant in batch culture conditions 213
6.3 *Strep*-tag II affinity purification of recombinant N_2OR expressed under copper sufficient conditions 214
6.4 *Strep*-tag II affinity purification of recombinant N_2OR expressed under copper limited conditions 215
6.5 UV-vis spectra of purified *Strep*-tag II recombinant N_2OR by affinity chromatography 216
6.6 Ferricyanide-oxidised minus dithionite-reduced UV-vis difference spectra of N_2OR. 218
6.7 Methyl viologen activity assay of N_2OR proteins 219
6.8 UV-vis spectrum of N_2OR form I and form II 224

7.1 Proposed mechanisms of maturation of the Cu_A centre of nitrous oxide reductase from *P. denitrificans* 229
7.2 Multiple sequence alignment of proteins containing a thioredoxin motif encoded in *P. denitrificans* 231
7.3 Concentration of copper in soil of the European Union. 232

A.1 Clustal X Colour Scheme 239

List of Tables

1.1 Comparison of copper *vs.* iron enzymes that catalyse similar reactions. 12

2.1 Bacterial strains used . . . 34
2.2 Constituents of complete lysogeny broth . . . 34
2.3 Core constituents of *Paracoccus denitrificans* defined mineral salts medium. . . . 35
2.4 Constituents of the Vishniac and Santer trace elements solution. . . . 35
2.5 Standard restriction digestion reaction . . . 43
2.6 T4 DNA ligation standard recipe . . . 43
2.7 Primers used . . . 45
2.8 High-Fidelity Phusion polymerase PCR reaction recipe . . . 47
2.9 High-Fidelity Phusion polymerase cycling instructions . . . 47
2.10 MyTaq DNA polymerase PCR reaction recipe. . . . 47
2.11 MyTaq DNA polymerase cycling instructions . . . 47
2.12 Composition of a standard 15 % SDS-PAGE gel . . . 51
2.13 Peptide mass fingerprinting results and mascot scores . . . 53
2.14 Plasmids used . . . 57
2.15 Partial specific volumes calculated using Sednterp . . . 66

3.1 Calculated M_w of $ScoB_{sol}$ by AUC . . . 96
3.2 Copper binding properties and thioredoxin activity of known Sco proteins . . . 105

4.1 Estimated Cu^{1+} dissociation constants for $PCuC_{WT}$ . . . 149
4.2 Estimated Cu^{1+} dissociation constants for $PCuC_{Nt}$ . . . 149
4.3 Estimated Cu^{1+} dissociation constants for $PCuC_{Ct}$ . . . 149

5.1 Calculated M_w of $PCuC_{Nt}$ by AUC . . . 166
5.2 Calculated M_w of $PCuC_{Ct}$ by AUC . . . 168
5.3 Calculated M_w of $PCuC_{WT}$ by AUC . . . 171
5.4 Crystallisation conditions where PCuC crystals were produced . . . 172
5.5 Data collection and structure refinement statistics for $PCuC_{Nt}$ . . . 174

5.6 Bond lengths and angles of the Cu-binding site of $PCuC_{Nt}$ 179
5.7 Data collection and structure refinement statistics for $PCuC_{Ct}$ . . . 182
5.8 Bond lengths and angles of the Cu-binding site of $PCuC_{Ct}$ 183
5.9 Bond lengths and angles of the special position copper of $PCuC_{Ct}$. 188
5.10 Cu^{2+} binding properties of CopC and LPMO proteins 197

6.1 Summary of the characteristics of recombinant N_2OR proteins purified from *P. denitrificans* 225

7.1 Summary of dissolved trace metal concentrations. 233

A.1 Antibiotics and supplements 237
A.2 Templates used for Phyre2 ScoB model 240
A.3 Signal peptide prediction for $PCuC_{Nt}$ and YcnI 240

Abbreviations

AEC	Anion exchange chromatography
Anammox	Anaerobic ammonium oxidation
AUC	Analytical ultracentrifugation
ASEC	Analytical size exclusion chromatography
ATP	Adenosine triphosphate
Az	Azurin
BCA	Bicinchoninic acid
BCS	Bathocuproine disulfonic acid
BLAST	Basic local alignment search tool
BSA	Bovine serum albumin
Car	Carbenicillin
$CC_{1/2}$	Pearson's correlation coefficient
CopC	Copper resistance protein
Cox	Cytochrome *c* oxidase
CV	Column volume
Cyt bc_1	Cytochrome bc_1
Cyt c_{550}	Cytochrome c_{550}
DETC	Diethyl-dithio-carbamate
DMS	Dimethyl sulfoxide
DNA	Deoxyribonucleic acid
DNRA	Dissimilatory nitrate reduction

DSC	Differential scanning calorimetry
DTT	Dithiothreitol
DUF	Domain of unknown function
ECD	Electron capture detector
ECuC	Extracytoplasmic copper chaperone-like protein
EDTA	Ethylenediaminetetraacetic acid
EPR	Electronic paramagnetic resonance
FeS	Iron-sulphur cluster
FNR	Fumarate and nitrate reductase regulator
GC	Gas chromatography
Gen	Gentamicin
GSH	Reduced glutathione
HEPES	4-(2-hydroxyethyl)-1-piperazineethanesulfonic acid
HMM	Hidden Markov models
HTH	Helix-turn-helix
IAA	Iodoacetamide
ICP-AES	Inductively coupled plasma atomic emission spectroscopy
IMAC	Immobilised metal affinity chromatography
IMS	Intermembrane space
ITC	Isothermal titration calorimetry
LB	Lysogeny broth
LMCT	Ligand to metal charge transfer
LPMO	Lytic polysaccharide monooxygenases
Km	Kanamycin
MALDI	Matrix-assisted laser desorption/ionization mass spectrometry
MCO	Multicopper oxidase
MFS	Major facilitator superfamily
MGD	Molybdopterin guanine dinucleotide
MMO	Methane mono-oxygenase
MR	Molecular replacement
MOPS	3-(N-morpholino)propanesulfonic acid

MS	Mass spectrometry
Mw	Molecular weight
N_2OR	Nitrous oxide reductase
Nar	Membrane-bound nitrate reductase
Nap	Periplasmic nitrate reductase
NCS	Non-crystallographic symmetry
NGC	*nos* gene cluster
Nir	Nitrite reductase
NMR	Nuclear magnetic resonance
NnrR	Nitrite and nitric oxide reductase regulator
Nor	Nitric oxide reductase
Nos	Nitrous oxide reductase
OD	Optical density
PA	Pseudoazurin
PAGE	Polyacrylamide gel electrophoresis
PBS	Phosphate-buffered saline
PCR	Polymerase chain reaction
PCu_AC	Periplasmic Cu_A chaperone protein
PCuC	Periplasmic copper chaperone protein
$PCuC_{Ct}$-6His	Recombinant PCuC C-terminal domain
$PCuC_{FL}$-6His	Recombinant PCuC full length
$PCuC_{Nt}$-6His	Recombinant PCuC N-terminal domain
$PCuC_{WT}$	PCuC wild type
PDB	Protein data bank
pMMO	particulate methane monooxygenase
PrrC	Photosynthetic regulatory response
Ps az	Pseudo azurin
PVDF	Polyvinylidene difluoride
RO	Reverse osmosis
Rif	Rifampicin
RMSD	Root-mean-square deviation

RNA	Ribonucleic acid
RO water	Reverse osmotic water
$R_{p.i.m}$	Precision-indicating merging R factor
RT	Room temperature
SAD	Single-wavelength anomalous diffraction
SAXS	Small angle X-ray scattering
Sco	Synthesis of cytochrome oxydase protein
$ScoB_{sol}$-6His	Recombinant soluble ScoB protein
SDS	Sodium dodecyl sulfate
SEC	Size exclusion chromatography
SenC	Sensor of cytochrome oxydase protein
RND	Resistance-nodulation cell division system
SOD	Superoxide dismutase
SAXS	Small-angle X-ray scattering
Spec	Spectinomycin
Strep	Streptomycin
SUI	Cytochrome *c* oxidase subunit I
SUII	Cytochrome *c* oxidase subunit II
Tau	Taurine
TEMED	Tetramethylethylenediamine
Thr	Thioredoxin
T_m	Melting temperature
TOF	Time of flight
Tris	Tris(hydroxymethyl)aminoethane
UQH_2	Ubiquinol
UV-Vis	Ultraviolet-visible electronic absorbance spectroscopy
VECSUM	Vector sum of bond valences
WB	Western-Blot
WT	Wild-type

Acknowledgements

First of all I would like to thank my supervisors Andrew Gates, Gary Rowley and David Richardson for having given me this opportunity, mentored and guided trough out this scientific adventure. Secondly I want to thanks Marcus Edward and Matthew Sullivan for your patience, and being always willing to help and dedicate some of your time to all the demanding PhD students around you.

I also want to thank to all NORA members, it has been a fantastic experience being part of this group. We should definitely join for a last summer school (but without drama)!

Thanks to all the people from lab 2.30 for being such as fantastic group. Likewise, I want to give an special thank you to all people of Manuel Pineda and Lola Roldán groups from Cordoba specially to Pedro, Fran, Goyi, Victor... thanks for encouraging me in my early years when I was just an undergrad student. I also want to thank Yao Pan and Eiko Kuramae, I remember my time at Wageningen and all the people from NIOO-KNAW with special affection. In addition, I want to thank Hector, Maite and Vanesa for being my friends and colleagues during my stay in Madrid, I miss those all-together breakfasts!

A warm thank you goes for all my friends from Linares and Cordoba I know I can always count on you, and hopefully, now that the PhD is finished we will spend more time together! I also want to thank for all the love and support to my

family specially my parents Manuel and Maria del Carmen, my sister Mamen, my grandmother Rosa, David, Martin, Noelia, Alejandro and so many more. I have really missed you all in the distance.

Last but not least, I want to give the most special and warmest thank you to my partner Lola. Thank you for being by my side during these four last years, you brighten and give colour to my day to day. Together, the two of us we can take down any obstacle.

Para mis padres Manuel y Maria del Carmen

1 Introduction

1.1 Biogeochemical nitrogen cycle

Nitrogen is a common element in the universe, for instance it is the seventh most abundant element in the Milky Way and the Solar System, and on Earth it accounts for 78 % of the atmospheric gases. The element is an essential constituent of all known forms of life, it is found in amino acids, the nucleic acids and in the so called molecular unit of currency adenosine triphosphate (ATP) [6]. The biogeochemical nitrogen cycle describes the set of reactions by which the element circulates between the atmosphere and the biosphere in different organic and inorganic forms. NO_3^- can be considered as a junction key point of the N-cycle, it can be reduced down to NH_4^+ by plants and prokaryotes in a process called assimilatory nitrate reduction [7]. Alternatively, microbes can use NO_3^- as an electron acceptor under anaerobic conditions and also generate NH_4^+, this process is called dissimilatory nitrate reduction (DNRA). Anammox (anaerobic ammonium oxidation) is another process that was discovered almost twenty years ago whereby bacteria from the phylum *Planctomycetes* convert aerobically NO_2^- and NH_4^+ into N_2 [8]. However, one of the most relevant steps of the N-cycle for the purpose of this work is the dissimilatory anaerobic reduction of NO_3^- into N_2 called denitrification. N_2 is then reintroduced into the biosphere by nitrogen fixation. Finally, the cycle is closed with the process of nitrification by which NH_4^+ is oxidised into NO_2^- followed by the oxidation of the NO_2^- into NO_3^- (see figure 1.1).

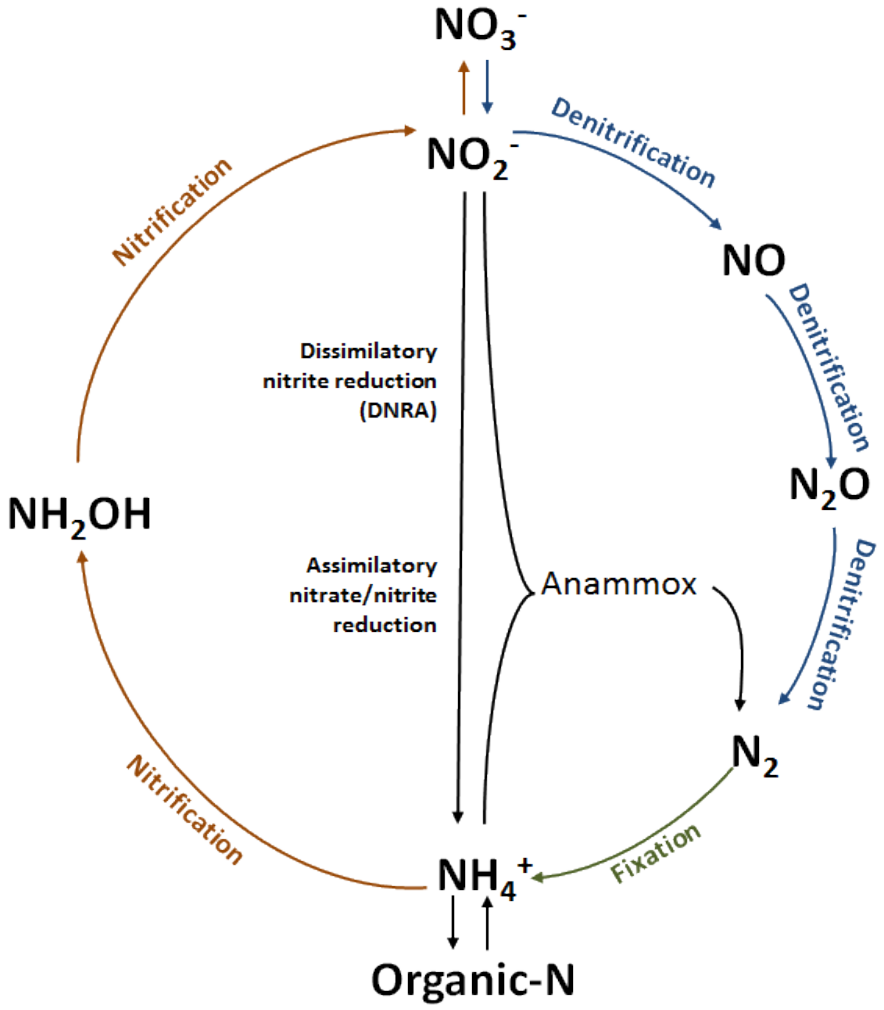

FIGURE 1.1: Schematic representation of the biogeochemical nitrogen cycle.

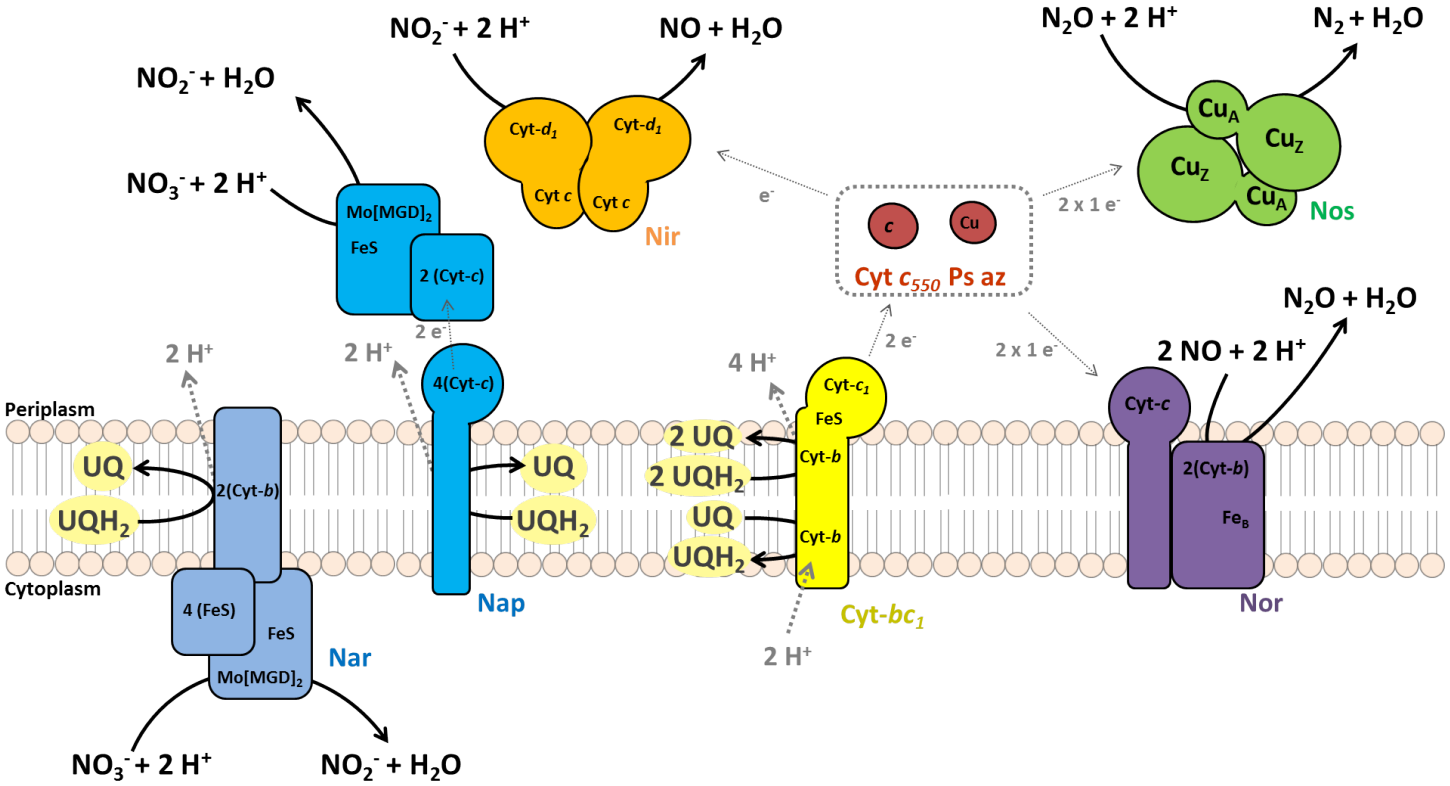

FIGURE 1.2: Schematic illustration of denitrification enzymes and their cellular location in *Paracoccus denitrificans*. Some organisms contain a copper-containing (NirK) nitrite reductase instead of a heme-containing reductase (NirS). The ubiquinol pool is the source of electrons for each reaction which then has to be replenish from the oxidation of organic carbon or inorganic electron donors. A net movement of protons across the membrane is generated, the resultant proton motive force can be used for ATP synthesis. Abbreviations: Nar, nitrate reductase; Nir, nitrite reductase; Nor, nitric oxide reductase; Nos, nitrous oxide reductase; Cyt bc_1, cytochrome bc_1; Ps az, pseudo azurin; UQH_2, ubiquinol; FeS, iron-sulphur centre; MGD, molybdopterin guanine dinucleotide; *b*, *c* and d_1 are different types of heme cofactors.

Denitrification is an intriguing example of the vast respiratory flexibility displayed by prokaryotes, whereby many microorganisms may thrive during anaerobic conditions using nitrogen oxyanions and nitrogen oxides as alternative electron acceptors in the absence of oxygen [9]. Denitrification involves the transformation of nitrate (NO_3^-) to nitrite (NO_2^-), NO_2^- to nitric oxide (NO), NO to nitrous oxide (N_2O) and N_2O to N_2. Each stage is catalysed by a different multidomain metalloprotein, for example the active sites of nitrate reductases (Nar or Nap) requires molybdenum as a part of the *bis*-molybdopterin guanine dinucleotide cofactor, nitrite reductase (Nir) may exist in two forms that contain either heme iron (NirS) or copper (NirK), nitric oxide reductase (Nor) requires heme and non-heme iron and the function of nitrous oxide reductase (Nos) is dependent on copper. Nevertheless, denitrification is a matter of general public interest since the use of nitrogen based fertilisers in agriculture is affecting the health of ground and coastal water environments and the atmospheric nitrous oxide global emissions [10].

Nitrous oxide is a colourless and highly soluble gas in water, which can persist in the atmosphere up to 150 years due to its low reactivity, compared to most of the atmospheric gases. Besides, each molecule of N_2O has 300 times the warming potential of a CO_2 molecule [1] and it may be removed from the stratosphere via UV photolysis, with the subsequent ozone layer depletion. At a global level, N_2O accounts a 9% to the total radiative forcing of greenhouse gas emissions and in the future this contribution is likely to be significantly higher since N_2O atmospheric loading is increasing at a 0.25% per year.

The reduction of N_2O to N_2 requires two electrons and two protons and this reaction is strongly exergonic (denoted by the large negative value of the free energy, ΔG^o):

$$N_2O + 2H^+ + 2e^- \longrightarrow N_2 + H_2O \quad [E^{\circ\prime}pH7 = +1.35V; \Delta G^{\circ\prime} = -339.5\ \mathrm{kJ\,mol^{-1}}] \tag{1.1}$$

At room temperature, this step needs the catalysis of nitrous oxide reductase (N_2OR) in order to occur in a cellular environment, since N_2O is very stable and

barely reactive [11, 12]. N_2OR exists as a functional dimer, each monomer binds 6 copper ions distributed in two distinct copper centres [13] (see chapter 6 for more information). Located at the N-terminal domain there is an unique catalytic Cu_Z centre whereas at the C-terminal domain a Cu_A electron transfer centre is found. Considering the high demand on copper that the enzyme imposes to the microorganism and the relatively limited reward from a bioenergetic point of view, it is not surprising that in electron acceptor-rich environments, such as nitrate fertilised fields, microorganisms may simply opt to avoid reducing N_2O. As a result, denitrification is interrupted with the consequent release of N_2O into the atmosphere [14–16].

1.2 Heme-copper oxidases from *Paracoccus denitrificans*

The Gram negative bacterium *Paracoccus denitrificans* was isolated for the first time in 1908 by the Dutch microbiologist Martinus Beijerinck [17] but we had to wait almost a hundred years until the genome of the bacterium was fully sequenced [18]. Since it was discovered, *P. denitrificans* has been the subject of numerous studies and one of the reasons why this bacteria has been used over the years as a model organisms is due to the similarity of its aerobic electron transport chain to that of mitochondria [19]. One of the main characteristics that distinguish the respiratory chain of *P. denitrificans* is its great metabolic complexity and versatility which is highly branched and can end in up to five different terminal reductases and four terminal oxidases [19, 20]. Among these terminal oxidases, three of them belong to the diverse family of heme-copper oxidases, which are characterised by the diversity of their subunit composition, cofactor content, electron donor and oxygen affinity [21, 22]. In terms of their subunit compositions, all heme-copper oxidases share the presence of a transmembrane subunit I (SUI) that contains a low spin heme (of *a*- or *b*-type) and a binuclear metal centre composed of a high spin heme (of *a*-, *o*-, or *b*-type, also named a_3, o_3 or b_3)-iron, and a Cu ion. The

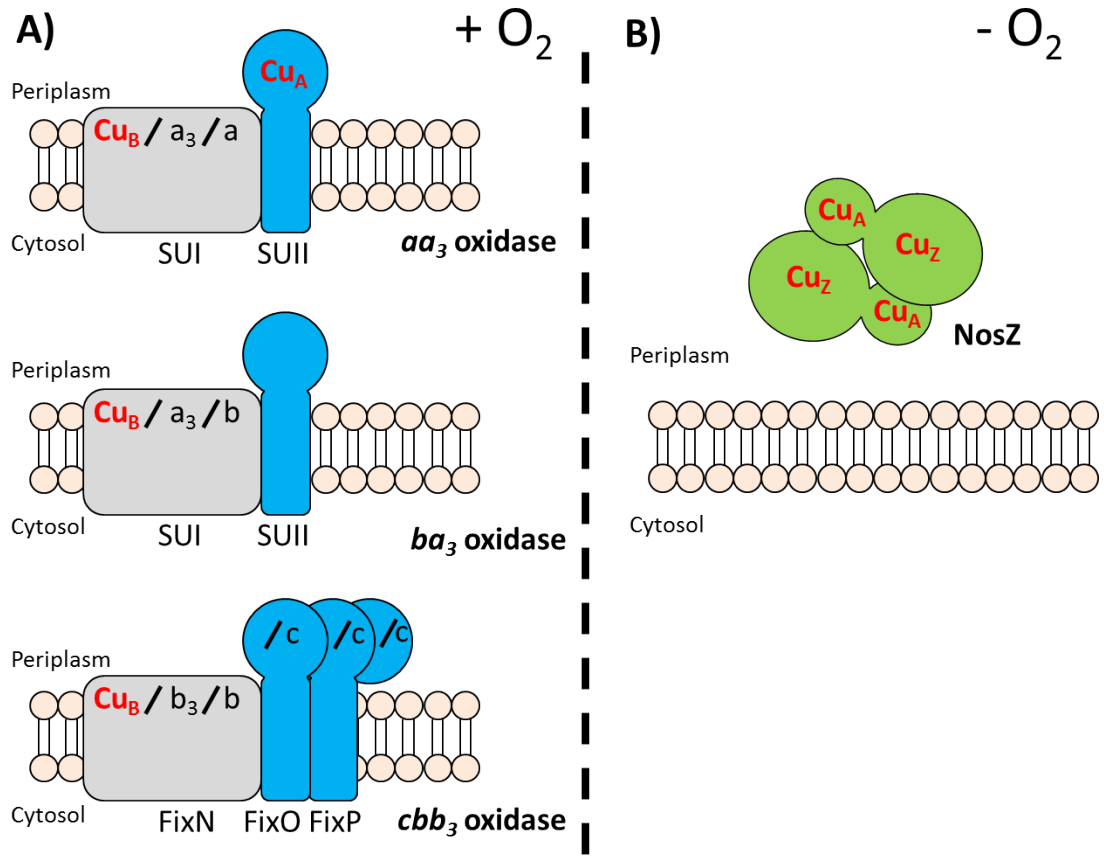

FIGURE 1.3: Copper dependent terminal reductases from *Paracoccus denitrificans*. **(A)** Under aerobic conditions *P. denitrificans* can express up to three different heme-copper oxidases: an aa_3, ba_3 or cbb_3. Only aa_3 contains a Cu_A centre. **(B)** Under anaerobic growth *P. denitrificans* expressing a Cu_A containing NosZ and use N_2O as an electron acceptor.

low spin heme is responsible for transferring the electrons to the catalytic binuclear centre (Cu_B) where the O_2 is reduced to H_2O [21, 23]. Subunit II (SUII) is also frequently shared among heme-copper oxidases, is the primary electron acceptor, and it can either hold a binuclear Cu centre (Cu_A) or a *c*-type cytochrome.

Heme-copper oxidases can be further classified into three different classes (A, B and C) regarding to their subunit composition and key residues involved in proton transfer pathways [23]. *P. denitrificans* happens to harbour one of each type of cytochrome *c* oxidase (Cox): an aa_3-Cox (type A), a ba_3-Cox (type B) and a cbb_3-Cox (type C) (see figure 1.3).

The terminal oxidase from *P. denitrificans* that has been more extensively studied is the heme-copper aa_3-type cytochrome *c* oxidase (cytochrome aa_3) [19, 24]. This Cox is made up of four-subunits [25] three of them with mitochondrial equivalents [26]. Within SUI a heme *a* and a heme a_3 are found together with the catalytic Cu_B centre whereas SUII presents an electron transfer Cu_A centre. In addition, aa_3 Cox has two different proton pathways (K and D) and an affinity for oxygen in the order of the micromolar ($K_M \sim 1\ \mu M$).

The ba_3-type oxidase is a quinol oxidase [27] made up of two subunits. SUI contains a heme *b* and a heme a_3 in addition to the Cu_B centre whereas SUII compared to aa_3-type oxidase does not present a Cu_A centre although some other ba_3-type oxidases can have it such as in the case of ba_3-type oxidase from *T. thermophilus* [5]. In contrast to aa_3, ba_3-type oxidases have only a K proton pathway and a higher affinity for oxygen ($K_M \sim 0.1\ \mu M$) [28].

The cbb_3-type oxidase was initially discovered in endosymbiotic rhizobia as the type of Cox that the microbe uses at extremely low oxygen concentration within the root nodules ($K_M \sim 7$ nM) [29]. This oxidase has three subunits, SUI contains a *b* and a b_3 heme as well as a Cu_B centre while the other two subunits are heme containing membrane proteins that act as electron entry sites.

When oxygen levels drop and anaerobic conditions prevail, *P. denitrificans* can utilise NO_3^- as an alternative electron acceptor and sequentially reduced it down to

N_2 [19]. Among all the terminal reductases that *P. denitrificans* carries cytochrome *c* oxidase aa_3, ba_3, cbb_3 and N_2OR require copper as a redox active cofactor (see figure 1.3). However, only aa_3 and N_2OR share structural homology in their electron transfer Cu_A centre (ba_3 from *P. denitrificans* lacks a Cu_A centre).

1.2.1 Eukaryotic cytochrome *c* oxidase Cu_A centre maturation

The eukaryotic cytochrome *c* oxidase that is part of the electron transport chain of the mitochondria is a macromolecular complex made up of nearly 13 subunits. The majority of these subunits are encoded in the nuclear chromosome with the exception of SUI and SUII which are encoded within the mitochondrial genome. Likewise, the intervention of a multitude of accessory factors that originate from the two sides the mitochondrial membrane are required [30]. Therefore, in order to produce an active enzyme the process of membrane insertion and maturation of each individual subunit as well as their cognate partners and the assemblage of the cofactors has to be finely tuned and coordinated.

In particular, the maturation process of the Cu_A centre of SUII requires the action of the Cu chaperones Cox17, Sco1, and Sco2 that perform step-specific functions. Cox17 is a small Cu-binding protein that can transfer Cu to both Sco1 and Sco2, the Sco proteins in turn are part of a diverse family of proteins that can have thioredoxin and/or Cu-binding activity (see Chapter 3). However, there are some subtle differences in the metal interchange process. For instance, Cox17 can simultaneously reduce the metal-binding cysteine residues of oxidised Sco1 and transfer a Cu^{1+} ion, while electron transfer-coupled metallation of Cox17 to oxidised apo-Sco2 is not possible and copper delivery has to be done to the reduced apo-protein [31]. Once Sco1 and Sco2 have been metallated by Cox17, Cu^{1+}-Sco2 interacts with the newly synthesised SUII stabilizing it, then Sco1 is recruited in the Sco2-SUII complex and passes one Cu^{1+} to SUII to form the Cu_A site [32] (see figure 1.4 A). The thioredoxin activity of Sco is considered to play a relevant role in the reduction and maintenance of the cysteine residues of the Cu_A [32].

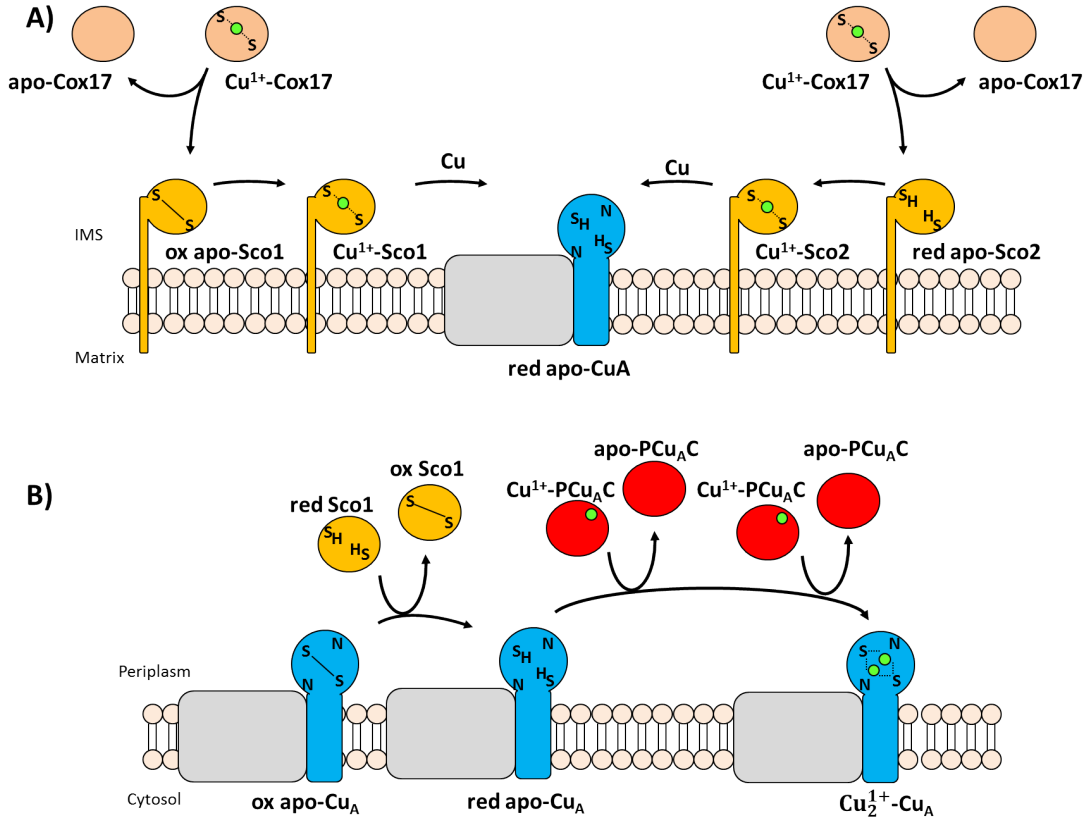

FIGURE 1.4: Pathway of copper insertion into the Cu_A centre of cytochrome *c* oxidase. **(A)** Maturation of mitochondrial aa_3 oxidase. Cu^{1+}-Cox17 can deliver copper to oxidised apo-Sco1 coupled with electron transfer. However, Cu^{1+} donation from Cu^{1+}-Cox17 to apo-Sco2 only take places when the metal centre of the protein is reduced. Holo Sco1 and Sco2 are then responsible for the metallation of reduced apo-Cu_A. **(B)** Maturation of ba_3 oxidase from *T. thermophilus*. In this case, Sco prepares the Cu_A centre of SUII by reducing the cysteine residues of the binuclear site, then two Cu^{1+} transfer event take place from holo PCu_AC to reduced Cu_A centre. The small green spheres represent Cu^{1+} ions. For simplification Sco1 has been represented as a periplasmic protein although the native protein is bound to the cell membrane.

1.2.2 Prokaryotic cytochrome *c* oxidase Cu_A centre maturation

The process of maturation of the prokaryotic Cu_A-containing ba_3 cytochrome *c* oxidase has been recently studied in depth in the Gram negative bacterium *Thermus thermophilus* [5]. Prokaryotic microorganisms in general do not contain *cox17* genes and instead two protein families have been found to be required. The first family consist of small periplasmic Cu^{1+}-binding proteins called PCu_AC [33] (see chapter 4) and the second one consist of the Sco proteins previously mentioned. Both *sco* and pcu_AC genes are encoded within the same gene cluster in *T. thermophilus*. Contrary to the model of Cu_A maturation of Eukaryotic Cox, the Sco protein of *T. thermophilus* was found to be unable to deliver copper to the Cu_A centre of SUII, instead it worked as a thiol-disulfide oxidoreductase keeping the cysteine residues of the Cu_A centre reduced. The copper chaperoning role was played by PCu_AC which in turn selectively and sequentially deliver two Cu^{1+} ions to reduced apo-Cu_A giving rise to the Cu_2^{1+}-Cu_A site of SUII (see figure 1.4 B).

1.3 Copper and microbiology

Copper like many other metals originated at the heart of massive stars although on Earth is just a trace element that accounts for only 0.00005 % of the lithosphere [34]. The transition metal can be found in two oxidation states Cu^{1+} and Cu^{2+}. The oxidised form of Cu has a 3 d^9 outer electronic configuration while the reduced ion is a closed shell d^{10} ion and therefore is diamagnetic.

At the formation of the Earth 4.5 billion years ago, oxygen was absent and microbial life was anaerobic, principally based on Fe^{2+}, while copper was in its Cu^{1+} state sequestered by sulphur compounds into mineral precipitates. It was not until the development of an oxic atmosphere 2 billion years later due to the metabolism of photosynthetic cyanobacteria when Cu^{1+} began to be oxidised to the water soluble Cu^{2+} ion and soluble Fe^{2+} was converted to the insoluble Fe^{3+} [35]. This event

had enormous impact on life and consequently microorganisms had to develop mechanisms for iron acquisition and at the same time the redox properties of copper began to be used in enzymes such as cytochrome oxidase or multi-copper oxidases. In fact, the evolution of cupredoxins can be traced back to the appearance of photosynthesis [35]. Many examples can be found of copper- *vs.* iron-containing enzymes that catalyse similar reactions (see table 1.1).

An inevitable side effect of Cu metabolism is that, as a result of its redox biology, it catalyses the Fenton reaction with hydrogen peroxide and produces highly toxic reactive oxygen species that principally target iron sulphur cluster containing proteins (see equation 1.2) [35–37].

$$Cu^{1+} + H_2O_2 \longrightarrow Cu^{2+} + OH^- + OH^{\cdot} \tag{1.2}$$

Copper toxicity is such that the current understanding is that no free Cu is found within the cell. Instead, the transition metal gets to its final destination bound to copper binding proteins or Cu chaperones, or to low molecular mass ligands such as reduced glutathione (GSH) [38–41]. Indeed, for many years it has been considered that most microorganisms do not even possess copper-containing enzymes in their cytoplasm with the notable exception of the metal storage protein Csp1 from *Methylosinus trichosporium* OB3b, which is folded in the cytosol where it presumably acquires Cu before being exported [42, 43]. Overall, cells have developed mechanisms of Cu transport, sequestration and compartmentalization in order to be capable of tightly controlling Cu levels and to avoid Cu derived toxicity effects [44].

1.3.1 Bacterial cuproenzymes

Superoxide dismutase (SOD) is an enzyme with an important antioxidant function that catalyses the dismutation of O_2^- radical into either O_2 or H_2O_2. Two different types of bacterial SOD can be distinguished based on the metal co-factors present

Function	**Iron**	**PDB**	**Copper**	**PDB**
O_2 transport	Hemoglobin	1A3N	Hemocyanin	1JS8
Hydroxylation	Cytochrome P_{450}	1AMO	Particulate MMO	1YEW
Oxidation	Catechol dioxygenase	2AZQ	Dinuclear catechol oxidase	1BUG
Electron transfer	Cytochrome c_{550}	155C	Pseudoazurin	3ERX
Terminal oxidase	Diiron alternative oxidase		Cytochrome *c* oxidase	1OCC
			N_2O reductase	1FXW
Anti-oxidant	FeSOD	1COJ	CuZnSOD	1ESO
NO_2^- reduction	NirS	2AKJ	NirK	1OE2

TABLE 1.1: Comparison of copper *vs.* iron enzymes that catalyse similar reactions. SOD, superoxide dismutase; MMO, methane mono-oxygenase.

in their catalytic centres. SodA contains Mn^{2+} whereas SodC Cu^{1+} and Zn^{2+} (and in same cases Fe^{2+}) [45]. The Cu containing SOD is exported to the periplasm through the Sec system where it is supposed to receive the transition metal from a copper chaperone such as CueP from *Salmonella typhimurium* (see figure 1.5) [46, 47].

The periplasmic protein CueO is a multicopper oxidase (MCO) similar to PcoA (described below). This MCO is up-regulated in the presence of copper through the *cueR* regulon [48] and is considered to provide copper periplasmic tolerance by oxidizing Cu^{1+} into the less toxic Cu^{2+} ion (see figure 1.5) [49, 50].

1.3.2 Copper import mechanisms

Overall, most of the research studies in relation to Cu homeostasis have addressed the systems involved in Cu export while less attention has been paid to the mechanisms required for Cu uptake. Copper ions are small and hydrophilic and could potentially enter the bacterial cells utilizing the porin pathway, such as the outer membrane proteins OmpF and OmpC from *Escherichia coli* (see figure 1.5) [51, 52].

Alternatively, Cu can be sequestered from the extracellular environment by secreting small ligands with great affinity and specificity to copper termed chalkophores. For

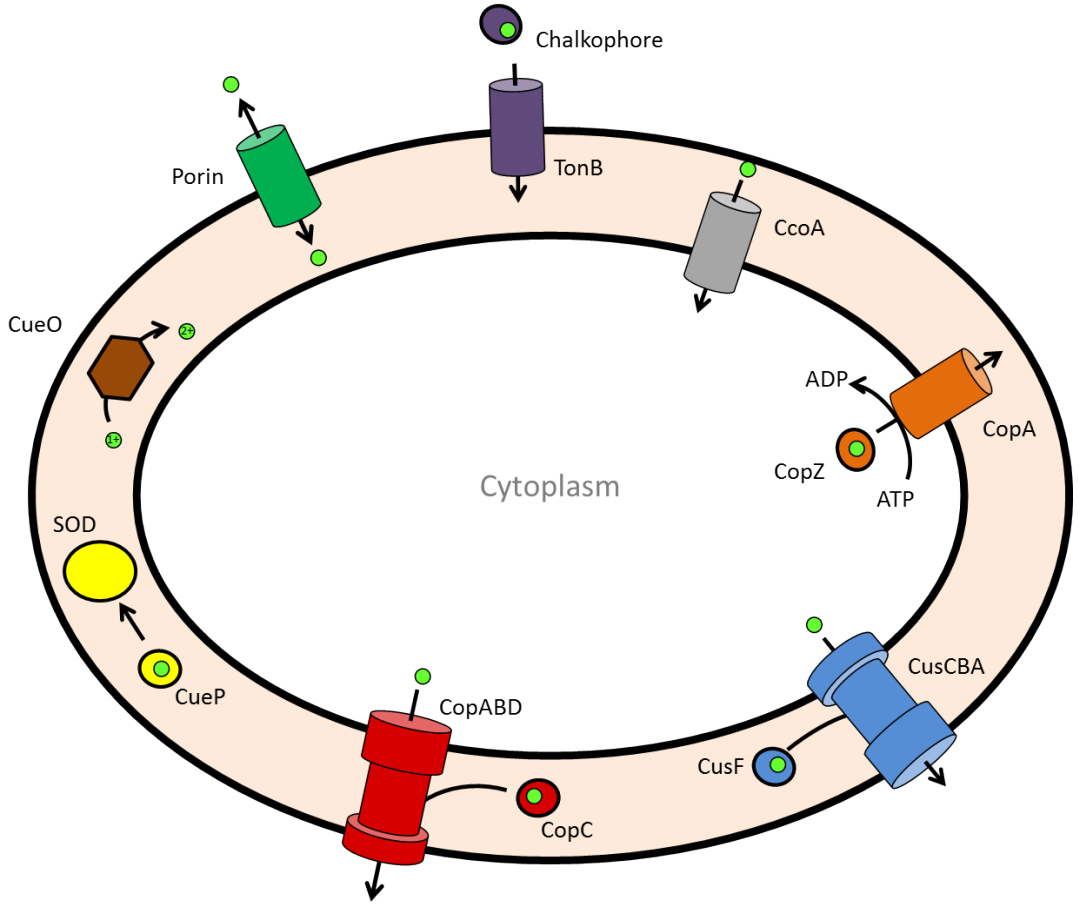

FIGURE 1.5: Summary of characterised prokaryotic cuproenzymes responsible for copper homeostasis of the cell. Cu can enter the cell through porins or bound to chalkophores that interact with TonB proteins. CcoA has been proposed as a system for Cu import into the cytoplasm. CusCFBA and CopABDC are four-component Cu efflux pumps. CueP is a considered as a SOD chaperone. CueO is involved in detoxification of Cu^{1+} through oxidation of the metal into Cu^{2+}. The small green spheres represent Cu ions.

instance, methanotrophic organisms secrete a Cu^{1+}-binding compound named methanobactin when the organisms are grown under copper limiting conditions [53]. Instead of using porins, Cu loaded methanobactins are thought to be internalised by energy dependent TonB transporters [54]. Likewise, *P. denitrificans* releases coproporphyrin III when is grown in a Cu deprived media and is thought to be incorporated through a TonB-dependent heme receptor/transporter that is encoded in the vicinity of the *nos* gene cluster (see figure 1.5) [55].

In addition, a member of the major facilitator superfamily (MFS) has been proposed to function as a Cu importer [56, 57]. In *R. capsulatus* CcoA is required for cytochrome cbb_3 oxidase synthesis since deletion of *ccoA* decreases intracellular Cu and cbb_3 activity (see figure 1.5) [56, 57].

1.3.3 Cu export systems

1.3.3.1 Cu-transporting P-type ATPases

Copper homeostasis in the cytosol is maintained by the P_{1B}-type ATPase protein CopA that removes excess of copper. The expression of this protein in *E. coli* is induced in the presence of copper [58] and in *B. subtilis* copper transport is aided by the periplasmic chaperone CopZ (see figure 1.5) [59]. CopA is supposed to interact with other periplasmic copper chaperones such as CueP [60]

1.3.3.2 Cus system

The Cus system, which is exclusively present in Gram-negative bacteria, has been proposed to act as a defence mechanism towards cytosolic derived copper toxicity. It consists of six genes organised in two operons *cusRS* and *cusCFBA* [61]. CusRS and CusCFBA are a two-component regulatory system and a resistance-nodulation cell division system (RND), respectively. CusA is an inner membrane homotrimeric protein that captures Cu ions from the cytoplasm and the periplasm and interacts directly with the periplasmic protein CusB [62, 63]. CusC is a trimeric outer

membrane protein that interacts with CusAB and forms a channel that bridges the periplasmic space. In addition, CusF is a small periplasmic protein capable of transferring Cu to the CusCBA complex (see figure 1.5). Deletion of any of these four genes increased copper sensitivity in a *cueO* deletion background [64].

1.3.3.3 CopCD/PcoCD system

The CopCD/PcoCD pair is a system that confers copper resistance, in *Enterobacteriaceae* is predominantly encoded on plasmids while among *Pseudomonadaceae* and *Xanthomonadaceae* is found in the chromosomal DNA. For instance, The *E. coli* strain APEC O1 carries an additional plasmid with the seven-genes cluster *pcoABCDRSE* [65]. PcoRS are proteins of a two-component regulatory system while PcoABCD showed homology to the CopABCD proteins from *P. syringae* [66, 67]. The protein PcoB/CopB is located in the outer membrane. PcoA/CopA is a periplasmic multicopper oxidase that can bind up to 11 copper atoms. PcoC/CopC is a periplasmic Cu binding protein which can bind up to two Cu ions [68–71]. PcoD/CopD is cytoplasmic membrane protein involved in copper uptake (see figure 1.5) [72, 73]. YcnJ is a particular CopCD fusion protein from *B. subtilis* that will be explained in more detail in section 4.

1.4 Nitrous oxide reductase

Nitrous oxide reductase (N_2OR) was isolated for the first time in 1972 by Matsubara *et al.* as a new type of copper binding protein that the researchers discovered as a by-product of cytochrome cd_1 purification [74]. However, scientists required 10 more years to identify the function of the protein, which they eventually achieved through a thorough identification of the metal requirement for anaerobic respiration of N_2O [75, 76].

1.4.1 Patterns in *nos* gene clusters

The coding gene for N_2OR was initially identified within the *nos* genes cluster (NGC) of *P. stutzeri* by mapping genomic insertions of the transposon Tn*5* [77]. However, a subsequent bioinformatic study by Sanford and collaborators distinguished at least two distinctive NGC that can be generally classified in the following two groups: those that harbour a type-I or typical *nosZ* gene and those with a type-II or atypical *nosZ* [16, 78].

1.4.1.1 Typical *nos* gene clusters

The structural arrangement of typical NGC is characterised for being largely conserved among prokaryotic denitrifiers. Within the gene cluster that contains the functional gene for N_2OR there are also coded a set of accessory genes involved in the optimal transcription and assembly of N_2OR, particularly the Cu_Z centre. The most regular pattern of the accessory genes is a tricistronic *nosDFY*, along with *nosL* downstream of *nosY*. Occasionally more than one copy of *nosF* and *nosY* are present although *nosL* is the gene more likely to be redundant (see figure 1.6) [79–82].

Less conserved than *nosDFY* but still worth mentioning is the presence of the gene neighbours *nosC*, *nosR* and *nosX*. The gene *nosC* codes for a putative cytochrome *c* protein and is usually found preceding *nosZ*, or in certain occasions is divergently encoded such as in *Ralstonia eutropha*. Another commonly conserved gene is *nosR* which is usually located upstream of *nosZ*, but it may also be found between *nosZ* and *nosD* or at the end of the gene cluster. Members of the α-proteobacteria group occasionally contains a gene termed *nosX* that may follows or leads the NGC (see figure 1.6) [79–82].

In the research of Sanford *et al.*, the investigators determined that typical NGC are generally present in genomes of α-, β- and γ-proteobacteria. The organisms from these groups represent an ecophysiologically homogeneous group of complete

denitrifiers and facultative aerobes ($\sim$ 85 % of the genomes studied), which are able to switch from aerobic respiration to denitrification when soil conditions become anoxic [16, 78].

1.4.1.2 Atypical *nos* gene clusters

Atypical *nos* gene clusters are generally made up of 10 to 11 genes. These genes show limited apparent organisation aside from the presence of a gene encoding a putative transmembrane protein of unknown function that is frequently located downstream of *nosZ*. At least five genes are shared in common with typical NGC. Here, the *nosDFYL* genes are often found downstream the gene that codes for the putative transmembrane protein and a *c*-type cytochrome homologous to *nosC* that contains a CX_2CH motif is also present (see figure 1.7) [78].

Noticeably, *nosR* and *nosX* genes are completely absent in atypical NGCs. Instead three distinctive genes that code for putative polypeptides with the following motifs are found: a protein with two [4 Fe−4 S] motifs ($CX_2CX_2CX_3CP$), a protein with a [2 Fe−2 S] motif ($CXHX_nCPCH$) and another protein with a cytochrome -*b* domain. These three proteins together with the product of *nosC* are predicted to be involved in electron transport processes (see figure 1.7).

Sandford and collaborators determined that atypical NGC are found distributed within diverse microbial taxa and in a considerable higher percentage ($\sim$ 56 % of genomes) of organisms that are not considered full denitrifiers. Overall, they shape an ecophysiological diverse group present in a broad range of habitats, including anoxic, microaerophilic, oxic or psychrophilic environments.

1.4.2 Mechanism of action of N_2OR

Since 1982 when the enzymatic activity of N_2OR from *P. stutzeri* was characterised for the first time [83] and until 2011 when the structure of N_2OR in its active form

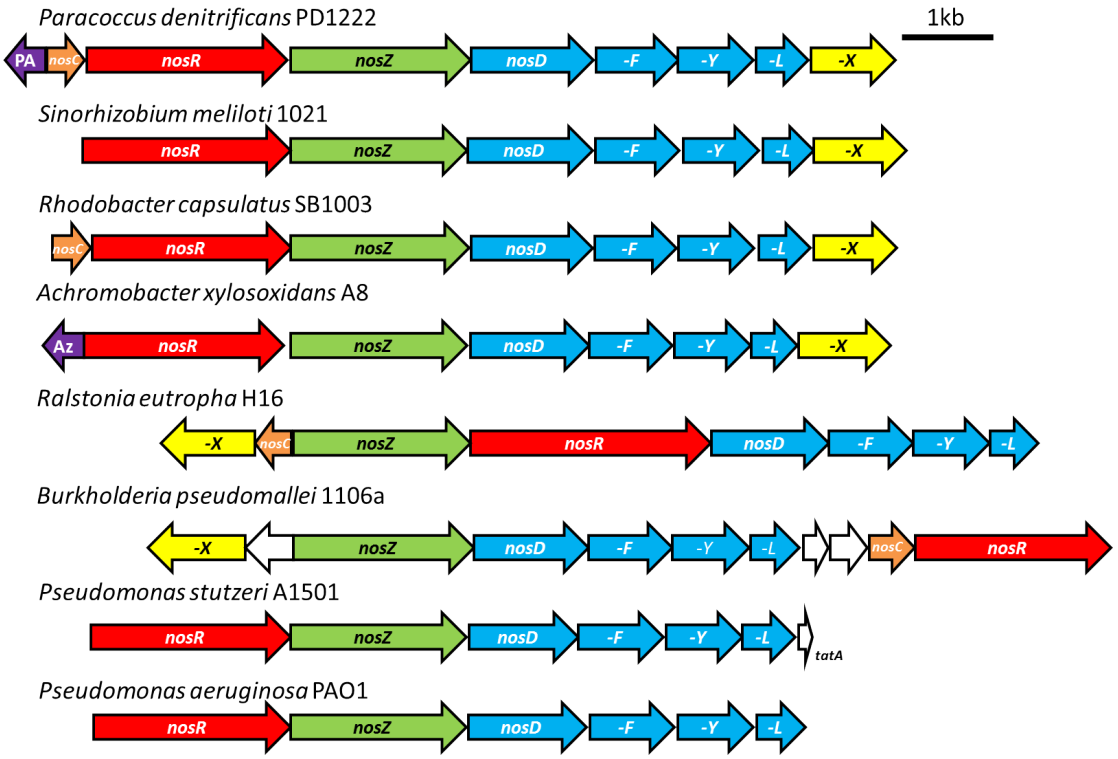

FIGURE 1.6: Comparison of the organisation of typical *nos* gene clusters. The genes have been annotated as follow, pseudoazurin (PA); azurin (Az); protein containing *c*-type cytochrome (*nosC*); twin-arginine translocation (*tatA*). White arrows stand for hypothetical proteins.

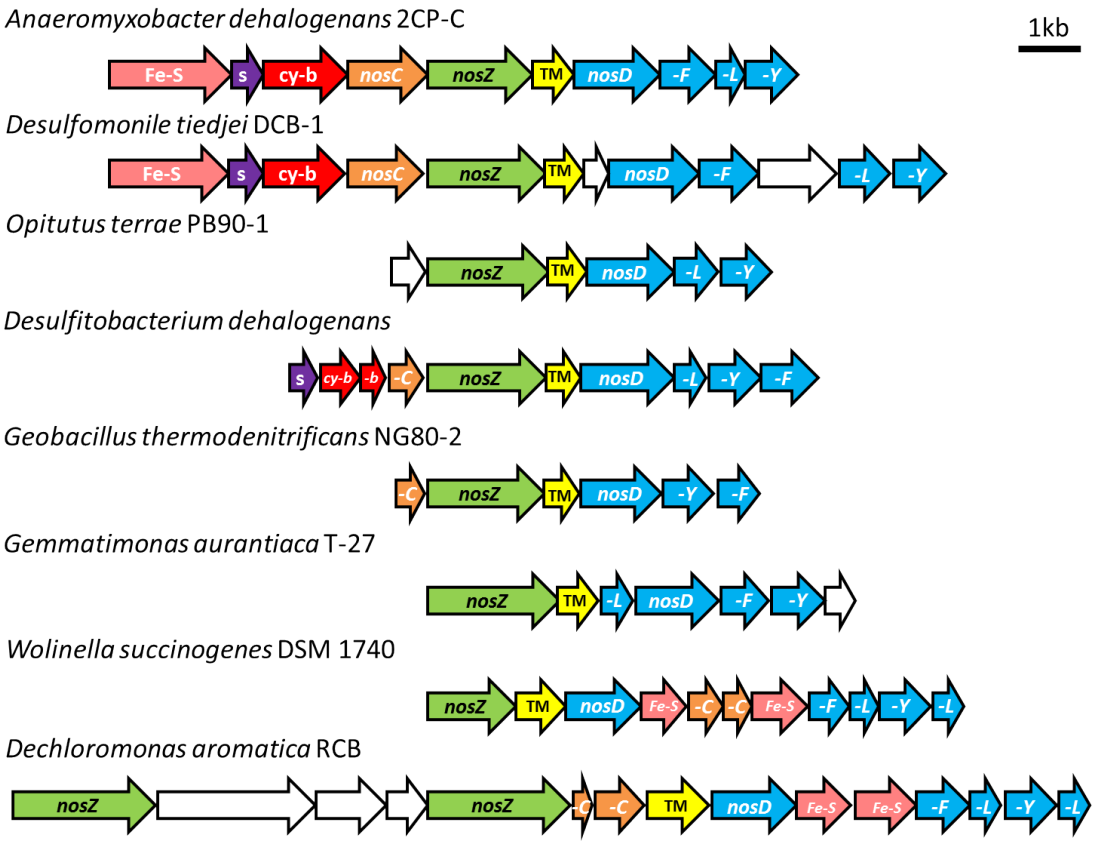

FIGURE 1.7: Comparison of the organisation of atypical *nos* gene clusters. The genes have been annotated as follow: predicted iron–sulphur-binding proteins (labelled "Fe-S"), Rieske iron–sulphur proteins (S), *b*- (cy-b) or *c*-type (*nosC*) cytochromes, transmembrane protein (TM) and accessory genes (*nosD*, *nosF*, *nosY*, *nosL*).

was published [13], around eight N_2OR proteins from different microorganisms have been purified and described [83–90]. Several forms of N_2OR with different redox properties were reported over this period of time depending on the genomic background and purification procedure used, and an intense debate emerged about the mechanism of action of the protein. According to the spectroscopic characteristics and redox state of N_2OR at least three different forms can be distinguished: form I (or purple N_2OR) is isolated under anoxic conditions, is catalytically active with artificial electron donors and analysis of the UV-vis spectra indicates that the Cu_A and Cu_Z centres were in their oxidised [$Cu^{1.5+}$-$Cu^{1.5+}$] and [2 Cu^{2+}-2 Cu^{+}] states, respectively. Form II and form III are pink and blue, respectively; both are isolated in the presence of oxygen but in the case of form III a reductant is added to the preparation. The Cu_Z centre of both forms is in a [Cu^{2+}-3 Cu^{+}] redox state and they differ in their Cu_A centre that is oxidised in form II and fully reduced in form III. In both cases the enzyme is inactive as purified and has to be re-activated by prolonged reduction with reduced methyl viologen.

Finally, Pomowski and co-workers settled the discussion when in 2011 they published the structure of N_2OR purified from anaerobic conditions [13]. The crystal structure of N_2OR form I from *P. stutzeri* most likely represents its physiologically active form and overall is similar to all previous solved structures [13]. N_2OR is a homodimer of approximately 130 kDa, each monomer is composed of two domains, the N-terminal domain is a seven-bladed β-propeller domain and binds the tetranuclear Cu_Z catalytic centre, while the C-terminal domain adopts a conserved cupredoxin fold, typical for copper-binding proteins, and contains a binuclear Cu_A electron transfer centre (see figure 1.8). The two monomers are arranged within an inverted disposition where the two different copper centres from each monomer are brought together at the very close distance of 10 Å. The main difference of N_2OR form I is the presence of a second sulphur atom within the Cu_Z centre (see extended description in section 1.4.2.2).

1.4.2.1 The Cu_A electron transfer centre of N_2OR

Located at the C-terminal region of N_2OR there is a cupredoxin-like domain that contains a Cu_A centre similar to the one found in cytochrome *c* oxidase [25]. Both Cu_A centres are binuclear metal sites that perform a single electron transfer reaction. The copper ions are coordinated by two cysteine ligands, two histidines, a methionine and a backbone carbonyl oxygen from a tryptophan residue (see figure 1.8). The two cysteine residues bridge the two copper atoms (Cu_{A_1} and Cu_{A_2}), while the other residues bind only Cu_{A_1} (His and Met) or Cu_{A_2} (His and Trp). Cu_A centres have a positive redox potential and a characteristic mix-valence high spin [${Cu_{A_1}}^{+1.5}$:${Cu_{A_2}}^{+1.5}$] $S = 1/2$ state in its oxidised form. An unpaired electron delocalised over two nuclei with a nuclear spin of $I_{Cu} = 3/2$ is deduced from a narrow 7-line hyperfine splitting in the g_{II} region of the electron paramagnetic resonance (EPR) spectrum [91].

Based on the analysis of the structure of N_2OR of *P. stutzeri* it was attributed a molecular gating role for His^{583} that coordinates Cu_{A_1} [13]. Under anoxic conditions, the imidazole side chain of the residue is rotated to form a short hydrogen bond with the side chain of residue Ser^{550}. At the same time, His^{583} preserves its hydrogen bond to the conserved residue Asp^{576}, which reaches the surface of the protein and in a previous study of *Marinobacter hydrocarbonoclasticus* N_2OR it has been proposed to be the electron entry point to Cu_A [92]. Only when Cu_Z is degraded upon O_2 exposure, or when N_2O binds to the Cu_Z site, does the conformation of His^{583} revert to the state commonly observed in Cu_A centres. This event is indicative of functional coupling of the two metal centres and suggests that binding of the substrate has to take place before electrons can be transferred to Cu_A centre [93].

1.4.2.2 The Cu_Z catalytic centre of N_2OR

The Cu_Z cluster lies within the N-terminal region of N_2OR. This metal centre is coordinated by seven histidine residues that originate from six of the seven

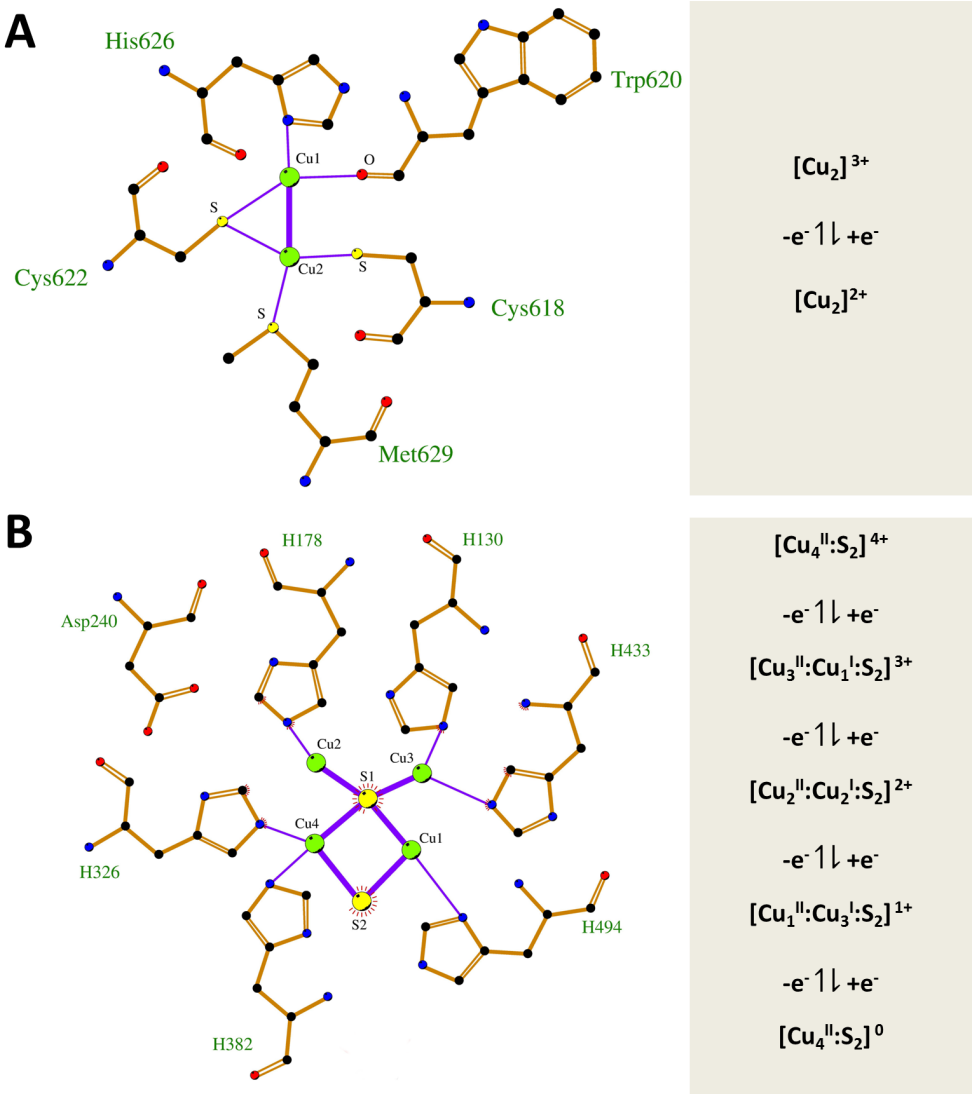

FIGURE 1.8: Schematic diagram of the copper centres of N_2OR. **(A)** The binuclear Cu_A centre and **(B)** the tetranuclear Cu_Z centre. Picture generated using the software LigPlot [94]

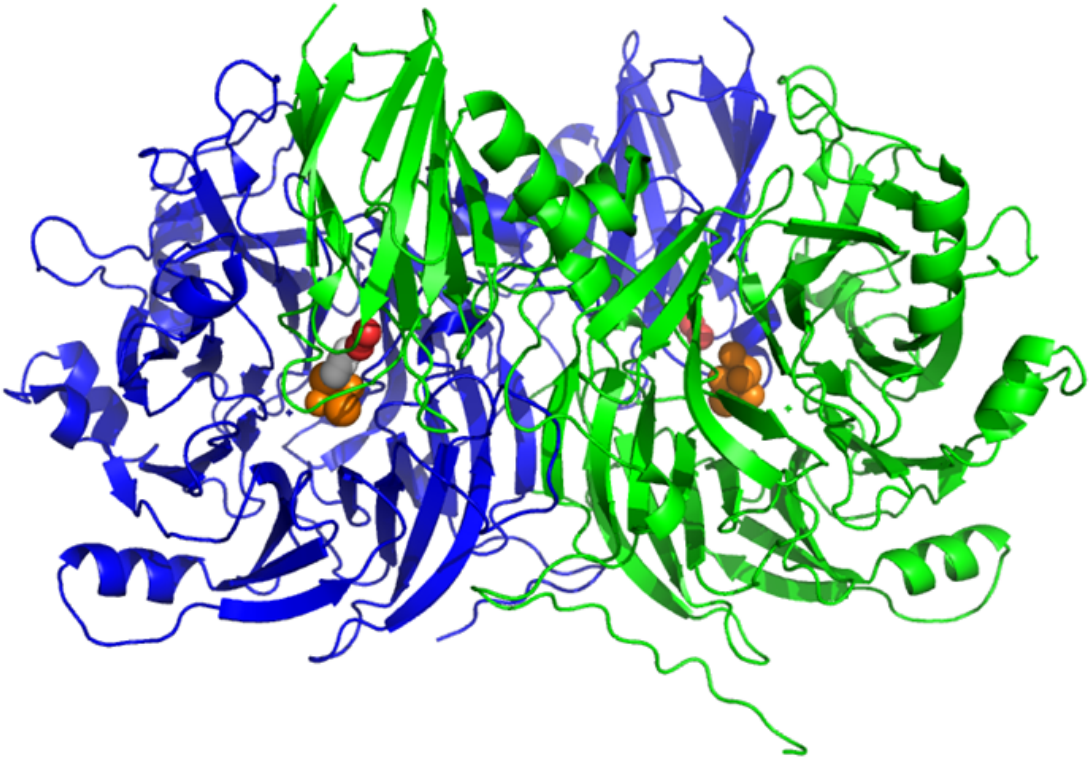

FIGURE 1.9: Cartoon representation of nitrous oxide reductase from *Pseudomonas stutzeri*. Protein monomers are coloured in blue and green while the Cu_A and Cu_Z centres are represented as red and orange spheres. Note that a molecule of N_2O is bound to the blue monomer and it has been drawn as a white sphere (PDB accession code: 3SBR)

β-strands that form a β-propeller structure. As we mentioned above, three different forms of N_2OR have been distinguished in the literature, which apart from their different spectroscopic features and the purification procedure used, crucial structural differences are also found in their Cu_Z centre. N_2OR form I is considered to represent the functional form of the protein and it is characterised for presenting a Cu_Z with a [4Cu:2S] stoichiometry (Figure 1.8). Alternatively, the Cu_Z of N_2OR forms II and III share the central μ_4-bridging sulfido ligand, although they lack a second S atom which instead has being substituted by a water molecule or a hydroxo ligand.

In fact, the presence of the labile sulphur within the Cu_Z of N_2OR form I can be identified spectroscopically. The reduced UV-vis spectrum of N_2OR shows a characteristic maximum at 538 nm that is the result of the contribution of both Cu centres. This combined spectra can be easily deconvoluted into the subspectra of the two the Cu_A and Cu_Z centres. With a mild reductant such as ascorbate the Cu_A can be selectively reduced to a colourless form while a Cu_Z deficient strain can be used to identify the bands of the Cu_A centre [90, 95]. Once the spectrum of both metal sites has been isolated, the subspectrum of the Cu_Z site can be modelled with two transitions at 552 and 650 nm which have been assigned to distinct charge transfer to a copper ion, originating from atoms S_{Z_2} and S_{Z_1}, respectively [13]. It is therefore considered that during purification of N_2OR forms II and III S_{Z_2} atom is lost along with the 552 nm band. The result is a single remaining band at 650 nm that was previously described as the Cu_Z^* state.

1.4.2.3 N_2O binding at the Cu_Z centre of N_2OR

Currently, the only structural data available of the mode of binding of the nitrous oxide substrate to N_2OR comes from the work of Pomowski and co-authors [13]. In this study, the researchers pressurised anoxically purified N_2OR crystals with N_2O and they identified the gas molecule located in the vicinity of the Cu_Z centre in a side-on manner of the cluster face made up by atoms Cu_{Z_2}, Cu_{Z_4} and S_{Z_1} [13]. However, the distance of the gaseous molecule to the cluster is peculiarly

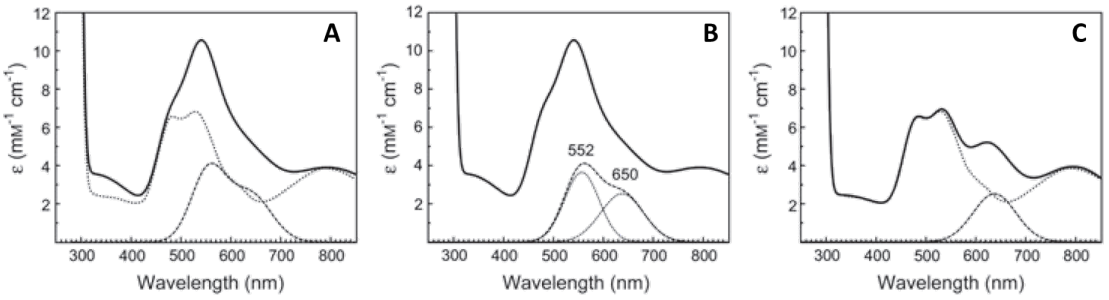

FIGURE 1.10: UV-visible spectra of *P. stutzeri* N_2OR. **(A)** Spectral features of N_2OR form I (solid line) and deconvoluted Cu_A (grey dotted line) and Cu_Z (dark dotted line) centres. **(B)** Spectral features of N_2OR form I (solid line) and deconvoluted Cu_Z site showing the contribution of S_{Z_2} and S_{Z_1}. **(C)** Spectral features of N_2OR form II showing Cu_Z^* that lacks S_{Z_2}. The figure has been adapted from Zumft *et al* [96].

too long for covalent or even coordinative interactions. Therefore, the authors hypothesised that within the catalytic cycle, a first reduction step and a consequent structural conformational change might be responsible for a tighter binding of N_2O to Cu_Z site [13]. This assumption is based on the fact that although N_2OR form I is catalytically active as purified, the activity of the enzyme is low and has to be activated by prolonged incubation with a strong reductant in order to acquire maximum activity [97]. Alternatively, the only other piece of evidence for the mechanism of action comes from synthetic chemistry studies. Bar-Nahum and co-workers generated a mixed-valence $[Cu_3S_2]^{2+}$ cluster that converts N_2O to N_2 at low temperature. The authors suggested a mechanism of action involving a pre-equilibrium formation of a di-copper complex and a subsequent reduction of N_2O via a transition state that features bridging of substrate between the two copper ions through a single O atom [98].

1.4.3 Regulation of *nos* genes

While the biochemistry of nitrous oxide reduction has been extensively characterised, the signals and transcriptional regulators controlling this process have received considerably less attention. In addition, there is a high degree of diversity in the organisation of regulatory networks, even among phylogenetically closely related

organisms. Oxygen, nitric oxide and copper are the three most important signals that are known to affect the expression of N_2OR.

1.4.3.1 FNR transcriptional factor

The first FNR (fumarate and nitrate reductase regulator) protein was initially described in *Escherichia coli* [99] were it is considered to be responsible for the control of the transition between aerobic and anaerobic respiration [100]. Structurally, these proteins are divided in two domains. The N-terminal domain binds either a $[4\,Fe{-}4\,S]^{2+}$ or a $[2\,Fe{-}2\,S]^{2+}$ cluster through four cysteine residues [101] while the C-terminal region presents a DNA-binding helix-turn-helix (HTH) domain. Under anoxic conditions, monomeric FNR acquires $[4\,Fe{-}4\,S]^{2+}$ cluster dimerises and specifically bind to the FNR box present within the promoter of target genes [102]. Exposure to oxygen causes oxidation of the $[4\,Fe{-}4\,S]^{2+}$ cluster and the dissociation of the protein from the promoter.

Paracoccus denitrificans has three FNR paralogues that orchestrate the regulation of the expression of the denitrification genes [103, 104]: NarR is a nitrate sensor involved in the regulation of NO_3^- reductase (Nar). NnrR (nitrite and nitric oxide reductase regulator) is a heme-containing NO sensor that regulates the expression of nitrite (Nir), nitric oxide (Nor) and nitrous oxide reductases (Nos). FnrP is an O_2 sensor that regulates the transcription of N_2OR [105].

1.4.3.2 NosR and NosX

The presence of a *nosR* gene is characteristic of typical *nos* gene clusters [78] and in *P. denitrificans* is found adjacent to and upstream of *nosZ*. NosR is a membrane-bound polypeptide of 78 kDa that contains a large N-terminal flavin-binding domain that faces the periplasm. Within the C-terminal domain two CX_3CP motifs and a ferredoxin-like domain that binds two [4Fe:4S] clusters are found [106]. Zhang and co-workers showed recently that NosR can bind flavin *in vitro* and *in vivo* [107] and the presence of the two [4Fe-4S] clusters has been pro-

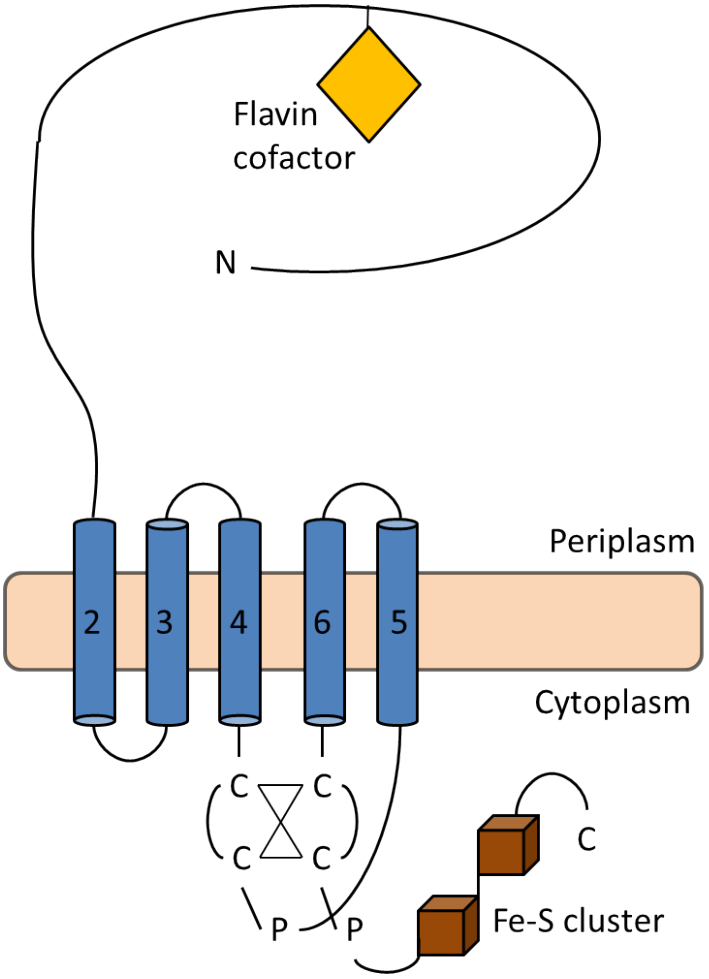

FIGURE 1.11: NosR topology model. The transmembrane helix 1 is cleaved upon membrane insertion and is not part of the mature protein. The predicted transmembrane core is composed of 5 helices. Helices 4 and 6 have been placed arbitrarily adjacent to emphasise a plausible interaction (X) of the CX_3CP motifs by a metal or –SH redox chemistry.

posed by Zumft *et al.* based on EPR and metal content analysis [79] (see figures 1.11 and 6.1). In addition, the cytoplasmic location of the C-terminal domain of NosR has been inferred from structural homology comparison of *E. coli* NapH [108]. The deletion of the cofactors binding residues of NosR resulted in the generation of holo N_2OR that showed altered spectroscopic and redox properties of the Cu_Z centre. N_2OR protein was catalytically active *in vitro* using an artificial electron donor despite the inability of the whole cells to reduce N_2O [106]. All together, these phenotypes point NosR as the likely electron donor for N_2OR *in vivo*. Moreover, NosR has been found to be required for the proper expression of *nosZDFY* in *P. stutzeri* [106, 109–111] and *P. denitrificans* [3] even though it is located in the membrane and lacks a DNA-binding motif. Alternatively, it has been proposed that this role could be accomplished through the interaction with other transcriptional factors such as DnrD [106].

The *nosX* gene is another ancillary gene of typical *nos* gene clusters, and when is present the gene is either heading or tailing the NGC. NosX is found among α-(e.g. *P. denitrificans*) and β-proteobacteria (e.g. *R. capsulatus*) although is absent in γ-proteobacteria. NosX is a 32 kDa flavoprotein exported to the periplasm through the Tat pathway. A redox role has been attributed based on Zhang and co-workers study where they observed the flavin transfer reaction from the NosX paralogue ApbE to NosR [107]. Moreover, *nosX* mutants lose whole-cell nitrous oxide reductase activity, but fully assembled N_2OR is still produced [112].

1.4.3.3 NasS-NasT

NasS-NasT is a two component regulatory system that controls the expression of the *nas* and *nos* gene clusters in response to extracellular NO_3^-/NO_2^- levels [113, 114]. NasTS are broadly distributed in Gramnegative bacteria. NasS is a cytosolic NO_3^-/NO_2^- sensor that contains a binding motif similar to the one described for NrtA, the periplasmic component of the NO_3^- and NO_2^- ABC-type uptake system of the cyanobacteria *Synechocystis sp.* PCC 6803 [115]. NasT contains an ANTAR (AmiR and NasR transcription antitermination regulator) domain and is predicted

to be a transcription anti-terminator [116]. Both proteins, form a complex that dissociates in the presence of micromolar levels NO_3^- [113, 117]. Sánchez and co-workers have recently identified a region within the *nosR* 5'-leader sequence that is involved in the termination of *nos* transcription. In the presence of nitrate, NasT interact with *nosR* mRNA and induces *nos* expression [114, 117].

1.4.3.4 Copper regulation

Denitrification is a highly copper demanding respiratory pathway [76, 118–120]. Depending on the organism, up to three copper containing proteins involved in this process can be identified: pseudoazurin (Paz), nitrite reductase (NirK) and nitrous oxide reductase (NosZ). Pseudoazurin contains a single Cu atom, NirK is a homotrimer with two copper atoms per monomer [121] and a functional N_2OR requires 12 copper atoms per homodimer. Although there are copper-independent alternatives for Paz and NirK, there is no recognised copper independent alternative for N_2OR for reducing N_2O to N_2.

Matsubara *et al.* pointed for the first time in 1982 that in *Pseudomonas perfectomarinus* the end product in a copper limited media during anaerobic respiration of NO_3^- was N_2O [76]. Thirty years later, Felgate and co-authors explored the effect of copper limitation in species with distinct Fe-dependent (i.e. *P. denitrificans*) and Cu-dependent (i.e. *Achromobacter xylosoxidans*) nitrite reductase enzymes [122]. The researchers found that under NO_3^- sufficient and copper depleted conditions *A. xylosoxidans* releases about 40% of NO_3^- consumed as NO_2^- while *P. denitrificans* releases a similar proportion as N_2O [122]. Furthermore, the biomass produced by *P. denitrificans* under both copper sufficient or depleted conditions remained fairly constant, but the N_2O emissions in copper limited conditions were more than a 1,000-times the rate of copper sufficient cultures. A year later Sullivan *et al.* provided the first experimental evidence of a genetic control of the *nos* genes based on extracellular copper levels [3]. In this transcriptomic study, the NGC of *P. denitrificans* was strongly downregulated under copper limiting conditions and this transcriptional control seemed to be mediated through NosC and NosR proteins. In

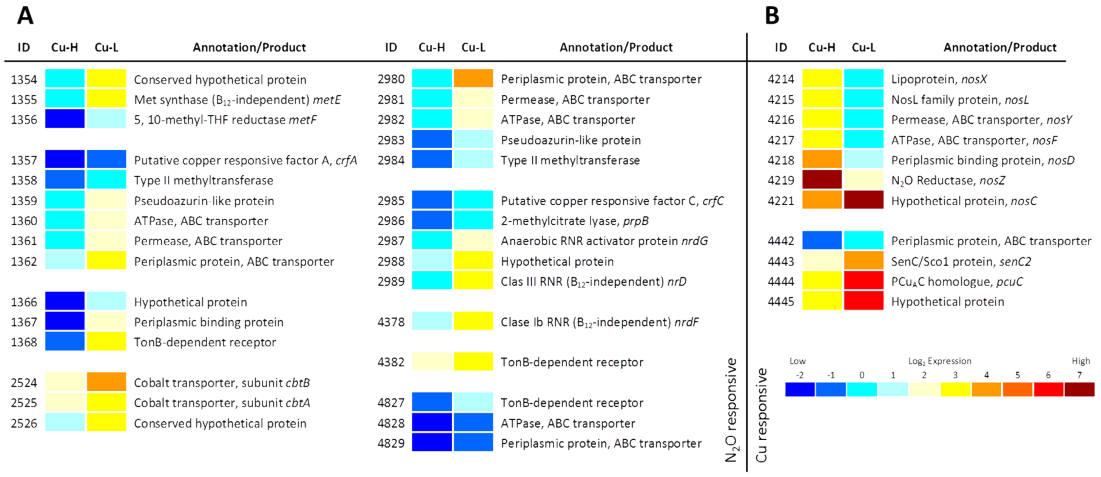

FIGURE 1.12: Heat map representing the gene expression profile of *P. denitrificans* PD1222 under copper sufficient and limited regimes. (A) Genes regulated by B_{12} riboswitches that are modulated by N_2O. (B) The Cu-responsive genes for N_2O reduction and Cu-metabolism. Colours ranging from blue to red indicate average $\log_2$ normalised expression values between three biological replicates. Data used to produce the figure was obtained from Sullivan *et al.* [3]

addition, the accumulation N_2O in copper deficient cultures induced the expression of vitamin B_{12}-independent genes controlled by vitamin B_{12} riboswitches [3].

1.5 Experimental Aims

Whether *P. denitrificans* uses O_2 or NO_3^- as a terminal electron acceptor during aerobic or anaerobic respiration, a high demand for acquiring Cu is imposed on the cells. Cytochrome *c* oxidases and nitrous oxide reductase require the transition metal as a redox active cofactor and they even share structural homology at their electron transfer Cu_A centre (see figure 1.3). However, almost all the current knowledge about the maturation process of this binuclear centre comes from the extensive study of prokaryotic and eukaryotic Cox [5, 32]. Whereas it is still debated and speculated how the Cu required for N_2OR activity is chaperoned around the cell and delivered to apo-N_2OR. A recent transcriptomic analysis from *P. denitrificans* by Sullivan and co-workers highlighted a putative *hypothetical-pcuC-ScoB* gene cluster as a candidate system that could function either inserting or maintaining Cu-centres of N_2OR [3]. Hence the purpose of this thesis has been

to systematically study the growth phenotypes of the deletion mutants of *scoB* and *pcuC* as well as their genetic complementations. In addition, recombinant ScoB and PCuC have been purified and characterised biochemically in order to prove copper binding to the proteins and to estimate the affinity of the binding events. We have also solved the crystallographic structure of the two domains that conform PCuC and identified the copper binding residues within the protein. In the last part of this study, we tried to explore the effect of *scoB* and *pcuC* deletion mutants on N_2OR Cu-centre assembly by isolating the terminal reductase from different genomic backgrounds.

2 Materials and Methods

2.1 Media and conditions for bacterial growth

Two different types of culture media were used in this thesis: a complete medium for cell propagation and a defined minimal salt medium for physiological studies. All culture media were prepared using water purified by reverse osmosis (RO, *Purelab Prima, ELGA*) and sterilised by autoclaving at 121 °C for 15 minutes before use.

2.1.1 Complete medium

A complete lysogeny broth (LB) medium essentially as described by Luria and Bertani [123, 124] was used in routine culture of the *Escherichia coli* and *Paracoccus denitrificans* PD1222 (a derivative of *P. denitrificans* DSM 413^T [125]) strains outlined in table 2.1. Although the original recipe has been modified over the years, the standard recipe used throughout this work is given below in table 2.2.

LB cultures of *E. coli* and *P. denitrificans* were routinely grown with agitation at 37 and 30 °C, respectively. Antibiotics were added to the media as outlined in table A.1 of the appendix. Solid media contained 1.5 % (w/v) of agar.

Bacteria	Characteristics	Source
Escherichia coli		
E. coli 803	*Met*$^-$; used as host for transformation with large plasmids	[126, 127]
E. coli JM101	Used as host for small plasmids	[128, 129]
P. denitrificans		[125]
PD1222 (PdWT)	Wild-type strain, rif^R, Spec^R	[3]
PD2304 (Pden 4445)	Non-polar str^R mutant of Pd1222, deficient in Pden 4445, rif^R	[3]
PD2305 (*pcuC*$^-$)	Non-polar str^R deletion mutant of Pd1222, deficient in *pcuC*$^-$, rif^R	[3]
PD2306 ($\Delta senC$)	Non-polar deletion mutant of Pd1222, deficient in $\Delta senC$, rif^R	[3]
PD2422 (gPdWT)	Non-polar insertion mutant of Pd1222, insertion of *nosZ* 3' StrepII sequence, rif^R	This study
PD2404 (*g4445*$^-$)	Non-polar insertion mutant of PD2304, insertion of *nosZ* 3' StrepII sequence, str^R, rif^R	This study
PD2405 (*gpcuC*$^-$)	Non-polar insertion mutant of PD2305, insertion of *nosZ* 3' StrepII sequence, str^R, rif^R	This study
PD2406 ($g\Delta senC$)	Non-polar insertion mutant of PD2306, insertion of *nosZ* 3' StrepII sequence, rif^R	This study

TABLE 2.1: Bacterial strains used

Chemical	g L^{-1}
Yeast extract	5
Tryptone	10
NaCl	10

TABLE 2.2: Constituents of complete lysogeny broth

2.1.2 Minimal medium

A defined minimal salts medium was used for the examination of microbial physiological traits and in the determination of growth requirements of *P. denitrificans* strains [130–132]. Minimal medium was prepared at pH 7.5 as standard containing the core components outlined below in Table 2.3. Here, succinate and ammonium were used as sole carbon and nitrogen sources respectively, while nitrate served as the respiratory electron acceptor during anaerobic growth. In addition to these core components, minimal medium was also supplemented with essential trace metals (each given at their final concentration) as outlined in table 2.4. The trace element supplement (also named Vishniac and Santer solution) was prepared as a 500-times stock solution and the pH was adjusted to 6.2 using KOH [131, 132]. For preparation of copper (Cu)-low minimal medium, the $CuSO_4$ salt was omitted from the standard trace elements solution recipe (see table 2.4).

Chemical	**M_w**	**mM**	**g L^{-1}**
Na_2HPO_4	141.96	29.0	4.12
KH_2PO_4	136.09	11.0	1.50
NH_4Cl	53.49	10.0	0.53
$MgSO_4$	246.48	0.4	0.10
$NaNO_3$	89.99	20.0	1.70
Succinate	270.14	30.0	8.10

TABLE 2.3: Core constituents of *Paracoccus denitrificans* defined mineral salts medium.

Compound	**M_w**	**μM**	**g L^{-1}**
EDTA	292.24	342.2	50.00
$ZnSO_4 \cdot 7H_2O$	287.55	15.3	2.20
$MnCl_2 \cdot 4H_2O$	197.91	51.1	5.06
$FeSO_4 \cdot 7H_2O$	278.01	35.9	4.99
$(NH_4)_6Mo_7O_{24} \cdot 4H_2O$	1235.9	1.8	1.10
$CuSO_4 \cdot 5H_2O$	249.68	12.6	1.57
$CoCl_2 \cdot 6H_2O$	237.93	13.5	1.61
$CaCl_2 \cdot 2H_2O$	147.02	99.8	7.34

TABLE 2.4: Constituents of the Vishniac and Santer trace elements solution.

The standard Vishniac and Santer solution (termed Cu-high, containing 13 μM $CuSO_4$) displays an intense green colour when freshly prepared that changes to

a deep purple colour over time. While, a freshly prepared Cu-low trace elements solution is of a pale orange-colour that ends up turning red. This colour change is indicative of a time-dependent oxidation process between transition metal salts of different oxidation states that equilibrate in air over time. Importantly, the equilibration of the trace metal solution can be accelerated by sparging solutions with compressed air or by adding small amounts of hydrogen peroxide. This process can also be followed using UV-visible electronic absorbance spectroscopy (Figure 2.1 A and B). Given that the bioavailability of individual trace metals may depend on their oxidation states, this was an important observation that may impact on the denitrification process and bacterial growth. A series of control experiments that when freshly-prepared solutions are used directly, the growth of *P. denitrificans* both aerobically and anaerobically can be significantly compromised (Figure 2.1 C and D). For the purpose of reproducibility of the results presented in this work and given that the work of Sullivan and co-workers [3] has shown that N_2O respiration is dependent on Cu-availability, fully oxidised Vishniac and Santer stock solutions were used. After preparing Vishniac and Santer solutions the UV-vis spectra of the solutions were checked periodically to ensure no further spectral changes were observed and that equilibrated "mature" stock solutions were ready to be stored at 4 °C and used in experiments after filter sterilise them. Here, growth and production of N_2O of PD1222 was consistent with previous studies (Figure 2.1), providing a solid platform for further comparative physiological studies presented in this work.

To ensure maximum aeration of cultures during aerobic growth experiments, bacterial strains were grown at 30 °C in 250 mL conical flasks containing 50 mL of autoclaved media and agitated at 200 rpm.

For anaerobic growth, *P. denitrificans* was cultured in batch using 500 mL Duran bottles filled with 400 mL of minimal salts media and sealed with screw-cap lids and gas-tight silicone septa. The cultures were incubated without agitation at 30 °C, allowing cells to consume residual oxygen present within the limited headspace and to transition from aerobic to anaerobic respiration. For inoculation, 8 OD-units (measured at 600 nm) of a stationary phase minimal medium pre-culture were added per vessel. Importantly, special care was taken when preparing culture ve-

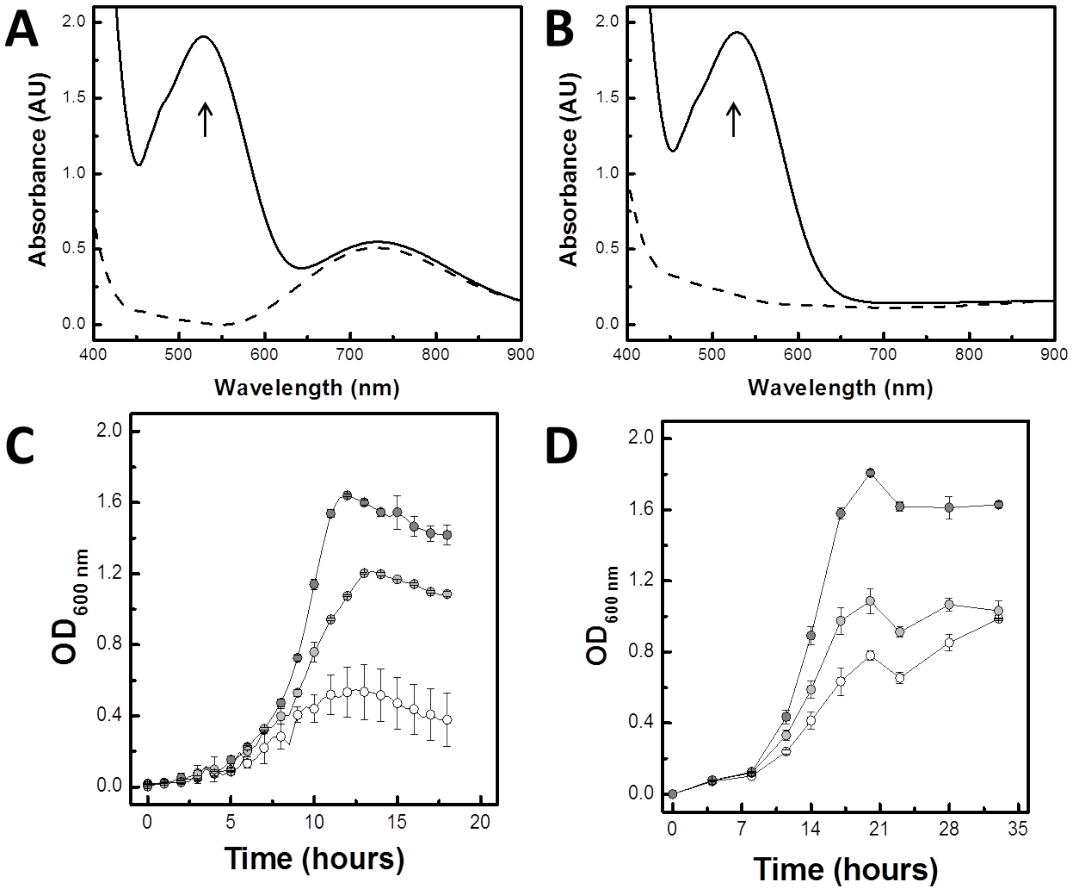

FIGURE 2.1: The impact of Vishniac and Santer trace element solution on bacterial growth. UV-vis spectra of a fresh (dash line) and oxidised (solid line) **(A)** Cu-high and **(B)** Cu-low solutions. **(C)** Aerobic and **(D)** anaerobic growth of *P. denitrificans* supplemented with Cu-H trace element solutions at three different stages of maturation: fully oxidised (•), intermediate state (◉) and freshly prepared (○).

ssels and all glassware was pre-washed thoroughly with 50 % (v/v) nitric acid followed by RO water to remove trace metal contaminants.

2.2 Analytical Methods

2.2.1 Measurement of nitrate and nitrite in cultures

Nitrite and nitrate levels from anaerobic batch cultures were quantified by ion chromatography using a Dionex ICS-5000 instrument with suppressed conductivity detection (*Thermo Scientific*). The following set-up was used for the analysis: Dionex Ion Pac^{TM} AG18 guard column (50 mm x 2 mm); Dionex Ion Pac^{TM} AS18 analytical column (250 mm x 2 mm); column oven temperature 30 °C; gradient elution with KOH from 12 to 34 mM and a flow rate 0.25 mL min^{-1}. Media samples were diluted 400 times in analytical grade water, filtered and loaded onto the column using an autosampler (injection volume: 10 μL). The instrument was calibrated using a range of five mixed $NaNO_2$ and $NaNO_3$ standards (see figure 2.2 A). The data were processed using Chromeleon software 6.8 (*Thermo Scientific*).

2.2.2 Measurement of nitrous oxide in cultures

Nitrous oxide levels in anaerobic batch cultures were determined by sampling the head space gas (220 mL) of sealed Duran culture bottles. For each time point, a 3 mL gas sample was recovered using a 5-mL gas-tight syringe (*Hamilton*). Over the course of the experiments less than 5 % of the head space was removed for analysis of each technical replicate.

Gas samples were transferred and stored in pre-evacuated screw cap vials (*Labco Exetainer*) prior to analysis on a Clarus 500 Gas Chromatograph (*Perkin Elmer*). Head space gases were separated using an Elite-Q PLOT Phase Column (length: 30 m, inner Diameter: 0.53 mm) and detected with a ^{63}Ni Electron Capture Detector (ECD). The carrier and auxiliary gases used were supplied by BOC (UK)

an consisted of zero-grade N_2 (*BOC*) and a 95% (v/v) argon/5% (v/v) methane mixture, respectively. A sample volume of 50 μL was manually injected onto the column using a 250 μL gas-tight syringe (*Hamilton*). The following instrument parameters were used for N_2O detection: carrier gas flow, 60 psi; auxiliary gas flow, 58 psi; injector temperature, 115 °C; column temperature, 90 °C and ECD temperature, 350 °C. This configuration gave a retention time for N_2O of 5.2 min.

In order to prevent column and detector saturation and to generate sharp defined peaks suitable for analysis, a 20 or 95 sample split was used (with 6, 5 and 3 attenuation) depending on the sample concentration. The instrument was calibrated for each method using a set (see figure 2.2 B) of pre-made N_2O standards (*Scientific and Technical Gases*). The total amount of N_2O was calculated using a Henry's Law constant for N_2O (at 30 °C) of $K_H^{cc} = 0.5392$ [3].

2.2.3 Analysis of metal content in protein samples

Trace element analysis of protein solutions was determined by inductively coupled plasma atomic emission spectroscopy (ICP-AES) using a Vista Pro ICP (*Varian*) equipped with a Helix spray chamber, glass expansion concentric nebuliser, and a SPS-5 auto sampler. All standards and samples were measured in triplicate, and the RSDs in most cases were lower than 2 %. Samples were prepared by addition of 100 μL of 21.7 % HNO_3 to 100 μL of protein sample (0 - 200 μM) and the mixture was incubated at 95 °C for 30 min. Samples were cooled to room temperature and volume adjusted to 3 mL with analytical grade water.

2.2.4 Determination of protein concentration

Protein concentration was determined using the Bradford colorimetric method [133], which is based on the binding of an acidic dye to the basic and aromatic amino acid residues (particularly arginine) of a protein solution. A standard curve of known concentrations of bovine serum albumin (*Sigma*) was used to obtain relative measurement of protein concentrations (see figure 2.2 C).

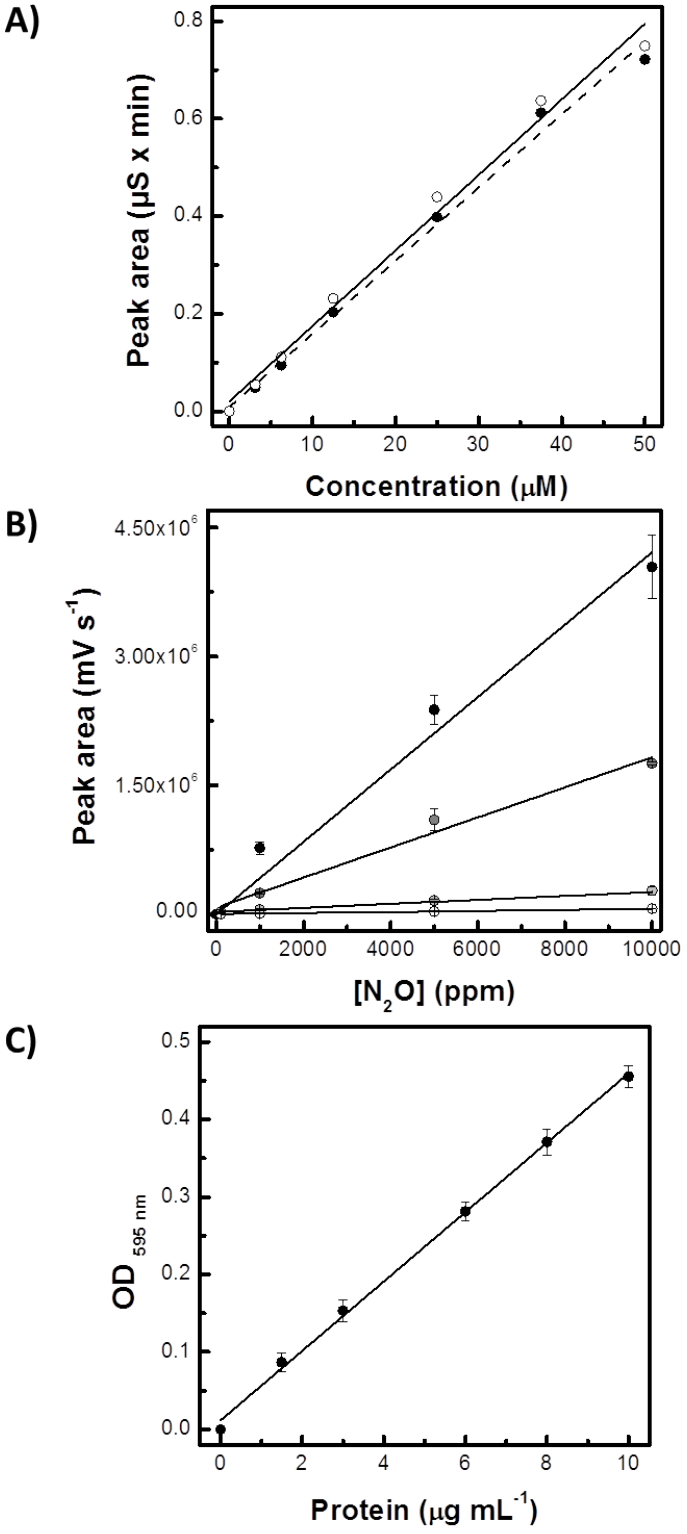

FIGURE 2.2: Representative standard curves. **(A)** $NaNO_2$ and $NaNO_3$ analysis of culture samples. Solid and dash lines represent fits for $NaNO_2$ and $NaNO_3$, respectively. **(B)** N_2O analysis of culture samples. Data was recorded using the following instruments parameters: 20 sample spit (•), 95 sample spit with 6 (◉), 5 (◉) and 3 (○) attenuation correction. **(C)** Determination of protein concentration with bovine serum albumin

Typically the reaction mixture would consist of 200 μL of Protein Assay Dye Reagent (*BioRad*), the protein sample to be analysed and water to make up to 1 mL. Then, the reactions were incubated 5 min. at room temperature and the absorbance values were measured at 595 nm.

2.2.5 Enzymatic assay for nitrous oxide reductase activity

The enzymatic activity of isolated nitrous oxide reductase (N_2OR) was assayed *in vitro* using reduced methyl viologen as an artificial electron donor according to Kristjansson *et al.* [87]. All the reagents and material used were thoroughly degassed and left to equilibrate for 24 hours in the glove box prior to the experiment.

Stocks of 100 mM methyl viologen and 97 mM sodium dithionite were routinely prepared. A concentrated N_2O solution was prepared by aliquoting 1 mL of the reaction buffer (20 mM HEPES, 150 mM NaCl pH 7.5) into a 50 mL GC air tight glass vial. Then, the flask was flushed for 5 minutes with N_2O (*BOC*) and the overpressure was released and equilibrated to atmospheric pressure using a simple airlock (made up with a needle and a syringe, without the plunger, filled with water).

The protein was incubated for five minutes in 3 mL plastic cuvettes containing 10 – 15 μL of methyl viologen, 2 – 5 μL sodium dithionite and the reaction buffer. Once the sample had been equilibrated the spectrophotometer was set up in time-resolved mode at 600 nm. The absorbance of the cuvette was measured for a few seconds in order to acquire a stable baseline before adding N_2O solution using a 50 μL gas-tight syringe (*Hamilton*).

2.3 Preparation of nucleic acids

2.3.1 Isolation of genomic DNA

Genomic DNA from bacteria was performed using the Wizard Genomic DNA Purification Kit (*Promega*). This method is based on a four-step process: cell lysis, RNase digestion, protein precipitation and genomic DNA concentration and elution. Purified gDNA is suitable for PCR, digestion with restriction endonucleases and membrane hybridizations (e.g., Southern and dot/slot blots).

The cells of a 5 mL overnight culture were typically used and the DNA was generally resuspended in 100 μL of H_2O overnight at 4 °C.

2.3.2 Preparation of plasmid DNA

The isolation of plasmid DNA (up to 20 μg) was routinely performed using a Spin Miniprep Kit (*QIAGEN*). This kit is based on alkaline lysis of bacterial cells followed by adsorption of DNA onto a silica membrane in the presence of high salt. Typically plasmid DNA was extracted from 3 mL of an overnight culture of *E. coli* and centrifugation steps were performed in a 5424 microcentrifuge (*Eppendorf*). The DNA was eluted with DNase and RNase free water (*Sigma*) after incubating the column for 5 - 10 min before elution. Concentration and quality of DNA was measured at 260 and 280 nm using a nanodrop 2000 UV-Vis Spectrophotometer (*Thermo Scientific*).

2.3.3 Restriction enzyme digestion

Restriction enzymes were purchased from New England Biolabs (*NEB*). NEB restriction digestions are carried out using SmartCut reaction buffer for all their enzymes, therefore simplifying multiple digestion reactions. A typical reaction contained 1 μg of plasmid DNA and was incubated for at least 15 min at 37°C.

Component	Reaction
Restriction enzyme	1 μL (10 units)
Plasmid DNA	1 μg
NEB CutSmart Buffer 10X	5 μL
Water	to 50 μL

TABLE 2.5: Standard restriction digestion reaction

2.3.4 Ligation of DNA fragments

DNA inserts were ligated into the desired vector using a commercial T4 DNA ligase from New England Biolabs (*NEB*) in a 20 μL reaction at 16 °C overnight. This enzyme catalyses the formation of a phosphodiester bond of both blunt and cohesive ends of DNA. Typically, 50 ng of vector were used per reaction and up to three molar ratio (1:1, 1:3, 1:5) of plasmid to insert were tested using equation 2.1. A representative ligation reaction can be found in table 2.6.

$$\frac{Kb\ insert}{Kb\ vector} x\ ng\ of\ vector\ x\ molar\ ratio\ of\ \frac{insert}{vector} = ng\ of\ insert \tag{2.1}$$

Component	Reaction
T4 DNA Ligase Buffer (10x)	2 μL
Vector DNA	1 (50 ng)
Insert DNA	x ng
T4 DNA Ligase	1 μL
Water	to 20 μL

TABLE 2.6: T4 DNA ligation standard recipe, where x is given by equation 2.1. The water used was molecular biology reagent

2.3.5 Agarose gel electrophoresis

DNA gel electrophoresis was routinely performed using 1 % (w/v) agarose dissolved in TAE buffer (45 mM Tris-acetate, 1 mM EDTA, pH 8) made from a 50-times stock solution (*ForMedium*^{TM}) and supplemented with 2 μM ethidium bromide (*Sigma-Aldrich*) to stain the DNA. The agarose gel was then placed in a electrophoresis tank and submerged in TAE buffer solution. DNA samples pre-mixed with GelPilot

DNA Loading Dye 5-times (*QIAGEN*) were loaded into the gel together with a 1 kb hyperladder (*BioLine*) as a DNA molecular weight standards. Typically, an electric current of 120 mA was applied during 30 to 60 min and gels were latter on imaged using a Gel Doc XR UV-transilluminator (*BioRad*).

2.3.6 Recovery of DNA from agarose gels

DNA was extracted and purified from agarose gels using a QIAquick gel extraction kit (*QIAGEN*). This kit allows the recovery of DNA fragments from 70 bp to 10 kb that are suitable for subsequent molecular biology applications.

Experiments were performed essentially as stated in the manufacturer's instructions with special care of not exceeding the 400 mg limit of agarose per spin column and to add the colorimetric pH indicator of the QG buffer provided with the kit. This buffer should remain yellow or the DNA recovery would be drastically reduced, if necessary a small amount of sodium acetate was added to the reaction in order to lower the pH of the sample. The purified DNA was eluted in 50 μL of nuclease free water (*Sigma*).

2.3.7 DNA sequencing

Sequencing of plasmid DNA and purified PCR products was carried out by MWG Eurofins Genomics (Ebersberg, Germany). Plasmid DNA was provided at a concentration of 50 - 100 ng μL^{-1} while purified PCR products were provided at a concentration of 2 - 10 ng μL^{-1} alongside with 150 pmol of the relevant primers.

2.4 Amplification of DNA using the polymerase chain reaction (PCR)

2.4.1 Oligonucleotide design

DNA oligonucleotides were designed using Primer 3 Plus, FastPCR (*PrimerDigital*) and Artemis Genome Browser (*Sanger*) software [134–136] and ordered from MWG Eurofins Genomic (Ebersberg, Germany). The list of primers used for this thesis can be found in table 2.7.

For each oligonucleotide, an optimal length of 18-22 bases, a GC content below 60% and a melting temperature (T_m) of 60 °C was generally sought during primer design. Primer modifications such as phosphate groups or restriction sites were added to the 5' end of the primers, including on occasions several extra bases upstream the restriction sites in order to facilitate optimal cutting efficiency.

Name	Sequence	Use
pLMB509_F1	tgccagggtcgaccaactga	pMSL001
pLMB509_R1	tcagttggtcgaccctggca	
PCuC_NdeI_F1	aacatatgagaacgatcatgcagaacc	pMSL003
PCuC_XmaI_R1	aacccggggtgcccgccatggccatctcc	
$PCuC_{Nt}$_F1	cacggccatggccatggcgat	pMSL005
$PCuC_{Nt}$_R1	ggccggggcctctgaccgctc	
$PCuC_{Ct}$_F1	ggcgcgcaaaaaggagat	pMSL006
$PCuC_{Ct}$_R1	atcgccatggccatggccgtg	
scoB_NdeI_F1	aacatatgatggcgggcactgaacgcaaatc	pMSL007
scoB_NdeI_R1	aaggatccatggcgggcactgaacgcaaatc	
scoB_XmaI_R1	aacccggggctgctcagcaggcggcgcaggctggcca	pMSL008
nosZ3fln_F1	aactgcagcctcgatcctgtccgacatc	pMSL002
nosZ3fln_R1	aatctagaggcatcgagatccttgttcg	
nosZ_StrepII_F1	caatttgaaaaatgagtcccatgcgca	pMSL002
nosZ_StrepII_R1	ggggtggctccaggcctccttcggctc	

Table 2.7: Primers used

2.4.2 PCR of DNA using High-Fidelity Phusion Polymerase

The amplification of DNA fragments intended for cloning applications was performed using Phusion High-Fidelity DNA polymerase (*Thermo Scientific*). This polymerase is highly accurate due to its 3' → 5' exonuclease activity, it generates blunt end products and is suitable for amplifying long amplicons. The ligation of the PCR fragments generated has to be preceded by a phosphorylation event unless 5' phosphorylated primers are used.

PCR reactions were prepared in a 50 µl final volume according to the recipe presented in table 2.8 and performed using a thermocycler (*Techne*) adapting the PCR cycle protocol of table 2.9 to the T_m of the primers used.

2.4.3 Diagnostic PCR of DNA using *Taq* DNA polymerase

Routine PCR of DNA was carried out using MyTaq DNA polymerase (*BioLine*). The reaction buffer of this product contains all the reagents (dNTPs, $MgCl_2$, DNA polymerase, etc.) necessary for the PCR reaction reducing the number of pipetting steps and allowing a fast and efficient PCR.

PCR reactions were prepared in a 20 µl final volume according to the recipe presented in table 2.10 and performed using a thermocycler (*Techne*) adapting the PCR cycle protocol of table 2.11 to the T_m of the primers used.

2.4.4 Colony PCR

Colony PCR is a fast and conventional method employed to examine the genotype of a bacterial strain. This methods has the advantage of eliminating the need to grow colonies in liquid culture and isolate its genomic or plasmid DNA. However, cell content and media compounds may cause inhibition of the PCR reaction.

Usually, 5 - 10 colonies were picked from an LB-agar plate, resuspended in 20 µl of molecular-grade water (*Sigma*), incubated at 100 °C for 5 - 10 min and then let to

Component	**Reaction (µl)**
5 x Phusion HF Buffer	10.0
Forward primer (20 µM)	5.0
Reverse primer (20 µM)	5.0
dNTPs (10 mM)	5.0
Template (100 ng/µl)	1.0
Phusion DNA polymerase	0.5
Water	to 50.0

TABLE 2.8: High-Fidelity Phusion polymerase PCR reaction recipe. The water used was molecular biology reagent

Cycle step	**Temperature (°C)**	**Time (s)**	**Cycles**
Initial denaturation	98	60	1
Denaturation	98	5 - 10	
Annealing	45 - 72	10 - 30	35
Extension	72	15 - 30	
Final extension	72	600	1

TABLE 2.9: High-Fidelity Phusion polymerase cycling instructions

Component	**Reaction (µl)**
MyTaq Mix (2x)	10.0
Forward primer (20 µM)	0.4
Reverse primer (20 µM)	0.4
Template	1.0
Water	to 20

TABLE 2.10: MyTaq DNA polymerase PCR reaction recipe. The water used was molecular biology reagent

Cycle step	**Temperature (°C)**	**Time (s)**	**Cycles**
Initial denaturation	95	60	1
Denaturation	95	15	
Annealing	45 - 72	15	35
Extension	72	10	
Final extension	72	600	1

TABLE 2.11: MyTaq DNA polymerase cycling instructions

cool on ice. Then, the suspension was spun down at maximum speed for 1 min and 1 µl of the supernatant was used as a template for the reaction shown in table 2.10. The presence or absence of PCR amplicons and size of the products can be determined by electrophoresis on an agarose gel.

2.4.5 Purification of DNA PCR products

PCR products required for cloning and sequencing were purified using QIAquick PCR purification kit (*QIAGEN*). This protocol is based on a similar principle as the Miniprep kit used for isolation of plasmid DNA previously described, where the DNA binds to a silica membrane in the presence of high salt concentrations. This kit was favoured when a single PCR product was observed on an agarose gel in order to remove excess of primers that could affect downstream applications. Protocol was carried out according to manufacturer's instructions using a 5424 microcentrifuge (*Eppendorf*) and DNA was eluted in 50 μL water (*Sigma*).

2.5 Transformation of *E. coli* with plasmid DNA

2.5.1 Preparation of competent cells

Chemically competent cells were routinely prepared using a modification of the $CaCl_2$ protocol from Cohen *et al.* [137]. To that end, a 50 mL LB culture of the desired *E. coli* strain at early exponential phase was prepared ($OD_{600} = 0.4 - 0.6$). The cells were harvested by centrifugation at 6,000 rcf for 10 min at 4 °C, resuspended in 15 mL of sterile 0.1 M $CaCl_2$ and incubated at 4°C for 30 min. Next, the cells were collected again by centrifugation, resuspend in 2 mL 0.1 M $CaCl_2$ and incubate at 4°C for another 2 hours. The competence of the cells can be increased by storing them at 4°C overnight before transformation. After this, the cells were ready to transform.

2.5.2 Transformation of competent cells

E. coli strains WA803 [126, 127] and JM101 [128, 129] were routinely used to prepare competent cells and used in cloning applications. These strains have a high tolerance for cytosine methylation, are optimal host for M13mp vectors and show a high transformation efficiency.

Normally, 200 μL of $CaCl_2$-competent cells were transferred to a sterile pre-chilled tube were the DNA (no more than 50 ng in a volume of 10 μL or less) was added. The content was carefully mixed by swirling and stored on ice for 30 minutes. After this, the tubes were transferred to a rack, placed in a preheated 42 °C water bath and incubated for 2 minutes without agitation. Then, the samples were quickly transferred to an ice bath where they were allowed to chill for 1-2 minutes. Next, 500 μL of LB medium was added to each tube and the cultures were incubated for 45-60 minutes at 37 °C to allow the bacteria to recover and to express the antibiotic resistance marker encoded by the plasmid. Finally, the cells were recovered by centrifugation (2 min at 6,000 rcf) and plated onto an agar LB medium containing the appropriate antibiotic.

2.6 *in vivo* genetic manipulations

Plasmids not self-transmissible were mobilised from *E. coli* strains (donor) to *P. denitrificans* (recipient) by tri-parental matings with *E. coli* containing the plasmid pRK2013 (helper) [138].

2.6.1 Conjugation via patch crosses

This method [139] was mainly used for the transmission of plasmids with a high efficiency such as in the case of protein expression plasmids. A loopful of each strain (donor, helper and recipient) was deposited in a LB-agar plate without antibiotics, mixed and incubated overnight at 30 °C. Then, single colonies of transconjugants

of *P. denitrificans* were selected by streaking some of the cells, from the conjugation plate, into a LB-agar plate with spectinomycin plus the corresponding antibiotic of the transferred vector.

2.6.2 Conjugation via filter crosses

When the selection of a rare event is required, such as in the generation of mutants, filter crosses were used [140]. For this purpose, three 50 mL LB cultures were prepared: one in stationary phase of the recipient strain and two in early exponential phase of the donor and helper strains ($OD_{600} \sim 0.6$). The cells were then harvested by centrifugation (10 min at 6,000 rcf and 4 °C) and resuspended all together in 1 mL of 50 % (v/v) glycerol. Next, the mixture was pipetted on top of a filter (*Whatman*), that was previously placed on a solid LB-agar plate without antibiotics, and let to dry close to the flame until the plate could be safely moved without causing spillages. After two days of incubation at 30 °C, the cells were recovered in 1 mL of 50 % (v/v) glycerol, which was then used to prepare serial dilutions. A volume of 50 µL of each sample was plated on a LB-agar plate with the appropriate antibiotics and incubated at 30 °C until single colonies of *P. denitrificans* could be identified.

2.7 Polyacrylamide gel electrophoresis

2.7.1 Resolution of proteins by SDS-PAGE

Protein samples were assessed by polyacrylamide gel electrophoresis (PAGE) under denaturing conditions [141] and using a discontinuous system [142] in order to produce high resolution and optimal band definition. Standard SDS-PAGE gels were produced according to the recipe shown in table 2.12 below.

Protein samples were prepared by mixing them with 0.2 volumes of a five times concentrated sample buffer (300 mM Tris-Cl pH 6.8, 10 % SDS, 50 % glycerol,

25 % β-mercaptoethanol, 0.05 % bromophenol blue) and boiled at 95 °C for 5 minutes. Then, they were left to cool on ice and briefly spun down before loading into the gel. Typically, 5 μL of Precision Plus Protein^{TM} Prestained Standard (*BioRad*) were used as a marker per gel. The electrophoresis was performed, using a Mini-protean II electrophoresis system (*BioRad*) filled with running buffer (25 mM Tris-Cl, 192 mM glycine, 0.1 % SDS (w/v)), at constant current of 30 mA for approximately 1 hour at room temperature. Once the electrophoresis had finished, gels were submerged in InstantBlue Coomassie stain solution (*Expedeon*) and left to incubate in a rocket platform for 30 mins.

Component	**Separating Gel**	**Stacking Gel**
Polyacrylamide	15 % (v/v)	4 % (v/v)
Tris-Cl pH 8.8	375 mM	-
Tris-Cl pH 6.8	-	125 mM
SDS	0.1 (w/v)	0.1 (w/v)
Ammonium persulphate	0.05 (w/v)	0.05 (w/v)
Tetramethylethylenediamine (TEMED)	0.03 (v/v)	0.03 (v/v)

TABLE 2.12: Composition of a standard 15 % SDS-PAGE gel

2.7.2 Western-Blot analysis

Western-Blot (WB) was performed routinely as a diagnostic test for the identification of recombinant proteins. A Trans-Blot SD Semi-Dry Electrophoretic Transfer Cell (*BioRad*) in combination with a three buffer system [143, 144] was used to transfer proteins from SDS-PAGE gels to polyvinylidene difluoride (PVDF) membranes (Amersham Hybond^{TM}-P, *GE Healthcare*).

The three buffer system mentioned above comprises a cathode 1 (C1) solution and two anode buffers (A1 and A2). Buffer C1 (25 mM Tris, 40 mM ε-aminocaproic acid pH 9.4) contains ε-aminocaproic acid which acts as a trailing ion which migrates through the gel from the cathode towards the anode. Buffer A1 (0.3 M Tris pH 10.4) is used to neutralise the excess of protons generated on the surface of the anode plate. Buffer A2 is composed of 25 mM Tris pH 10.4. The solutions were supplemented with methanol to a final 20 % (v/v) concentration, this helps to stabilise the dimensions of the gel and to remove complexed SDS from polypeptides.

Western-blots were initiated by incubating an SDS-PAGE gel in a clean tank containing buffer C1 for 15 minutes. In the meantime, three pieces of blotting paper (*Fisher Scientific*) were soaked in buffer A1, three in buffer A2 and six in solution C1. Also, the PVDF membrane was activated by immersing it in methanol for 15 seconds (a colour change in the membrane should be perceived which turned from opaque to semitransparent). Next, the membrane was carefully transferred into a tank with analytical grade water in order to remove methanol excess and then was placed into a tank with buffer A2 where it was left to equilibrate for at least 5 minutes. Once the 15 minutes had elapsed, the three segments of blotting paper previously soaked in A1 were placed in the centre of the anode electrode plate, followed by the three segments of blotting papers soaked in A2. In order to ensure an even transfer, air bubbles between layers of blotting paper were removed by carefully rolling a pipette tip between each layer in the stack. Then, the membrane was laid on top of the soaked papers followed by the SDS-PAGE gel and the six segments of blotting paper soaked in C1.

The transfers were set at a constant current of 60 mA for approximately 45 minutes and once it had finished, the membrane was incubated in a clean tank containing 20 mL of blocking solution (5 % (w/v) skimmed milk powder in PBS: 137 mM NaCl, 2.7 mM KCl, 10 mM Na_2HPO_4, 1.8 mM KH_2PO_4) for at least 60 minutes at room temperature. After this incubation period, Monoclonal Anti-polyHistidine-Peroxidase Antibody (*Sigma*) was added to the blocking solution to a working dilution of 1:20,000 and incubated overnight at 4 °C. Recombinant strepII tag proteins were incubated with Monoclonal Anti-StrepII-Peroxidase Antibody (*IBA*) in PBS (therefore the blocking solution had to be thoroughly washed before addition of the antibody) at a working dilution of 1:10,000. The next day, the membrane was washed three times with PBS-T (PBS with 0.05 % (v/v) TWEEN20) for 10 minutes and once with PBS for another 10 minutes. The chemiluminescent reaction was initiated by addition of SuperSignal West Pico Chemiluminescent Substrate solution (*Thermo Scientific*) to the membrane which was then incubated in the dark for 5 minutes. Western-blot images were recorded using a LAS-3000 gel imager (*Fujifilm*).

2.8 Mass Spectrometry of proteins

The proteins of interests were identified by peptide mass fingerpinting after trypsin digestion on a Bruker Autoflex Speed Maldi-TOF/TOF at John Innes Centre Proteomics Facility (Norwich Research Park). Prior to sample submission, gel slices had to be destained with 30 % (v/v) ethanol and reduced with 10 mM dithiothreitol (DTT). Then, free cysteines were alkylated with 30 mM iodoacetamide (IAA) which reacts with free sulfhydryl groups of cysteine residues irreversibly and cannot be reoxidised to form disulfide bonds (this step is important for allowing trypsin maximum digestion of the protein). Finally, samples were dehydrated using acetonitrile and delivered to John Innes Centre Proteomics Facility where they were digested with trypsin.

Raw data was extracted with BioWorks (*Thermo Fisher Scientific Inc*) and the resulting peak list was used for a database search using an in-house Mascot 2.4 server (*Matrix Science*) on all bacterial sequences of the UniProt Swiss-Prot/TrEMBL database (release 20170418). The searches were performed with a peptide tolerance of 5 ppm and a fragment tolerance of 0.6 Da. Iodoacetamide derivative of cysteine was selected as a fixed modification, oxidation of methionine as variable, and trypsin as the protease used (with up to three missed cleavages allowed).

Protein	**Significance Score**	**Sequence Coverage (%)**	**Expect Value**
$PCuC_{WT}$	143	61	2.4 x 10^{-11}
$PCuC_{FL}$-6His	146	64	1.2 x 10^{-11}
$PCuC_{Nt}$-6His	66	56	3.7 x 10^{-05}
$PCuC_{Ct}$-6His	43	32	1.2 x 10^{-02}
$ScoB_{sol}$-6His	52	16	2.2 x 10^{-02}
NosZ-SII	117	17	9.4 x 10^{-09}

TABLE 2.13: Peptide mass fingerprinting results and mascot scores (values greater than 49 were considered to be significant ($p < 0.05$).)

2.9 Protein structure prediction

The Phyre2 web server (http://www.sbg.bio.ic.ac.uk/phyre2) in intensive mode was used to predict the tertiary structure of $ScoB_{sol}$ (Pden_4443) [145]. Phyre2 uses the alignment of hidden Markov models for homology-based protein modelling and incorporates the *ab initio* folding simulation to model regions with no detectable homology to known structures. The predicted protein structure was visualised using the software Pymol [146].

2.10 Synthesis of pLMB510 and pLMB511 plasmid vectors

The taurine inducible expression vector for *Alphaproteobacteria* pLMB509 [147] (Figure 2.3 A) allows high-throughput cloning and expression of His-tagged proteins for purification. However, it presents certain limitations, such as a single NdeI restriction site for cloning procedures and it is only adequate for the expression of C-terminally His-tagged proteins. Therefore, two different derivatives of pLMB509 named pLMB510 and pLMB511 were generated (see figure 2.3 A and B). Both plasmid have a new multicloning site (NdeI, BamHI, XmaI and EcoRI) and are suitable for the expression of Factor X cleavable N-terminally tagged proteins or enterokinase cleavable C-terminally tagged proteins. The main difference between these two vectors is that pLMB510 contains 6His as affinity tag while pLMB511 codes instead a StrepII tag.

The generation process of pLMB510 and pLMB511 required the removal by inverse PCR of the EcoRI site located in position 1107 bps in pLMB509 that precedes the T1 terminator. Then the PCR product was digested with DpnI (*NEB*), PCR purified (*QIAGEN*) and the DNA was phosphorilated (*NEB*), religated (*NEB*) and transformed into *E. coli* 803. Afterwards, the resultant plasmid was digested with NdeI and EcoRI (*NEB*) in order to remove the fragment ranging from base 170

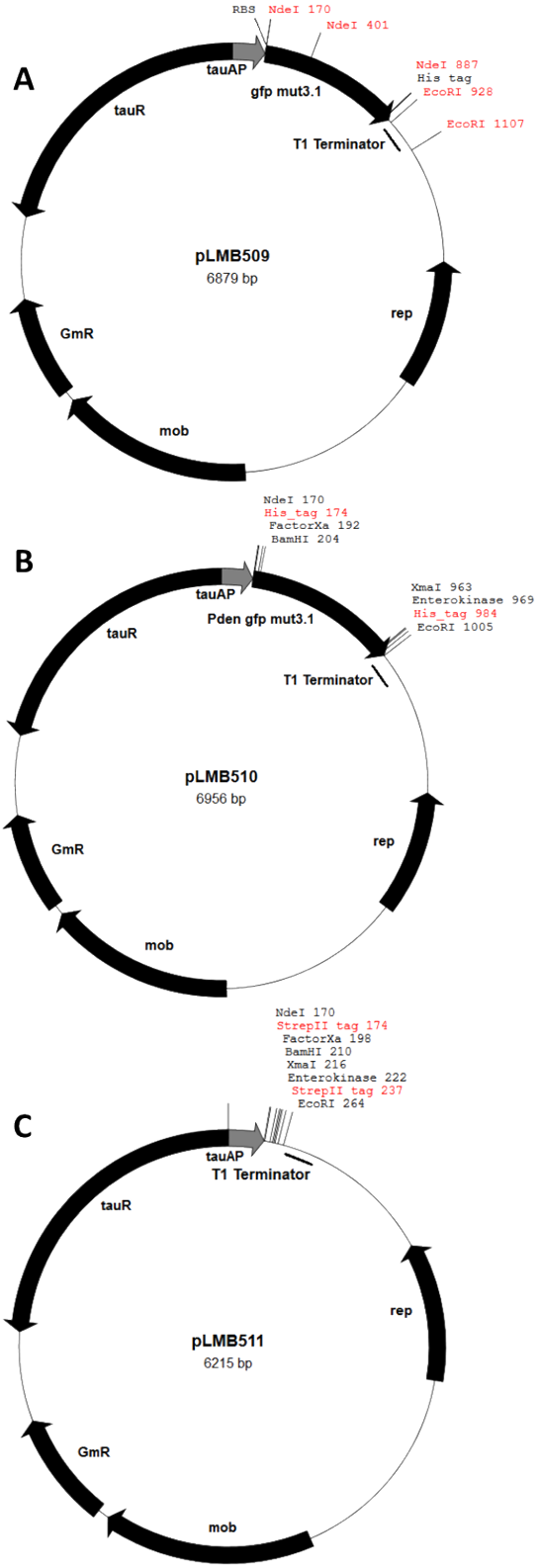

FIGURE 2.3: The taurine inducible expression vectors for *Alphaproteobacteria*. **(A)** pLMB509: C-terminal His-tagged proteins. **(B)** pLMB510: cleavable N- or C-terminal His-tagged proteins. **(C)** pLMB511: cleavable N- or C-terminal StrepII-tagged proteins [148]

to 928. Vectors pLMB510 and pLMB511 were produced by cloning the NdeI - EcoRI fragments derived from the synthetic constructs supplied by GenScript (see appendix section A.2).

2.11 Construction of knock-in mutants

Unmarked insertion mutants were generated in *P. denitrificans* using the mobilizable multi-purpose cloning vector pK18*mobsacB* (Figure 2.4 and table 2.14) [149]. A fragments of ∼1 kbp flaking the stop codon of *nosZ* was amplified by PCR (see figure 2.5 A), using a pair of primers containing PstI and XbaI restriction sites (see appendix table 2.7), and cloned into pJET1.2 (*Thermo Scientific*). Then, a StrepII tag sequence was introduced upstream the stop codon of *nosZ* by inverse PCR using phosphorylated primers (see figure 2.5 B). The PCR product was then DpnI (*NEB*) digested, religated and transformed into *E. coli* 803. Next, the resultant plasmid was digested using PstI and XbaI and the digestion fragment was cloned into pK18*mobsacB*.

The plasmid pK18*mobsacB* containing the StrepII flaking region of *nosZ* (from now on pMSL01) was then conjugated into wild-type *P. denitrificans* (PD1222), *Pden_4445*$^{-}$ (PD2304), *pcuC*$^{-}$ (PD2305) and Δ*scoB* (PD2306) by triparental mating using the filter cross technique as described above.

The basic principle of generating mutants using this system is that pK18*mobsacB* is not replicative in *P. denitrificans*. Therefore, under the presence of a selective pressure, such as the addition of kanamycin to the media, the only way the bacteria can survive is by undergoing an homologous recombination event. As a result, the whole plasmid is integrated in the chromosome at the location of the cloned flanking regions (see figure 2.5 C). Single cross over recombination events were initially selected by plating the cells from the conjugation into LB with spectinomycin and kanamycin and identified by colony PCR (using universal M13 primers targeting the multicloning site of pK18*mobsacb*).

Plasmid	**Characteristics**	**Source**
pRK2013	Used as mobilizing plasmid in triparental crosses, kan^R	[138]
pK18*mobsacB*	Allelic exchange suicide plasmid, sucrose-sensitive, *mob*$^+$, kan^R	[149]
pJET1.2	Eco47IR, cloning vector, Amp^R	*Thermo Scientific*
pUC57	*lacZ*, cloning vector, Amp^R	*GenScript*
pLMB509	expression plasmid, *tauP*, *mob*$^+$, gen^R	[147]
pLMB510	pLMB509-derivative, EcoRI (1107 bps) deficient, expression plasmid of his tagged proteins, *tauP*, *mob*$^+$, gen^R	This study
pLMB511	pLMB509-derivative, EcoRI (1107 bps) deficient, expression plasmid of strepII tagged proteins, *tauP*, *mob*$^+$, gen^R	This study
pMSL001	pLMB509-derivative, EcoRI (1107 bps) deficient, expression plasmid, *tauP*, *mob*$^+$, gen^R	This study
pMSL002	pK18mobsacB derivative, construct for *nosZ* StrepII sequence insertion, kan^R	This study
pMSL003	pLMB509-derivative, expression construct for $PCuC_{FL}$-6His, gen^R	This study
pMSL004	pLMB510-derivative, expression construct for $PCuC_{FL}$-6His, gen^R	This study
pMSL005	pMSL003-derivative, expression construct for $PCuC_{Nt}$-6His, gen^R	This study
pMSL006	pMSL003-derivative, expression construct for $PCuC_{Ct}$-6His, gen^R	This study
pMSL007	pLMB509-derivative, expression construct for ScoB-6His, gen^R	This study
pMSL008	pLMB510-derivative, expression construct for a soluble ScoB-6His, gen^R	This study

Table 2.14: Plasmids used

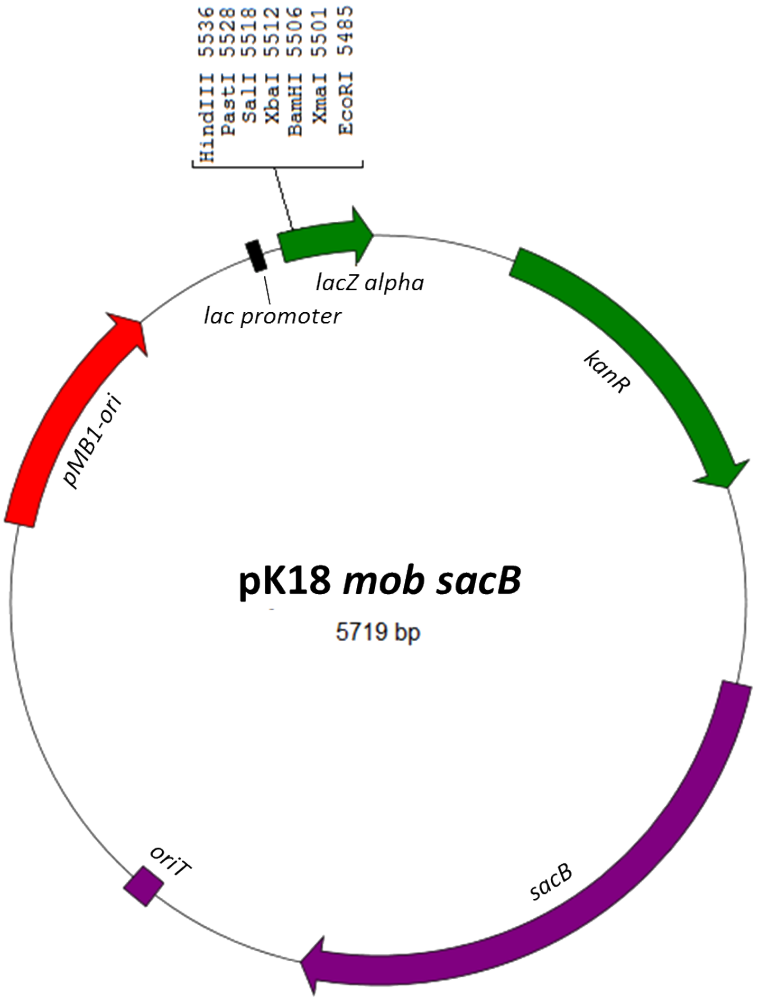

FIGURE 2.4: Map of the mobilizable multi-purpose cloning vector pK18*mobsacB* used for construction of insertion mutants.

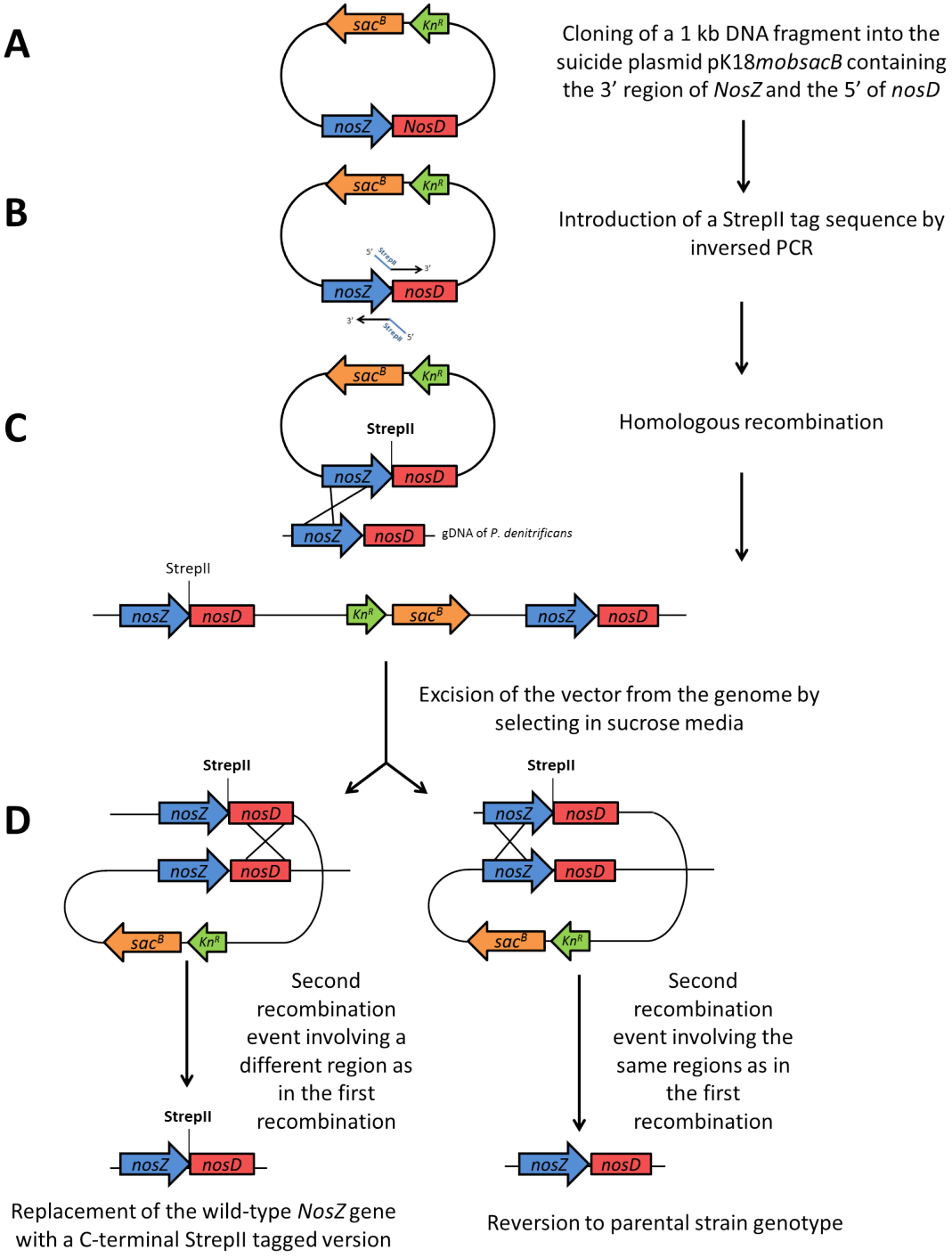

FIGURE 2.5: Schematic representation of the genetic events leading to generation of knock-in mutants. **(A)** Cloning of the flanking regions of *nosZ*. **(B)** Introduction of a StrepII sequence by inverse PCR **(C)** First integrative homologous recombination event. **(D)** Second recombination event with two possible outcomes: mutant generation or reverting parental strain

The mutant is finally generated by forcing the bacteria to undergo a second recombination event where the plasmid is excised from the chromosome. The selective pressure in this case is driven by the expression of levansucrase, which is an enzyme encoded by the *sacB* gene. Levansucrase uses sucrose as a substrate to polymerise levans, a polysacharide that is then accumulated in the cytoplasm and results in the lysis of the bacteria in hypotonic media (10 g L^{-1} tryptone, 5 g L^{-1} yeast extract, 4 g L^{-1} NaCl and 6 % (w/v) sucrose). The cells that were able to grow in this media had either restored back to the wild-type phenotype or resulted in the mutant strain (see figure 2.5 D). Mutants were screened by colony PCR and the PCR products were sequenced for confirmation.

2.12 Protein overexpression and purification

Protein purification of recombinant soluble ScoB (here after $ScoB_{sol}$), PCuC full length ($PCuC_{FL}$), PCuC Nt-domain ($PCuC_{Nt}$), PCuC Ct-domain ($PCuC_{Ct}$) and NosZ was carried out from the following strains: *P. denitrificans* WT (PD1222) carrying the plasmid pMSL008 for the purification of recombinant $ScoB_{sol}$ and *P. denitrificans pcuC*$^{-}$ (PD2305) containing the expression plasmid pMSL004, pMSL005 or pMSL006 for the isolation of recombinant PCuC proteins. *P. denitrificans* gWT (PD2422), *gpcuC*$^{-}$ (PD2405) and *P. denitrificans g*Δ*scoB* (PD2406) are knock-in mutants for the purification of recombinant NosZ.

The preparative steps, of protein overexpression and cell lysis, prior to the purification were in general common for $ScoB_{sol}$, PCuC, PCuC Nt-domain and PCuC Ct-domain. Typically, a 18 L LB culture (18 x 1 L conical flasks) was inoculated with a 1 % inoculum of the corresponding strain and antibiotic (gentamicin). Then, the cultures were incubated at 30 °C with agitation (150 rpm) until $OD_{600} \sim 0.6$ - 0.9, at which point, expression was induced by the addition of taurine (10 mM final concentration).

After 16 hours, cells were harvested by centrifugation at 6,000 g for 20 minutes at 4 °C using an Avanti^{TM} J-20 centrifuge (*Beckman Coulter*) and $ScoB_{sol}$ was

resuspended in 0.01 culture volumes of buffer A (20 mM Hepes, 500 mM NaCl and 25 mM Imidazole, pH 7.5) while PCuC, PCuC Nt-domain and Ct-domain were resuspended in buffer B (20 mM Hepes, 150 mM NaCl and 25 mM Imidazole, pH 7.5). DNase 1 from bovine pancreas (*Sigma*) and a protease inhibitor mixture (cOmplete, EDTA-free, *Roche*) were added to the cell suspension before cell disruption by French Press. Two passes at 1,000 psi (6.89 MPa) were needed to completely break the cells, after which, the cell lysate was centrifuged at 205,000 g for 2 hours using an Optima X100-K ultracentrifuge (*Beckman Coulter*). Next, the soluble fraction was recovered and filtered using a 0.45 μM nitrocellulose filter paper (*Sartorius Stedim*).

2.12.1 Purification of $ScoB_{sol}$-6His and $PCuC_{WT}$

Recombinant $ScoB_{sol}$ and $PCuC_{WT}$ were purified using an ÄKTA FPLC system (*GE Healthcare*) fitted with a UPC-900 high precision monitor, that was set to track the absorbance at a wavelength of 280, 360 and 460 nm, and a sample loading pump that was used to load the filtered cell lysate. Three chromatographic steps were needed to fully purify the protein: immobilised metal affinity (IMAC), anion exchange (AEC) and size-exclusion chromatography (SEC). Firstly, the filtered cell lysate was applied into a 5-mL Ni^{2+} column (HiTrap Chelating HP, *GE Healthcare*) which had been previously equilibrated with buffer A. Next, unbound protein was removed by applying 10 column volumes (CV) of buffer A. $ScoB_{sol}$ and $PCuC_{WT}$ were eluted from the column after the application of a linear gradient of imidazole 25-500 mM for 10 CV with a flow rate of 1 mL min^{-1}. Fractions containing $ScoB_{sol}$ and $PCuC_{WT}$ were combined and diluted 50 times in buffer C (20 mM HEPES pH 8). The diluted protein was loaded into a 5-mL HiTrap Q HP anion-exchange column (*GE Healthcare*) and unbound protein was removed by washing with Buffer C for 10 CV. $ScoB_{sol}$ was eluted from the anion-exchange column by applying a linear gradient of 0 - 1000 mM NaCl over 10 CV with a flow rate of 0.2 mL min^{-1}. Peak fractions containing $ScoB_{sol}$ and $PCuC_{WT}$ were pooled, dialysed against buffer D (20 mM HEPES, 150 mM NaCl pH 7) and concentrated by ultrafiltration. The

concentrated sample was loaded into a 116-mL preparative size-exclusion column (Sephacryl S-75 high resolution, *GE Healthcare*) pre-equilibrated with Buffer D and eluted with a flow rate of 0.2 mL min^{-1}.

2.12.2 Purification of recombinant PCuC proteins

Recombinant $PCuC_{FL}$-6His, $PCuC_{Nt}$-6His and $PCuC_{Ct}$-6His were purified using an ÄKTA FPLC system (*GE Healthcare*) fitted with a UPC-900 high precision monitor, that was set to track the absorbance at a wavelength of 280 and 410 nm, and a sample loading pump that was used to load the filtered cell lysate. Three chromatographic steps were also needed to fully purify the proteins: IMAC, AEC and SEC. The filtered cell lysate was applied into a 5-mL Ni^{2+} column (HiTrap Chelating HP, *GE Healthcare*) which had been previously equilibrated with buffer B. Next, unbound protein was removed by applying 10 column volumes (CV) of buffer A. Finally, the recombinant protein was eluted from the column after the application of a linear gradient of imidazole 25-500 mM for 10 CV with a flow rate of 1 mL min^{-1}. Fractions containing the recombinant protein were combined and diluted 20 times in buffer C (20 mM HEPES pH 8). The diluted protein was loaded into a 5-mL HiTrap Q HP anion-exchange column (*GE Healthcare*) and unbound protein was removed by washing with Buffer C for 10 CV. The recombinant protein was eluted from the anion-exchange column by applying a linear gradient of 0 - 1000 mM NaCl over 10 CV with a flow rate of 0.2 mL min^{-1}. Peak fractions containing the recombinant protein were pooled, dialysed against buffer D (20 mM HEPES, 150 mM NaCl pH 7) and concentrated by ultrafiltration. The concentrated sample was loaded into a 116-mL preparative size-exclusion column (Sephacryl S-75 high resolution, *GE Healthcare*) pre-equilibrated with Buffer D and eluted with a flow rate of 0.2 mL min^{-1}.

2.12.3 Purification of recombinant N_2OR

Nitrous oxide reductase was purified from *P. denitrificans* grown anaerobically under two different copper regimes. Typically 3 L (3 x 1 L Duran bottle) of minimal medium were sufficient for the purification of NosZ under copper high conditions, while 20 - 30 L (2 - 4 x 5 L acid washed Duran bottle) of minimal medium where normally needed to purify NosZ under copper limited conditions. Flasks were inoculated with a 1 % inoculum of preconditioned cells of *P. denitrificans* gPdWT, *gpcuC*$^{-}$ or *g*Δ*senC* (Pd2422, Pd2305 or Pd2306), sealed with screw-cap lids and gas-tight silicone septa and incubated at 30 °C without agitation.

After 24 hours, cells were harvested by centrifugation at 6,000 g for 20 minutes at 4 °C using an Avanti^{TM} J-20 centrifuge (*Beckman Coulter*) and resuspended in 0.01 culture volumes of Buffer E (100 mM Tris-Cl, 150 mM NaCl, pH 8.0). DNase 1 from bovine pancreas (*Sigma*) and a protease inhibitor mixture (cOmplete, EDTA-free, *Roche*) were added to the cell suspension before cell disruption by French Press. Two passes at 1,000 psi (6.89 MPa) were needed to completely break the cells, after which, the cell lysate was centrifuged at 205,000 g for 2 hours using an Optima X100-K ultracentrifuge (*Beckman Coulter*). Next, the soluble fraction was recovered and filtered using a 0.45 μM nitrocellulose filter paper (*Sartorius Stedim*).

Recombinant NosZ was purified using an ÄKTA FPLC system (*GE Healthcare*) with the UPC-900 high precision monitor set at 280, 480 and 640 nm. The filtered cell lysate was loaded into a pre-equilibrated 5-mL StrepII column (*IBA*) using the sample loading pump and unbound protein was removed by applying 10 column volumes (CV) of buffer E. Finally, the recombinant protein was eluted from the column after applying a step gradient of buffer F (100 mM Tris-Cl, 150 mM NaCl, 20 mM Biotin pH 8.0) for 5 CV at a flow rate of 1 mL min^{-1}.

2.13 N-terminal sequencing of PCuC

2.13.1 Edman degradation

A pure sample of $PCuC_{WT}$ (10 μg) was applied onto a SDS-PAGE gel and transferred into a PVDF blotting membrane as described previously. Then, a clean scalpel was used to cut around the PCuC band, using a coomassie stained SDS-PAGE gel as a reference, and placed inside of a clean microcentrifuge tube. Sample was submitted to Cambridge Peptides Ltd (Birmingham, UK) by ordinary mail for analysis. The identified sequence was NH_2-HATLE.

2.13.2 Protein sequencing by in source decay MALDI-TOF

A sample of 50 μL of pure $PCuC_{WT}$ (1 nmole) was submitted to the John Innes Centre Proteomics Facility (Norwich Research Park) for N-terminal sequencing by in source decay (ISD) MALDI-TOF. The identified sequence was NH_2-HATLERSEAPAGAAYRAVIRIGHGC.

2.14 Addition of Cu ions to Cu-binding proteins

The ability to bind Cu^{1+} or Cu^{2+} of $ScoB_{sol}$, $PCuC_{WT}$, $PCuC_{Nt}$ and $PCuC_{Ct}$ and the stoichiometry of the binding was tested by titrating a copper solution into the proteins and following the changes of the UV-vis and fluorescence spectra.

As purified proteins were incubated with a 50-times excess of a mixture of the high affinity Cu^{1+} and Cu^{2+}-binding chelators diethyl-dithio-carbamate (DETC) and ethylenediaminetetraacetic acid (EDTA) for $\sim$ 10 min at room temperature. DETC develops an intense yellow colouration and becomes highly hydrophobic when it binds to the metal. Therefore, the complexes were removed from the solution by hydrophobic interaction chromatography (HIC) in flow-through mode

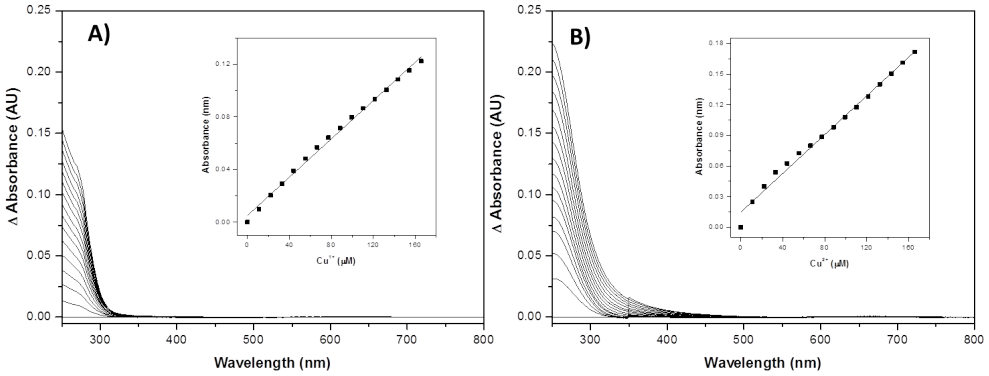

FIGURE 2.6: UV-visible spectra of CuCl and $CuSO_4$. **(A)** UV-visible absorbance spectra of 0 to 105 µM CuCl in 100 mM MOPS and 150 mM NaCl pH 7.5. The insert represents the absorbance changes at 270 nm; **(B)** UV-visible absorbance spectra of 0 to 105 µM $CuSO_4$ in 100 mM MOPS and 150 mM NaCl pH 7.5. The insert represents the absorbance changes at 270 nm

a technique that is commonly used within the pharmaceutical industry to remove aggregates from the production of monoclonal antibodies [150]. For this purpose, the mixture was loaded into a 1-mL HiTrap Phenyl HP column (*GE Healthcare*) and the flow-through was collected and buffer exchanged several times by ultrafiltration in order to remove any trace of free DETC or EDTA into 100 mM MOPS and 150 mM NaCl pH 7.5 using a spin-concentrator (*Merck Millipore*). The protein was then introduced in the glove box (*mBraun*) were oxygen was kept below 0.5 ppm, and reduced with 5-times excess of DTT, which was later on removed by several steps of ultrafiltration using a centrifugal filter (*Merck Millipore*).

Substoichiometric additions of Cu^{1+} were performed in the form of copper chloride dissolved in 100 mM HCl and 500 mM NaCl solution, while Cu^{2+} was prepared from copper sulphate dissolved in 500 mM NaCl. UV-visible absorbance spectra were recorded during the titration using a Cary 4000 spectrophotometer (*Agilent technologies*). The spectroscopic data were not corrected against buffer with Cu, since both free CuCl and $CuSO_4$ absorb within the 250 to 280 nm region which therefore interferes with the small UV-vis changes appreciated of the Cu-protein bound form (see Figure 2.6 A). The relative absorbance at 270 nm of the titration of CuCl and $CuSO_4$ result in a straight line (see Figure 2.6 B). While, the relative absorbance of CuCl or $CuSO_4$ bound to the protein of interest will result in a linear

increase up to one equivalent and a breakpoint that will continue to increase with a significantly less pronounce slope due to the contribution of free Cu in solution (see Figures 3.9, 3.10, 4.19, 4.20, 4.21, 4.22 and 4.23). At the same time, Cu-binding events were followed by fluorescence spectroscopy. The emission spectra of the same samples were recorded using a Varian Cary Eclipse fluorescence spectrophotometer (*Agilent technologies*) with excitation at 280 or 295 nm, emission slit widths of 5 nm and a 290 nm cut-off band pass filter was applied.

2.15 Analytical ultracentrifugation

Protein samples for sedimentation equilibrium experiments were prepared as described previously in section 2.14 and applied, under anaerobic conditions, into 12-mm charcoal-filled Epon double-sector cells with quartz windows. The sample and reference sectors were loaded with 105 µl of sample and 120 µl of buffer, respectively. The cells were placed in a AN-50 Ti rotor and run in a XL-I analytical ultracentrifuge (*Beckman Coulter*) at 25 °C.

Absorbance data was acquired at 280 nm and samples were spun until equilibrium was reached (noted by the absence of changes in the profile of scans collected 4 h apart). The partial specific volume of the analysed proteins was calculated from the amino acid composition (see table 2.15) and the density of the buffer was estimated as 1.006 mL g^{-1} using the software Sednterp (v. 20130813 BETA) [151]. Absorbance data was analysed using Ultrascan (v. 9.9) [152].

Protein	**Partial specific volume (mL g^{-1})**
$ScoB_{sol}$	0.72
$PCuC_{WT}$	0.73
$PCuC_{Nt}$	0.72
$PCuC_{Ct}$	0.73

TABLE 2.15: Partial specific volumes calculated using Sednterp [151]

2.16 Analytical size exclusion chromatography

Analytical size exclusion chromatography (ASEC) is a common technique used to calculate the molecular weight of proteins. Apo and metallated protein samples were analysed in a Superdex 200 column 10/300 GL (*GE Healthcare*) connected to an ÄKTA FPLC system (*GE Healthcare*) with the UPC-900 high precision monitor.

The column was equilibrated with 2 CV of deoxygenated buffer (20 mM HEPES, 150 mM NaCl and 0.25 mM DTT pH 7.5) and 0.15 mL of sample was injected at a flow rate of 0.25 mL min^{-1}. A commercial standard kit (*Sigma*) was used to generate a calibration curve under the conditions mentioned before (Figure 2.7).

The K_{av} of the standards was calculated according to the following equation:

$$K_{av} = \frac{V_e - V_0}{V_c - V_0} \tag{2.2}$$

Where K_{av} is the partition coefficient which is a proportion of pores available to the molecule and is a function of the elution volume (V_e), the column void volume (V_0) and the geometric column volume (V_c). V_c is equal to 24 mL for the column used and V_0 was calculated experimentally with Blue Dextran 2000 (*Sigma*) and is equal to 8.18 mL.

2.17 Estimation of metal dissociation constants using copper chelators

The binding of Cu^{1+} by $ScoB_{sol}$, PCuC, PCuC N- and C-terminal domain was investigated in the presence of bicinchoninic acid (BCA) or bathocuproine disulfonic acid (BCS). The affinity of this type of proteins for metals (M) is very tight (K_D

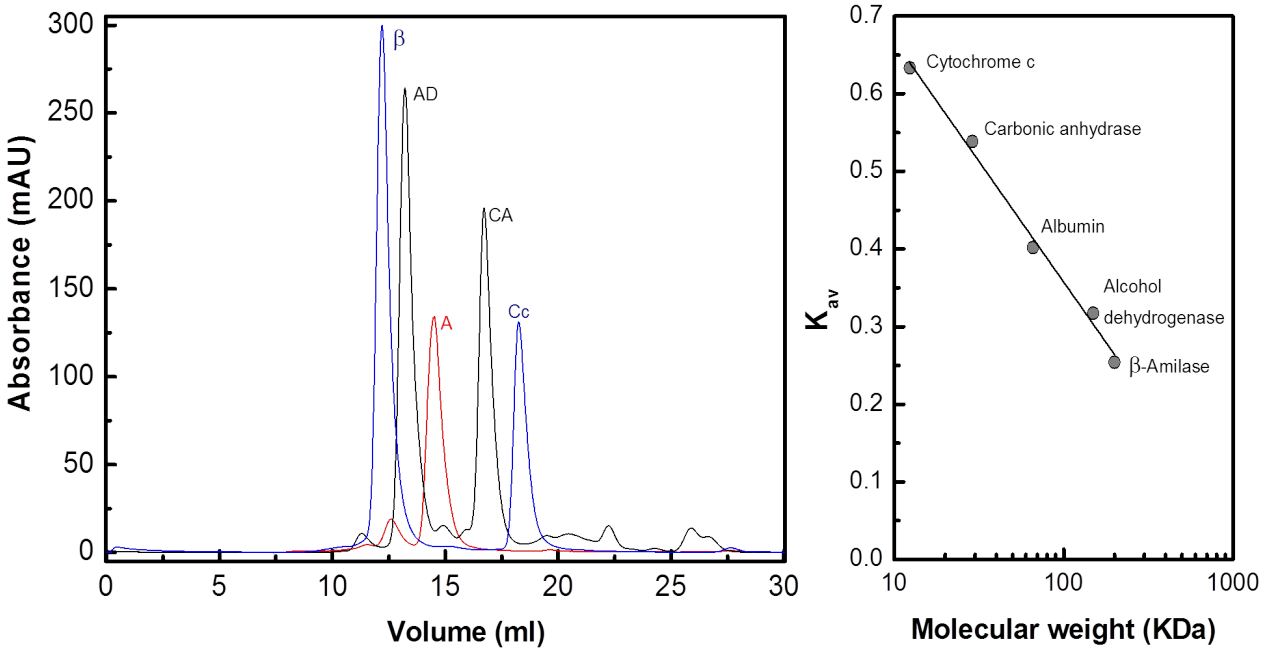

FIGURE 2.7: Analytical size exclusion chromatography standards. Cytochrome C (CC, 12.4 kDa), carbonic anhydrase (CA, 29 kDa), albumin (A, 66 kDa), alcohol dehydrogenase (AD, 150 kDa) and β-amilase (β, 200 kDa).

$< 10^{-7}$ M) and it cannot be measured by direct titration of metals into apo-proteins [153, 154], since the detection sensitivity of most of the methods is within the micromolar range. At such relatively high concentration, the system is not at equilibrium and all the protein is instead saturated with metal. As a result, the estimation of the derived K_D is limited by the protein concentration of the experiment.

BCA and BCS are ligands that bind Cu^{1+} quantitatively to produce 1:2 complex $[ML_2]$ (where L is either BCA o BCS) according to equation 2.3 and their overall formation constant (by convention denoted as β since is a cumulative constant) is $10^{19.8}$ and $10^{17.2}$ M^{-2}, respectively [43, 154].

$$M + 2L' \overset{\beta_A}{\rightleftharpoons} ML_2 \qquad \beta_A = \frac{[ML_2]}{[M][L']^2} \tag{2.3}$$

The binding of Cu^{1+} to a protein (P) that binds a single copper and the corresponding dissociation constant is given in equation 2.4:

$$M + P \underset{K_D}{\overset{K_A}{\rightleftharpoons}} MP \qquad K_D = \frac{1}{K_A} = \frac{[M][P]}{[MP]} \tag{2.4}$$

Equation 2.5 shows a typical experimental situation where two ligands compete for the same metal ion that is present at a limiting concentration:

$$MP + 2L' \overset{K_{ex_1}}{\rightleftharpoons} ML_2 + P \quad K_{ex_1} = \frac{[ML_2][P]}{[MP][L']^2} \tag{2.5}$$

$$K_{ex_1} = \left(\frac{[M][P]}{[MP]}\right)\left(\frac{[ML_2]}{[M][L']^2}\right) = K_D\beta_2' \tag{2.6}$$

Equation 2.6 can be transformed into equation 2.10 based on the mass balances of equations 2.7, 2.8 and 2.9:

$$[P] = [P]_{total} - [MP] \tag{2.7}$$

$$[L'] = [L]_{total} - 2[ML_2] \tag{2.8}$$

$$[M]_{total} - [MP] \approx [ML_2] \tag{2.9}$$

$$K_D\beta_2' = \frac{\frac{[P]_{total}}{[MP]} - 1}{\left(\frac{[L]_{total}}{[ML_2]} - 2\right)^2 [ML_2]} \tag{2.10}$$

Equation 2.10 can be used to calculate K_D, since the β_A values of BCS and BCA are known and $[ML_2]$ can be determined experimentally from the solution absorbance of the reaction equilibrium 2.5 ($L = BCS, \varepsilon_{483} = 12,500\ M^{-1}cm^{-1}$ and for $L = BCA, \varepsilon_{560} = 7,900\ M^{-1}cm^{-1}$) [43, 154].

Experiments were carried out in a glove box in both directions of equation 2.6. The forward reaction was prepared by titrating the apo-protein and maintaining the ligand concentration constant, while for the reverse reaction the ligand was titrated and the apo-protein kept constant. In both cases, copper concentration was maintained constant at 10 μM and prepared from a stock solution ($[Cu(CH_3CN)_4]PF_6$) dissolved in acetonitrile and then diluted in 20 mM HEPES and 150 mM NaCl pH 7.5. Each reaction was prepared independently, in triplicates and aliquoted into a 96 well plate which was sealed with SureSeal DWB plastic coverslips (*Molecular Dimensions*) and wrapped with parafilm. After 60 minutes of incubation, whole spectrum was collected in a Sense Microplate Reader (*HIDEX*). Reduced methyl viologen was also added to a separate well to check for oxygen leaking. Data was normalised at 800 nm and fitted using the script shown in appendix A.6 and A.7 for the software Dynafit (v. 4.07.096) [155].

2.18 Small-angle X-ray scattering

Small-angle X-ray scattering (SAXS) experiments were performed at beamline B21 Diamond Light Source (Harwell Science and Innovation Campus). PCuC and $ScoB_{sol}$ samples (10 mg mL^{-1}) were applied to a Sephadex 200 5/150 GL column (*GE Healthcare*) attached to an in-line 1200 series HPLC (*Agilent*) and eluted with a flow rate of 0.1 mL min^{-1}. The buffer (20 mM HEPES, 150 mM NaCl and 1 mM DTT pH 7.5) eluted after one column volume was used as a blank. SAXS images were continuously collected at 1 second intervals for a total exposure time of 10 minutes at 15 °C on a PILATUS3 2 M detector (*Dectris*) situated at 3.9 m from the sample and an X-ray wavelength of 1.0 Å.

Buffer subtractions and data merging were performed with the software SCATTER (v. 3.0j) [156]. Downstream analysis were done with the following programs from the ATSAS suite (v. 2.8.0) [157]: GNOM (v. 4.6) to calculate structural parameters such as the radius of gyration (Rg) and the pair distance distribution functions (p(r)) [158], DAMMIF (v. 1.1.2) was used to create 23 independent rapid *ab initio* bead models [159], DAMAVER (v. 5.0) to average the *ab initio* bead models [160], DAMMIN (v. 5.3) to further refine the previous models, SUPCOMB (v. 2.3) was used to fit the crystal structure into the resulting *ab initio* model [161], CRYSOL (v. 2.8.2) was used to assess the agreement between experimental and theoretical curves [162–164] and GASBOR to model protein surface envelops based on chain-like ensemble of *dummy residues* [165].

2.19 Protein crystallography

The selection of the crystallisation conditions, protein harvest, data collection and model building was performed in collaboration of the structural biologist Dr. Marcus Edwards.

2.19.1 Crystal formation

Protein crystals of $PCuC_{Nt}$ and $PCuC_{Ct}$ were formed by the vapour diffusion method in a sitting drop format. The crystallisation conditions for each protein were found using commercially available sparse matrix screening kits (*QIAGEN*). A volume of 50 µL of each solution was aliquoted into the reservoir well of 96-well MRC 2 drop plates (*Molecular Dimensions*). Then, an Oryx Nano protein crystallography robot (*Douglas Instruments*) was used to dispense protein samples and precipitant solution in drops of 0.6 μL which contained a ratio of precipitant:protein solution of 1:1 or 2:1. Plates were then sealed with SureSeal DWB plastic coverslips (*Molecular Dimensions*) and incubated at 16 °C. Protein crystal formation of $PCuC_{Nt}$ (10 mg mL^{-1}) was observed in 20 % PEG 8000, 200 mM magnesium chloride and 100 mM Tris-Cl pH 7.5. The optimal concentration of PEG 8000 and magnesium chloride was optimised by testing a range of concentrations from 16 - 26 % (in 2 % increments) and from 100 - 400 mM (following 100 mM increments), respectively. $PCuC_{Ct}$ (20 mg mL^{-1}) crystallised in 100 mM trisodium citrate, 200 mM potassium sodium tartrate and 2.0 M ammonium sulphate pH 5.6. This condition was further optimised by testing a set of concentration of ammonium sulphate following a gradient of 0.5 - 3.0 M (in 0.5 M increments) and by changing the concentration of potassium sodium tartrate from 50 - 400 mM (following 50 mM increments).

Crystals were harvested using 0.1 - 0.2 mm mounted LithoLoops (*Molecular Dimensions*) and then incubated for a few seconds in a cryogenic solution before flash freezing them in liquid nitrogen. The cryogenic solution was made up in precipitant solution containing 20 % (v/v) ethylene glycol for $PCuC_{Nt}$ and 35 % glycerol for $PCuC_{Ct}$.

2.19.2 Data collection

X-ray diffraction experiments were performed at beamline IO3 Diamond Light Source (Harwell Science and Innovation Campus). Typically, an exploratory screening of three test images using a 0.979 Å wavelength was performed on each

crystal to then prioritise the rest of the data collection session and determine a data collection strategy using MOSFLM [166] and/or EDNA [167].

2.19.2.1 $PCuC_{Nt}$

For $PCuC_{Nt}$, a crystal that initially diffracted to 1.5 Å and had a predicted P3 space group was selected to perform a single-wavelength anomalous diffraction (SAD) experiment. For this purpose, the wavelength was adjusted to 1.378 Å as required for anomalous scattering by copper and a total of 288 images were collected across 720° in 2.5° oscillations using a beam of 11 x 5 µm and 0.2 s exposures. These parameters had been calculated using the integrated software MOSFLM [166]. The images were then merged and scaled with XIA2 [168] that calculated a maximum resolution of 1.84 Å, although the data was adjusted to 2.00 Å using the software AIMLESS within the CCP4 suite [169] to improve the completeness statistic. This SAD dataset was used to determine the phases and an initial model was built using Crank2 pipeline component of the CCP4 on-line programs [170]. Two chains and a total of 323 residues were initially built.

Then the wavelength was adjusted to 0.979 Å and another $PCuC_{Nt}$ crystal that had been previously screened was used to collect a complete native dataset. A total of 450 images were recorded across 180° in 0.4° oscillations, 0.2 s exposures and an unattenuated 63 x 50 µm beam as indicated by MOSFLM [166]. After processing the images with XIA2 [168] a maximum resolution of 1.46 Å was calculated. The structure was then solved by molecular replacement with the program PHASER [170] using the coordinates from the experimentally phased structure. This was followed by manual inspection and iterative cycles of model building in COOT and crystallographic refinement using REFMAC5 [171].

2.19.2.2 $PCuC_{Ct}$

A crystal that initially diffracted down to 1.54 Å and had a $P2_1$ space group was selected to collect a full native dataset. The wavelength was set at 0.928 Å and

a total of 3600 images were collected across 180° in 0.05° oscillations using an unattenuated 63 x 50 µm beam and 0.04 s exposures. These parameters had been calculated using the integrated software MOSFLM [166]. The images were then merged and scaled with XIA2 [168] and the crystallographic structure was solved to a resolution of 1.6 Å by molecular replacement (MR) using the software MoRDa [172]. The initial model generated by MoRDa contained one polypeptide with 127 residues. MoRDa automatically selected the coordinates of the extracytoplasmic copper chaperone-like protein (ECuC) from *S. lividans* (PDB accession codes: 3ZJA) as a search template. The solution had space group $P2_1$, a MoRDa Q-factor of 0.673 out of 1 and a probability of correct solution of 3 over 3. The crystallographic unit contained a single protein molecule and continuous and well defined electron density was observed for 127 residues (out of 169 that were deduced from the genetic construct used to over-expressed the protein) ranging from position 54 to 184.

3 Biochemical characterisation of $ScoB_{sol}$

3.1 Introduction

Synthesis of cytochrome oxidase (Sco), sensor of cytochrome oxidase (SenC) [173], photosynthetic regulatory response (PrrC) [174] or YpmQ [175] are names that have been given to members of a protein family that has been mainly studied in relation to the biogenesis of copper and heme-dependent oxidases of the respiratory chain [32]. Genes encoding Sco proteins are present in all kingdoms of life, and often found in more than one copy within the same genome as a consequence of independent duplication events. This multiplicity of *sco* genes may be indicative of the possible functional divergence of the encoded proteins, which may differ between organisms belonging to the different kingdoms of life [176–178].

In eukaryotes, all *sco* genes are considered to derive from a gene present in the last common ancestor of choanoflagellates, plants and metazoans [179]. Flowering plants, yeast and vertebrate genomes contain two *sco* genes and in each case they are considered to result from independent duplication events [180]. In bacteria and archea the occurrence of *sco* genes is even more variable. For example, in a study where 311 prokaryotic genomes were analysed (285 from bacteria and 26 from archea) it was shown that, when *sco* genes are present, in most cases they are found in more than one copy. However, it was also shown that there are organisms or even entire groups of prokayotes (such as cyanobacteria) that do not contain any

Sco homologues at all [177]. In this study the co-occurrence of *sco*, *cox2* and *nosZ* genes was also assessed and the authors found that there seems to be a general correlation between *sco* and *cox2* genes (e.g. the genes are either both present or both absent in 82 % of the genomes analysed). Only 12 % of the organisms studied had *cox2* but not *sco* genes and 6% had *sco* but not *cox2* genes. Genes encoding NosZ proteins were identified in 27 organisms of the 311 analysed, and 25 of the NosZ containing organisms encoded at least one *sco* gene.

Sco are membrane proteins with a globular domain facing the intermembrane space (IMS) in eukaryotic mitochondria or the periplasm in bacteria, and a single N-terminal transmembrane helix that anchors them to the cell membrane. The globular domain exhibits a thioredoxin fold [181] that consists of a core of four-stranded β sheets (β_3, β_4, β_6, β_7) flanked by three α helices (α_3, α_5, α_6). Thioredoxin proteins are known to function as general disulfide oxido-reductase through a mechanism of reversible oxidation of two cysteine thiol groups to a disulfide, accompanied by the transfer of two electrons and two protons (see figure 3.1 A). As a result, a disulfide bond is exchanged with a thioredoxin to produce two dithiols on the substrate protein partner [181]. Some Sco proteins are known to have maintained thioredoxin activity (e.g. *P. putida* Sco [182], *R. sphaeroides* PrrC [183]) while others have completely lost this activity (e.g. *H. sapiens* Sco1 [184], *S. lividans* Sco [185]). The structure of thioredoxin and Sco proteins tolerates modifications in certain regions without disruption of their activity [180, 181]. In Sco proteins one of these alterations is an insertion at the N-terminus of an α-helix that anchors the protein to the membrane followed by a β-hairpin structure (β_1 and β_2) and an α-helix (α_2). Another region susceptible of modification is between β_4 and α_5, where a helix (α_4) and a strand (β_5) that forms a parallel β-sheet with β_4 are inserted (see figure 3.1 B). Lastly, eukaryotic Sco proteins present an extra β-hairpin at the loop that connects α_5 and β_6 [186, 187].

A recognised motif lies within the globular domain of Sco proteins that consists of two conserved cysteines and a histidine residue (see sequence alignment in Figure 3.2 A). In some Sco proteins this motif has been found to have conserve thioredoxin

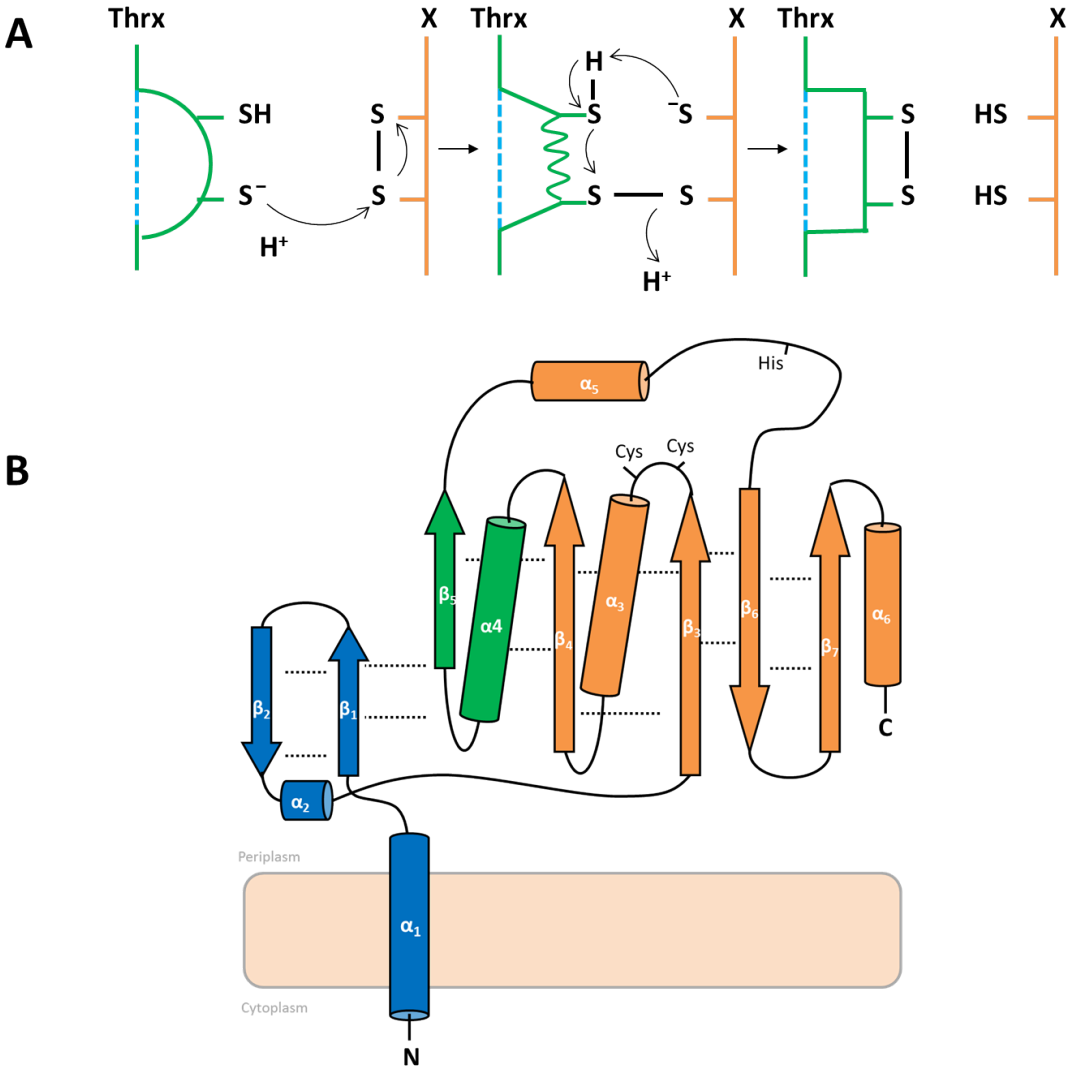

FIGURE 3.1: Proposed mechanism of action of thioredoxin proteins and schematic representation of the general fold topology of a bacterial Sco protein. **(A)** Proposed mechanism by which the thiolate group of a reduced thioredoxin (Thrx) undergoes a nucleophilic attack. As a result, a transient mixed disulfide is formed between Thrx and its protein partner (X) that acts as a substrate. A second nucleophilic attack of the deprotonated cysteine of Thrx generates a disulfide bond between the cysteines of Thrx and two reduced cysteines in the protein partner. **(B)** Schematic representation of the general fold topology of a bacterial Sco protein. The typical elements of a thioredoxin fold are coloured in orange and additional secondary structural elements are shown in blue (N-terminal transmembrane α-helix) and green (α_4 and β_5 forming a parallel β-sheet with β_4).

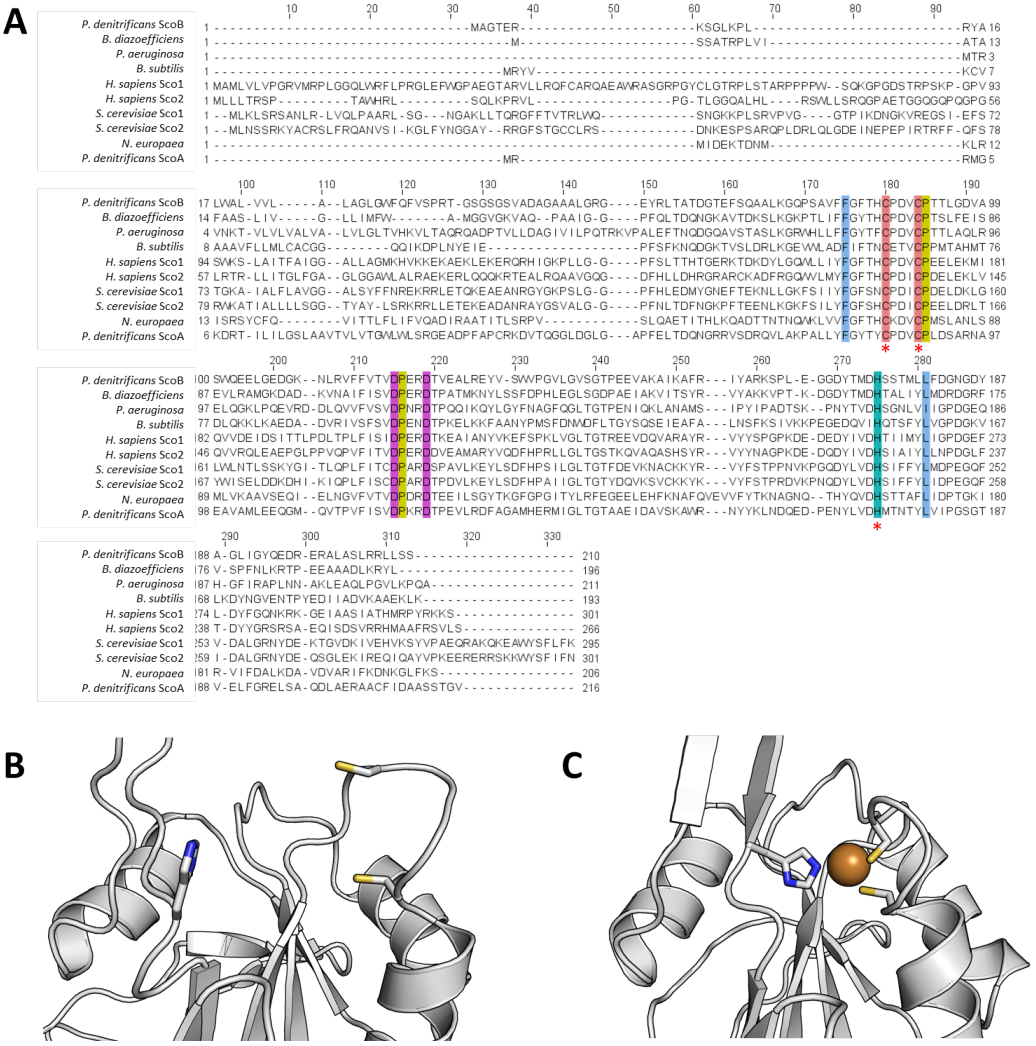

FIGURE 3.2: Sequence alignment and cartoon representation copper binding site of Sco proteins. **(A)** Sequence alignment of Sco proteins using the program MUSCLE [188], conserved residues have been coloured using Clustal X colour scheme (see appendix A.1). Residues involved in copper binding have been highlighted with a (⋆) symbol. Cartoon representation of the copper binding site of **(B)** apo-Sco1 and **(C)** Cu^{1+}-Sco1 from *H. sapiens* (PDB accession codes: 2GVP and 2GT6, respectively).

activity while in others had acquired the ability to bind both Cu^{1+} and Cu^{2+} species (see table 3.2). Mutation of any of the residues that forms the motif results in the loss of copper-binding ability by the Sco protein and a reduction in cytochrome *c* oxidase (COX) activity [189, 190]. Furthermore, copper binding is also known to drive a conformational change in the protein that alternates between an open-mobile form and a close-rigid form (see Figure 3.2 B and C) [184, 186]. This degree of conformational change is variable between Sco homologues, for instance eukaryotic Sco2 has shown higher flexibility in both states compared to Sco1 that is structurally more rigid [187]. This higher degree of flexibility has been proposed as one of the reasons for Sco2 plasticity, which is involved in other processes apart from Cu_A assembly [191, 192].

3.2 A Sco protein from *P. denitrificans* necessary for N_2O reduction

A BLAST search of *Paracoccus denitrificans* PD1222 genome showed the presence of two *sco* genes: *scoA* and *scoB* (Figure 3.3). A multiple sequence alignment of ScoA and ScoB using MUSCLE within the software package Jalview [193] was used to calculate a pairwise sequence identity and similarity of 29 and 39 % with the on-line service SIAS [194]. Both Sco proteins present features typical of members of the Sco family, such as, a N-terminal transmembrane helix, a globular domain with a general thioredoxin fold, a distinctive copper binding CX_3C motif and a conserved histidine residue (Figure 3.3 A). The *scoA* gene is encoded as part of a RegAB system and is present in chromosome 1 in a putative *scoA-regA-hvrA* gene cluster, with a *regB* gene divergently transcribed. *hrvA* codes for a histone-like protein that exhibits significant sequence similarity to *Escherichia coli* heat-stable nucleoid-structuring (H-NS) repressor [195]. RegAB is a redox regulatory system comprising a histidine sensor kinase and a partner DNA-binding response regulator [196]. In *B. japonicum* SenC is thought to be involved in the modulation of RegAB through the oxidation and reduction of a redox-active cysteine residue within RegB

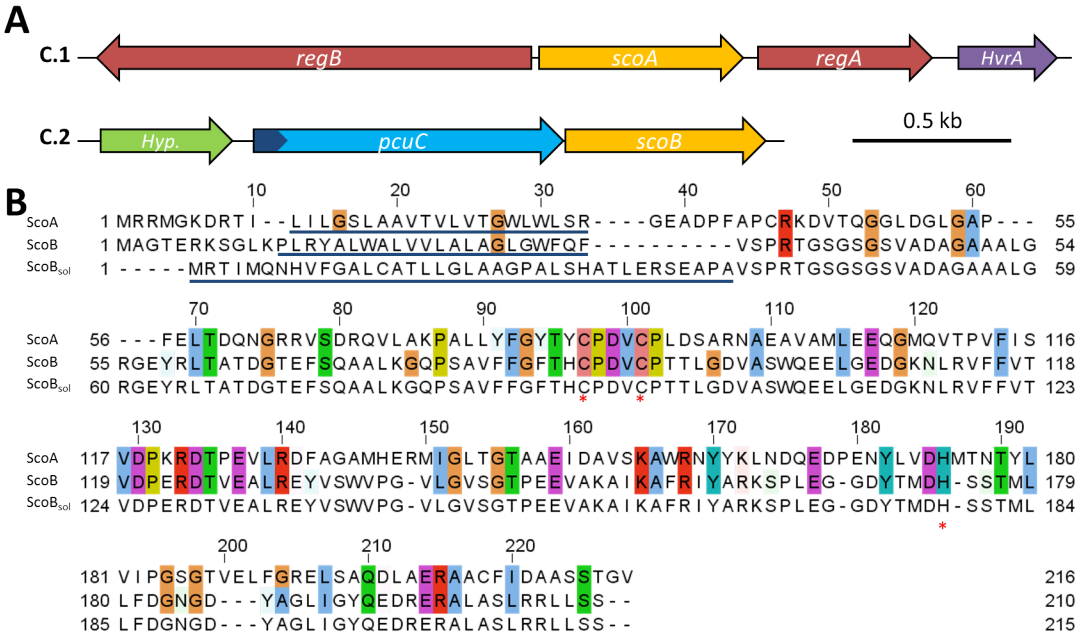

FIGURE 3.3: Properties of *scoA* and *scoB* genes from *P. denitrificans*. **(A)** Gene clusters of *scoA* and *scoB*. **(B)** Sequence alignment of ScoA, ScoB and $ScoB_{sol}$ polypeptides. The blue line below ScoB and ScoA denotes the location of the N-terminal α-helix, while in $ScoB_{sol}$ represents the the region replaced by PCuC signal peptide in $ScoB_{sol}$ sequence. Conserved residues have been coloured using Clustal X colour scheme (see appendix A.1)

[197]. In *P. denitrificans*, deletion of *scoA* showed no apparent phenotype on cytochrome *c* oxidase activity [198].

The *scoB* gene is present on chromosome two embedded in a putative *hypothetical-pcuC-Sco* gene cluster. The hypothetical gene (Pden_4445) is predicted to encode a membrane protein anchored to the cell membrane through a single N-terminal transmembrane helix and does not show sequence similarity to any other studied gene. The predicted gene product of *pcuC* is a polypeptide made up of the fusion of two proteins, a N-terminal YcnI-like domain [4] and a C-terminal domain homologous to the known copper chaperone PCu_AC that has been studied in *Deinococcus radiodurans* [33]. In contrast to *scoA*, deletion of *scoB* from *P. denitrificans* had a severe effect on cytochrome *c* oxidase activity [198]. Sullivan and co-workers showed that the gene expression of this whole gene cluster is sensitive to extracellular copper concentrations, and deletion of any of the three genes of this gene cluster attenuates N_2OR activity during anaerobic respiration [3].

In this chapter we focused our attention on ScoB. For the study of this protein we generated a soluble version of the protein in the periplasm ($ScoB_{sol}$) in order to avoid all the associated issues of performing subsequent analytical experiments in the presence of detergents. Using the software PHOBIUS [199] and SignalP [200] we predicted the location of the N-terminal α-helix for ScoB (see figure 3.3 B) and the signal peptide of the putative periplasmic PCuC protein found within the same gene cluster (see chapter 4 for more information), respectively. We therefore designed and synthesised (*GenScript*) a gene were the first 33 residues of *scoB* had been replaced with the first 38 residues of *pcuC*. Throughout this chapter, we report the properties of the resultant periplasmic protein upon addition of Cu^{1+} and Cu^{2+} and the effect of copper on its oligomeric state. Parallel *in vivo* studies have also been performed and revealed that ScoB is responsible for the maintenance of N_2O reductase activity under conditions where extracellular copper is limiting.

3.3 Phenotypical characterisation of *scoB*

To test if ScoB is involved in the assembly of terminal oxidases in *P. denitrificans*, we compared the growth of *scoB* in-frame unmarked deletion mutant (PD2306), wild-type and two *in trans* complemented strains. The complemented strains were generated by conjugating the low copy number taurine inducible plasmids pMSL007 and pMSL008 into Δ*scoB*. pMSL007 codes for a full length membrane-anchored ScoB protein ($ScoB_{FL}$) and pMSL008 a soluble ScoB ($ScoB_{sol}$) with the signal peptide of PCuC that directs the protein to the periplasm through the Sec system (see figure 3.3 for sequence comparison). Under aerobic conditions, the growth rate of the mutant and complemented strains was not affected whether the bacteria was grown in media with sufficient amounts of copper (e.g. average of 0.155 ± 0.003 h^{-1}) or in the absence of the metal (e.g. 0.154 ± 0.010 h^{-1}) (figures 3.4 A and B). The addition of the inducer to the media did not affect the growth phenotype of the strains under the two copper regimes studied (e.g. copper sufficient, 0.157 ± 0.013 h^{-1} and copper limited, 0.154 ± 0.033 h^{-1}) (figure 3.4 C and D).

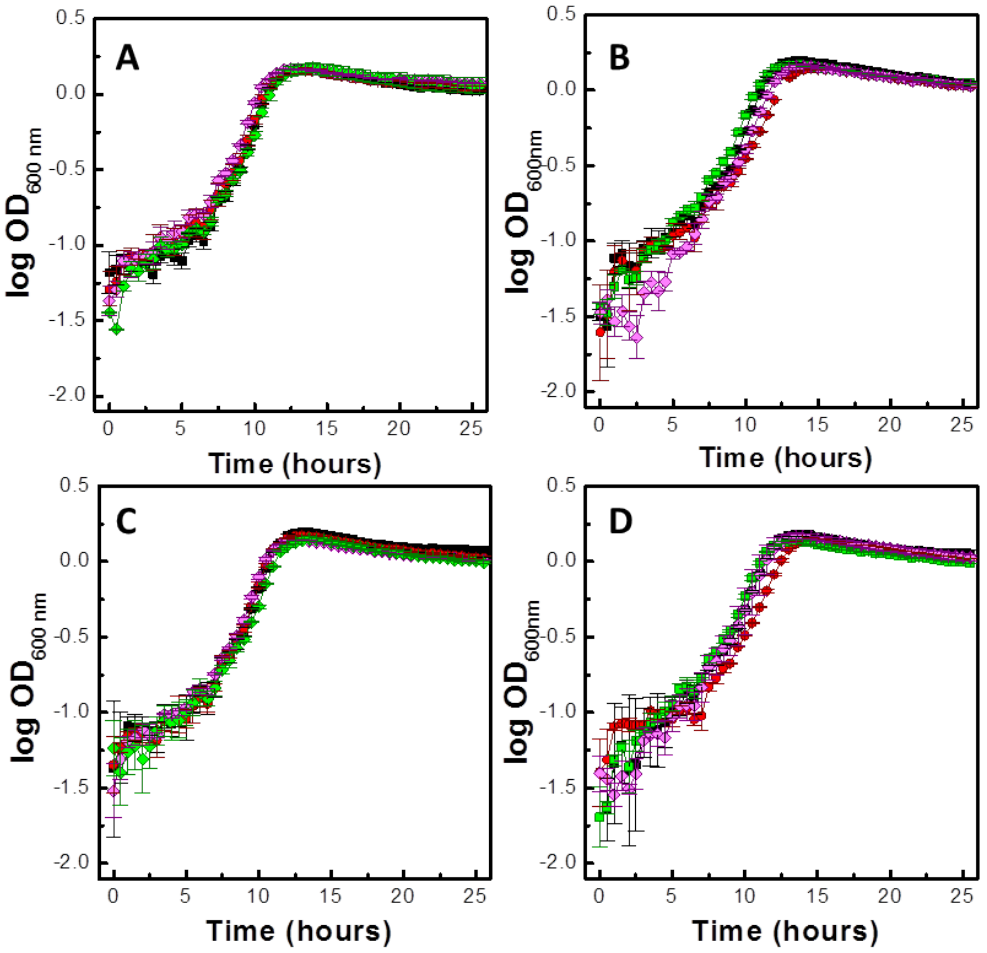

FIGURE 3.4: Aerobic growth characteristics of *P. denitrificans* WT (■), Δ*scoB* deletion mutant (●), ScoB_{FL} (■) and ScoB_{sol} (◆) complemented strains in batch culture conditions. The growth in the absence of taurine is shown in graphs **(A)** and **(B)**, and in the presence of the inducer in **(C)** and **(D)**. Cultures shown in the left and right column contained 13.5 and < 0.5 μM of copper, respectively. Standard errors of the mean are indicated by the error bars ($n = 3$).

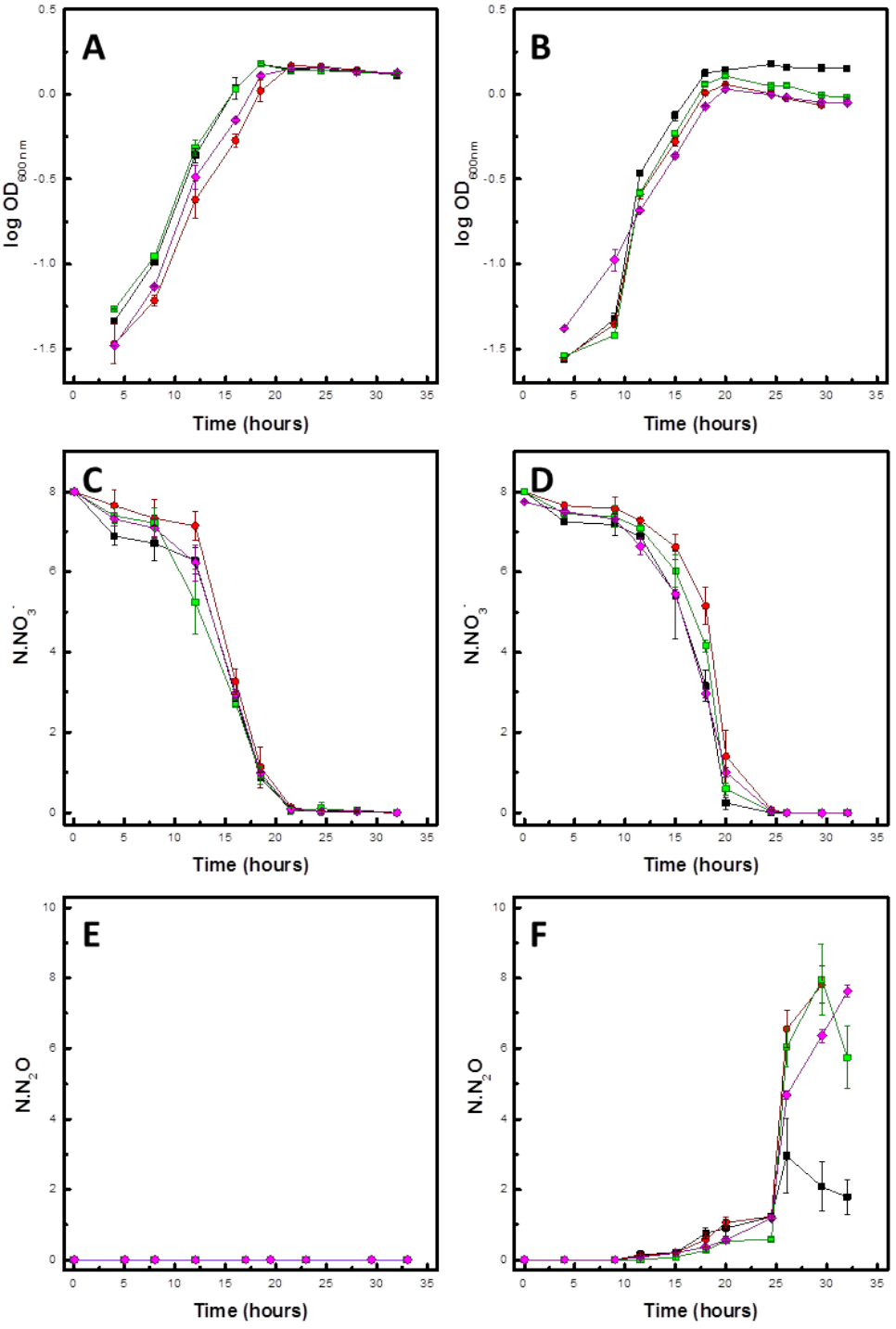

FIGURE 3.5: Growth characteristics of *P. denitrificans* WT (■), Δ*scoB* deletion mutant (●), $ScoB_{FL}$ (■) and $ScoB_{sol}$ (◆) complemented strains in batch culture conditions in the absence of taurine. The anaerobic growth is shown in graphs **(A)** and **(B)**. Plots **(C)** and **(D)** represent the consumption of NO_3^- in millimole of N in the form of NO_3^-. **(E)** and **(F)** show N_2O production in millimole of N in the form of N_2O. Cultures shown in the left and right column contained 13.5 and < 0.5 μM of copper, respectively. Standard errors of the mean are indicated by the error bars ($n = 3$).

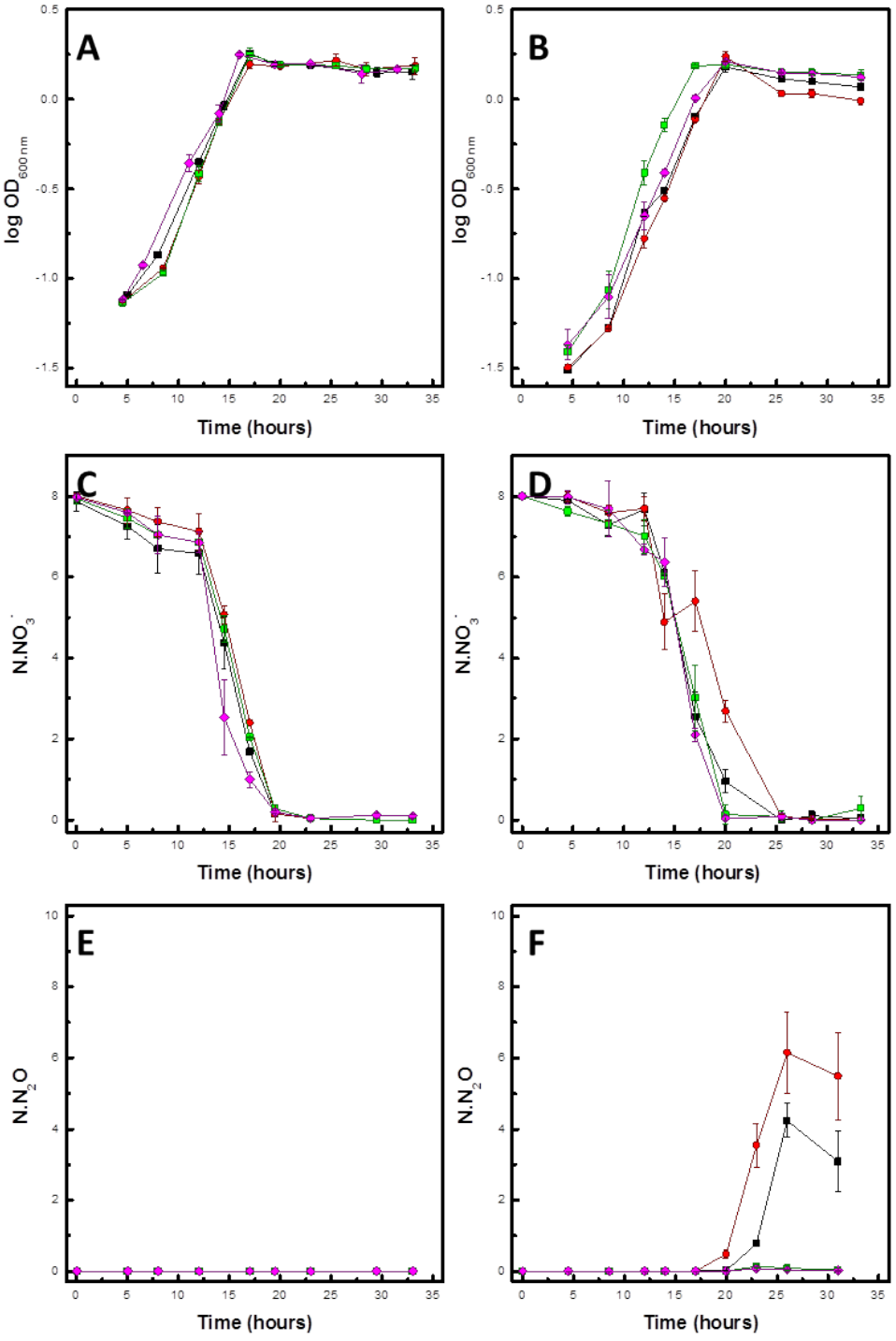

FIGURE 3.6: Growth characteristics of *P. denitrificans* WT (■), Δ*scoB* deletion mutant (●), $ScoB_{FL}$ (■) and $ScoB_{sol}$ (◆) complemented strains in batch culture conditions in the presence of 1 mM taurine. The anaerobic growth is shown in graphs **(A)** and **(B)**. Plots **(C)** and **(D)** represent the consumption of NO_3^- in millimole of N in the form of NO_3^-. **(E)** and **(F)** show N_2O production in millimole of N in the form of N_2O. Cultures shown in the left and right column contained 13.5 and < 0.5 μM of copper, respectively. Standard errors of the mean are indicated by the error bars ($n = 3$).

In a similar way, under anaerobic conditions the growth rate of the strains showed no significant change under copper sufficient (e.g. 0.102 ± 0.009 h^{-1}) and limited conditions (e.g. 0.111 ± 0.007 h^{-1}). Likewise, addition of the inducer to the media did not affect the growth capabilities of the strains (e.g. copper sufficient, 0.111 ± 0.017 h^{-1} and copper limited, 0.119 ± 0.022 h^{-1}) (figures 3.5 and 3.6 A and B). Moreover, all the nitrate was completely depleted throughout the growth without any remarkable difference in terms of rate of consumption between the strains (figures 3.5 and 3.6 C and D).

The most interesting result came from the analysis of N_2O production of the cultures. When sufficient extracellular copper concentration was present in the media no N_2O was detected independently of the addition of the inducer (figures 3.5 and 3.6 E). However, in copper depleted media and in the absence of inducer, Δ*scoB* mutant and the complemented strains accumulated N_2O above WT levels (figures 3.5 F). The excess of N_2O observed in Δ*scoB* complemented strains could be brought back to below wild-type levels after the addition of 1 mM taurine (figures 3.6 F) consistent with a higher N_2OR activity.

3.4 Soluble ScoB$_{sol}$-6His purification

Recombinant soluble ScoB protein was expressed and purified from whole cell extracts of *P. denitrificans*. The soluble fraction was applied to a Ni^{2+} IMAC column (Figure 3.7 A) and two main peaks were detected in the elution chromatogram. These two peaks corresponded with a 37 and 25 kDa band in a SDS-PAGE gel, that were confirmed by mass spectrometry as wild-type PCuC (PCuC$_{WT}$) and ScoB$_{sol}$, respectively. For the next step of the purification, the fractions containing both proteins were combined, reloaded into an anion exchange column and eluted with a gradient of salt. Once more, the chromatogram revealed the presence of two main species and the gel showed that the order of elution had reversed, ScoB$_{sol}$ eluted first followed by PCuC$_{WT}$ (Figure 3.7 B). For the final step of the purification, the fractions containing both proteins were combined, concentrated and loaded onto

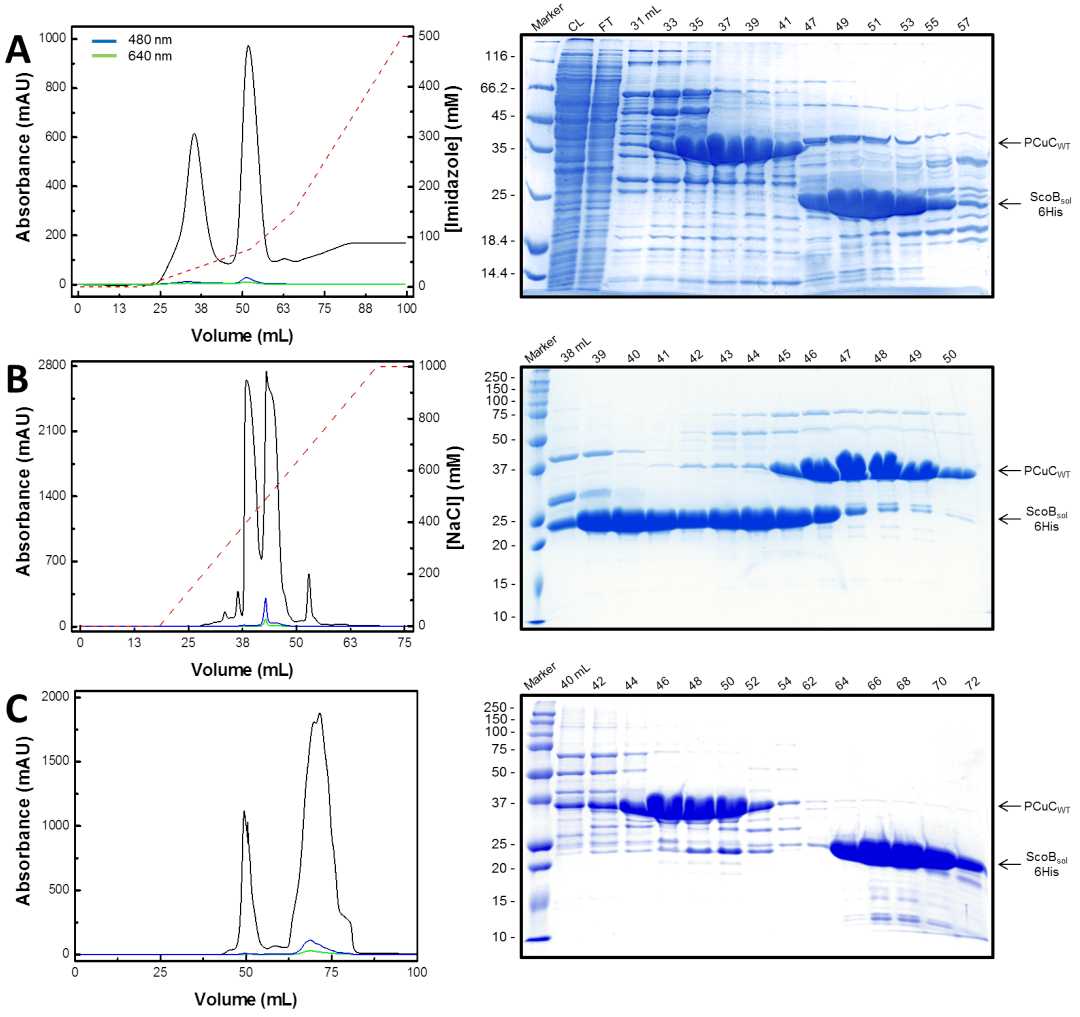

FIGURE 3.7: Steps of the purification of $ScoB_{sol}$-6His. Chromatograms and SDS-PAGE gels of **(A)** Ni^{2+} IMAC purification, **(B)** anion exchange chromatography and **(C)** Size exclusion chromatography.

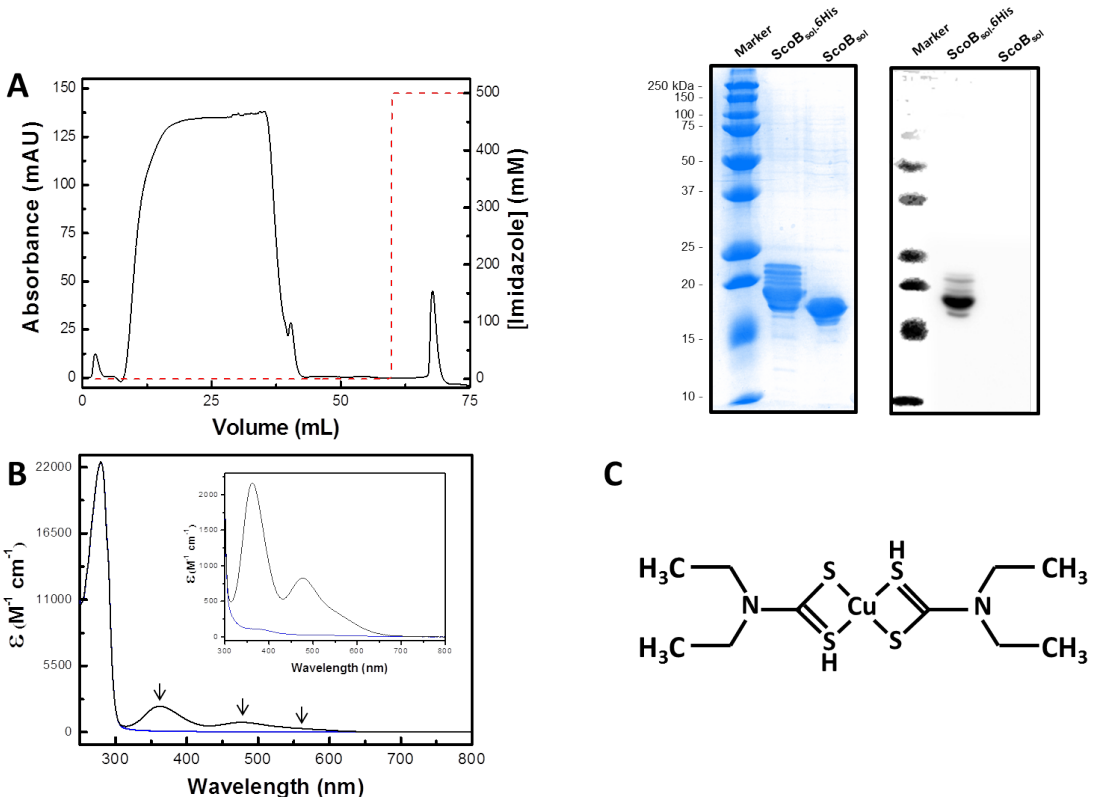

FIGURE 3.8: Cleavage of affinity tag and apo-$ScoB_{sol}$ generation. **(A)** Enterokinase digestion $ScoB_{sol}$-6His and western-blot of the cleaved and uncleaved forms using anti-6His primary antibody. **(B)** Representative UV-vis spectrum of $ScoB_{sol}$ as purified (-) and apo-$ScoB_{sol}$ (-). The arrows indicate the position of the absorbance peaks of a type 2 red copper protein.**(C)** Chemical structure of the copper bound form of DETC.

a gel filtration column which was successful in resolving both proteins as judged by the chromatogram and SDS-PAGE gels (Figure 3.7 C). An average yield of approximately 2.5 mg of purified $ScoB_{sol}$ protein was obtained from 18 L batch culture. Recombinant $ScoB_{sol}$-6His contained an unique enterokinase cleavable sequence in order to facilitate the removal of the histidine tag after purification.

Samples of $ScoB_{sol}$-6His were incubated with enterokinase (NEB) and uncleaved protein was separated by applying the protease reaction mixture to a Ni^{2+} IMAC column. The cleaved form was collected in the flow through while the uncleaved form was retained and eluted with 500 mM imidazole (Figure 3.8 A).

The protein as purified showed an spectrum characteristic of type 2 red copper proteins (Figure 3.8 B) with peak absorbance present at 363, 467 and 565 nm that have been attributed to arise from S(Cys)-Cu^{2+} charge transfer band [201, 202]. Apo-$ScoB_{sol}$ was generated as described in section 2.14 [203] after treatment with diethyl-dithio-carbamate (DETC) as deduced from the spectrum from Figure 3.8 B.

3.5 UV-visible absorbance and fluorescence spectroscopy characterisation of copper binding to $ScoB_{sol}$

To determine whether ScoB binds Cu^{1+} and/or Cu^{2+} and how many copper equivalents is able to bind, reduced apo-ScoB was titrated with solutions of either CuCl or $CuSO_4$. When apo-ScoB was titrated with Cu^{1+} high energy absorbance bands (below 280 nm) appeared due to S(Cys)→Cu ligand to metal charge transfer (LMCT) transitions [204, 205]. The absorbance increase at 250, 260, 270, 290 nm was plotted as a function of Cu^{1+} per $ScoB_{sol}$ and showed a linear increase up to one copper equivalent above which the absorbance stopped increasing and remained constant (Figure 3.9 A and B). The copper-binding behaviour of $ScoB_{sol}$ was also followed by fluorescence spectroscopy. Since $ScoB_{sol}$ contains two tryptophans when

excitation is applied at 295 nm intrinsic tryptophan fluorescence is observed from the protein which can be used to follow metallation that causes a quench in fluorescence [206]. Excitation of reduced apo-$ScoB_{sol}$ at 295 nm gave rise to an emission spectra with a maxima at 336 nm. A plot of the fractional fluorescence against Cu^{1+} concentration over $ScoB_{sol}$ shows that the addition of Cu^{1+} quenched 60 % of the fluorescence linearly with a clear inflection point at one copper equivalent, and subsequent additions of Cu^{1+} did not affect the fluorescence emission spectrum (Figure 3.9 C and D).

By contrast, additions of Cu^{2+} to reduced apo-$ScoB_{sol}$ gave rise to high (below 280 nm) and low energy bands (peak absorbance present at 363, 467 and 565 nm, as previously mentioned) that have also been attributed to S(Cys)→Cu LMCT transitions [201, 202, 204, 205]. Increase in absorbance at 363 nm observed in response to copper additions was plotted as a function of Cu^{2+}/$ScoB_{sol}$ and showed again a distinctive copper-binding phase up one copper equivalent (Figure 3.10 A and B). Binding of Cu^{2+} was also followed by fluorescence spectroscopy during titrations. Excitation at 295 nm also gave an emission spectrum with a maximum at 336 nm. Addition of Cu^{2+} quenched 80 % of the fluorescence in a similar fashion as Cu^{1+}, but with the particularity that it showed a blue shift of λ_{max} from 336 to 322 nm with increasing concentrations of Cu^{2+} (Figure 3.10 C and 3.11). This deviation is indicative of a conformational change of $ScoB_{sol}$ that shifts the Trp residues towards a more hydrophobic environment [207]. Both Cu^{1+} and Cu^{2+} UV-vis and fluorescence spectroscopy titrations are consistent with a 1:1 stoichiometry.

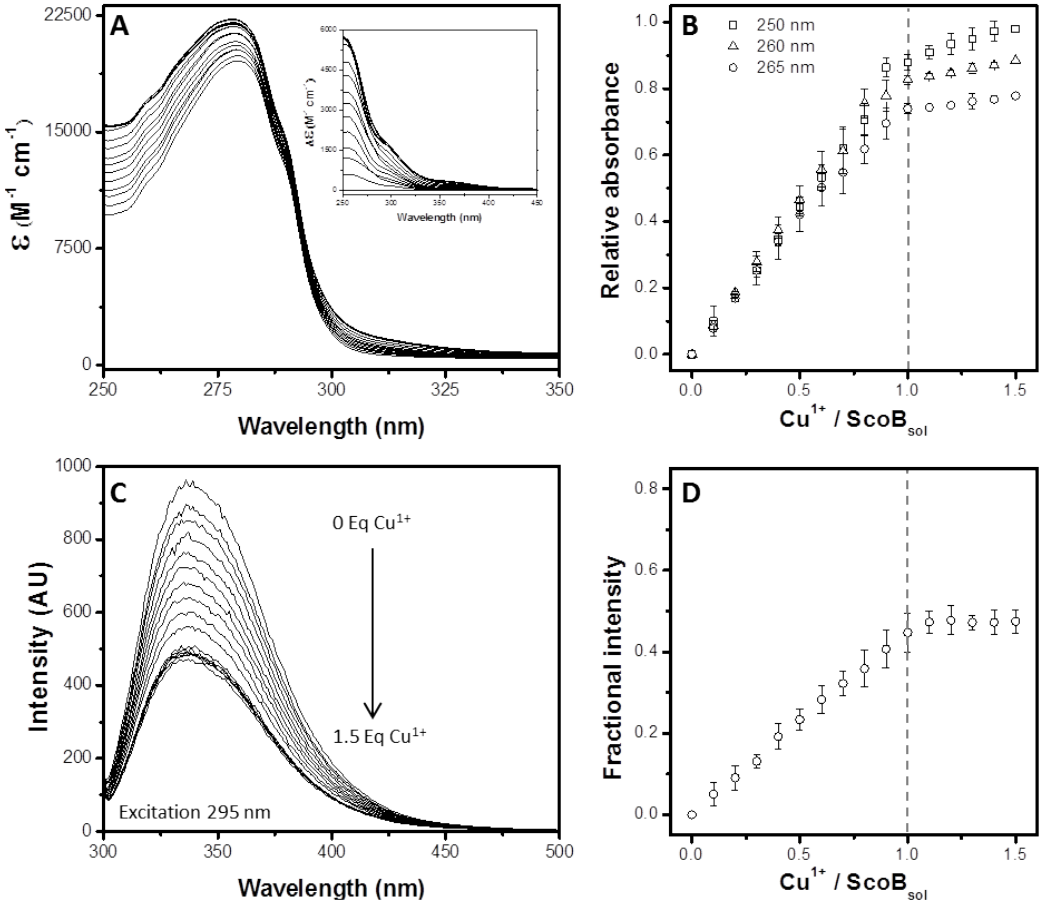

FIGURE 3.9: Absorbance and fluorescence studies of Cu^{1+} binding by reduced apo-$ScoB_{sol}$. **(A)** UV-visible absorbance spectra following the addition of 0 - 1.5 Cu^{1+} ions per protein; **(B)** Plot of absorbance changes at 250 (□), 260 (△) and 265 nm (○) as a function of Cu^{1+} per $ScoB_{sol}$; **(C)** Fluorescence quench of the tryptophan emission peak in response to increasing concentrations of copper (excitation wavelength of 295 nm); **(D)** Plot of the maximal fractional fluorescence intensity as a function of Cu^{1+} per $ScoB_{sol}$. The concentration of $ScoB_{sol}$ was determined using the colorimetric Bradford reagent as 70 μM in 100 mM MOPS and 150 mM NaCl, pH 7.5. Standard errors of the mean are indicated by the error bars ($n = 3$).

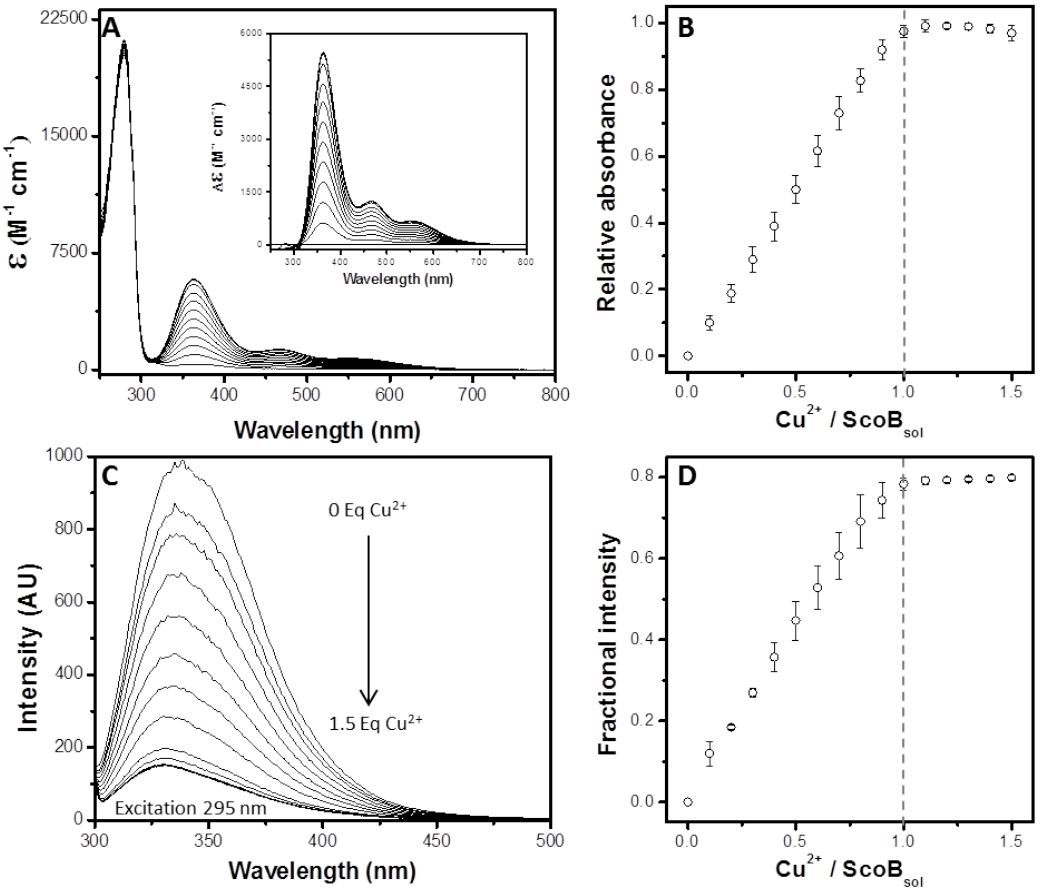

FIGURE 3.10: Absorbance and fluorescence studies of Cu^{2+} binding by reduced apo-$ScoB_{sol}$. **(A)** UV-visible absorbance spectra following the addition of 0 - 1.5 Cu^{2+} ions per protein; **(B)** Plot of absorbance changes at 365 nm (○) as a function of Cu^{2+} per $ScoB_{sol}$; **(C)** Fluorescence quench of the tryptophan emission peak in response to increasing concentrations of copper (excitation wavelength of 295 nm); **(D)** Plot of the maximal fractional fluorescence intensity as a function of Cu^{2+} per $ScoB_{sol}$. The concentration of $ScoB_{sol}$ was determined using the colorimetric Bradford reagent as 70 μM in 100 mM MOPS and 150 mM NaCl, pH 7.5. Standard errors of the mean are indicated by the error bars ($n = 3$).

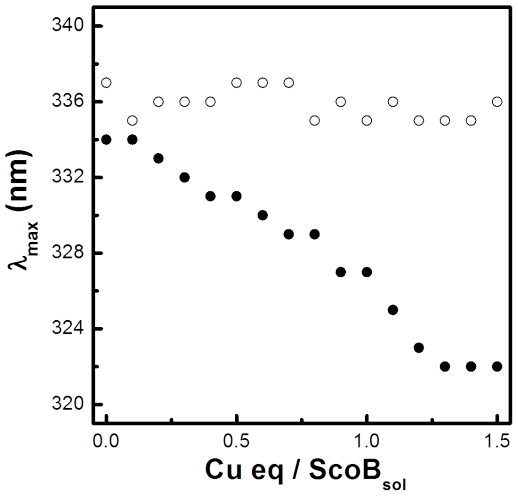

FIGURE 3.11: Copper binding solvatochromic effect of $ScoB_{sol}$. The position of λ_{max} of the emission peak remains $\sim$ 336 nm upon Cu^{1+} binding to $ScoB_{sol}$ (○), while Cu^{2+} binding shits the position $\sim$ 14 nm (●) towards the blue region

3.6 Investigating the solution state of $ScoB_{sol}$

The effect of Cu^{1+} and Cu^{2+} binding on the oligomeric state of reduced apo-$ScoB_{sol}$ was studied by sedimentation equilibrium analytical ultracentrifugation (AUC). Samples of $ScoB_{sol}$ containing 0.0, 0.5, 1.0 and 1.5 Cu^{1+} or Cu^{2+} equivalents per protein were prepared and sedimentations experiments performed at 10,000, 20,000 and 30,000 rpm. The data was plotted as a function of the absorbance at 280 nm versus the square of the radial distance of the sample at any position within the cell (r) minus the square of the radial position at a reference point (r^2_{ref}) (Figure 3.12 A and B). The data were fit to a single-component model shown as solid lines. The residual difference between the experimental data and the fitted curve were also shown. The calculated molecular mass of $ScoB_{sol}$ was 20,018 $\pm$ 2,485 Da which is in agreement with the theoretical mass (20,668 Da) and indicates that $ScoB_{sol}$ is a monomeric protein irrespective the concentration and redox state of copper.

In order to use a different technique to further validate the effect of copper loading on the oligomeric state of $ScoB_{sol}$ analytical size exclusion chromatography (ASEC) experiments were performed. Figures 3.13 A and B show the elution chromatograms of apo-$ScoB_{sol}$ and Cu^{2+}-$ScoB_{sol}$. Note that the copper binding to $ScoB_{sol}$ in Figure

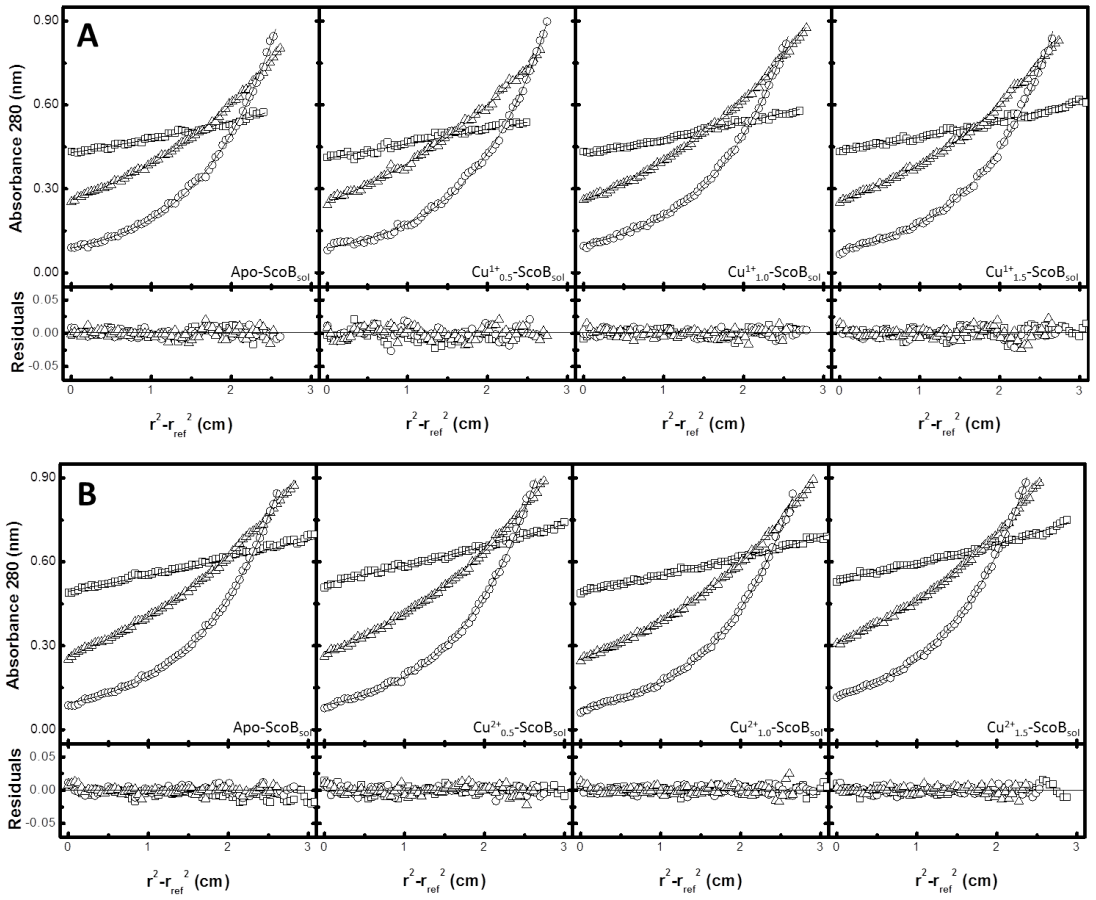

FIGURE 3.12: Effect of copper on the sedimentation equilibrium of $ScoB_{sol}$. **(A)** The top panel shows the profile of $ScoB_{sol}$ samples prepared with Cu^{1+} and **(B)** the lower panel with Cu^{2+}. Within each panel, the top graph represents the absorbance profiles of $ScoB_{sol}$ (25 μM) at 10,000 (□), 20,000 (△) and 30,000 (○) rpm at 20 °C and the lines the fits to a single-component model. The lower graphs show the residual differences between the experimental data and the fitted curves.

	Cu^{1+}		Cu^{2+}	
Sample	**M_w (kDa)**	**Std**	**M_w (kDa)**	**Std**
Apo-$ScoB_{sol}$	20.7	2.6	18.7	1.0
$Cu_{0.5}$-$ScoB_{sol}$	19.3	3.0	19.5	1.7
$Cu_{1.0}$-$ScoB_{sol}$	20.5	4.2	19.5	1.7
$Cu_{1.5}$-$ScoB_{sol}$	21.5	4.2	20.1	1.9

TABLE 3.1: Calculated M_w of $ScoB_{sol}$ by sedimentation equilibrium analytical ultracentrifugation. Standard errors of the mean of three technical replicates ($n = 3$).

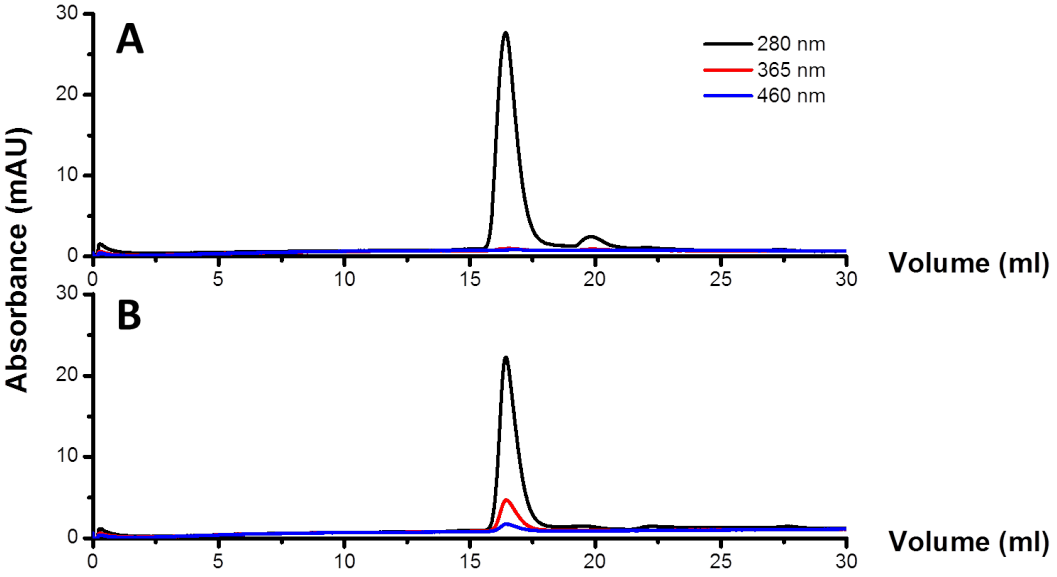

FIGURE 3.13: Analytical size exclusion chromatography of $ScoB_{sol}$. The graph shows the absorbance intensity at 280, 365 and 460 nm against elution volume (ml) of **(A)** apo-$ScoB_{sol}$ and **(B)** Cu^{2+}-$ScoB_{sol}$ (140 μM) in 20 mM HEPES, 150 mM NaCl and 0.25 mM DTT pH 7.

3.13 (B) can be appreciated by the absorbance increase at 365 and 460 nm that is absent in apo-$ScoB_{sol}$. In both cases, a single main peak could be detected at 16.4 mL that correspond to a molecular mass of 29 kDa. This result indicates that copper binding does not affect the oligomerization state of $ScoB_{sol}$, and is therefore consistent with the analytical ultracentrifugation results described in the previous section.

3.7 Small-Angle X-ray scattering of $ScoB_{sol}$

We also characterised the association state and conformation of $ScoB_{sol}$ in solution by small-angle X-ray scattering (see scattering curve in figure 3.14 A). Kratky analysis is often used to qualitatively asses the globularity and flexibility of proteins. Interpretation is based on the asymptotic behaviour of the intensity decay in the Guinier region in a q^2 x $I(q)$ vs. q plot [208]. The scattering profile of $ScoB_{sol}$ produced a bell-shaped plot with an incipient tail at higher q, which indicates that $ScoB_{sol}$ is in overall a globular protein with signs of flexibility (see figure 3.14 B), similar profiles have been found in other thioredoxin-like proteins [209]. The Kratky plot was also used to calculate the volume and molecular weight of $ScoB_{sol}$, since the integrated area of the graph is inversely proportional to the excluded volume of the hydrated particle. A volume of 4,100 $Å^3$ was measured for $ScoB_{sol}$ and a molecular weight and 26 kDa. These values are agreement with the AUC and ASEC results and indicate that $ScoB_{sol}$ is a globular monomeric protein in solution.

Information about the overall size of $ScoB_{sol}$ was obtained from a Guinier plot (Figure 3.14 C) that was generated from the representation of q^2 vs. $logI(q)$ and by making a linear fit at small scattering vectors (limited by q x Rg < 1.3). A radius of gyration (R_g) of 17.6 Å and a forward scattered intensity ($I(0)$) of 6.3 x 10^{-3} was calculated for $ScoB_{sol}$.

The pair-wise distance distribution function was estimated by Fourier inversion of the experimental intensities using Scatter [156]. This is a real space representation

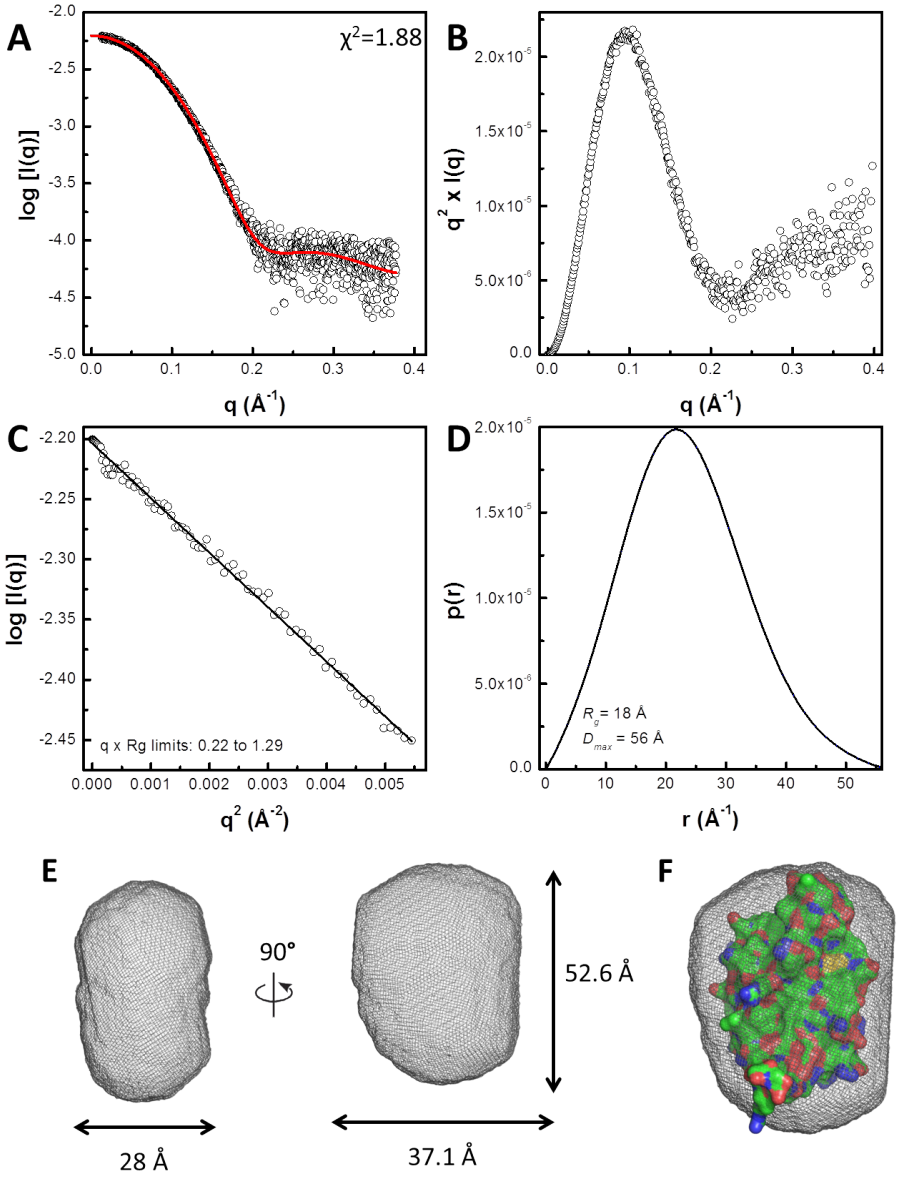

FIGURE 3.14: Solution characterization of $ScoB_{sol}$ by SAXS. **(A)** Scattering curve of $ScoB_{sol}$ and fitting of the calculated scattering curve from the homology model of $ScoB_{sol}$ (red line); **(B)** Kratky plot showing that $ScoB_{sol}$ is a globular protein with signs of flexibility; **(C)** Guinier plot and calculated R_g value; **(D)** P(r) distribution function of $ScoB_{sol}$, R_g and D_{max} values are indicated; **(E)** Front and side view of the overall envelope generated from shape reconstruction using DAMMIF and DAMMIN [210] represented as a grey mesh; and **(F)** homology model of $ScoB_{sol}$ monomer docked into the SAXS envelope using SUPCOMB [161]

of the scattering data which can be used to extract shape features of the particle. P(r) function of $ScoB_{sol}$ generated a bell-shaped profile with a maximum at 21 Å and a D_{max} of 56 Å. Typical globular particles have peak maximums at $D_{max}/_2$, the offset of the peak from 28 to 21 Å might suggest that the overall geometry of $ScoB_{sol}$ is a spheroid with either prolate (elongated) or oblate (flattened) characteristics. The real space R_g from the P(r) function was calculated to be 17.6 Å and is consistent with the reciprocal R_g obtained from the Guinier Plot (Figure 3.14 D).

The theoretical scattering curve for the homology model of $ScoB_{sol}$ was calculated using the software package Scatter [156] and compared to the experimental scattering curve with the program Crysol [164] (Figure 3.14 A). The fit determined in Crysol indicated that the homology model of $ScoB_{sol}$ (generated with the software Phyre2 [145] in intensive mode) is in good agreement with the experimental X-ray scattering data, with a χ^2 of 1.88. As a result, 78 % of the residues were modelled at >90 % of confidence. The predicted model of ScoB was derived from 6 previously described Sco structures with a high confidence (see table A.2 from the appendix section).

The real space distribution can be also used for *ab initio* shape-determination in order to generate a surface envelope of the protein. Initially, an averaged model was generated from 23 different models using the program DAMMIF [159] in slow mode. The averaged model was then used to feed the software DAMMIN [210] for further refinement. The final model contained 1,277 atoms with a total volume of 44,686 $Å^3$ (see figure 3.14 E) which correspond to a protein of 26.3 kDa. Docking of the homology model was achieved using the program SUPCOMB [161].

3.8 Discussion

Sco proteins have been primarily studied in relation to copper metabolism in both eukaryotic and prokaryotic organisms [5, 203] (see table 3.2). In particular, the Sco protein from *T. thermophilus* was found to be required for the maintenance of the correct redox state of the Cu_A centre of cytochrome *c* oxidase before metallation

by PCu_AC [5]. By contrast, nitrous oxide reductase is another copper containing terminal reductase responsible for N_2O consumption in *P. denitrificans*. N_2OR carries two different multi-copper sites, an active site Cu_Z and an electron transfer centre Cu_A. The Cu_Z site of N_2OR is located at the N-terminal domain while the Cu_A site is at the cupredoxin-like C-terminal domain and is structurally similar to the Cu_A site from COX. However, the protein chaperones responsible for the copper insertion into both Cu_Z and Cu_A centres and their mechanism of action still remain unknown. In this work, we have attempted to gain insight into the role of ScoB in the maturation process for N_2OR from *P. denitrificans* which is naturally found encoded in a copper responsive gene cluster (*hypothetical-pcuC-scoB*) [3].

The *in vivo* study of *scoB* mutant conducted under aerobic conditions did not distinguish a significant phenotype compared to the wild-type strain. Interestingly, in a previous study from *P. denitrificans* where *scoB* was mutated they found a decrease in cytochrome *c* oxidase activity under copper limiting conditions that could be rescued by addition of copper [198]. However, the authors did not report if this reduction in activity was also associated with a decrease in growth capacity. Taking both observations together, we consider that the lack of a growth phenotype and the reduction in COX activity in the *scoB* mutant could be potentially explained by the bacterial growth being supported by the activity of cytochrome ba_3 oxidase which expression is increased by 3.7-fold in copper limited aerobic cultures (personal communication from Dr. M. Sullivan). By contrast, during the *in vivo* study carried out under anaerobic conditions and copper limitation ScoB showed to be necessary for the correct functioning of N_2OR. The reduction of N_2O could be rescued by *in trans* complementation of *scoB* (with either full length or periplasmic $ScoB_{sol}$) or by supplementation with copper. It is also worth mentioning the fact that $\Delta scoB$ complemented strains produced even less N_2O than wild-type. This could be due to the fact that production of ScoB under the control of the taurine inducible promoter could reach even higher levels than in wild-type, and therefore being able to scavenge even more copper. Similarly, previous studies from *P. aeruginosa* [211], *R. capsulatus* [212], *S. lividans* [185] and *B. subtilis* [175] showed that mutation of *sco* produced a reduction in

terminal reductase activity in a copper depleted media that could also be recovered by genetic complementation or supplementing growth media copper. The fact that addition of copper to the media is enough to restore the enzymatic activity of the terminal reductase has generally been attributed to two possible factors: spontaneous self-assembly or the possibility that a different protein partner could take the role of assembling the copper centre in the absence of Sco.

The *in vitro* reconstitution of reduced apo-$ScoB_{sol}$ from *P. denitrificans* with copper has shown that the protein can bind one equivalent of either Cu^{1+} or Cu^{2+}. Binding of Cu^{1+} to Sco proteins has been previously demonstrated in human Sco1 and Sco2 [203, 213, 214], *B. subtilis* BsSco [215], *S. lividans* Sco [185, 216] and *T. thermophilus* Sco [5], and it has also been reported for yeast Sco1 [189, 217]. On the other hand, Cu^{2+} binding to Sco proteins has been reported for human Sco1 and Sco2 [203, 213, 214], *S. cerevisiae* Sco1, *B. japonicum* Sco [218], *R. capsulatus* ScoB [212], and *T. thermophilus* Sco [5] and it has only been demonstrated for *B. subtilis* BsSco [215], *S. lividans* Sco [185, 216] and *R. sphaeroides* PrrC [183]. Copper binding to *P. denitrificans* ScoB is vastly tight as deduced from the UV-vis and fluorescence titrations. Since metal–ligand and metal concentrations cannot be simultaneously measured in the reaction with enough accuracy, a K_D of $\sim 10^{-7}$ M has to be used as an upper limit for both Cu^{1+} and Cu^{2+} binding unless titrations in the presence of well-characterised copper chelators of known K_D are performed [154]. An initial exploratory experiment of $ScoB_{sol}$ with Cu^{1+} and the copper chelator BCA resulted in a K_D of $1.50 \pm 0.28 \times 10^{-16}$ (see figure 3.15). This value is within the range of other Sco proteins from the literature that span from 10^{-12} M (e.g. *B. subtilis* BsSco) to 10^{-17} M (e.g. *S. lividans* Sco [218]). However, up to date it has not been reported any Cu^{2+} K_D performed by direct competition using a divalent copper chelator and the only known values are from calorimetric titrations ($K_D \sim 10^{-12}$ M [215]) or stopped-flow ($K_D \sim 10^{-12}$ M [185]) that could be imposing an upper limit to the detection of an accurate K_D.

An additional piece of evidence supporting the role of ScoB as a copper chaperone in *P. denitrificans* comes from the fact that periplasmic recombinant ScoB purified from soluble cell extracts of *P. denitrificans* contained copper ($\sim$ 0.375 equivalents

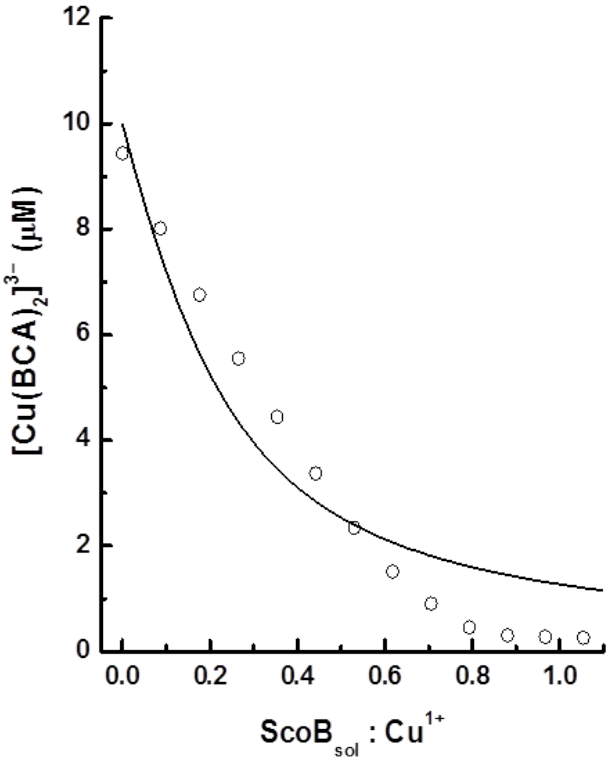

FIGURE 3.15: Estimation of Cu^{1+} binding affinity of $ScoB_{sol}$ at pH 7.5 using the ligand BCA. The plot shows the forward reaction in which $ScoB_{sol}$ was titrated into a solution of $[Cu^{1+}BCA_2]^{3-}$. The graph represents the absorbance changes as a function of $ScoB_{sol}$:Cu^{1+} indicating the binding of Cu^{1+} by $ScoB_{sol}$.

of Cu as calculated from the extrapolation of the Cu^{2+} titration performed in section 3.5). Apo-$ScoB_{sol}$ could be generated for subsequent experiments by incubation with DETC (as described in section 2.14) which is a chelator with a very high affinity for Cu^{1+} [203]. Similarly, other Sco proteins such as human and yeast Sco1 contained copper when they were purified from either bacteria or yeast [189, 219]. The amount of copper bound to *P. denitrificans* ScoB could draw attention since a higher metallation could in theory be expected considering the high affinity of the protein for Cu. A reason for this could be that LB broth used for the overexpression of the protein is in fact Cu-limiting. Another point to have in consideration is the difference between total copper and bioavailable copper within the medium as it has already being suggested in Chapter 2 section 2.1.2.

An interesting observation about Cu^{1+}-$ScoB_{sol}$ is that the UV-vis spectrum does not show any recognisable feature. Therefore, the copper binding can only be followed by the increase of the high energy absorbance bands (e.g. below 280 nm) due to

S(Cys)→Cu LMCT transitions [204, 205]. Alternatively, the UV-vis spectrum of the Cu^{2+} bound form of $ScoB_{sol}$ presents an intense electronic absorption band at 362 nm (ε = 5902 M^{-1} cm^{-1}) due to Sp_{σ}(Cys)→Cu^{2+} LMCT, a lower band at 465 (ε = 1364 M^{-1} cm^{-1}) due to Sp_{π}(Cys)→Cu^{2+} LMCT and a low-energy minor absorption band at 558 nm (ε = 727 M^{-1} cm^{-1}) [201, 202, 204, 205]. The UV-vis spectrum of Cu^{2+}-ScoB is similar to other known Sco proteins [185, 220] and is characteristic of a tetragonal type 2 Cu thiolate [221, 222]. Fluorescence titrations using Cu^{1+} and Cu^{2+} generated a similar result as UV-vis titrations with the interesting remark that the position of λ_{max} of the emission peak of Cu^{2+} shifted $\sim$ 12 nm towards the blue region and the shift was accompanied by a reduction in the intensity (Cu^{1+} quenched 60 % of the fluorescence and Cu^{2+} 80 %). This shift was not observed with Cu^{1+} and is indicative of a conformational change in the protein in which the tryptophan residues move towards a more hydrophobic environment (see figure 3.16) [207]. As it has been described in the introduction, it is known that copper binding drives a conformational change in the protein that alternates between an open and mobile form and a close and rigid form [184, 186]. Therefore, it is possible that the blue shift observed could be indicative of the protein adopting a closed form upon Cu^{2+} binding.

Characterisation of the soluble polypeptide by analytical ultracentrifugation and size exclusion chromatography as well as small angle x-ray scattering indicates that $ScoB_{sol}$ is a monomeric globular protein of 25.2 ± 4.8 kDa, which is a close to the theoretical calculated molecular weight of the recombinant protein (21.5 kDa). Homology $ScoB_{sol}$ model showed reasonable agreement with the SAXS-based *ab initio* envelope. Other recombinant Sco proteins have been found to be monomeric such as *B. subtilis* BsSco [223, 224], human Sco1 and Sco2 [187, 213], *P. putida* Sco [182] and *R. sphaeroides* PrrC [183, 225]. Peculiarly, the oligomeric state of $ScoB_{sol}$ was not altered upon copper binding independently of the redox form of the metal added unlike other known copper binding proteins such as CopA [226] or CopZ [227] that oligomerised in their holo form. However, it is plausible that ScoB may form oligomers *in vivo* driven by the transmembrane region of the protein, in the same way that it is thought to occur in human and yeast Sco proteins

[228, 229]. Anyhow, the oligomeric state of ScoB from *P. denitrificans* does not seem to be relevant for function since $ScoB_{sol}$ was also capable of restoring $\Delta scoB$ denitrification phenotype.

In conclusion, the periplasmic soluble fraction of ScoB ($ScoB_{sol}$) from *P. denitrificans* is a metalloprotein capable of binding a single Cu^{1+} or Cu^{2+} ion. Furthermore, $ScoB_{sol}$ is a monomeric globular protein which does not oligomerise upon copper binding or due to the redox state of the metal bound. The absence of ScoB under copper limiting conditions results in N_2OR inactivation with the consequent accumulation N_2O. However, the activity of N_2OR can be restored by supplementing the media with micromolar levels of copper or by expressing *in trans* ScoB or the periplasmic soluble version of the protein.

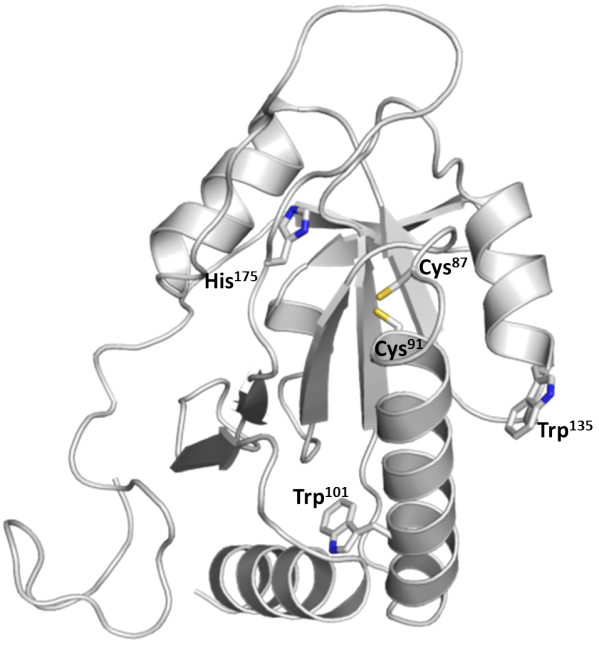

FIGURE 3.16: Cartoon representation of the predicted structure of apo-$ScoB_{sol}$. Copper binding residues and tryptophans have been represented as sticks. The model was generated with the software Phyre2 [145]

Sco protein	Cu^{1+} Binding	Cu^{1+} K_D	Cu^{2+} Binding	Cu^{2+} K_D	Thrx activity
H. sapiens Sco1	Yes	3.1 x 10^{-15} (competition) [203, 214]	Yes [213]	–	No [184]
H. sapiens Sco2	Yes	3.7 x 10^{-15} (competition) [203]	Yes [213]	–	–
S. cerevisiae Sco1	Yes [189, 217]	–	Yes [217]	–	–
		< 1.9 x 10^{-5} (titration) [215]		3.5 x 10^{-12} (DSC) [215]	
B. subtilis	Yes	10^{-12} (competition) [202]	Yes	< 6.5 x 10^{-8} (ITC) [230]	–
		–		Adventitious (titration) [224]	
B. japonicum	–	–	Yes [218]	–	–
P. putida	Yes	Weak (titration) [182]	No [182]	–	Yes [182]
R. capsulatus	–	–	Yes [212]	–	–
R. sphaeroides	–	–	Yes [183, 225]	–	Yes [183]
S. lividans	Yes	4.6 x 10^{-17} (competition)[216]	Yes	$< 10^{-12}$ (stopped−flow) [185]	No [185]
T. thermophilus	Yes	$< 10^{-10}$ (titration) [5]	Yes	–	–

TABLE 3.2: Copper binding properties and thioredoxin activity of known Sco proteins. Abbreviations used: differential scanning calorimetry (DSC); isothermal titration calorimetry (ITC).

4 Biochemical characterisation of PCuC

4.1 Introduction

Neighbouring *scoB* there is another gene within the same gene cluster that encodes a putative periplasmic copper-binding protein termed PCuC (see figure 4.6). In *Paracoccus denitrificans* the N-terminal domain of PCuC is similar to the YcnI protein from *B. subtilis* [4] and is fused through a linker region to a C-terminal domain homologue to PCu_AC (periplasmic Cu_A chaperone protein) from *T. thermophilus* [5, 33]. YcnI proteins are thought to be part of a mechanism for copper acquisition and/or resistance, while PCu_AC proteins have been mainly studied in relation to the maturation process of cytochrome *c* oxidase. In this chapter we focus our attention on the study of *P. denitrificans* PCuC (we use the nomenclature $PCuC_{WT}$ to refer to the native protein and $PCuC_{FL}$ to a full length affinity-tagged recombinant protein expressed in *P. denitrificans*). Specifically, the ability of this protein to bind copper will be investigated and its involvement in the maturation process of nitrous oxide reductase. For this purpose we have studied the biochemical characteristics of each domain of PCuC individually as well as the properties of the full-length protein.

4.1.1 The novel two-domain fusion protein PCuC

YcnI and PCu_AC are two different types of proteins involved in copper metabolism that typically occur as single domain proteins in a range of organisms (i.e. 656 and 1687 sequences predicted as YcnI and PCu_AC single domain polypeptides, respectively; as deposited in Pfam by July 30, 2018). However, they may also be found combined with other known copper-binding proteins such as Sco, CopC and CopD (see figure 4.1). Importantly, there are at least 76 examples where they are encountered fused together as a two-domain YcnI-PCu_AC protein configuration, such as that present in *P. denitrificans*. A phylogenetic analysis of non-redundant PCuC sequences revealed that the overwhelming majority of the organisms that carry a copy of a *pcuC* gene are Gram-negative bacteria that belong to the phylum proteobacteria. Within proteobacteria, 92 % are members of the alphaproteobacteria group with just 8 % representatives among betaproteobacteria. Of the alphaproteobacteria microorganisms, the three most abundant groups were rhizobiaceae, methylobacteriaceae and hyphomicrobiaceae, while all betaprotebacteria belonged to the burkholderiales. A further inspection of the genome of these organisms revealed that 96 % of them contained a gene in their genome that codes for a Cu_A containing protein, of which 17 % where N_2OR (see figure 4.2).

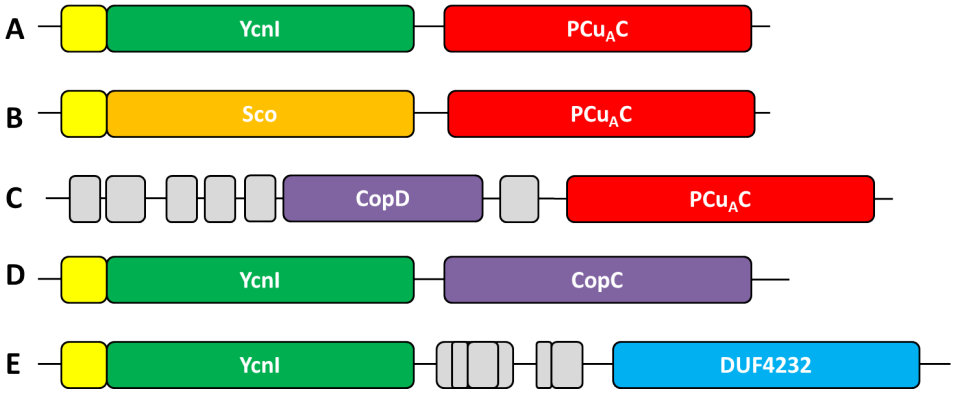

FIGURE 4.1: Representation of the domain configuration of YcnI and PCu_AC proteins. Examples of each type of protein can be found in **(A)** *P. denitrificans*, **(B)** *Gemmatimonas aurantiaca*, **(C)** *Sphingomonas hengshuiensis*, **(D)** *Conexibacter woesei* and **(E)** *Arthrobacter nitrophenolicus*. The yellow boxes represent the signal peptide sequence and the grey boxes transmembrane regions.

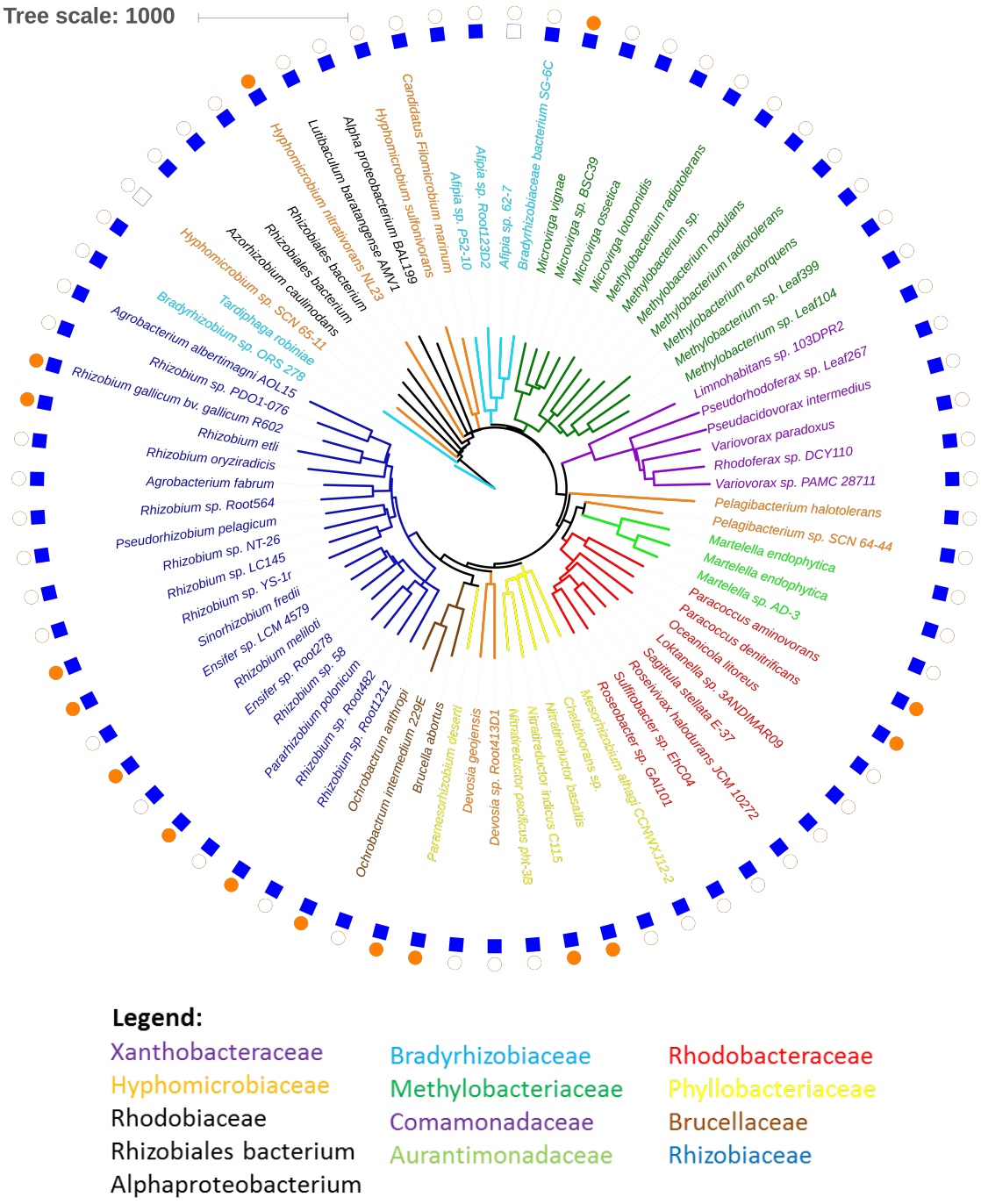

FIGURE 4.2: Cladogram of PCuC proteins. Identified species are shown for each entry, blue boxes represent the presence of a cytochrome *c* oxidase subunit II gene and the orange circles the presence of a N_2OR gene. The maximum likelihood tree was constructed with the software Jalview [193] and the cladogram was drawn with the on-line program iTOL [231]

This represents a good correlation between YcnI-PCu$_A$C and potential N_2O reducing bacteria.

Further inspection of the neighbouring genes of 15 representative organisms that belong to the principal families shown in figure 4.2 revealed that in all cases *pcuC* is preceded by a small hypothetical gene (see figure 4.3) homologous to Pden_4445 (Uniprot ref. A1BAG5) from *P. denitrificans*. This hypothetical gene codes for a putative protein of $\sim$ 130 amino acids of unknown function and together with *pcuC* is frequently found forming a binomial *hyp-pcuC* gene cluster. However, it is not unusual to encounter a *tonB*-dependent transporter gene located between the hypothetical gene and *pcuC*, or either a *sco* and another pcu_AC gene at the end of the gene cluster. The putative product of the hypothetical gene is predicted to be a membrane-anchored protein that is fixed to the cell membrane by an N-terminal transmembrane region spanning residue 21 to 38 according the program PRED-TAT [232]. The amino acidic composition of the putative hypothetical protein is rich in alanine, leucine and proline residues. A multiple sequence alignment of hypothetical protein reveals the presence of three conserved cysteine residues (Cys^{73}, Cys^{100} and Cys^{103}) in what seems to be a CX$_{27}$CX$_2$C motif, which could also potentially bind copper and a rich proline region at the C-terminus of the protein (see figure 4.4). However, attempts to overexpress Pden_4445 in *P. denitrificans* using the low-copy number plasmid pLMB509 [147] have so far been unsuccessful.

As described above, *P. denitrificans* PCuC is a novel two-domain protein and this is clearly apparent through a multiple sequence alignment analysis (see figure 4.5). The YcnI N-terminal domain comprises approximately the first 190 amino acids and the PCu$_A$C C-terminal domain nearly 170 amino acids. Within the N-terminal domain two histidine and two cysteine residues (His^{28}, His^{50}, Cys^{52}, Cys^{145}) are conserved within a putative HX$_{21}$HXCX$_{93}$C motif that could potentially bind copper. In addition, the C-terminal domain contains the well-defined H(M)X$_{10}$MX$_{21}$HXM motif present in PCu$_A$C proteins [33]. The gene product of *pcuC* from *P. denitrificans* is also predicted to be a Sec substrate and thus exported to the periplasm. The most likely cleavage site is located at position 1 - 29 accor-

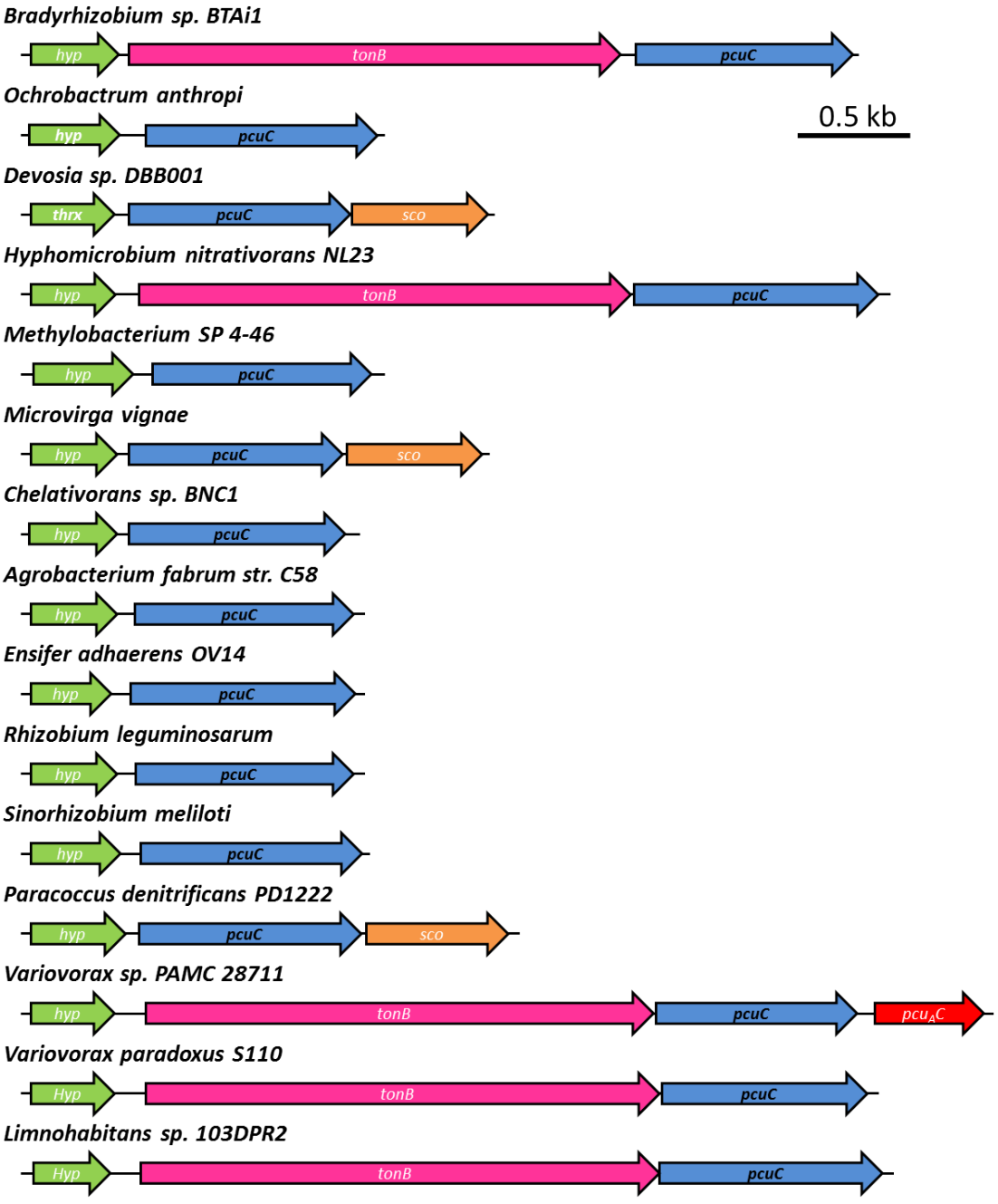

FIGURE 4.3: Overview of the gene neighbourhood of *pcuC* genes in bacteria. The gene clusters of 15 representative organisms that belong to the principal families shown in figure 4.2 have been represented.

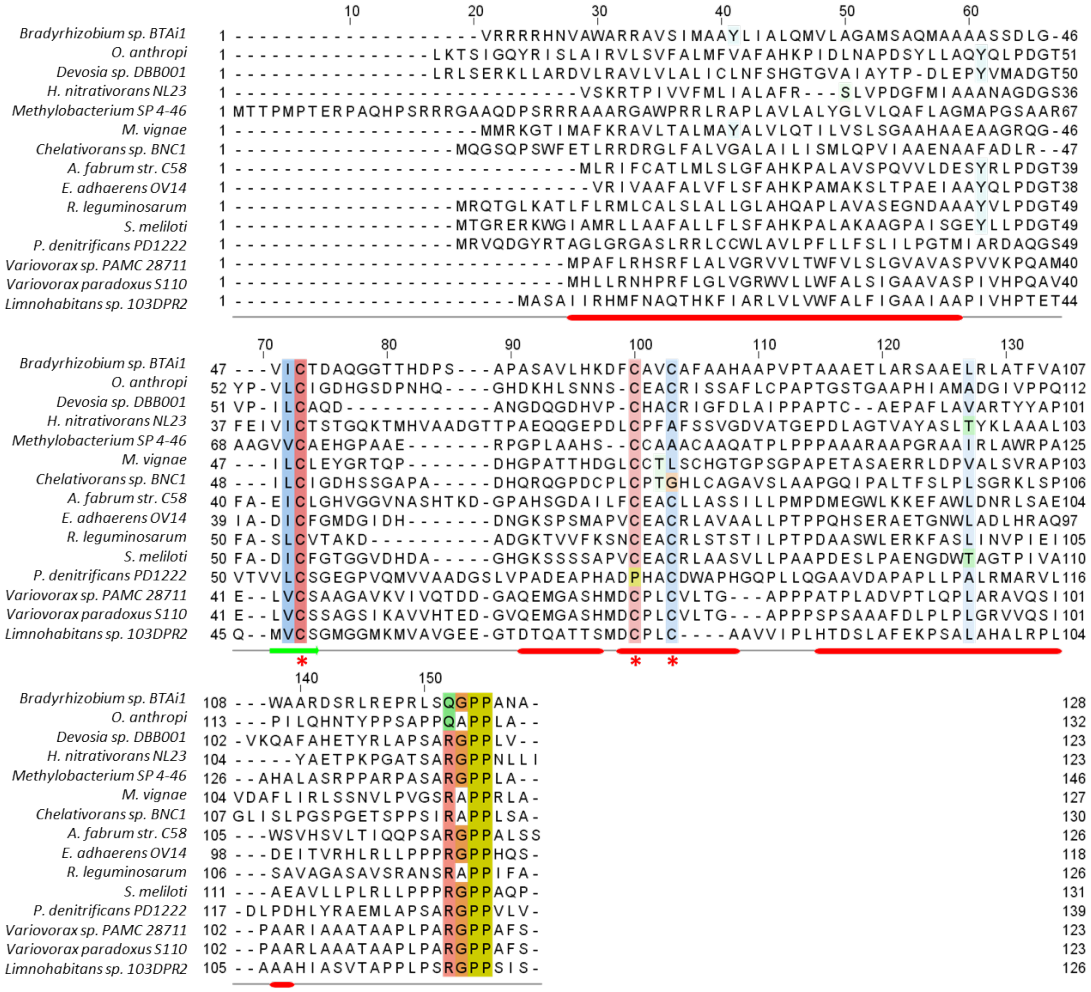

FIGURE 4.4: Multiple sequence alignment of hypothetical gene products homologous to Pden_4445 using the program Jalview [188]. Conserved residues have been coloured using Clustal X colour scheme (see appendix A.1) and conserved cysteines are highlighted using the symbol (⋆). Below the alignment the secondary structure prediction of *P. denitrificans* hypothetical gene product has been displayed, green arrows represent β-strands and red bars the α-helices.

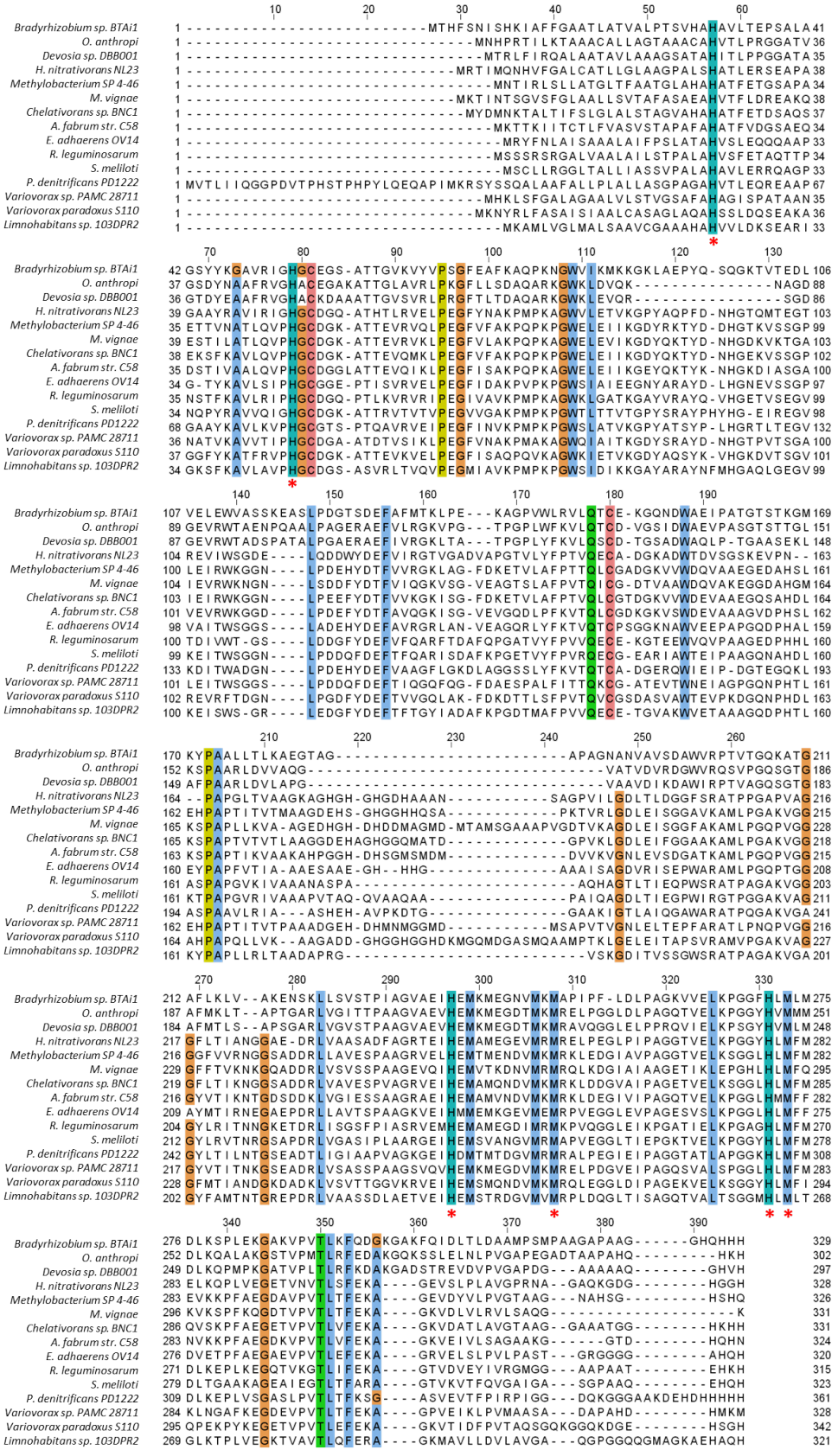

FIGURE 4.5: Multiple sequence alignment of PCuC proteins using the program Jalview [188]. Conserved residues have been coloured using Clustal X colour scheme (see appendix A.1) and conserved copper-binding residues are highlighted using the symbol (⋆)

ding to the program PRED-TAT [232]. Consequently, the mature protein would consist of a polypeptide of $\sim$ 300 amino acids with two domains connected through a linker region. This bridging region has a length of $\sim$25 residues and is rich in glycines ($n = 7$), alanines ($n = 5$) and histidines ($n = 4$).

A BLAST search using *B. subtilis* YcnI or *T. thermophilus* PCu_AC amino acid sequences (Uniprot ref. YCNI_BACSU and Q5SGY7, respectively) as a query resulted in the identification of three different proteins. Firstly, a gene encoding a PCu_AC-like single domain protein (Pden_0519, Uniprot ref. A1AZD7) within chromosome one. Secondly, a YcnI-PCu_AC two-domain protein encoded in chromosome two (Pden_4444, Uniprot ref. A1BAG4) which is the main focus of this chapter. Thirdly, a YcnI-like single domain protein (Pden_5009, Uniprot ref. A1BC25) encoded within the megaplasmid of *P. denitrificans* (see figure 4.6 A). Both, the predicted mature single-domain YcnI protein and the N-terminal YcnI-containing domain of PCuC have a pairwise sequence identity and similarity of 35.2 and 33.0 % as calculated from a multiple sequence alignment generated using the MUSCLE algorithm within the software package Jalview [193] and the on-line service SIAS [194] (see figure 4.6 B). While mature single-domain PCu_AC and the C-terminal domain of PCuC have a relatively higher pairwise sequence identity and similarity of 40 and 47 % (see figure 4.6 C).

The two-domain PCuC protein is encoded within the *hypothetical-pcuC-scoB* gene cluster that has been described in section 3.2 (see figures 3.3 and 4.6). In contrast, the gene encoding the single-domain YcnI protein is found within a considerably large gene cluster that encodes components for an acyl-CoA dehydrogenase, an alkane monooxygenase, an ABC transporter and a *copCD* gene. Similarly, other copper resistance genes are often located in megaplasmids that confer copper resistance to the microorganism such as CopC that is encoded in pPT23D plasmid in *Pseudomonas syringae* [71, 233]. Moreover, the single-domain pcu_AC gene is encoded within a putative *hypothetical-sod-*pcu_AC*-lipase-copA* gene cluster. An analysis using the program SignalP [200] predicted PCu_AC as a cytosolic protein, alternatively the software Phobius [199] and PRED-TAT [232] detected the presence

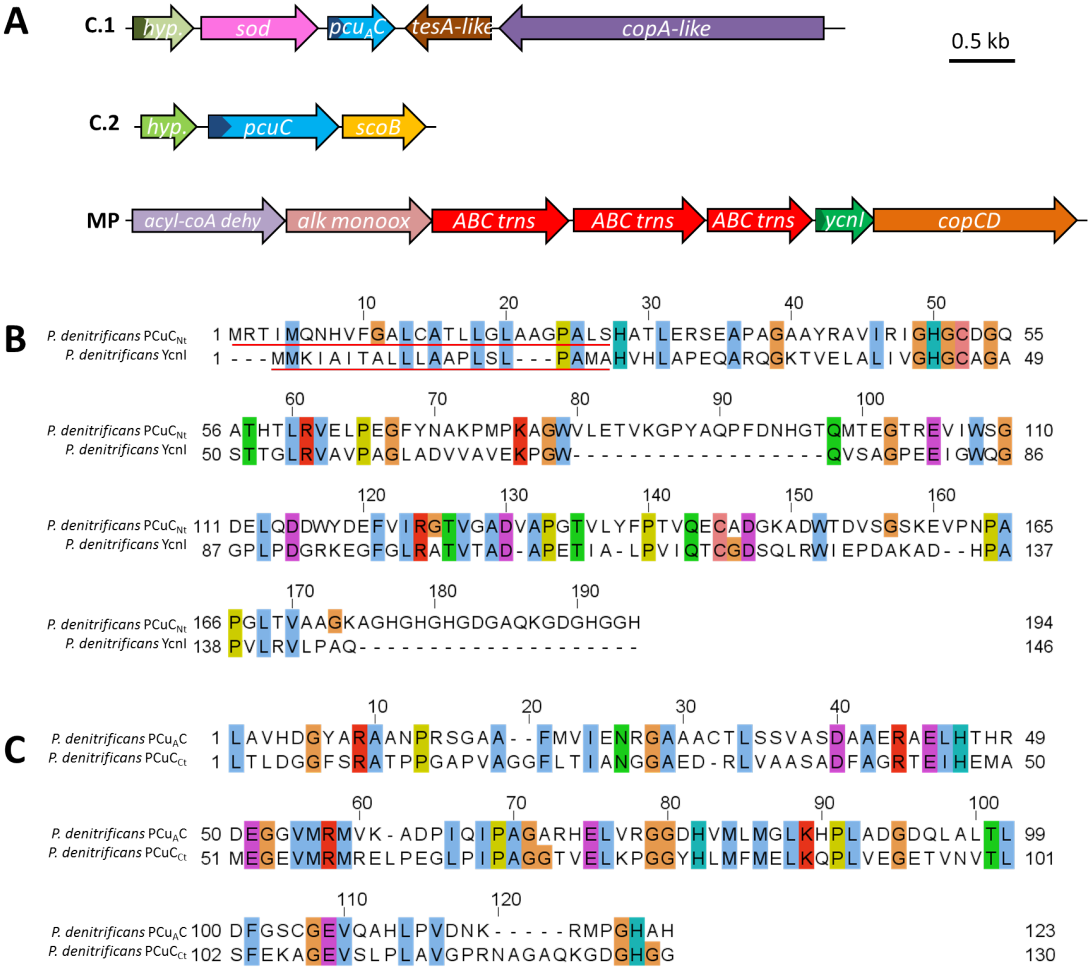

FIGURE 4.6: Properties of YcnI and PCu_AC domain containing proteins from *P. denitrificans*. **(A)** Gene clusters of pcu_AC, *pcuC* and *ycnI*. **(B)** Sequence alignment of YcnI proteins from *P. denitrificans* using the program Jalview [188]. The location of signal peptide has been underlined in red. **(C)** Sequence alignment of matured single-domain PCu_AC protein and C-terminal domain of PCuC, numbering is relative to the position of the first residue of processed PCu_AC. Conserved residues have been coloured using Clustal X colour scheme (see appendix A.1).

of a Sec leader sequence. The most likely cleavage site was identified between residues 29 to 53 and would result in a mature protein of 123 amino acids. The hypothetical gene found within the same gene cluster is also predicted to be exported to the periplasm through the Sec system although its function is unknown. Downstream of the hypothetical gene, there is a gene that codes for a putative cytoplasmic Fe/Mn-type superoxide dismutase probably involved in detoxification and protection against cell damage caused by reactive species of oxygen [234]. Divergently transcribed to *pcu$_A$C* there is a putative *tesA* gene that codes for a periplasmic protein similar to the well-characterised TesA from *Escherichia coli*. TesA is a lipase with thioesterase, esterase, arylesterase, protease and lysophospholipase activity [235]. Upstream of *tesA*, there is also a putative Cu^{2+}-exporting ATPase that shows sequence homology to the copper resistance protein CopA [236].

Importantly, Sullivan and co-workers observed in a transcriptomic study from *P. denitrificans* that the expression of the whole gene cluster where the *pcuC* gene is encoded was sensitive to extracellular copper concentration [3]. In addition, the three genes of this short gene cluster (*hypothetical*, *pcuC* and *sco*) had a crucial role in achieving correct N_2OR activity in a copper depleted media [3]. Shortly after, Dash and co-authors found that deletion strains of *pcuC* (Pden_0519) and *pcu$_A$C* (Pden_4444) genes had no apparent effect on cytochrome *c* oxidase activity [198]. Interestingly, inspection of the transcriptomic data of Sullivan *et al.* showed that the gene clusters of YcnI and PCu_AC were constitutively expressed irrespective of copper concentration.

4.1.2 The N-terminal YcnI domain of PCuC

Overall the literature concerning YcnI-like proteins is rather scarce. Currently no more than six or seven research studies can be found where a reference to a YcnI protein or a protein containing the domain of unknown function 1775 (DUF1775) is mentioned. The first record of an YcnI protein in the literature is given in 2008 by Karlsen *et al.* who identified the first YcnI type of protein called 'MCA0347' as

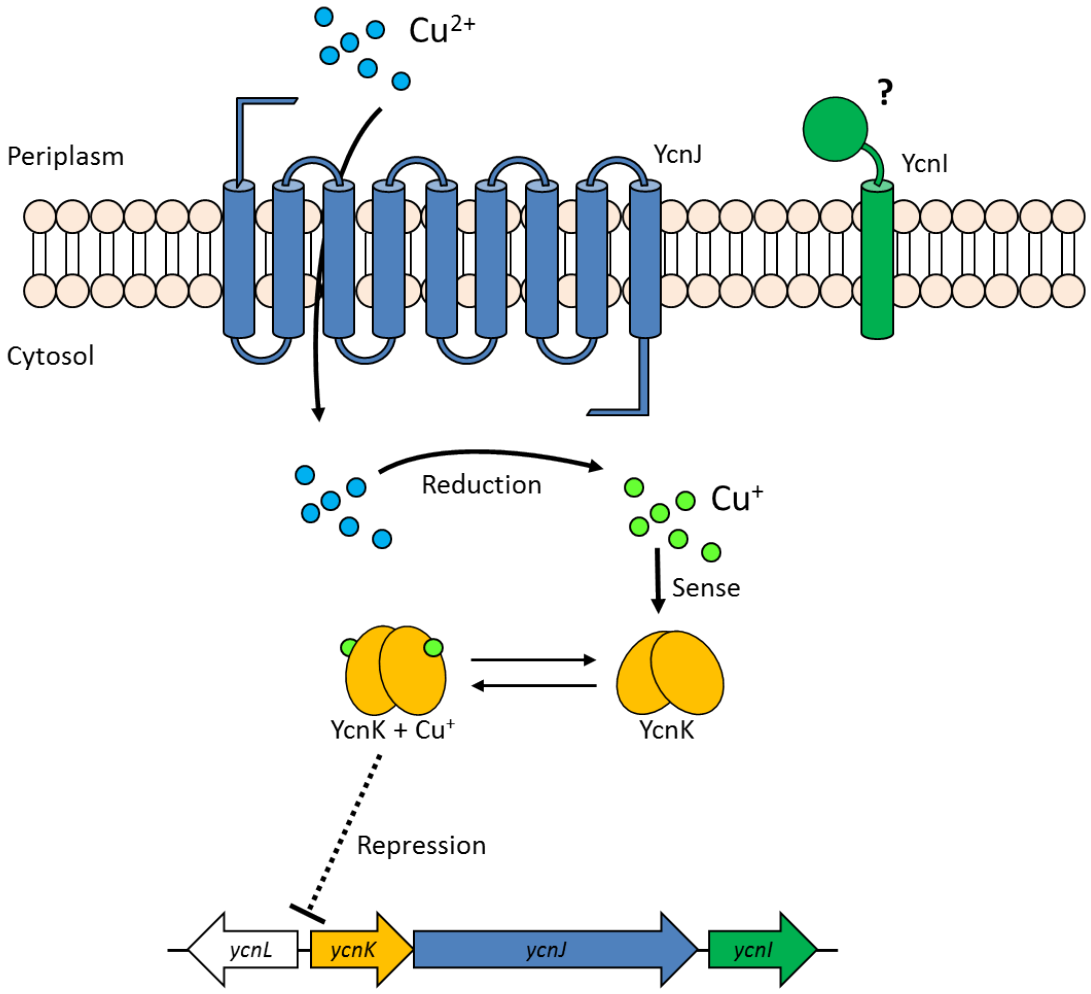

FIGURE 4.7: Proposed mechanism of action of YcnLKJI in *Bacillus subtilis*. Adapted from Hirooka *et al.* [237]

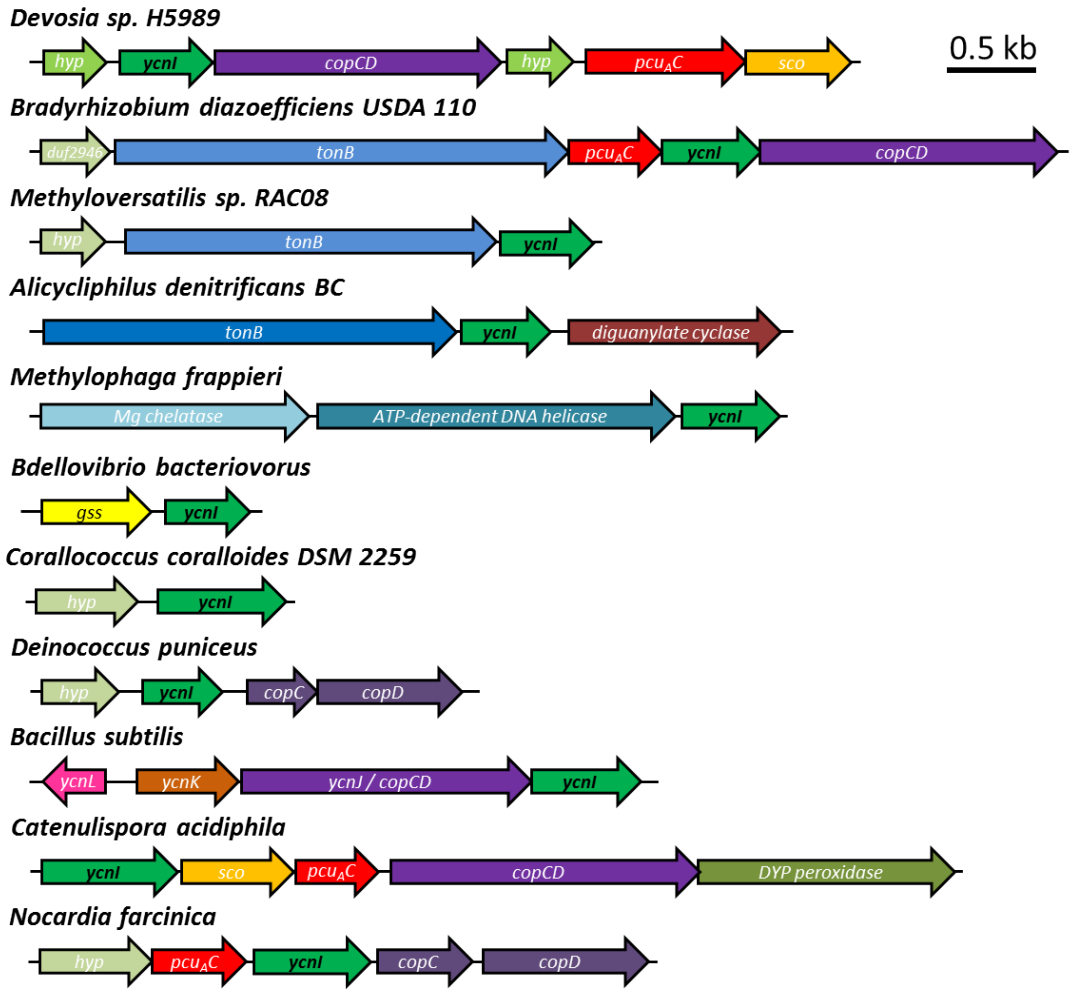

FIGURE 4.8: Overview of the gene neighbourhood of *ycnI* genes in bacteria. Abbreviations used, *hyp*: hypothetical gene, *gss*: glutathione synthetase.

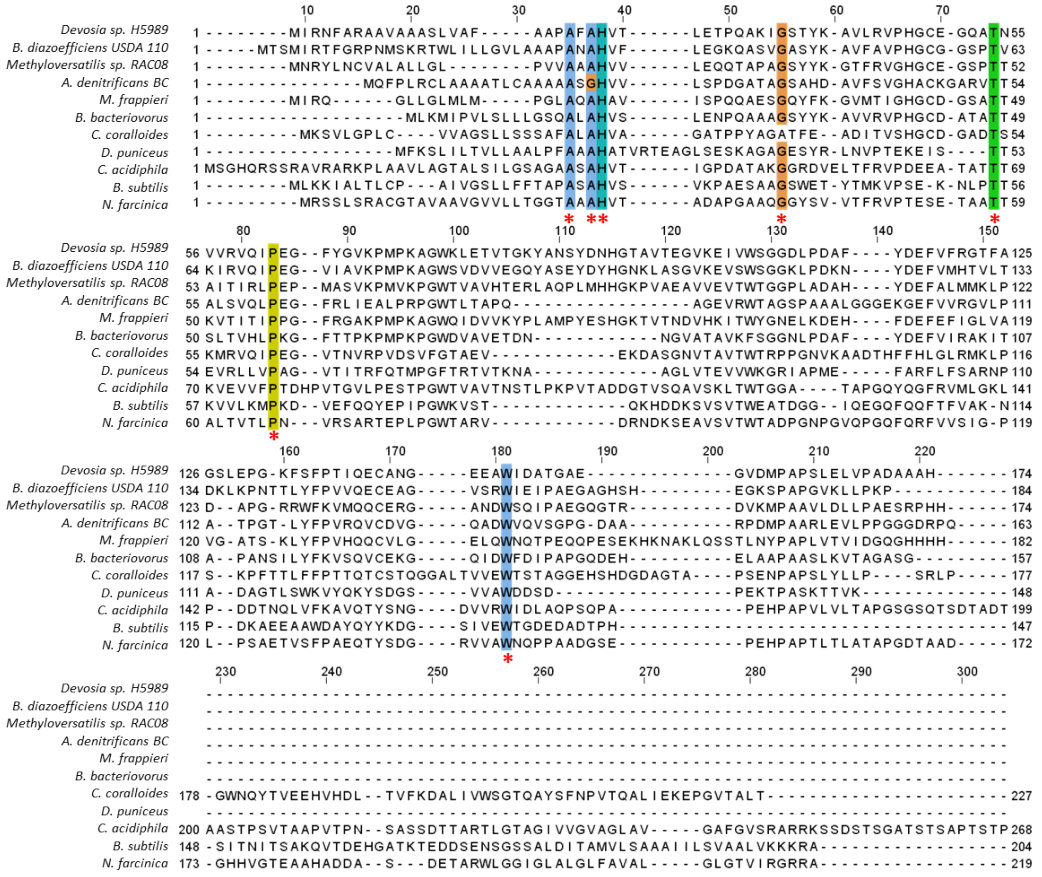

FIGURE 4.9: Multiple sequence alignment of YcnI proteins using the program Jalview [188]. Conserved residues have been coloured using Clustal X colour scheme (see appendix A.1) and conserved residues are highlighted using the symbol (⋆)

part of the surfactome of the methanotrophic bacterium *Methylococcus capsulatus* (Bath) at low copper concentrations [238, 239]. Later, Chillippagari and co-workers described the presence of the *ycnI* gene within a copper-import system in *B. subtilis* although its function was not determined [4]. Serventi *et al.* identified an *ycnI*-like gene present in a copper-responsive gene cluster that also contained a pcu_AC and a *copCD* gene [240]. The most recent mention is from Akanuma and co-authors, where SGR3624, another YcnI homologue, was identified in enriched membrane fractions from *Streptomyces griseus*. SGR3624 was found to be co-transcribed with a Sco protein and showed a delayed growth in solid medium [241]. Of these three organisms, the system of *B. subtilis* is the one that has been studied in most detail.

The *Bacillus* YcnI protein is encoded within a gene cluster that is up-regulated under copper-limiting conditions and consists of *ycnL-ycnK-ycnJ-ycnI* (see figure 4.7). The gene *ycnL* is located upstream and in the opposite direction to *ycnK* and codes for a putative reductase or disulfide isomerase. The gene *ycnK* in turn, encodes a two-domain transcriptional repressor [237, 242]. The N-terminal domain of YcnK contains an helix-turn-helix motif of the DeoR/GlpR family of transcriptional regulators, while the C-terminal domain contains a putative Cu-binding motif from the NosL superfamily. Downstream of *ycnK* lies *ycnJ*, which has a high-sequence similarity to the membrane protein CopCD [66]. The N-terminal region of YcnJ is homologous to the periplasmic copper-binding protein CopC [71], while the C-terminal transmembrane region presents a domain homologous to the inner membrane copper transport protein CopD of *Pseudomonas syringae* [66, 233].

Despite the limited information concerning YcnI protein family members are fairly well distributed. For example, a search of YcnI protein sequences using the Hidden Markov Model [243] deposited in Pfam (date of accession: July 30, 2018) as a query in the HMMER web server [244] identified 924 sequences from 746 microorganisms. Of these 924 sequences, 892 belonged to bacteria while at least 31 of them were from eukaryotic microorganisms principally among fungi, oomycetes and ichthyosporea. Nearly 80 % of the microorganisms analysed contained only one copy of a *ycnI* gene, 16 % of them had two and 3.5 % more than two, with some extraordinary exceptions

such as *Kutzneria sp.* 744 an actinobacteria isolated from the mycorrhizal root tips of Norway spruce seedlings [245] that carries up to five copies. The gene neighbourhood of *ycnI* was analysed using the web service STRING [246] which confirmed that *ycnI* genes are often found next to *sco*, pcu_AC and *copCD* (see figure 4.8).

A multiple sequence alignment (MSA) of the YcnI proteins from the organisms displayed in figure 4.8 highlighted the presence of seven highly-conserved residues including Ala-X-Ala-His-X_{16}-Gly-X_{19}-Thr-X_7-Pro-X_{97}-Trp (see figure 4.9). It is also worth noticing that *P. denitrificans* single-domain YcnI protein and the YcnI N-terminal domain of PCuC (see figure 4.6) only share two of these conserved residues (His and Trp). Considering that principally histidines and cysteines are typically involved in copper coordination, a single histidine and a tryptophan would not provide sufficient ligands for copper coordination [221, 247]. In addition, a signal peptide is predicted at the N-terminus of all YcnI sequences analysed, and interestingly, certain examples of YcnI proteins, such as the one from *B. subtilis*, *N. farcinica* and *Catenulispora acidiphila* present a hydrophobic region at the C-terminus that could potentially anchor the protein to the cell membrane.

4.1.3 The C-terminal PCu_AC-like domain of PCuC

The periplasmic Cu_A chaperone protein (PCu_AC) is a type of copper-binding protein involved in the maturation of the Cu_A site of cytochrome *c* oxidase [5]. This protein was initially identified after a gene neighbourhood analysis of *sco* genes by Artesano *et al.* [178] and shortly after this study, the copper binding properties and biological structure were described by the same group [33]. PCu_AC proteins are exclusively present in prokaryotes, specifically the majority of them belong to Gram-negative bacteria and in a lesser extent to some Gram-positive organisms [178]. In general, only one pcu_AC gene is encoded within the same organism although quite often two or more can be present within different genetic contexts [178]. Artesano and co-workers also analysed the gene neighbourhood of

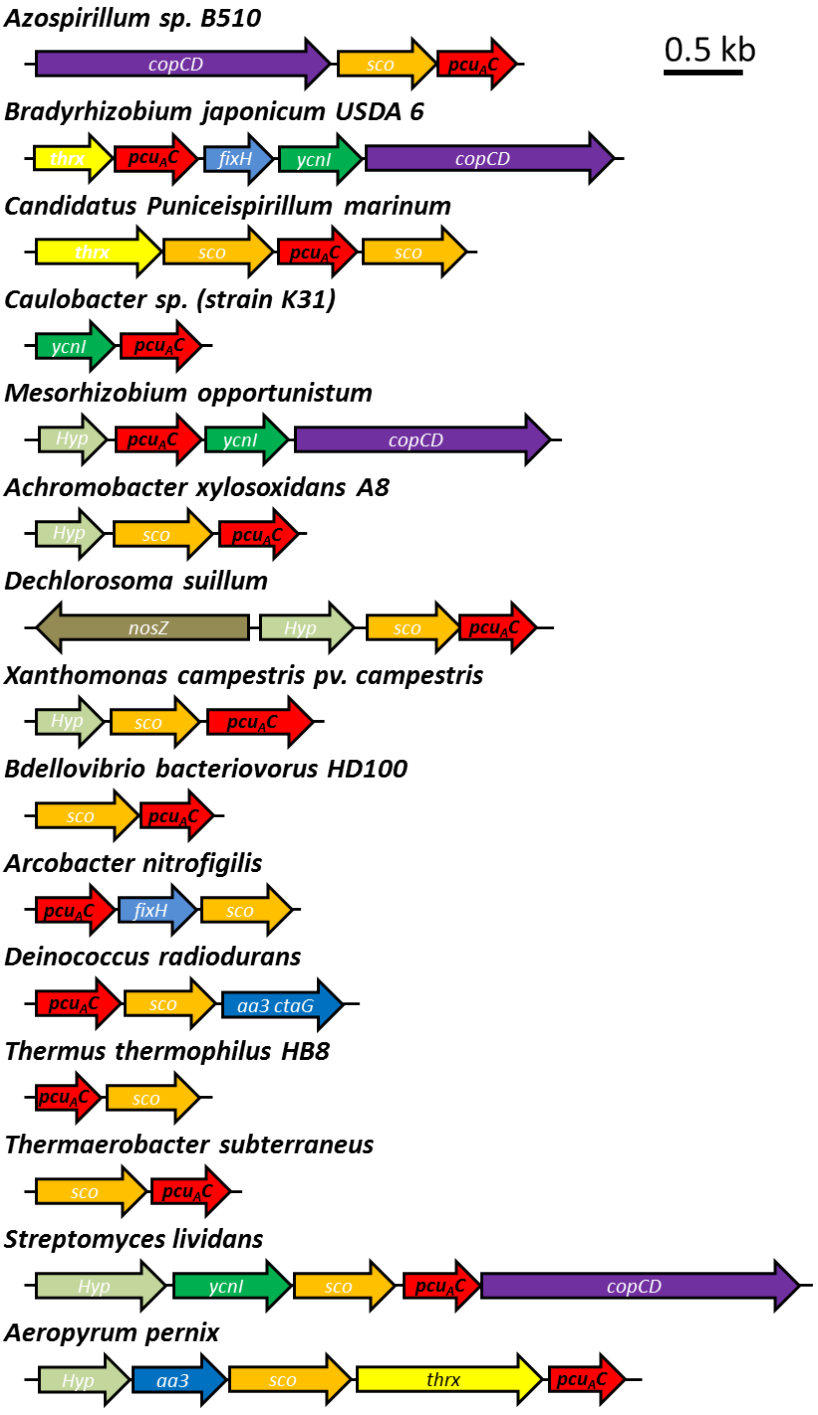

FIGURE 4.10: Overview of the gene neighbourhood of pcu_AC genes in bacteria. Abbreviations used, *hyp*: hypothetical gene, *thr*: thioredoxin.

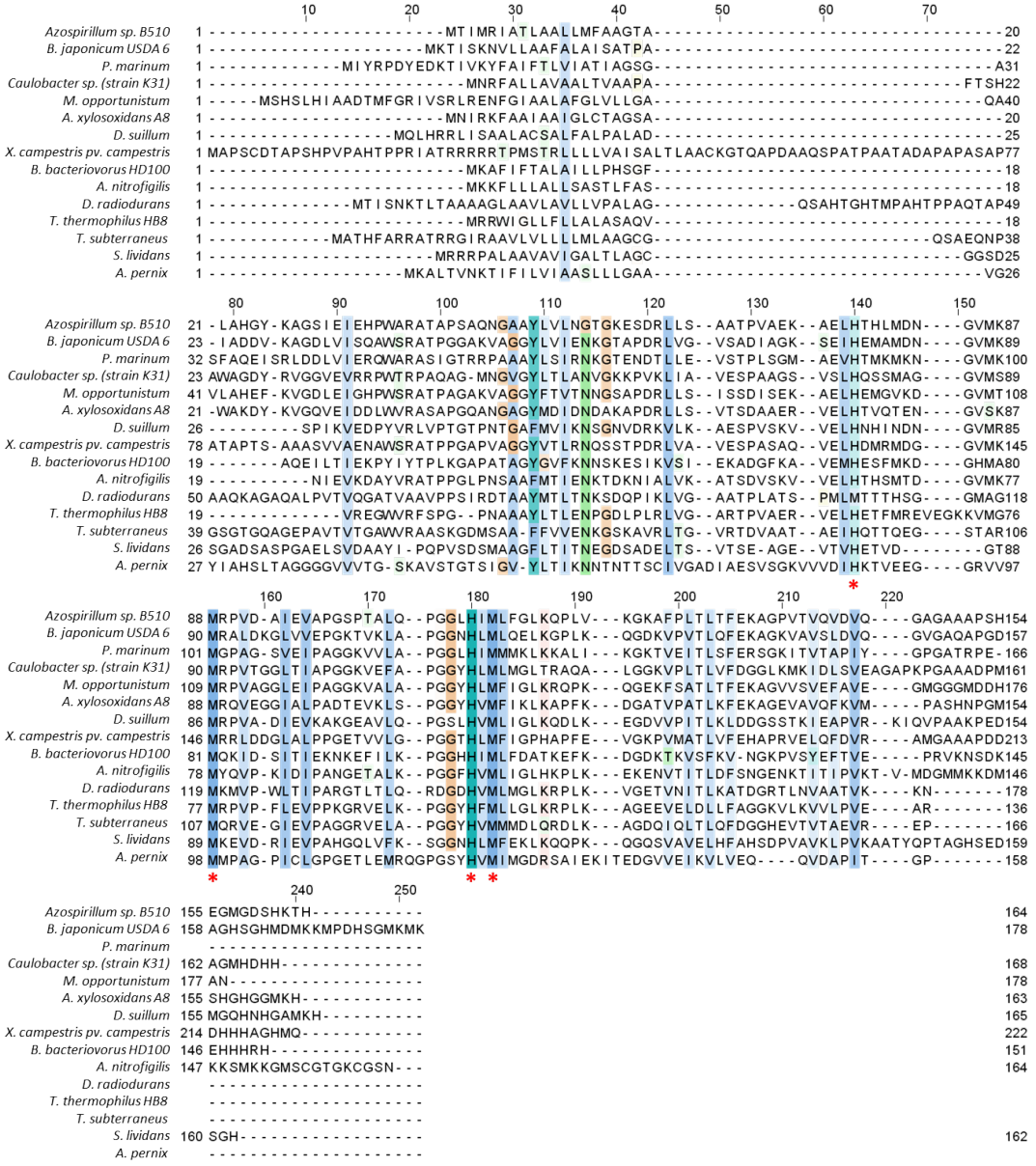

FIGURE 4.11: Multiple sequence alignment of PCu_AC proteins using the program Jalview [188]. Conserved residues have been coloured using Clustal X colour scheme (see appendix A.1) and conserved copper-binding residues are highlighted using the symbol (⋆)

$pcu_A C$ genes and found that they frequently appear together with *sco* genes, *ycnI*-like genes [4] of unknown function and a gene made up of the fusion of the copper-binding proteins CopC and CopD [248]. It is also striking how in some organisms *$pcu_A C$* genes are encoded surrounding genes that code for Cu-dependent terminal reductases, such as cytochrome *c* oxidase in *Deinococcus radiodurans* and *Aeropyrum pernix* or N_2OR in *Dechlorosoma suillum* (see figure 4.10). A multiple sequence alignment (MSA) of pcuc proteins from the organisms displayed in figure 4.10 highlighted the presence the previously mentioned H(M)X_{10}MX_{21}HXM motif (see figure 4.11).

4.2 Generation of the tools for the study of PCuC from *P. denitrificans*

As a first approach, we generated three different genetic constructs for the study of PCuC (see figure 4.12). One for the overexpression of the full-length protein (hereafter, $PCuC_{FL}$-6His) and two for each individual domain, the N-terminal domain ($PCuC_{Nt}$-6His) and the C-terminal domain ($PCuC_{Ct}$-6His). The *pcuC* gene (987 bps) from *P. denitrificans* was subcloned into pLMB509 plasmid (termed pMSL003, see appendix table 2.14). After that, pMSL003 was used as a template

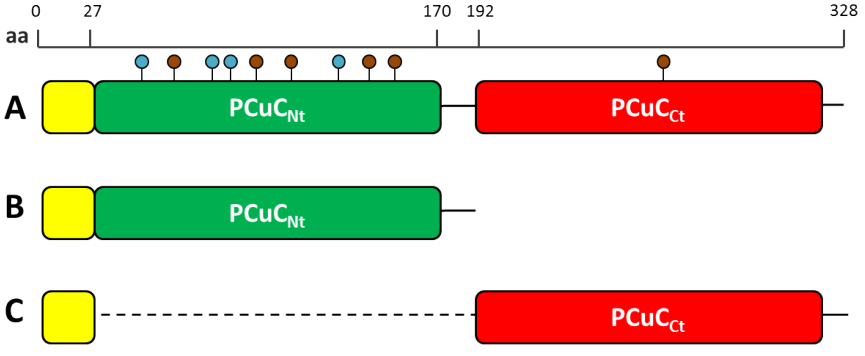

FIGURE 4.12: Representation of recombinant $PCuC_{FL}$, $PCuC_{Nt}$ and $PCuC_{Ct}$. The top ruler represent the approximate number of the residues of the proteins, the yellow box indicates the location of the signal peptide that is not present in the mature protein. The dotted line is the region that has been deleted in $PCuC_{Ct}$. The aromatic composition of PCuC has been drawn with coloured pins (tryptophans are in blue and tyrosines in brown)

to generate two plasmid derivatives by inverse PCR, for $PCuC_{Nt}$-6His construct (named pMSL005) a pair of primers was designed to truncate the last 402 bps of *pcuC* (see figure 4.12 B). While for $PCuC_{Ct}$-6His construct (termed pMSL006), 471 bps were truncated (see figure 4.12 C) after the initial 114 bps where the signal peptide had been predicted using the software SignalP [200].

Once the genetic constructs had been generated, they were subsequently conjugated into *P. denitrificans* wild-type and *pcuC*$^{-}$ non-polar deletion mutant (PD2305) and used in an initial small scale exploratory experiment in order to test their expression. From this initial small scale exploratory experiment we deduced that for future experiments the purification of $PCuC_{FL}$-6His, $PCuC_{Nt}$-6His and $PCuC_{Ct}$-6His should be performed from a *pcuC*$^{-}$ knock-out mutant. The reason is that a strong interaction was observed with $PCuC_{WT}$ when the proteins were purified from a *P. denitrificans* WT background (this will be further explored in chapter 5).

4.3 Characterisation of *pcuC*$^{-}$ deletion strains

To test whether PCuC is involved in the assembly of terminal oxidases in *P. denitrificans*, we examined the growth of a *pcuC*$^{-}$ in-frame deletion mutant (PD2305) versus WT and three different *in trans* complemented strains. The complemented strains were generated by conjugating the low-copy number taurine inducible plasmids pMSL003, pMSL005 and pMSL006 into *pcuC*$^{-}$. The plasmid pMSL003 codes for a full-length $PCuC_{FL}$-6His protein, while pMSL005 and pMSL006 code for each individual domain $PCuC_{Nt}$ and $PCuC_{Ct}$, respectively.

The growth of the strains studied was unaltered in the presence of oxygen when 13.5 µM of copper was present in the culture media (e.g. average of 0.184 ± 0.012 h^{-1}, see figure 4.13 A) and addition of taurine did not affect significantly the growth rate (e.g. 0.177 ± 0.010 h^{-1}, see figure 4.13 C). Interestingly, when extracellular copper was limiting (below 0.5 µM) only WT remained able to grow (e.g. 0.178 ± 0.004 h^{-1}). $PCuC_{FL}$ showed a reduced growth rate (e.g. 0.089 ± 0.004 h^{-1}) pro-

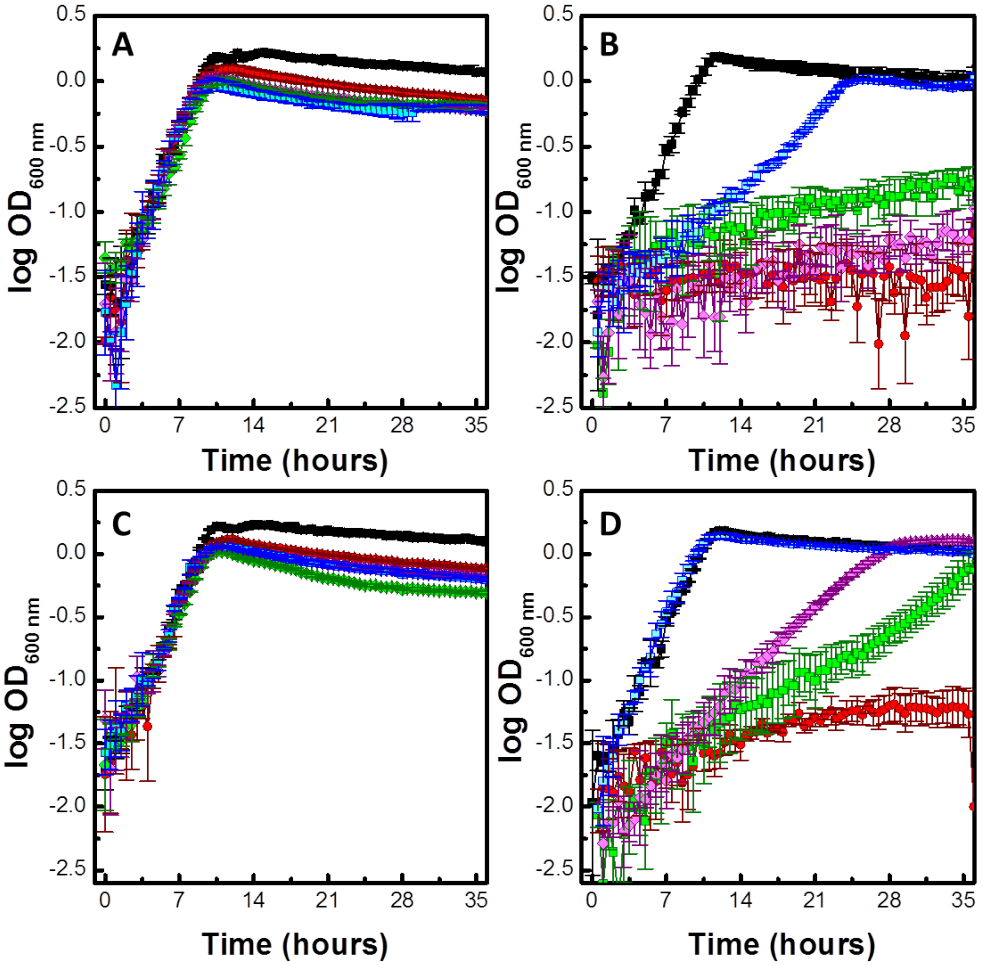

FIGURE 4.13: Aerobic growth characteristics of *P. denitrificans* WT (■), *pcuC*⁻ (●), and three *pcuC*⁻ strains complemented with recombinant $PCuC_{FL}$ (■), $PCuC_{Nt}$ (◆) and $PCuC_{Ct}$ (◆). The growth in the absence of taurine is shown in graphs **(A)** and **(B)**, and in the presence of the inducer in **(C)** and **(D)**. Cultures shown in the left and right columns contained 13.5 and < 0.5 µM of copper, respectively. Standard errors of the mean are indicated by the error bars ($n = 3$).

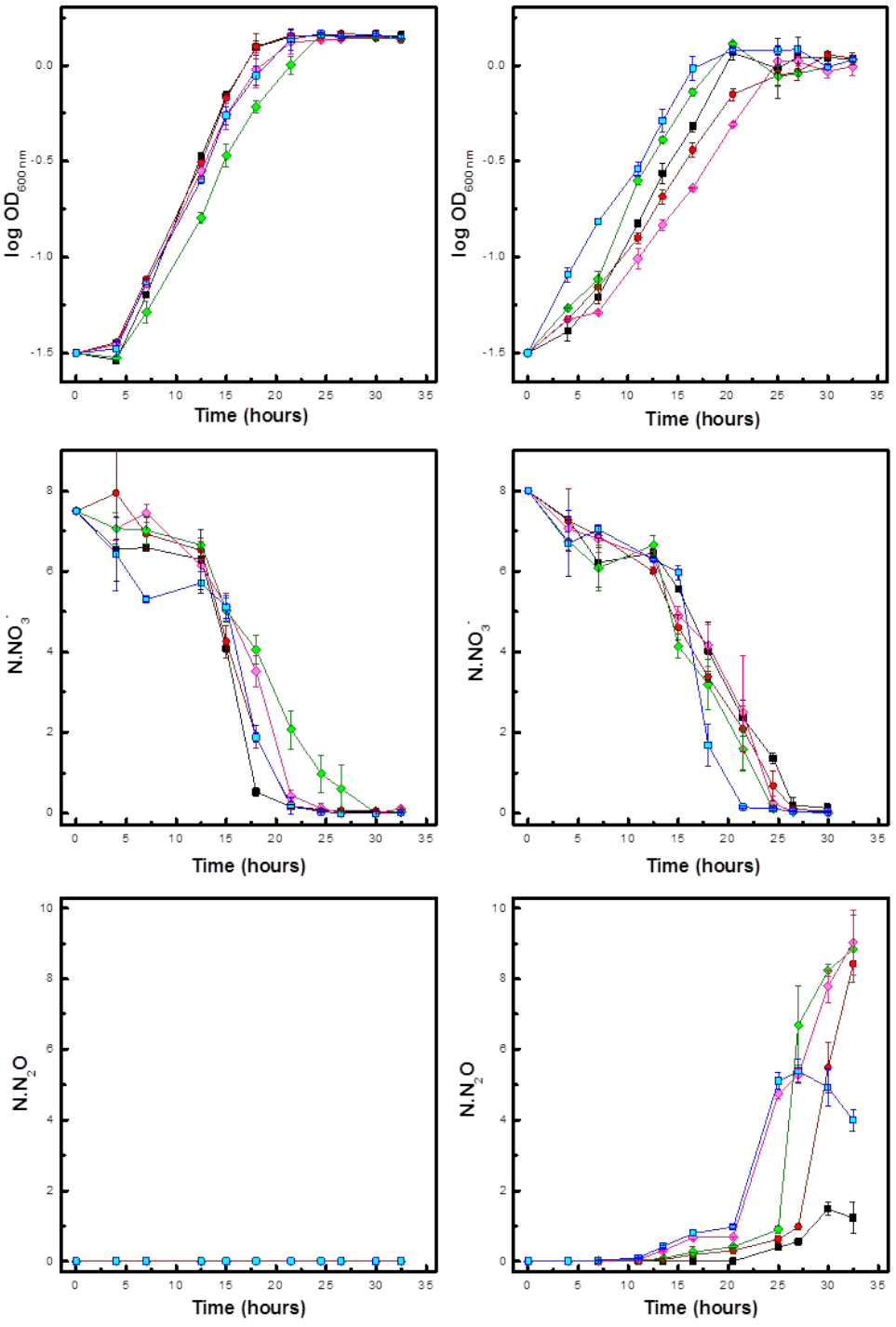

FIGURE 4.14: Anaerobic growth characteristics of *P. denitrificans* WT (■), *pcuC*⁻ (●), and three *pcuC*⁻ strains complemented with recombinant $PCuC_{FL}$ (■), $PCuC_{Nt}$ (◆) and $PCuC_{Ct}$ (◆) in the absence of taurine. The growth is shown in graphs **(A)** and **(B)**. Plots **(C)** and **(D)** represent the consumption of NO_3^- in milimoles of N in the form of NO_3^-. **(E)** and **(F)** show N_2O production in milimoles of N in the form of N_2O. Cultures shown in the left and right columns contained 13.5 and < 0.5 µM of copper, respectively. Standard errors of the mean are indicated by the error bars ($n = 3$).

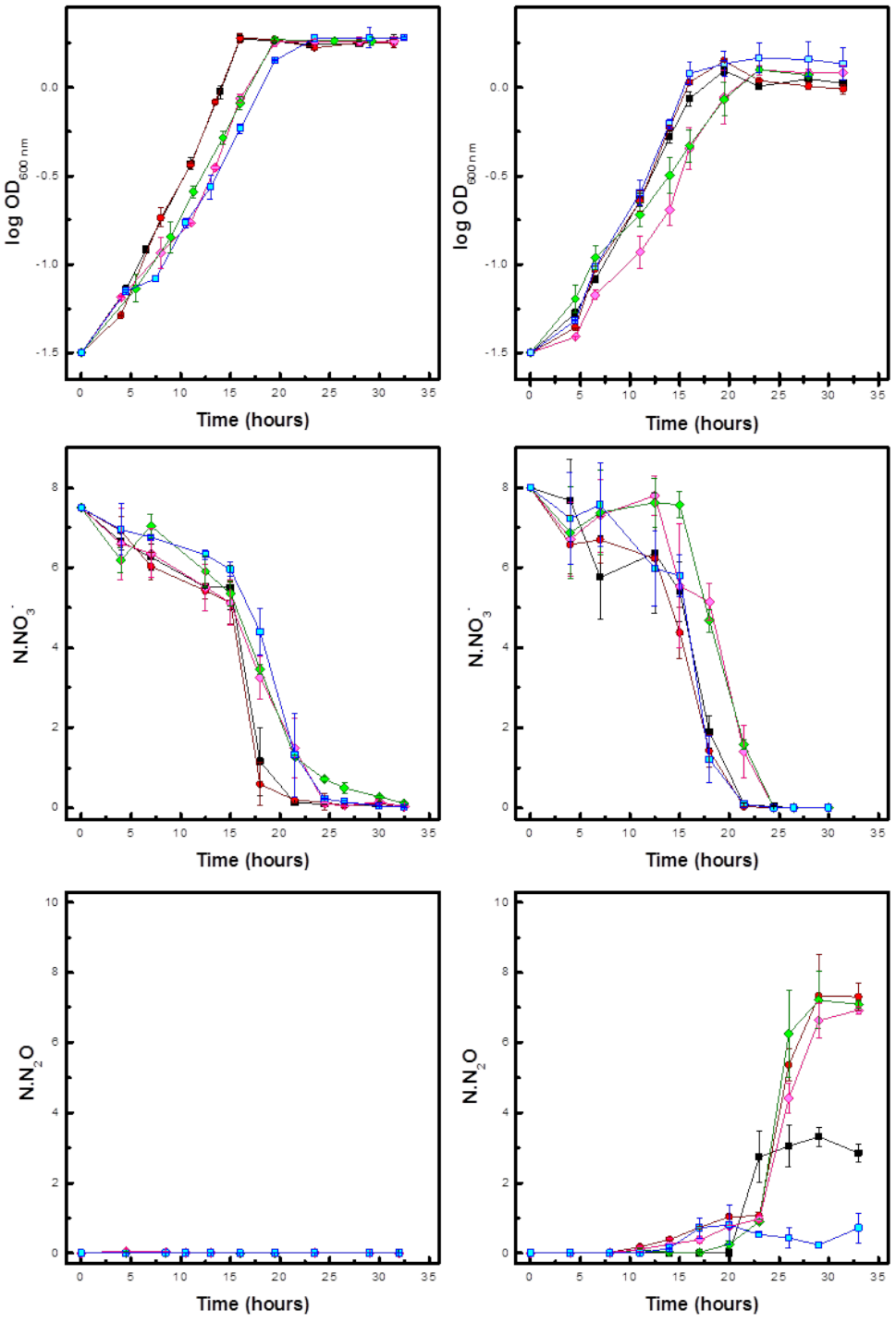

FIGURE 4.15: Anaerobic growth characteristics of *P. denitrificans* WT (■), *pcuC*⁻ (●), and three *pcuC*⁻ strains complemented with recombinant $PCuC_{FL}$ (■), $PCuC_{Nt}$ (◆) and $PCuC_{Ct}$ (◆) in the presence of 1 mM taurine. The growth is shown in graphs **(A)** and **(B)**. Plots **(C)** and **(D)** represent the consumption of NO_3^- in milimoles of N in the form of NO_3^-. **(E)** and **(F)** show N_2O production in milimoles of N in the form of N_2O. Cultures shown in the left and right columns contained 13.5 and < 0.5 µM of copper, respectively. Standard errors of the mean are indicated by the error bars ($n = 3$).

bably due to leaky expression of the plasmid while the rest of the strains were severely affected (e.g. average of 0.023 ± 0.014 h^{-1}, see figure 4.13 B). Addition of taurine to the media stimulated protein production from the relevant complementation vector. Expression of recombinant $PCuC_{FL}$ managed to fully restore the growth of the mutant (e.g. 0.200 ± 0.018 h^{-1}), while expression of $PCuC_{Nt}$ (e.g. 0.100 ± 0.008 h^{-1}) and $PCuC_{Ct}$ (e.g. 0.106 ± 0.017 h^{-1}) barely recovered it (see figure 4.13 D). $PCuC_{Nt}$ and $PCuC_{Ct}$ showed significantly longer lag-phases of 20 and 30 hours, respectively, compared to ∼ 7 hours for WT.

In contrast, under anoxic conditions the growth rate observed of the strains in the present of copper (e.g. average of 0.110 ± 0.012 h^{-1}) was very similar to the one observed when the metal was limiting (e.g. 0.095 ± 0.013 h^{-1}) (see figures 4.14 and 4.15 A and B). During denitrification, nitrate was added to the system as the initial electron acceptor and its consumption was monitored throughout the experiment. In all cases, the strains studied were able to consume all the NO_3^- added to the media (Figure 4.14 and 4.15 C and D). However, the most remarkable finding came from the analysis of the N_2O generated in the cultures (Figure 4.14 and 4.15 E and F). When copper was added to the media, the cultures rapidly converted the N_2O into N_2, i.e. full denitrification. Meanwhile, when copper and taurine were omitted from the culture media, *P. denitrificans* WT accumulated ∼ 2 milimoles of N_2O and *pcuC*$^-$ mutant and the complementations were completely unable to reduce N_2O. Addition of 1 mM taurine to the culture media only restored N_2O reduction in $PCuC_{FL}$, which managed to reduce N_2O below WT levels.

4.4 Production of PCuC proteins for biochemical analyses

4.4.1 Purification of recombinant $PCuC_{FL}$-6His protein

Although for subsequent experiments $PCuC_{WT}$ (previously purified in section 2.12.1 and 3.4) was used to characterise the biophysical properties of the protein. As a

proof of concept, recombinant $PCuC_{FL}$-6His used for phenotypical studies (section 4.3) was purified from *P. denitrificans pcuC*$^-$ mutant. The clarified cell lysate of a 12 L LB culture was applied to a Ni^{2+}-IMAC column and bound proteins were eluted using an imidazole gradient (25 - 500 mM). A main single peak was detected in the chromatogram that eluted at high concentrations of imidazole and the coomassie SDS-PAGE gel of eluted fractions revealed that it was predominantly composed of $PCuC_{FL}$-6His. In order to increase the purity of $PCuC_{FL}$-6His, fractions were diluted 10 - 15 times in binding buffer (buffer C from section 2.12.2) and applied to an anion exchange column. The elution chromatogram showed a main peak that eluted with 50 % of elution buffer (comparable to what was observed in section 3.4 where $PCuC_{WT}$ co-purified with $ScoB_{sol}$-6His) and the SDS-PAGE gel confirmed it as a main band of 35 kDa that corresponds to the predicted molecular weight of monomeric $PCuC_{FL}$-6His. However, the latest fractions displayed a green colour and their UV-vis spectrum had a pronounced band at 410 nm indicative of the presence of an hemoprotein contaminant. Therefore, $PCuC_{FL}$-6His samples were combined, concentrated and further purified by gel filtration. The chromatogram showed a dominant peak that eluted at 50 mL (similarly to the behaviour of $PCuC_{WT}$ in section 3.4) and SDS-PAGE gel confirmed it as mainly $PCuC_{FL}$-6His (Figure 4.18 C). Fractions containing the contaminant were separated from the remaining fractions, combined, concentrated and re-loaded into a preparative gel filtration column in order to remove the hemoprotein that may obscure the UV-vis spectra of subsequent experiments.

The PCuC protein as purified does not show any recognisable feature in the UV-vis spectrum and ICP-AES analysis revealed that contained <1 copper atom per protein as purified. Apo-$PCuC_{WT}$ was generated as described in section 2.14 after treatment with DETC to remove residual copper.

4.4.2 Purification of recombinant $PCuC_{Nt}$-6His protein

Recombinant PCuC N-terminal domain ($PCuC_{Nt}$-6His) was expressed and purified from whole cell extracts of *P. denitrificans pcuC*$^-$ mutant since the protein cannot

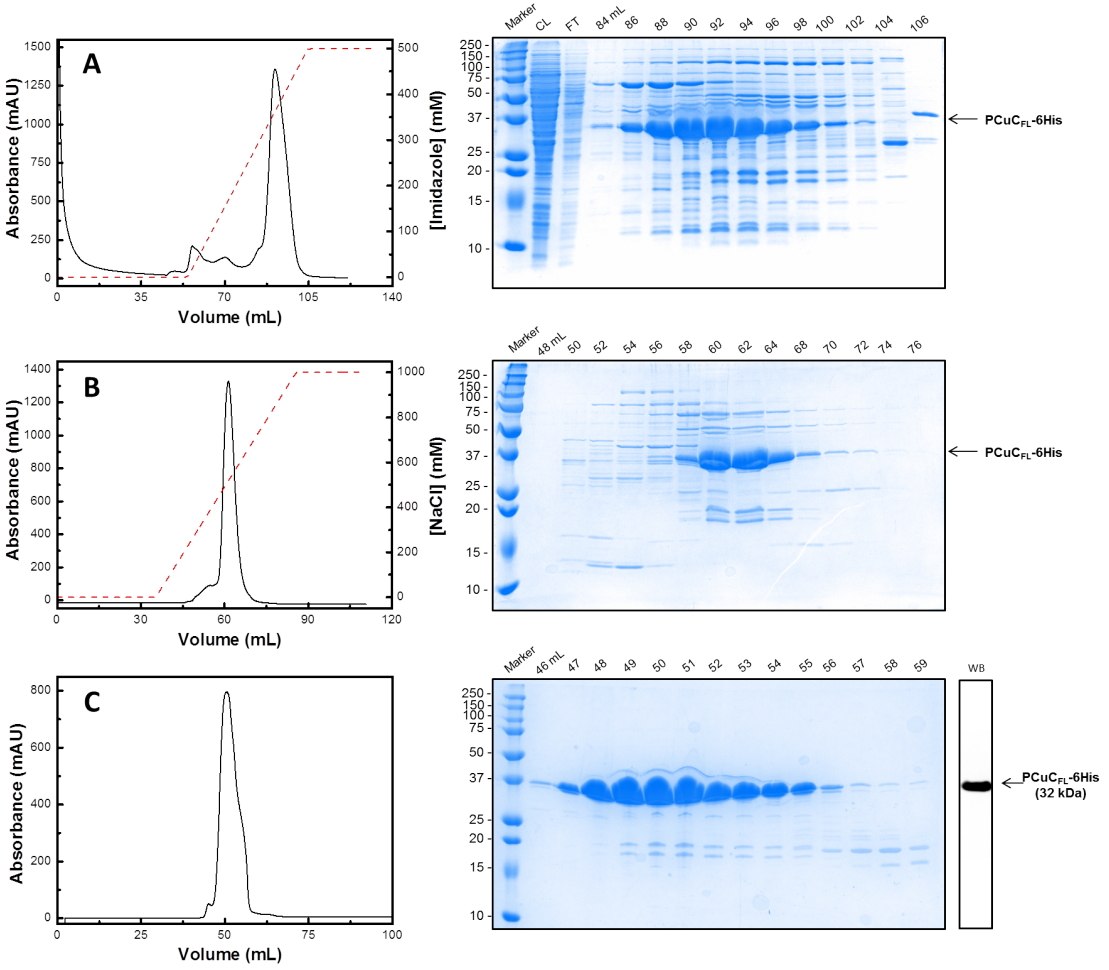

FIGURE 4.16: Purification of PCuC$_{FL}$-6His from *P. denitrificans pcuC*$^{-}$ mutant. Chromatograms and coomassie SDS-PAGE gels of **(A)** Ni^{2+}-IMAC affinity, **(B)** anion exchange and **(C)** gel filtration chromatography with western-Blot using anti-6His primary antibody.

be fully isolated from WT due to a strong interaction of $PCuC_{Nt}$ with native PCuC (as commented in section 4.2 and further discuss in chapter 5). The clarified soluble fractions from a typical 18 L LB cell culture was applied to a Ni^{2+}-IMAC column (Figure 4.17 A). The elution chromatogram showed a series of small intensity peaks at low imidazole concentrations composed of non-specific proteins, and a main peak that eluted with 500 mM imidazole containing the vast majority of $PCuC_{Nt}$-6His. For the next step of purification, samples of $PCuC_{Nt}$-6His were diluted 15 - 20 times in binding buffer (buffer C from section 2.12.2) and loaded into a Q-Sepharose column. In this case, the elution chromatogram showed the presence of two closely-spaced peaks and $PCuC_{Nt}$-6His could be found in both of them as deduced visually from a coomassie SDS-PAGE gel (Figure 4.17 B). However, the UV-vis spectrum of the fractions corresponding to the second peak indicated the presence of a hemoprotein contaminant with a band in the UV-vis spectrum with a λ_{max} at 410 nm. Despite this observation, the contaminant represented a very small proportion of the eluted protein (not clearly detectable in a SDS-PAGE gel), in order to fully isolate $PCuC_{Nt}$-6His, fractions of the second peak were combined, concentrated and loaded into a preparative gel filtration column that was used to fully purify $PCuC_{Nt}$-6His (Figure 4.17 C) for study. Similarly to what was observed in section 4.4.1, during the purification of $PCuC_{FL}$-6His, the recombinant as purified $PCuC_{Nt}$-6His protein does not show any recognisable feature in the UV-vis spectrum, and ICP-AES analysis revealed that contained $\sim$ 0.2 equivalents of copper per protein. Apo-$PCuC_{Nt}$ was generated as described in section 2.14 after treatment with DETC.

4.4.3 Purification of recombinant $PCuC_{Ct}$-6His protein

In order to characterise the C-terminal domain of PCuC and to test whether this protein is also able to bind copper *in vitro*, we expressed and purified $PCuC_{Ct}$-6His from whole cell extracts of *P. denitrificans pcuC*$^{-}$. The clarified soluble cell lysate of a typical 18 L LB culture was loaded into a Ni^{2+}-IMAC column and bound proteins were eluted with a 25-500 mM imidazole gradient. The elution chromatogram sho-

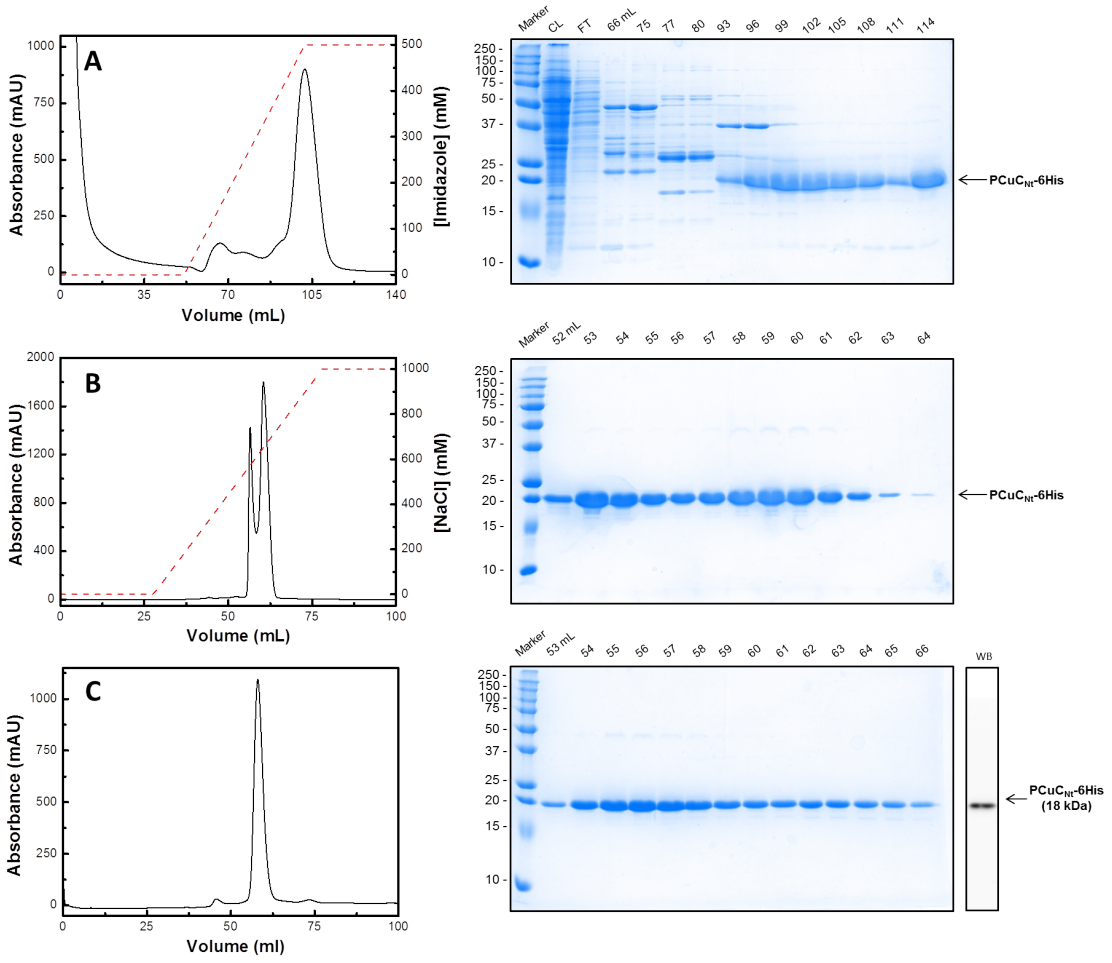

FIGURE 4.17: Purification of PCuC$_{Nt}$-6His from *P. denitrificans pcuC*$^{-}$ mutant. Chromatograms and coomassie SDS-PAGE gels of **(A)** Ni^{2+}-IMAC affinity, **(B)** anion exchange and **(C)** gel filtration chromatography with western-Blot using anti-6His primary antibody.

wed two closely-spaced peaks of similar intensity and, $PCuC_{Ct}$-6His could be identified visually in a coomassie SDS-PAGE gel as a $\sim$ 15 kDa band predominantly present in the second peak (see figure 4.18 A). As the purity of $PCuC_{Ct}$-6His was quite low, the protein was subjected to a second purification step by anion exchange chromatography. Fractions containing $PCuC_{Ct}$-6His were combined and diluted 10 - 15 times in binding buffer (buffer C from section 2.12.2), applied to the column and eluted with a 0.0-1.0 M NaCl gradient. The elution chromatogram also showed a double peak but in this case $PCuC_{Ct}$-6His was mainly present in the first peak that eluted with $\sim$ 30 % elution buffer. Similar to what we observed during the purification of $PCuC_{FL}$-6His and $PCuC_{Nt}$-6His, the latest fractions of the anion exchange chromatography of $PCuC_{Ct}$-6His displayed an UV-vis spectrum with an absorption maxima at 410 nm indicative of the presence of an hemoprotein contaminant. For the last step of the purification, samples containing $PCuC_{Ct}$-6His were combined and concentrated before loading them into a preparative gel filtration column. The chromatogram showed a single dominant peak that SDS-PAGE gel confirmed as mainly $PCuC_{Ct}$-6His. The hemoprotein contaminant eluted ahead of $PCuC_{Ct}$-6His indicating that it is probably a protein with a higher molecular weight and non-interacting such that both species could be effectively separated (see figure 4.18 C). Fractions of $PCuC_{Ct}$-6His that showed signs of containing the contaminant were subjected to additional gel filtration runs to increase sample purity.

The recombinant $PCuC_{Ct}$-6His protein as purified does not show any recognisable feature in the UV-vis spectrum and ICP-AES analysis revealed that contained $\sim$ 0.3 equivalents of copper per protein. Apo-$PCuC_{Ct}$ was also generated as described in section 2.14 after treatment with DETC.

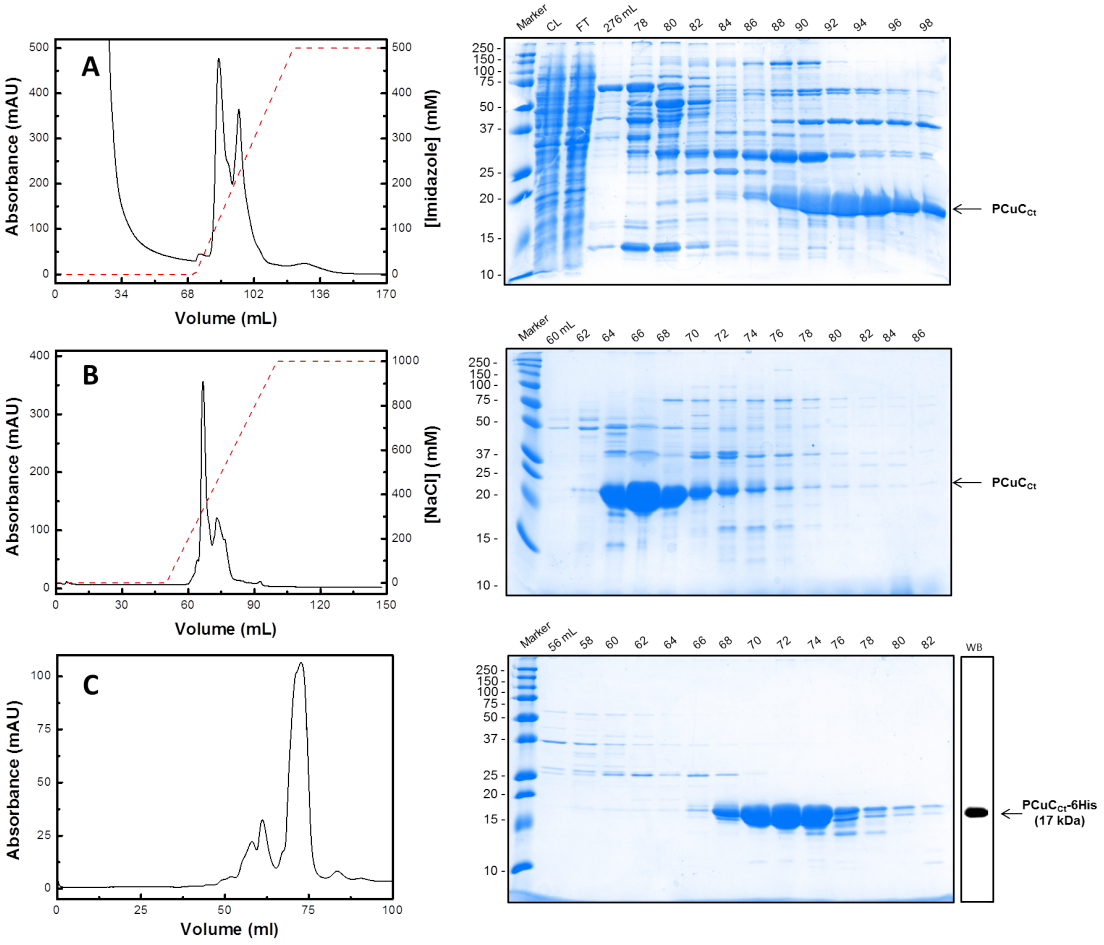

FIGURE 4.18: Purification of PCuC$_{Ct}$-6His from *P. denitrificans pcuC*$^{-}$ mutant. Chromatograms and coomassie SDS-PAGE gels of **(A)** Ni^{2+}-IMAC affinity, **(B)** anion exchange and **(C)** gel filtration chromatography with western-Blot using anti-6His primary antibody.

4.5 Investigating Cu-binding by PCuC

4.5.1 Cu-binding to wild-type PCuC

PCuC from *P. denitrificans* is an unusual polypeptide made up from the fusion of two different proteins: an N-terminal domain similar to YcnI from *B. subtilis* and a C-terminal domain homologue to PCu_AC from *T. thermophilus*. In order to determine whether PCuC is able to bind Cu^{1+} and/or Cu^{2+}, substoichiometric amounts of CuCl or $CuSO_4$ were added to reduced apo-$PCuC_{WT}$ and followed by UV-vis and fluorescence spectroscopy under stringent anaerobic conditions using a glove box.

Additions of Cu^{1+} to reduced apo-$PCuC_{WT}$ gave rise to high energy bands in the UV-vis spectrum (below 280 nm) likely due to N(His)→Cu LMCT transitions [249–251]. A plot of relative absorbance from 250 to 280 nm against Cu^{1+} equivalents per $PCuC_{WT}$ showed a linear increase from 0 to 2 and a plateau from 2 to 3 Cu^{1+} equivalents per $PCuC_{WT}$ (Figure 4.19 A). As the UV-vis response was modest, the intrinsic fluorescence of $PCuC_{WT}$ arising from the aromatic residues of the protein (Trp, $n = 4$) was also used to monitored Cu^{1+}-binding events to reduced apo-$PCuC_{WT}$ by fluorescence spectroscopy with an excitation wavelength of 295 nm. The emission spectra of reduced apo-$PCuC_{WT}$ had λ_{max} at 355 nm and 60 % of the fluorescence was steadily quenched upon the addition of two Cu^{1+} equivalents, after this point Cu^{1+} did not affect the spectrum significantly (Figure 4.19 B).

The Cu^{2+}-binding properties of reduced apo-$PCuC_{WT}$ were also studied by UV-vis and fluorescence spectroscopy. In contrast to what we observed for Cu^{1+}, additions of Cu^{2+} generated a plot of relative absorbance against Cu^{2+} per $PCuC_{WT}$ that increased linearly from 0.0 to 1.0 Cu^{2+} equivalents, after that the response continued increasing with a less pronounced slope (Figure 4.20 A and B). Fluorescence spectroscopy clearly showed a linear quench of 60 % of the fluorescence emission spectrum up to one Cu^{2+} equivalent after which no further quenching was observed. This result suggests that both N-terminal and the C-terminal domains of $PCuC_{WT}$

are able to bind one equivalent of Cu^{1+}, while only one of the two domains is capable of binding Cu^{2+} (see figure 4.20 C and D).

4.5.2 Cu-binding to $PCuC_{Nt}$

The N-terminal domain of PCuC is homologous to YcnI from *B. subtilis* which is an uncharacterised protein with a genetic context that points to a copper chaperoning role [4]. In order to explore if $PCuC_{Nt}$ has the ability to bind both Cu^{1+} and Cu^{2+} species and to define the stoichiometry of the binding, substoichiometric amounts of CuCl or $CuSO_4$ were added to reduced apo-$PCuC_{Nt}$ under anaerobic conditions. Reduced apo-$PCuC_{Nt}$ was obtained after treatment with DETC and DTT as described in section 2.14 and $\sim$ 0.02 copper equivalents per protein were detected by ICP-AES, revealing that the starting material was devoid of bound Cu. Cu^{1+}-binding events to apo-$PCuC_{Nt}$ were again monitored by UV-vis spectroscopy and gave rise to high energy absorbance bands (below 280 nm) due to N(His)$\rightarrow$Cu LMCT transitions [249–251]. A plot of the absorbance changes at 260 - 280 nm as a function of Cu^{1+} per $PCuC_{Nt}$ showed a linear increase with an inflection point at 1.0 Cu^{1+} equivalent (Figure 4.21 A), after this point, no further binding was observed. The intrinsic fluorescence of $PCuC_{Nt}$ was also used to monitor copper-binding to apo-$PCuC_{Nt}$. The fluorescence emission spectrum of apo-$PCuC_{Nt}$ has a λ_{max} at 355 nm and the addition of one copper equivalent quenched 60 % of the emission spectrum in a linear fashion and subsequent additions had no longer an effect on the fluorescence emission spectrum (Figure 4.21 B).

Comparative experiments assaying Cu^{2+}-binding behaviour of reduced apo-$PCuC_{Nt}$ were also performed and followed by UV-vis and fluorescence spectroscopy. Likewise to what was observed for Cu^{1+}, additions of Cu^{2+} showed an absorbance increase in the high energy region of the spectrum up to one equivalent of Cu^{2+} (see figure 4.22 A) and a 60 % quench of the fluorescence emission spectrum (see figure 4.22 B). In summary, these results indicate that $PCuC_{Nt}$ is in fact a copper-binding protein, which can bind one equivalent of either Cu^{1+} or Cu^{2+}.

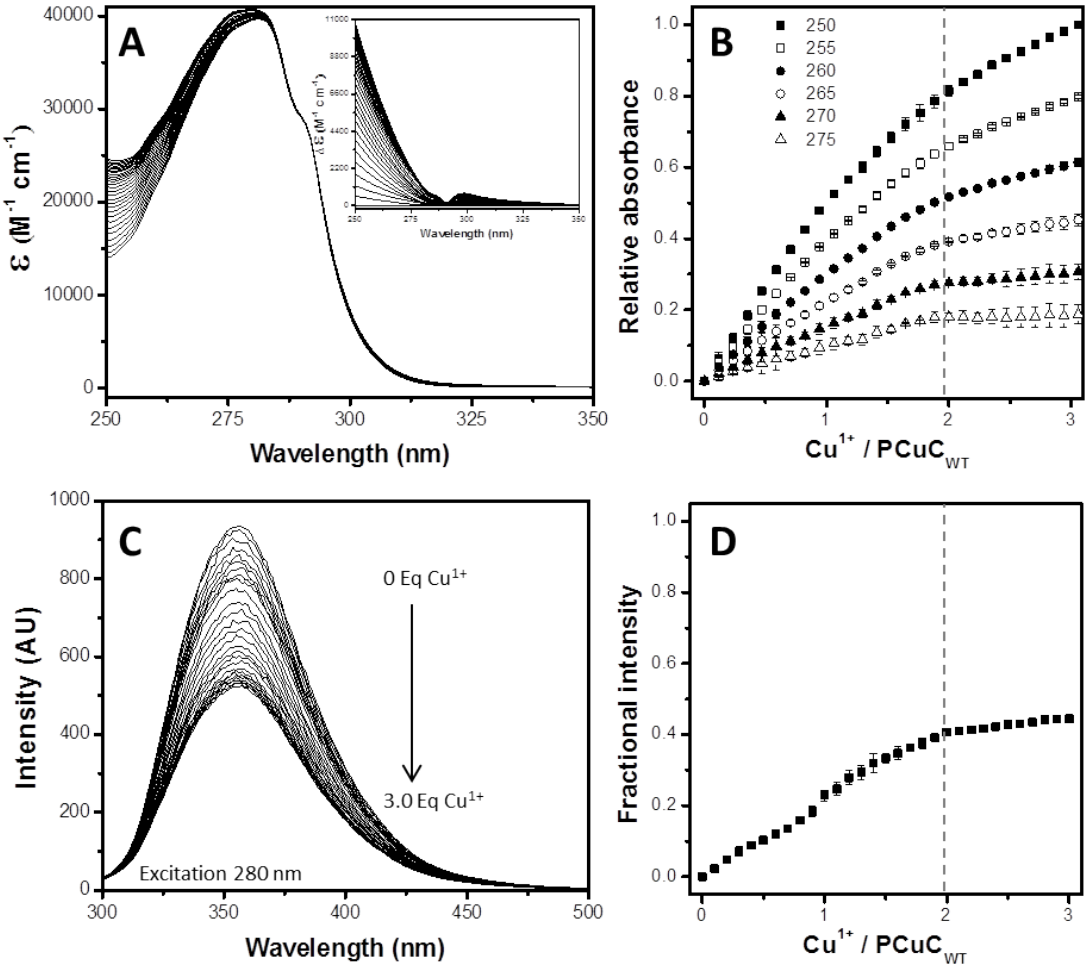

FIGURE 4.19: Absorbance and fluorescence spectroscopy studies of Cu^{1+} binding to reduced apo-$PCuC_{WT}$. **(A)** UV-vis absorbance spectra following the addition of 0.0 - 3.0 Cu^{1+} ions per protein; **(B)** Plot of relative absorbance changes from 250 to 275 nm as a function of Cu^{1+} per $PCuC_{WT}$; **(C)** Fluorescence quench of tyrosine and tryptophan emission peak in response to increasing concentrations of copper (excitation wavelength of 280 nm); **(D)** Plot of the maximal fractional fluorescence intensity as a function of Cu^{1+} per $PCuC_{WT}$. The concentration of $PCuC_{WT}$ was determined using the colorimetric Bradford reagent as 40 μM in 100 mM MOPS and 150 mM NaCl, pH 7.5. Standard errors of the mean are indicated by the error bars ($n = 3$).

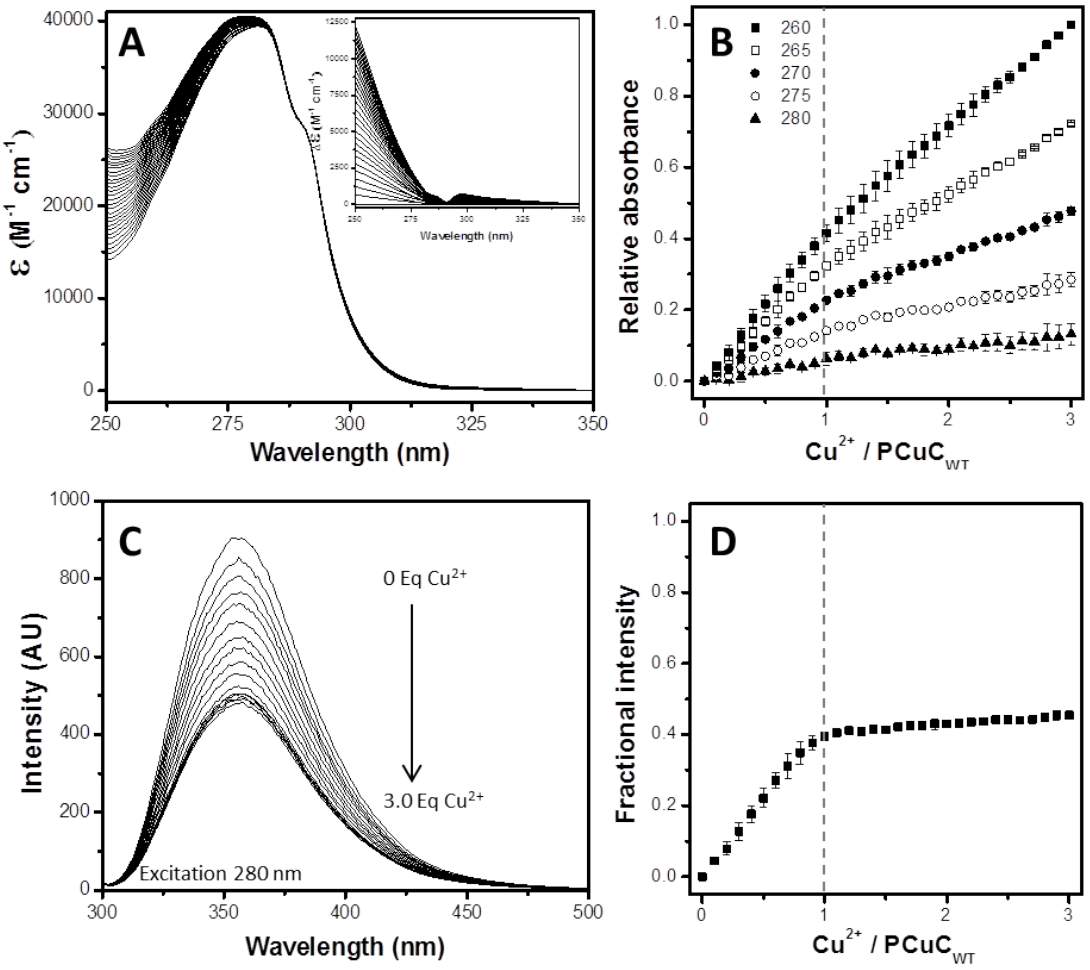

FIGURE 4.20: Absorbance and fluorescence spectroscopy studies of Cu^{2+} binding to reduced apo-$PCuC_{WT}$. **(A)** UV-vis absorbance spectra following the addition of 0.0 - 3.0 Cu^{2+} ions per protein; **(B)** Plot of relative absorbance changes from 260 to 280 nm as a function of Cu^{2+} per $PCuC_{WT}$; **(C)** Fluorescence quench of tyrosine and tryptophan emission peak in response to increasing concentrations of copper (excitation wavelength of 280 nm); **(D)** Plot of the maximal fractional fluorescence intensity as a function of Cu^{2+} per $PCuC_{WT}$. The concentration of $PCuC_{WT}$ was determined using the colorimetric Bradford reagent as 40 μM in 100 mM MOPS and 150 mM NaCl, pH 7.5. Standard errors of the mean are indicated by the error bars ($n = 3$).

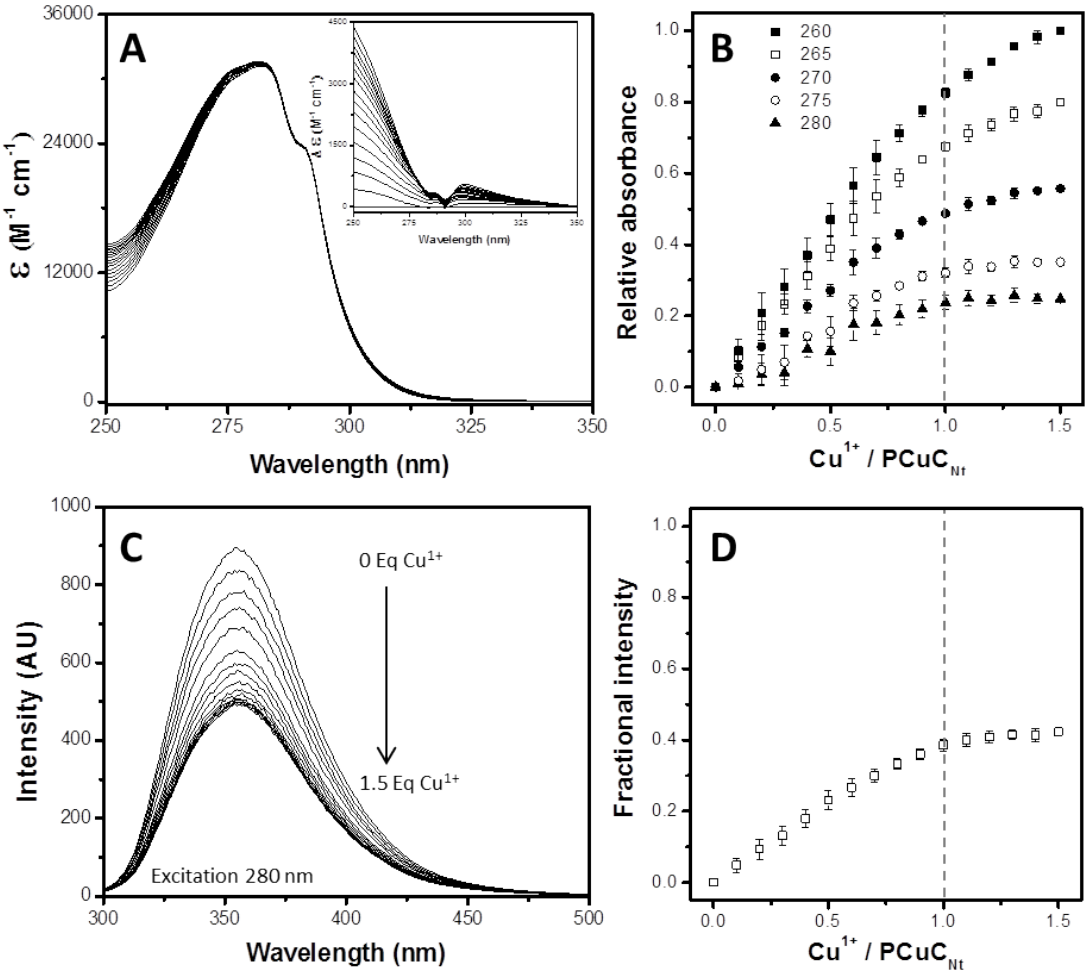

FIGURE 4.21: Absorbance and fluorescence spectroscopy studies of Cu^{1+} binding to reduced apo-$PCuC_{Nt}$. **(A)** UV-vis absorbance spectra following the addition of 0.0 - 1.5 Cu^{1+} ions per protein; **(B)** Plot of relative absorbance changes from 260 to 280 nm as a function of Cu^{1+} per $PCuC_{Nt}$; **(C)** Fluorescence quench of tyrosine and tryptophan emission peak in response to increasing concentrations of copper (excitation wavelength of 280 nm); **(D)** Plot of the maximal fractional fluorescence intensity as a function of Cu^{1+} per $PCuC_{Nt}$. The concentration of $PCuC_{Nt}$ was determined using the colorimetric Bradford reagent as 35 μM in 100 mM MOPS and 150 mM NaCl, pH 7.5. Standard errors of the mean are indicated by the error bars ($n = 3$).

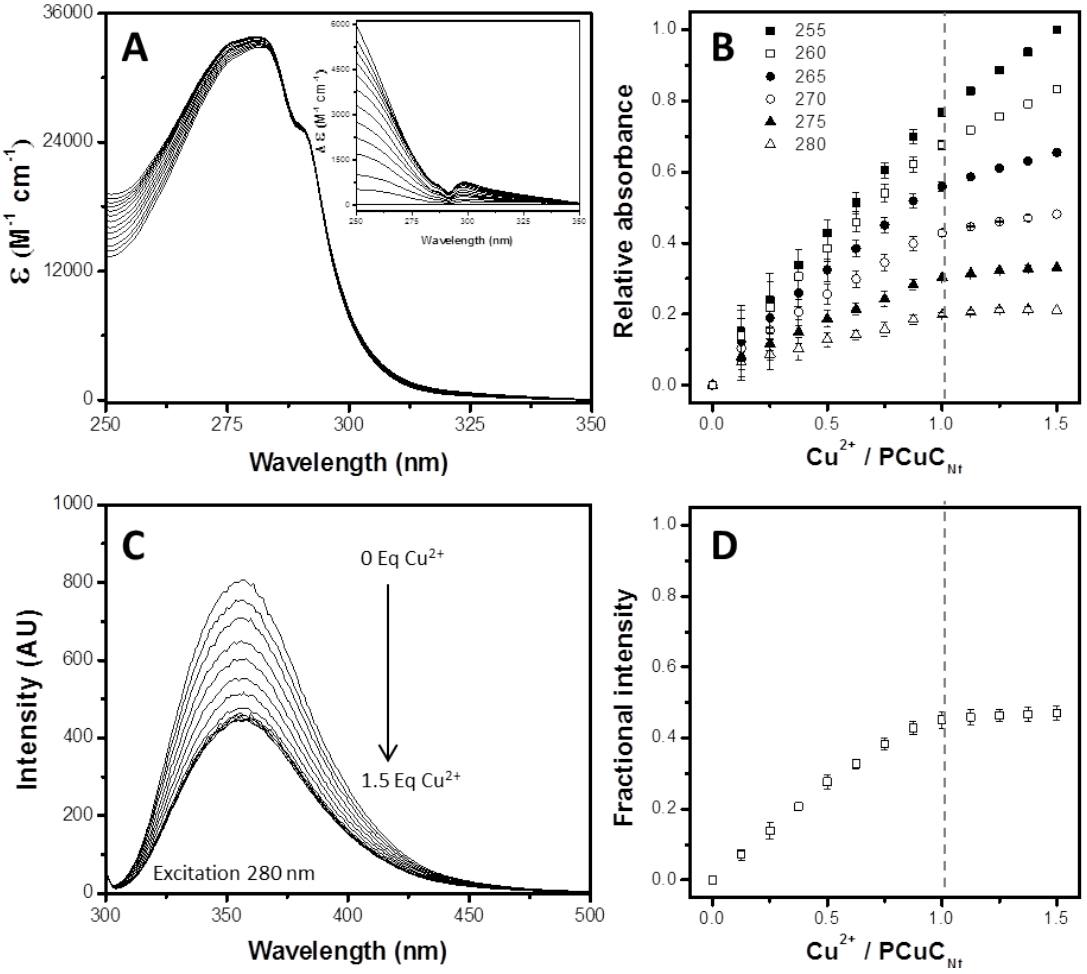

FIGURE 4.22: Absorbance and fluorescence spectroscopy studies of Cu^{2+} binding to reduced apo-$PCuC_{Nt}$. **(A)** UV-vis absorbance spectra following the addition of 0.0 - 1.5 Cu^{2+} ions per protein; **(B)** Plot of relative absorbance changes from 255 to 280 nm as a function of Cu^{2+} per $PCuC_{Nt}$; **(C)** Fluorescence quench of tyrosine and tryptophan emission peak in response to increasing concentrations of copper (excitation wavelength of 280 nm); **(D)** Plot of the maximal fractional fluorescence intensity as a function of Cu^{2+} per $PCuC_{Nt}$. The concentration of $PCuC_{Nt}$ was determined using the colorimetric Bradford reagent as 35 μM in 100 mM MOPS and 150 mM NaCl, pH 7.5. Standard errors of the mean are indicated by the error bars ($n = 3$).

4.5.3 Cu-binding to $PCuC_{Ct}$

PCu_AC family members are prokaryotic proteins known to be capable of binding copper through a conserved $H(M)X_{10}MX_{21}HXM$ motif [33]. Based on this previous knowledge, we attempted to determine whether the C-terminal domain of PCuC from *P. denitrificans*, that is homologue to PCu_AC from *T. thermophilus*, is also able to bind copper using similar spectroscopic methods as employed to study $PCuC_{WT}$ and the $PCuC_{Nt}$ variants. Within an anaerobic atmosphere substoichiometric amounts of CuCl were added to apo-$PCuC_{Ct}$ and the binding events of the metal to the protein were followed by UV-vis and fluorescence spectroscopy. High energy bands (below 280 nm) within the UV-vis spectrum were recorded for Cu^{1+}-$PCuC_{Ct}$ probably due to N(His)→Cu LMCT transitions [250, 251]. Analysis of the differential spectral changes from 250 to 275 nm as a function of Cu^{1+} per $PCuC_{Ct}$ showed a rapid and systematic linear increase from 0 to 1 Cu^{1+} equivalents per $PCuC_{Ct}$ and a slow binding after this point (see figure 4.23 A and B). However, the content of aromatic residues of $PCuC_{Ct}$ is very poor (1 Tyr and 5 Phe) and although a 20 % quench of the emission peak was recorded during the fluorescence titration, analysis of the fractional intensity did not show a significant trend and due to the high signal-to-noise ratio we cannot be certain that quench is not just collisional (see figure 4.23 C and D).

Titrations of Cu^{2+} into apo-$PCuC_{Ct}$ were also performed and measured by UV-vis and fluorescence spectroscopy (data not shown). However, unlike the profiles observed for $PCuC_{WT}$ and $PCuC_{Nt}$ the analysis of the relative absorbance and fractional intensity showed a continuous linear increase with no clear inflection. This result suggests that $PCuC_{Ct}$ does not show Cu^{2+}-binding features and is consistent with the Cu-binding profile of full-length PCuC.

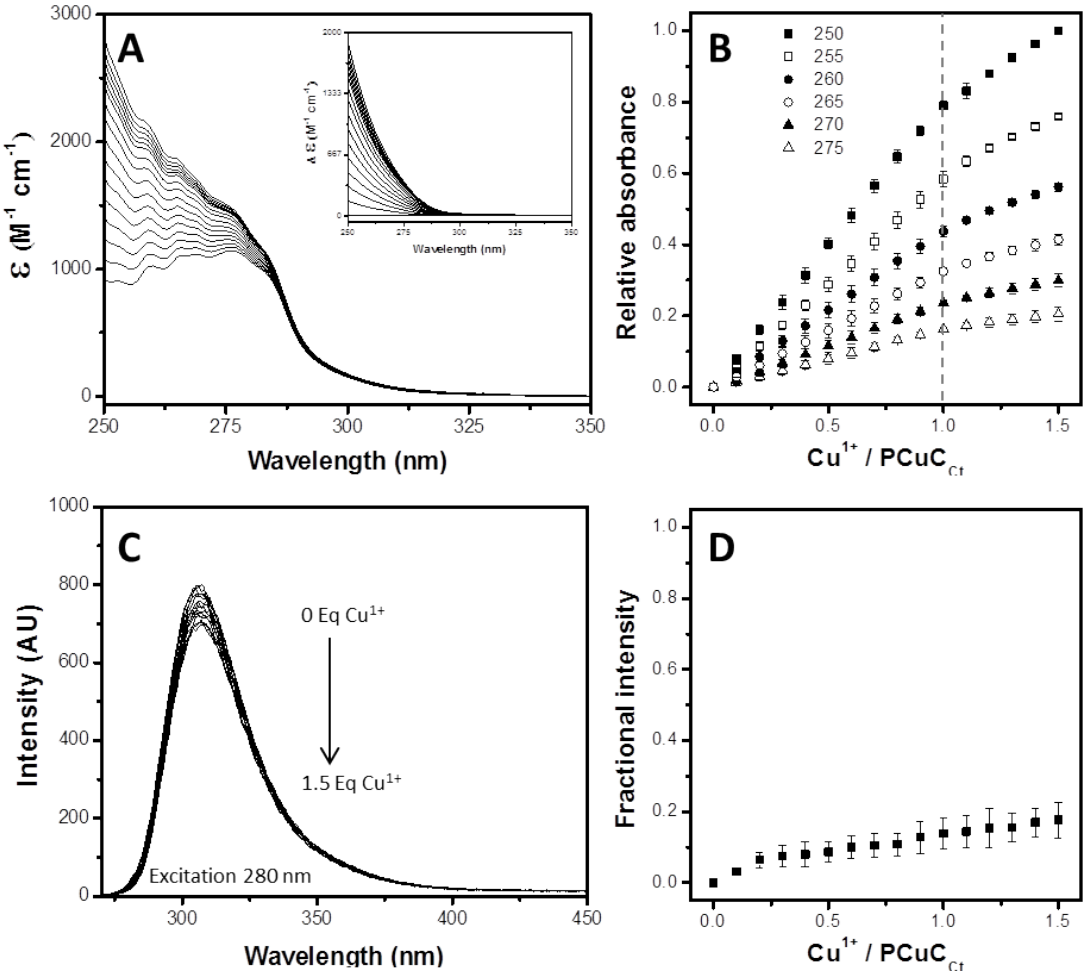

FIGURE 4.23: Absorbance and fluorescence spectroscopy studies of Cu^{1+} binding to apo-$PCuC_{Ct}$. **(A)** UV-vis absorbance spectra following the addition of 0.0 - 1.5 Cu^{1+} ions per protein; **(B)** Plot of relative absorbance changes from 250 to 275 nm as a function of Cu^{1+} per $PCuC_{Ct}$; **(C)** Fluorescence quench of tyrosine and tryptophan emission peak in response to increasing concentrations of copper (excitation wavelength of 280 nm); **(D)** Plot of the maximal fractional fluorescence intensity as a function of Cu^{1+} per $PCuC_{Ct}$. The concentration of $PCuC_{Ct}$ was determined using the colorimetric Bradford reagent as 105 μM in 100 mM MOPS and 150 mM NaCl, pH 7.5. Standard errors of the mean are indicated by the error bars ($n = 3$).

4.6 Cu^{1+} binding affinity of PCuC proteins

Copper binding proteins are frequently characterised for their extremely high metal binding affinities [154]. For this exceptional case, equation 4.1 is primarily shifted towards the formation of the metal-protein complex. UV-vis and fluorescence spectroscopy (such as the one presented in section 4.5) can generally only inform us about about the protein-bound form of the metal. This is typically indicative of systems that is not at equilibrium and estimation of the binding affinity cannot be made through direct interpretation of the titration data since copper binding proteins are actually capable of binding copper with submicromolar affinity (see section 2.17). Therefore, a different technique had to be put in place in order to accurately estimate the dissociation constant of proteins with such a high affinity. For this purpose, titrations were therefore performed in the presence of a competitive chelating agent of known K_D [154, 252]. BCA and BCS are two commonly used high affinity Cu^{1+} ligands ($\beta_2 = 10^{17.2}$ and $10^{19.8}$ M^{-2} for BCA and BCS, respectively [154]) that form 1:2 chromophoric complexes $[Cu^{1+}L_2]^{3-}$ that can be followed by UV-vis spectroscopy. Such methodology has been used to study other Cu-binding proteins in the past such as Sco, PCu_AC, CopC, Csp1, etc. [43, 68, 203]. The competition reactions were performed under anaerobic conditions in the glove box in both directions of equation 2.5 (see Chapter 2 section 2.17). For the forward reaction, the ligand and copper concentration was maintained constant while the protein was titrated. Reduction of the 562 nm band for BCA or the 483 nm for BCS indicated that the protein had managed to extract the copper from the ligands. Alternatively, for the reverse reaction of equation 2.5 the protein and copper concentration were maintained constant while in this case the ligands were titrated into the solution. Chelation of Cu^{1+} by the ligands from Cu^{1+}-protein complex was therefore followed by the increase of the 562 and 483 nm bands. Three different concentrations of ligand and protein were tested in triplicates for each reaction and always in excess over the copper concentration in order to ensure effective competition.

$$M + P \underset{K_D}{\overset{K_A}{\rightleftharpoons}} MP \tag{4.1}$$

4.6.1 Cu^{1+} binding affinity of wild-type PCuC

For the forward reaction $PCuC_{WT}$ was titrated into a solutions of 10 to 70 mM of BCA or 0.04 to 1.00 mM of BCS and the disappearance of the chromogenic UV-vis band was followed for each ligand. Meanwhile, for the reverse reaction the formation of $[Cu^{1+}L_2]^{3-}$ was measured when the copper chelators were titrated into a solutions of 10 to 60 µM of Cu^{1+}-$PCuC_{WT}$. Fitting of the data for titrations of apo-$PCuC_{WT}$ into $[Cu^{1+}BCA_2]^{3-}$ and BCA into Cu^{1+}-$PCuC_{WT}$ (see table 4.1 and figure 4.24 A and B) generated an average K_D value of 2.3 ± 4.8 x 10^{-21}. While titrations in the presence of the higher affinity ligand BCS estimated a K_D value of 1.5 ± 1.9 x 10^{-17} (see Table 4.1 and Figure 4.24 C and D).

4.6.2 Cu^{1+} binding affinity of $PCuC_{Nt}$

Since we have evidence from section 4.4.2 that $PCuC_{Nt}$ can bind copper we tried to estimate the affinity of the metal binding. For the competitive forward titration, $PCuC_{Nt}$ was added into solutions of 50 to 200 µM $[Cu^{1+}BCA_2]^{3-}$ or 25 to 45 µM $[Cu^{1+}BCS_2]^{3-}$ and the decrease in the absorbance maximum at 562 or 483 nm was followed, respectively. Alternatively, for the reverse reaction the formation of $[Cu^{1+}BCA_2]^{3-}$ or $[Cu^{1+}BCS_2]^{3-}$ was measured as an increase in the UV-vis spectrum (at 562 or 483 nm) when the ligands were titrated into solutions of 10 to 55 µM of Cu^{1+}-$PCuC_{Nt}$. Fitting of the data for titrations of apo-$PCuC_{Nt}$ into $[Cu^{1+}BCA_2]^{3-}$ and BCA into Cu^{1+}-$PCuC_{Nt}$ (see Table 4.2 and Figure 4.25 A and B) generated an averaged K_D value of 9.1 ± 7.3 x 10^{-15}. While titrations in the presence of BCS estimated a K_D value of 5.2 ± 1.8 x 10^{-15} (see Table 4.2 and Figure 4.25 C and D).

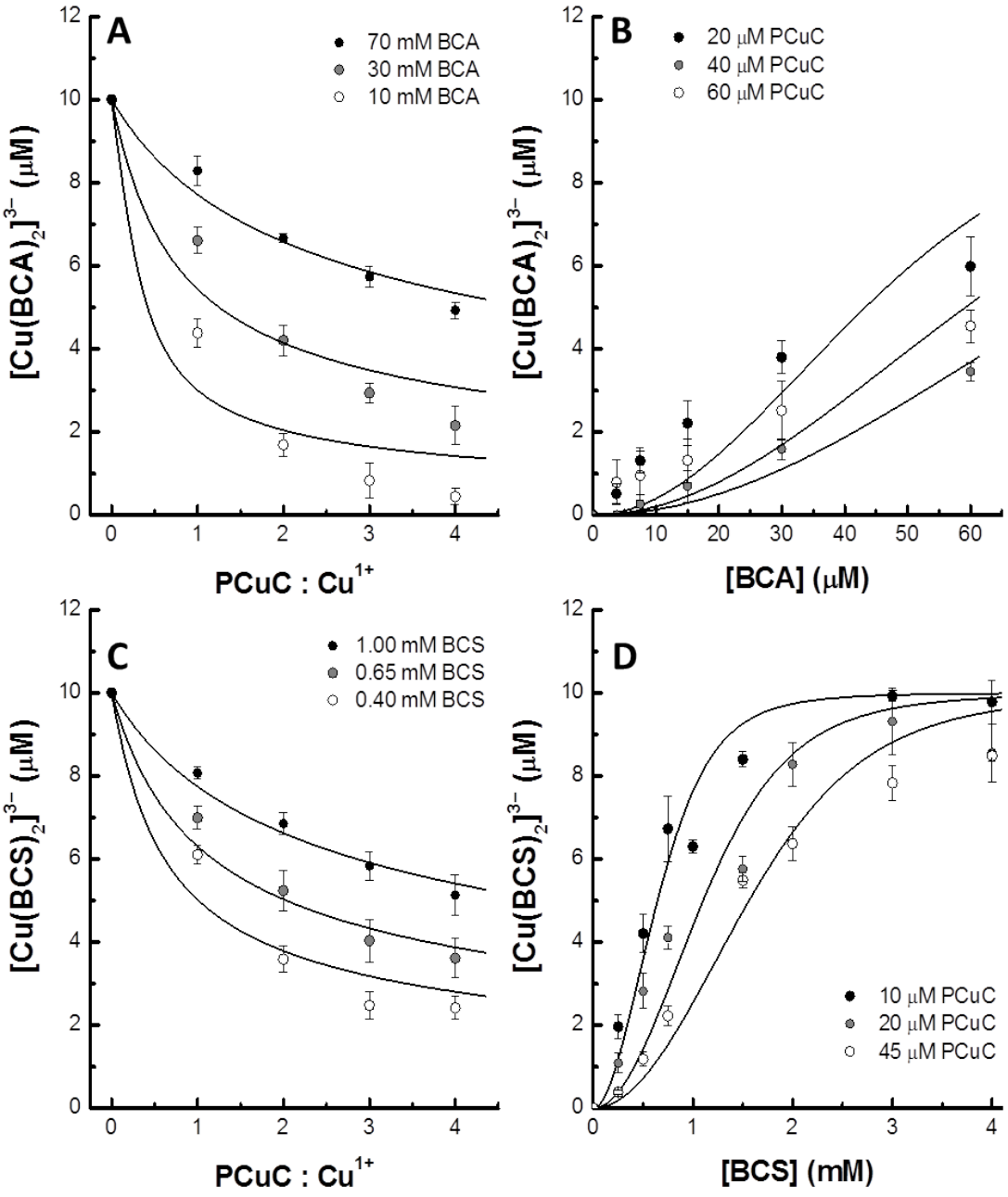

FIGURE 4.24: Estimation of Cu^{1+} binding affinity of $PCuC_{WT}$ at pH 7.5 using the ligands BCA and BCS. Plots **(A)** and **(C)** show the forward reactions in which $PCuC_{WT}$ was titrated into a solution of $[Cu^{1+}BCA_2]^{3-}$ and $[Cu^{1+}BCS_2]^{3-}$, respectively. The graphs represent the absorbance changes as a function of $PCuC_{WT}$:Cu^{1+} indicating the binding of Cu^{1+} by $PCuC_{WT}$. Plots **(B)** and **(D)** show the reverse reactions in which BCA or BCS was titrated into a solution of Cu^{1+}-$PCuC_{WT}$, in this case the absorbance changes of the plots represented as a function of BCA or BCS indicate the binding of Cu^{1+} by the ligands. Standard errors of the mean are indicated by the error bars ($n = 3$).

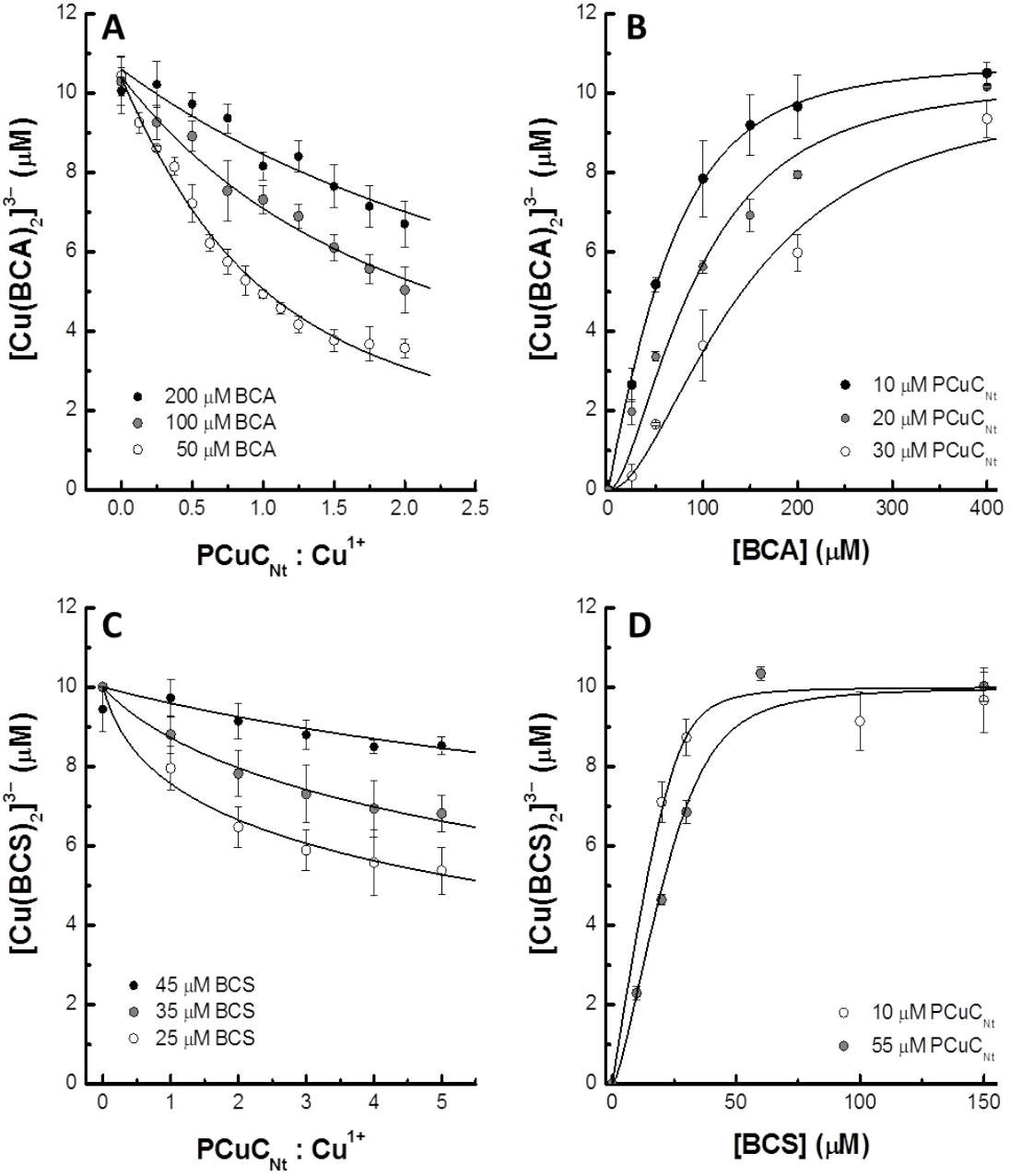

FIGURE 4.25: Estimation of Cu^{1+} binding affinity of $PCuC_{Nt}$ at pH 7.5 using the ligands BCA and BCS. Plots **(A)** and **(C)** show the forward reactions in which $PCuC_{Nt}$ was titrated into a solution of $[Cu^{1+}BCA_2]^{3-}$ and $[Cu^{1+}BCS_2]^{3-}$, respectively. The graphs represent the absorbance changes as a function of $PCuC_{Nt}$:Cu^{1+} indicating the binding of Cu^{1+} by $PCuC_{Nt}$. Plots **(B)** and **(D)** show the reverse reactions in which BCA or BCS was titrated into a solution of Cu^{1+}-$PCuC_{Nt}$, in this case the absorbance changes of the plots represented as a function of BCA or BCS indicate the binding of Cu^{1+} by the ligands. Standard errors of the mean are indicated by the error bars ($n = 3$).

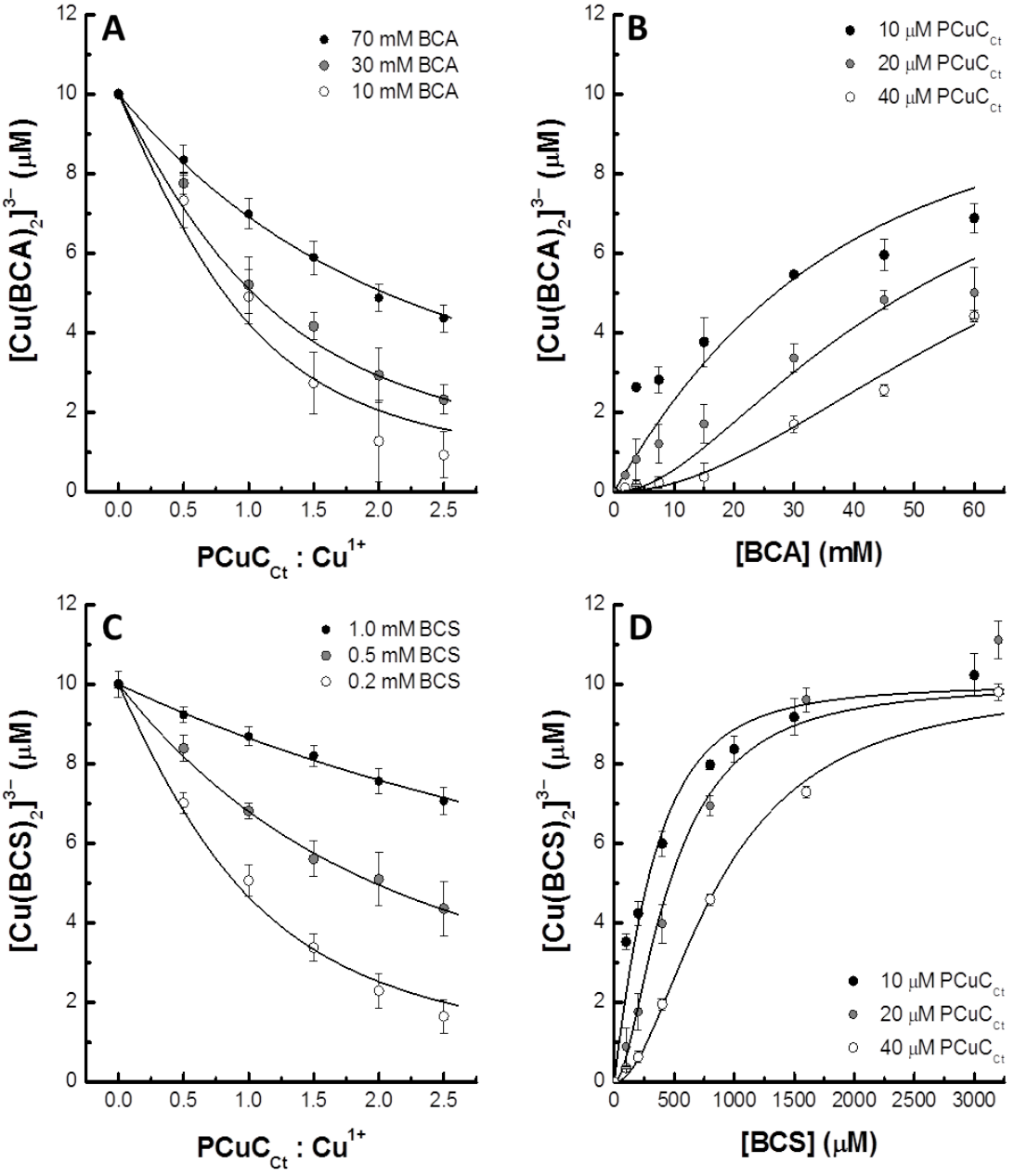

FIGURE 4.26: Estimation Cu^{1+} binding affinity of $PCuC_{Ct}$ at pH 7.5 using the ligands BCA and BCS. Plots **(A)** and **(C)** show the forward reactions in which $PCuC_{Ct}$ was titrated into a solution of $[Cu^{1+}BCA_2]^{3-}$ and $[Cu^{1+}BCS_2]^{3-}$, respectively. The graphs represent the absorbance changes as a function of $PCuC_{Ct}$:Cu^{1+} indicating the binding of Cu^{1+} by $PCuC_{Ct}$. Plots **(B)** and **(D)** show the reverse reactions in which BCA or BCS was titrated into a solution of Cu^{1+}-$PCuC_{Ct}$, in this case the absorbance changes of the plots represented as a function of BCA or BCS indicate the binding of Cu^{1+} by the ligands. Standard errors of the mean are indicated by the error bars ($n = 3$).

	Forward reaction			Reverse reaction		
	Ligand	***K_D app.***	**Std**	**$PCuC_{WT}$**	***K_D app.***	**Std**
BCA	10 mM	1.2×10^{-20}	3.2×10^{-21}	20 µM	3.1×10^{-22}	9.3×10^{-23}
	30 mM	7.8×10^{-22}	1.3×10^{-22}	40 µM	1.9×10^{-22}	5.1×10^{-23}
	70 mM	1.2×10^{-22}	8.5×10^{-24}	60 µM	1.1×10^{-22}	1.9×10^{-23}
BCS	0.40 mM	5.2×10^{-17}	6.7×10^{-18}	10 µM	7.3×10^{-18}	2.3×10^{-18}
	0.65 mM	1.7×10^{-17}	1.4×10^{-18}	20 µM	2.0×10^{-18}	8.6×10^{-19}
	1.00 mM	7.9×10^{-18}	4.7×10^{-18}	45 µM	1.7×10^{-18}	3.1×10^{-19}

TABLE 4.1: Estimated Cu^{1+} dissociation constants for $PCuC_{WT}$

	Forward reaction			Reverse reaction		
	Ligand	***K_D app.***	**Std**	**$PCuC_{Nt}$**	***K_D app.***	**Std**
BCA	50 µM	1.8×10^{-14}	1.3×10^{-15}	10 µM	1.6×10^{-14}	1.3×10^{-15}
	100 µM	1.2×10^{-14}	1.4×10^{-15}	20 µM	1.5×10^{-15}	4.8×10^{-15}
	200 µM	5.9×10^{-15}	9.2×10^{-16}	30 µM	9.2×10^{-15}	1.2×10^{-15}
BCS	25 µM	3.8×10^{-15}	4.0×10^{-16}	10 µM	6.3×10^{-15}	2.1×10^{-15}
	35 µM	3.0×10^{-15}	2.9×10^{-16}	50 µM	7.5×10^{-15}	1.7×10^{-15}
	45 µM	5.3×10^{-15}	9.4×10^{-16}			

TABLE 4.2: Estimated Cu^{1+} dissociation constants for $PCuC_{Nt}$

	Forward reaction			Reverse reaction		
	Ligand	***K_D app.***	**Std**	**$PCuC_{Ct}$**	***K_D app.***	**Std**
BCA	10 mM	2.9×10^{-19}	1.3×10^{-16}	10 µM	4.4×10^{-20}	2.4×10^{-17}
	30 mM	7.4×10^{-20}	4.8×10^{-17}	20 µM	4.4×10^{-20}	8.8×10^{-13}
	70 mM	4.3×10^{-20}	2.1×10^{-17}	40 µM	4.3×10^{-20}	2.1×10^{-17}
BCS	0.2 mM	1.8×10^{-18}	3.2×10^{-18}	10 µM	9.9×10^{-19}	3.8×10^{-17}
	0.5 mM	9.7×10^{-19}	3.7×10^{-18}	20 µM	1.1×10^{-18}	6.3×10^{-18}
	1.0 mM	9.1×10^{-19}	6.9×10^{-18}	40 µM	6.4×10^{-19}	8.5×10^{-18}

TABLE 4.3: Estimated Cu^{1+} dissociation constants for $PCuC_{Ct}$

4.6.3 Cu^{1+} binding affinity of $PCuC_{Ct}$

For the forward reaction of equation 2.5, apo-$PCuC_{Ct}$ protein was titrated into a solutions of 10 to 70 mM BCA or 0.2 to 1.0 mM BCS plus Cu^{1+}. Fitting of the data for titrations with the ligand BCA (see Table 4.3 and Figure 4.26 A and B) generated an average K_D value of 8.6 $\pm$ 6.7 x 10^{-20}, while titrations in the presence of the higher affinity ligand BCS estimated a K_D value of 1.2 $\pm$ 0.39 x 10^{-18} (see Table 4.3 and Figure 4.26 C and D).

4.7 Discussion

PCuC from *P. denitrificans* is an interesting protein apparently arising from the fusion of a YcnI and a PCu_AC protein. YcnI are proteins characterised for containing the domain of unknown function 1775 (DUF1775) and although in general have been poorly studied these proteins appear to be involved in copper metabolism. In contrast to YcnI, PCu_AC proteins have been extensively studied more often in relation to the maturation process of the Cu_A center of cytochrome *c* oxidase in *T. thermophilus* [5]. In this chapter we have attempted to gain additional evidence for the role of PCuC in the maturation process of N_2OR by identifying the metal binding properties of this novel two-domain high-affinity Cu-binding protein.

The *in vivo* study of *pcuC* showed that deletion of the gene had a severe effect on the aerobic growth of *P. denitrificans* and on N_2OR activity under copper limiting conditions. Interestingly, the presence of copper at micromolar levels in the growth medium was enough to fully restore the aerobic growth of the mutant and the activity of N_2OR during anaerobic respiration. However, none of the single domain complemented strains were capable of restoring either the aerobic or anaerobic phenotypes of the *pcuC*$^-$ mutant, which could only be convincingly recovered by complementation and expression using the full-length protein. As we discussed in section 3.8, a previous work from Dash *et al.* in *P. denitrificans* looked at the effect of *sco* and *pcu$_A$C* genes on cytochrome *c* oxidase activity [198].

Curiously, the authors did not observe a reduction on cytochrome oxidase aa_3 activity in a *pcuC* mutant, although they did not mention or explore the growth capabilities of such mutant. However, since we know that cytochrome oxidase ba_3 expression is up-regulated under copper limiting conditions (3.7-fold increase, personal communication from Dr. M. Sullivan) it could be argued that PCuC may be involved in both the maturation of cytochrome oxidase ba_3 and N_2OR. Similarly, it has been suggested in *B. japonicum* that a PCu_AC protein participates in the maturation of more than one copper dependent terminal reductase [240]. Moreover, the fact that only PCuC full length complementation could recover the observed phenotypes makes us wonder whether each domain work independently or on the contrary their mechanism of action requires them to be fused together through a linker region in order to exert their function.

4.7.1 The native full-length PCuC protein

The *in vitro* reconstitution of reduced native apo-PCuC protein (that was co-purified alongside $ScoB_{sol}$-6His, see section 3.4) with copper confirmed that the full-length protein is able to bind two equivalents per monomer of Cu^{1+}, but only one of Cu^{2+}. An increment proportional to the amount of Cu^{1+} added was observed in the high energy region of the spectrum which were attributed to N(His)→Cu LMCT transitions [249–251]. Analysis of the relative absorbance changes below 280 nm showed a clear linear increase from 0 to 2 copper equivalents after which no further binding was observed. Due to the relatively low signal-to-noise ratio of the Cu^{1+}-$PCuC_{WT}$ UV-vis bands fluorescence spectroscopy was also used to monitor the copper binding events. This technique could be applied since the full-length protein contains four tryptophan residues located in the N-terminal domain (see figure 4.12) and were used as intrinsic fluorescence probes. Similarly, the plots of the relative fractional intensity indicated that the protein is able to bind two equivalents of Cu^{1+} per monomer. By contrast, titrations with Cu^{2+} showed binding by UV-vis and fluorescence spectroscopy from 0 to 1 Cu^{2+} equivalents, and a clear and abrupt cessation of the binding with subsequent additions. The

Cu^{1+} and Cu^{2+} titrations of PCuC full-length protein are in strong agreement with the *in vitro* study of each individual domain (see sections 4.5.2 and 4.5.3). These results also imply that one of the domains of full-length PCuC can bind Cu^{1+} and Cu^{2+} (i.e. the YcnI-like N-terminal domain) while the other domain specifically binds only Cu^{1+} (i.e. the PCu_AC-like C-terminal domain).

The binding affinity of $PCuC_{WT}$ was also studied using the Cu^{1+} probes BCA and BCS. A 2-order magnitude difference between BCA and BCS competition experiments was observed. This disparity was also attributed to the relatively higher K_D of BCA compared to BCS. The Cu^{1+}-binding affinity of $PCuC_{WT}$ measured by competition with BCS was 1.5 $\pm$ 2.0 x 10^{-17} M which is an intermediate value between the K_D of $PCuC_{Nt}$ and $PCuC_{Ct}$ (see section 4.6.2 and 4.6.3). This calculated K_D is consistent with $PCuC_{WT}$ being a high-affinity copper scavenger capable of binding copper with an extremely low dissociation-constant and in turn could be part of the reason why the *pcuC*$^-$ phenotype is only observed at low copper levels at which this chaperone is optimally capable of responding to copper-levels. The conservation of such system in bacteria may point to the low bioavailability of this core life-sustaining metal.

4.7.2 PCuC N-terminal domain variant

YcnI are a family of proteins poorly studied and the only information currently present in the literature is from studies referring to copper metabolism. In fact, YcnI proteins are generally found within copper responsive gene clusters that are up-regulated during copper starvation such as in *B. subtilis* [4], *P. denitrificans* [3] and *Methylococcus capsulatus* Bath [238]. Furthermore, YcnI proteins are typically encoded along other copper-binding proteins such as Sco, PCu_AC and CopCD. All together at least provides circumstantial evidence for a role in metabolisms or binding of copper. However, the most important point regarding this work, is that YcnI proteins may be relevant during N_2O respiration. Sullivan and co-workers indicated for the first time that *P. denitrificans* deletion of the YcnI containing *pcuC* gene disrupted N_2O reduction under copper limiting conditions [3]. It has

been therefore the purpose of this chapter to shed further light on the role of YcnI and its involvement in the maturation process for N_2OR from *P. denitrificans*.

One of the first indicators of the YcnI domain of PCuC being capable of binding copper came from the detection of ~ 0.14 copper equivalents within the as purified $PCuC_{Nt}$ protein from *P. denitrificans*. It is immensely common that when copper-binding proteins are over-expressed in an heterologous organism such as *Escherichia coli*, the purified protein does not contain any metal bound to it such as for instance PCu_AC from *D. radiodurans* [33], PCu_AC from *T. thermophilus* [5], ECuC from *S. lividans* [216], Sco2 from *H. sapiens* [187], YcnI from *N. farcinica* [253], Csp1 from *Methylosinus trichosporium* OB3b [43], etc. However, more substantial evidence of Cu-binding was obtained when reduced apo-$PCuC_{Nt}$ was reconstituted *in vitro* with either Cu^{1+} or Cu^{2+}. Addition of copper to the reduced apo-protein developed low extinction coefficient bands in the high energy region of the UV-vis spectrum that were attributed to N(His) $\rightarrow$ Cu LMCT transitions [249–251]. Despite the low signal-to-noise ratio, plots of the absorbance changes below 280 nm showed a distinct copper binding phase from 0 to 1 copper atoms and no apparent binding above 1 copper equivalent per $PCuC_{Nt}$. Fluorescence spectroscopy was also used to monitor copper binding, sizeable spectroscopic changes were observed on copper-binding due to the presence of four tryptophan residues within $PCuC_{Nt}$ (see figure 4.12). Addition of one equivalent of copper to reduced apo-$PCuC_{Nt}$ quenched 60 % of the intrinsic fluorescence of the protein independently of the oxidation state of the copper added. Subsequent additions had no apparent effect on the fluorescence spectrum of the protein.

Given that the data presented so far indicates that $PCuC_{Nt}$ is a copper-binding protein, we thereby calculated the affinity with which the protein binds Cu^{1+} using the bidentate ligands BCA and BCS. Competition experiments showed that $PCuC_{Nt}$ is a high affinity copper-binding protein capable of chelating Cu^{1+} within the femtomolar range (see figure 4.25 and table 4.2). This is therefore the first reported K_D value of an YcnI-type protein and since we also know that $PCuC_{Nt}$ can bind Cu^{1+} as well as Cu^{2+} it would be reasonable to question whether the Cu^{2+} binding affinity of $PCuC_{Nt}$ is similar to the one for Cu^{1+} or if the protein shows any

preference for one of the two oxidation states of the metal, particularly considering that Cu^{2+} is likely to be a more physiologically relevant metal for $PCuC_{Nt}$ due to the more oxidizing location of the protein in the periplasm.

4.7.3 PCuC C-terminal domain variant

PCu_AC are Cu^{1+}-binding proteins involved in maturation of the Cu_A center of cytochrome oxidase ba_3 in *T. thermophilus* [5]. The model proposed by Abriata and co-workers requires the concerted action of PCu_AC and a Sco protein. Firstly the Sco protein with thioredoxin activity reduces the cysteine residues of the Cu_A center and then two Cu^{1+}-transfer events are carried out by PCu_AC proteins [5]. This maturation process may not be exclusive to cytochrome *c* oxidase Cu_A site if not potentially common to other terminal reductases such as the Cu_A containing N_2OR. Since Sullivan and co-workers found that *pcuC* gene was required for optimal N_2OR activation we therefore focused on elucidating the role of the C-terminal domain of PCuC in the maturation process of N_2OR.

Unfortunately, the C-terminal domain of PCuC from *P. denitrificans* has a very low extinction coefficient due to the poor aromatic composition of the protein (see figure 4.12). Despite this, *in vitro* addition of Cu^{1+} to apo-$PCuC_{Ct}$ did result in the development of low intensity bands in the high energy region of the UV-vis spectrum that were attributed to Cu → N(His) LMCT [250, 251]. Analysis of the relative absorbance of the titration spectra showed a rapid and linear increase from 0 to 1 Cu^{1+} equivalents per monomer and a slow absorbance raise after this point. Due to the lack of high fluorescence quantum yields tryptophan residues, titrations of Cu^{1+} into $PCuC_{Ct}$ did not reflect any significant change in the fluorescence emission spectrum and may thus result in non-specific collisional quenching of protein fluorescence by metals. By contrast, when Cu^{2+} was titrated into apo-$PCuC_{Ct}$ no apparent binging was detected under the experimental conditions. Therefore, it is not entirely clear whether other PCu_AC are able to bind Cu^{2+}. For example, Banci *et al.* were unable to detect an EPR signal of Cu^{2+}-PCu_AC from *D. radiodurans* and since the researchers observed that the NMR spectra of

apo-PCu_AC titrated with Cu^{1+} and Cu^{2+} were relatively similar they suggested that PCu_AC could have the ability of reducing Cu^{2+} to Cu^{1+} for binding to occur [33]. In *T. thermophilus* PCu_AC seems to be an specific Cu^{1+}-binding protein although the authors apparently did not explore the Cu^{2+} binding or reduction characteristics of the protein [5]. Blundell and co-workers reported the formation of Cu^{1+}–ECuC (extracytoplasmic copper chaperone) from *S. lividans* after addition of Cu^{2+} although they did not specify which technique was used to detect the binding [216]. The fact that $PCuC_{Ct}$ is unable to bind Cu^{2+} in *P. denitrificans* may be indicative of the specificity of $PCuC_{Ct}$ for Cu^{1+} *in vivo*. Nevertheless, another indicator of the ability of the protein to bind Cu is the presence of 0.34 ± 0.13 copper equivalents per $PCuC_{Ct}$ as purified from *P. denitrificans*.

The Cu^{1+}-binding affinity of $PCuC_{Ct}$ was also investigated with the Cu^{1+} ligands BCA and BCS. The measured K_D for $PCuC_{Ct}$ differed in two orders magnitude between BCA and BCS and this can be attributed to the experimental limitation of the probe BCA which is relatively a weaker ligand compared with BCS. Since BCA has a higher K_D (6.3 x 10^{-18} M) than BCS (1.6 x 10^{-20} M) an excess of ~ 1,000-times over the concentration of protein had to be used (compared to 75-times for BCS) in order to achieve effective competition. $PCuC_{Ct}$ K_D measured with BCS is extremely low suggesting that $PCuC_{Ct}$ is capable of binding copper within the attomolar concentration under our experimental conditions. The K_D value for *P. denitrificans* $PCuC_{Ct}$ is the lowest reported for this family of proteins, which is five orders of magnitude lower than the K_D of PCu_AC from *T. thermophilus* (2.2 ± 0.1 x 10^{-13} [5]) and two orders to the one of PCu_AC from *S. lividans* (2.0 ± 0.2 x 10^{-16} [216]). However, the K_D value of $PCuC_{Ct}$ is reasonable within the paradigm of absolute control of free copper within the cell and is comparable to the extremely low dissociation-constant values observed for other Cu-binding proteins such as Atx1 from *S. cerevisiae* (10^{-18}) [254], $Ccc2_a{}^f$ from *S. cerevisiae* (10^{-18}) [254] or CueR from *E. coli* (10^{-21}) [255].

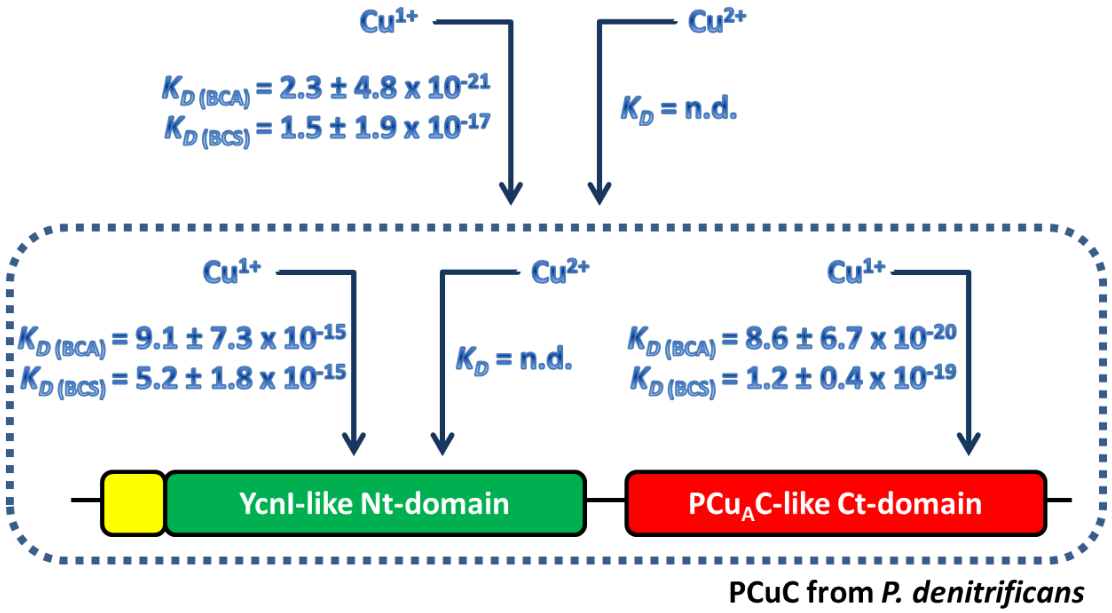

FIGURE 4.27: Summary of the Cu-binding properties of *P. denitrificans* PCuC and its constituent domains. The arrows indicate the Cu^{1+} and/or Cu^{2+} binding preference of the native full length PCuC protein (dotted line) and each individual domain. Average apparent K_D values obtained with the Cu^{1+} chelators BCA and BCS are also indicated. Abbreviation used, n.d. not determined.

5 Solution properties and structural resolution of PCuC

5.1 Introduction

PCuC from *Paracoccus denitrificans* is an unusual two-domain metallochaperone with an extremely high affinity for copper (K_D = 1.5 ± 1.9 x 10^{-17} M). As a consequence, the outcomes of the loss of the coding gene are in principle only appreciable amid copper-limited conditions. For instance, in *P. denitrificans* when copper is excluded from the formulation of the mineral salt medium the growth of *pcuC*$^{-}$ mutant is severely impaired during aerobic respiration, while under denitrifying conditions N_2O reduction is prevented. The N-terminal domain of PCuC is homologous to YcnI from *B. subtilis* [4] and in chapter 4 we have shown for the first time that this type of proteins can tightly bind copper (K_D = 5.2 x 10^{-15} ± 1.8 x 10^{-15} M). However, we were unable to infer a putative copper binding motif within $PCuC_{Nt}$ through bioinformatic analysis. In contrast to $PCuC_{Nt}$, the C-terminal domain of PCuC is very similar to PCu_AC, a known and structurally defined Cu-binding protein responsible for the metallation of the Cu_A center of cytochrome *c* oxidase in *T. thermophilus* [5]. The copper binding residues of $PCuC_{Ct}$ have been identified as well as the copper binding behaviour of the protein (K_D = 1.2 ± 0.4 x 10^{-18} M). However, we are still missing the mechanism by which both domains are organised within full length PCuC protein.

And this might be relevant in order to understand the physiology of the protein since both domains seem to be necessary for the proper functioning of N_2OR *in vivo*. Therefore, in this chapter we elucidate the solution properties and structural characteristics of $PCuC_{Nt}$, $PCuC_{Ct}$ and the PCuC full-length protein.

5.1.1 PCuC N-terminal domain

Apart from the work of Chillappagari and co-workers the other most relevant study concerning a member of the YcnI-family of proteins is the structure of YcnI from *N. farcinica*. This protein structure was solved by Bonanno *et al.* under the Protein Structure Initiative (PSI [256]), however there is no publication associated with this PDB entry since it was released in 2008 (PDB accession code: 3ESM [253]). An analysis of the overall structure of the protein with the on-line programs CATH [257] and PDBsum [258] revealed that it is composed of eleven β-strands that form three β-sheets arranged within a global β-sandwich configuration that resembles an immunoglobulin-like fold (see figure 5.1 A). However, the deposited structure presents several uncertainties, for instance it contains four point mutations of unknown purpose: Leu^{61} for Met, L^{76} for Met, Asp^{149} for the modified residue L-3-aminosuccinimide (SNN) and Gly^{150} for a molecule of acetic acid (ACY). In addition, a total of 44.3 % of the residues have not been modelled in the molecule. At the N-terminus, a signal peptide is predicted by the software SignalP [200] with a cleavage site between position 28 and 29. Instead 26 residues are missing and the sequence NH_2-SLHVTA is found where Ser^1 and Leu^2, that have positions 4 and 5 in the original sequence are followed by His^{29}. Furthermore, at the C-terminus where a transmembrane region is predicted from residue 192 to 219 a section of 71 residues is missing. Moreover, two molecules of SO_4^{2-} and one of dimethyl sulfoxide (DMS) are found in the surrounding of the protein, which may have originated from either the crystallisation conditions (100 mM citric acid pH 3.5, 2.0 M $(NH_4)_2SO_4$) or the cryoprotectant and therefore are unlikely to be relevant to the role of the protein.

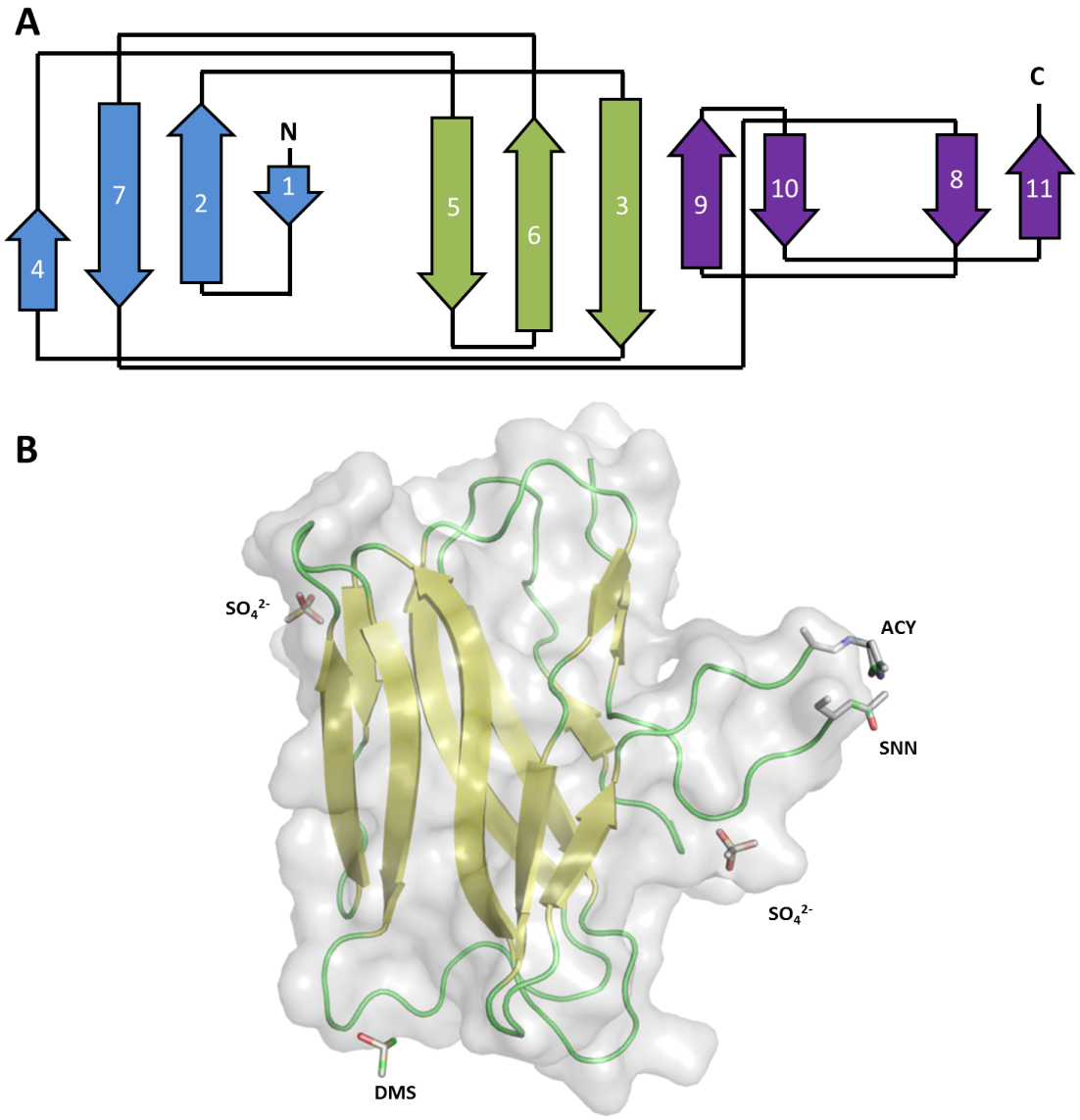

FIGURE 5.1: Structural representation of YcnI from *Nocardia farcinica* (PDB accession code: 3ESM). **(A)** 2D topology diagram representation of YcnI, the 3 β-sheets are coloured in blue, green and purple. **(B)** Cartoon and transparent surface representation. Abbreviations: ACY, acetic acid; SNN, L-3-aminosuccinimide; and DMS, dimethyl sulfoxide.

5.1.2 PCuC C-terminal domain

PCu_AC proteins are non-cytoplasmic proteins with a signal peptide that directs them to the periplasmic space and/or may anchor them to the cell membrane through an N-terminal transmembrane-spanning helix. In Gram-negative bacteria both cases of soluble and membrane associated PCu_AC protein are encountered while all Gram-positive are membrane proteins [33]. The soluble domain of PCu_AC is composed of 9 - 10 β-strands arranged in two β-sheets forming a Greek key motif that resembles to the cupredoxin-fold (see figure 5.2 A) [5, 33, 216]. Although the structure of PCu_AC proteins differs from the classical cupredoxin-fold and instead presents a flexible and solvent exposed β-hairpin comprising β_4 and β_5. Within the soluble domain of PCu_AC lies the recognised and highly conserved $H(M)X_{10}MX_{21}HXM$ motif responsible for copper binding (see figure 5.2) [33]. The histidine and methionine residues of this motif are responsible for the coordination of a single Cu^{1+} atom within a tetrahedral geometry [5, 33, 216]. Even though the Cu^{1+} ion is located close to the protein surface, the structural arrangement of Met^{61} within the copper-binding motif has the peculiarity of hindering sterically the metal. At the same time, Met^{61} has shown to be relatively flexible as shown by the apo- and holo-form structure determination (see figure 5.2). The displacement of this methionine upon recognition of a protein partner could be part of the mechanism of metal donation from PCu_AC to its partner protein [5, 33, 216].

5.2 Solution state characterisation of PCuC proteins

The effect of copper on the oligomeric state of $PCuC_{Nt}$, $PCuC_{Ct}$ and $PCuC_{WT}$ was studied by sedimentation equilibrium analytical ultracentrifugation (AUC) and analytical size exclusion chromatography (ASEC).

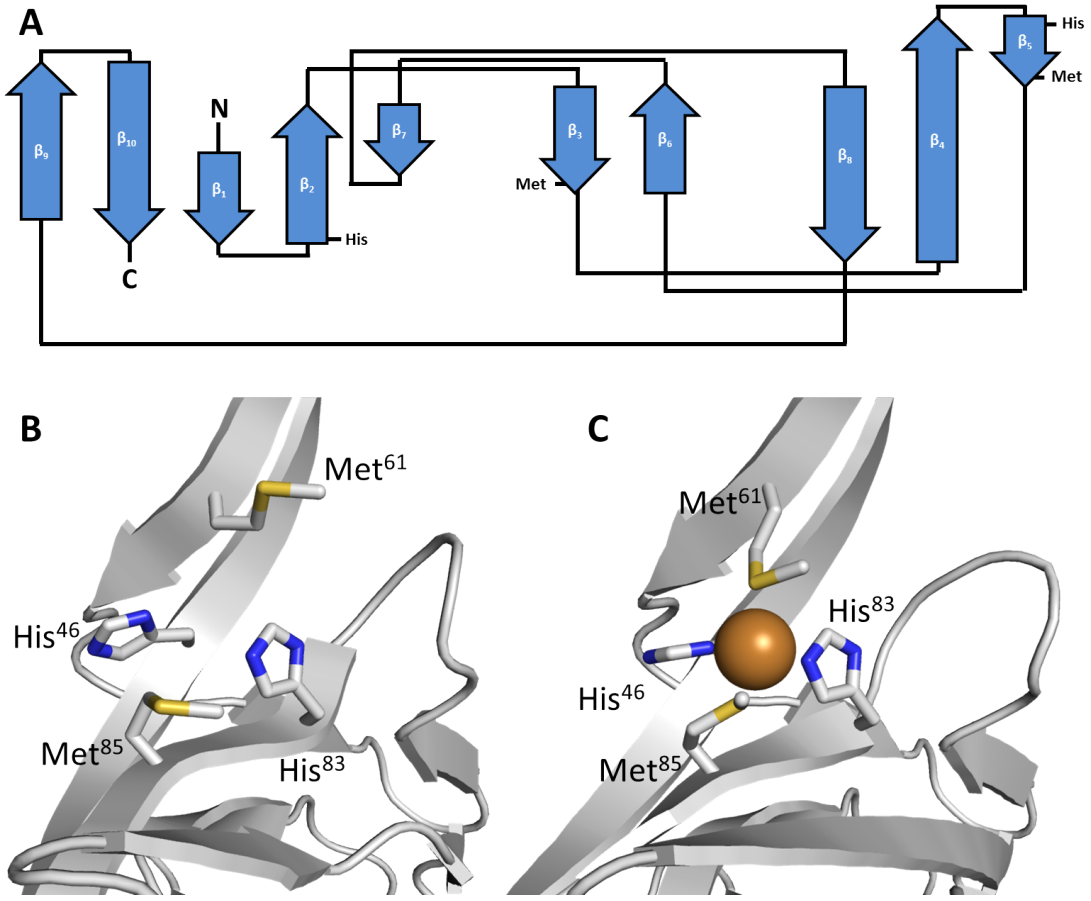

FIGURE 5.2: Structural representation of PCu_AC from *Thermus thermophilus*. **(A)** 2D topology diagram representation of PCu_AC, the β-sheet is coloured in blue and the position of the residues of the $H(M)X_{10}MX_{21}HXM$ motif involved in copper binding are also included. **(B)** Cartoon representation of the copper binding site of apo-PCu_AC and **(C)** Cu^{1+}-PCu_AC. The Cu^{1+} ion has been represented as an ochre sphere (PDB accession codes: 2K6W and 2K6Z, respectively).

5.2.1 Investigating the solution state of $PCuC_{Nt}$

Samples of reduced apo-$PCuC_{Nt}$ containing 0.0, 0.5, 1.0 and 1.5 equivalents of Cu^{1+} or Cu^{2+} were rotated at three different speeds i.e., 10,000, 20,000 and 30,000 rpm. The data was plotted as a function of the absorbance at 280 nm versus $r^2 - r_{ref}^2$ (Figure 5.3 A and B) and fitted to a single-component model. In the graph, the measured absorbance values have been represented with symbols and the theoretical as solid lines, the residual difference between the experimental data and the fitted curve is shown in a separate box. The averaged calculated molecular mass of $PCuC_{Nt}$ was 51.9 ± 3.0 kDa (see Table 5.1 for detailed M_w calculation of each sample) which is approximately three times the theoretical mass of a monomer (18.4 kDa) and indicates that $PCuC_{Nt}$ is a trimeric protein in solution. Regardless of the copper concentration the same sedimentation average molecular mass were observed, therefore the protein adopts an oligomer regardless copper status.

The oligomeric state of $PCuC_{Nt}$ in solution and the effect of Cu^{2+} loading were also studied by analytical size exclusion chromatography. Figure 5.4 shows the elution profiles of apo-$PCuC_{Nt}$ and Cu^{2+}-$PCuC_{Nt}$. In both cases, a single main peak was detected after 14.9 mL which is characteristic of a globular protein of 60.82 kDa. These results are consistent with the M_w calculated by AUC presented above which denoted $PCuC_{Nt}$ as a trimeric protein. In the same manner binding of the metal did not affect to the oligomerization state of the protein.

5.2.2 Investigating the solution state of $PCuC_{Ct}$

The molecular mass and assembly stoichiometry of $PCuC_{Ct}$ was studied by sedimentation equilibrium analytical ultracentrifugation. Equilibrium concentration gradients at lower centrifugal fields i.e., 20,000, 30,000 and 50,000 rpm of apo-$PCuC_{Ct}$ containing 0 to 1.5 of Cu^{1+} equivalents in 0.5 increments were fit to a single-component model (Figure 5.5). In the graph, the absorbance values has been represented with symbols and the theoretical data as solid lines, the residual difference between both data sets is shown in the lower panel. The calculated mole-

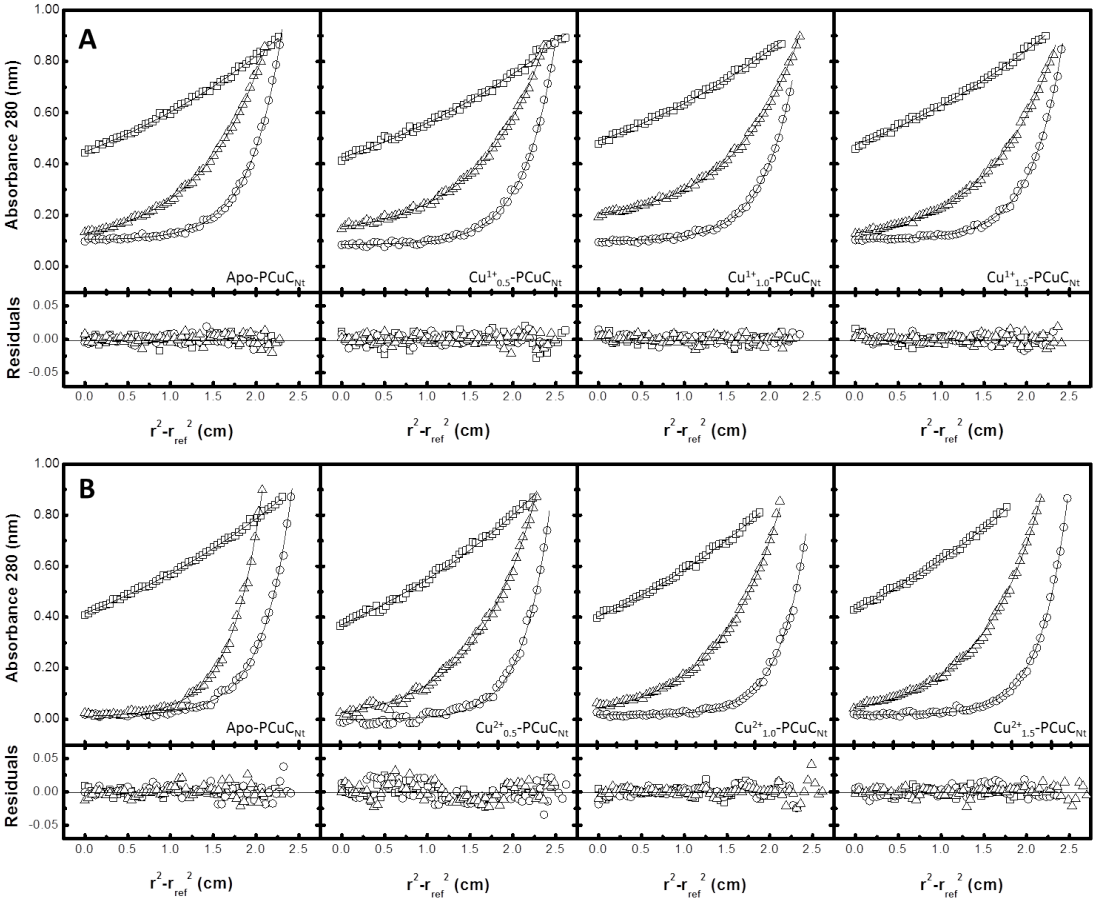

FIGURE 5.3: Effect of **(A)** Cu^{1+} and **(B)** Cu^{2+} on the sedimentation equilibrium of $PCuC_{Nt}$. Top graphs represent the absorbance profiles of $PCuC_{Nt}$ (16.8 μM) at 10,000 (□), 20,000 (△) and 30,000 (○) rpm at 20 °C and the lines the fits to a single-component model. Lower panels show the residual differences between the experimental data and the fitted curves.

	Cu^{1+}		Cu^{2+}	
Sample	**M_w** (kDa)	**Std**	**M_w** (kDa)	**Std**
Apo-$PCuC_{Nt}$	50.9	6.4	51.6	6.2
$Cu_{0.5}$-$PCuC_{Nt}$	50.6	8.3	50.8	1.2
$Cu_{1.0}$-$PCuC_{Nt}$	49.2	6.0	53.9	7.3
$Cu_{1.5}$-$PCuC_{Nt}$	49.8	6.4	58.5	6.9

TABLE 5.1: Calculated M_w of $PCuC_{Nt}$ by sedimentation equilibrium analytical ultracentrifugation. Standard errors of the mean of three technical replicates ($n = 3$).

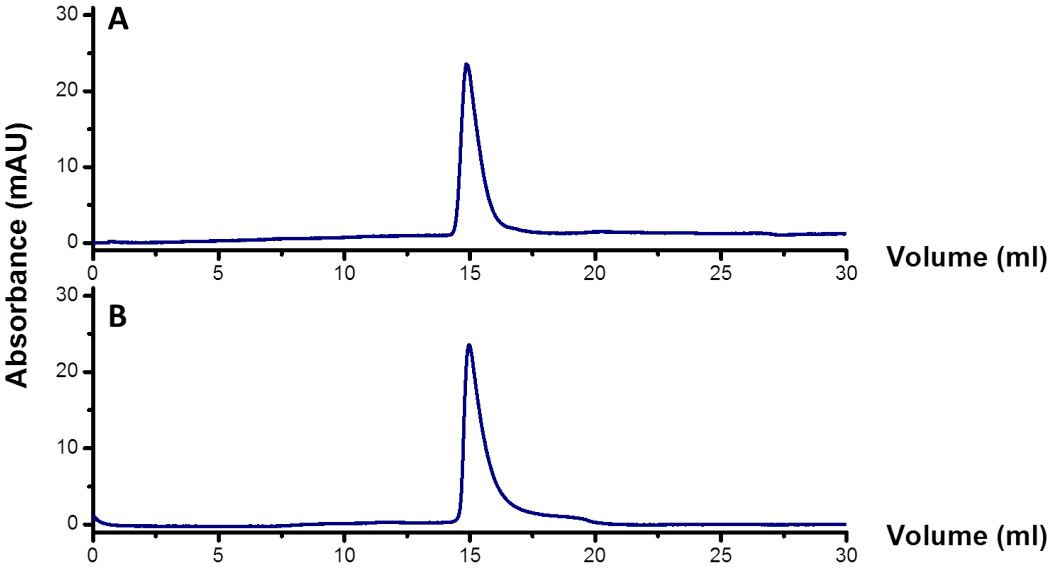

FIGURE 5.4: Analytical size exclusion chromatography of $PCuC_{Nt}$. Plots of the absorbance at 280 nm as a function of the elution volume for a 60 μM sample of **(A)** reduced apo-$PCuC_{Nt}$ and **(B)** Cu^{2+}-$PCuC_{Nt}$ in 20 mM HEPES, 150 mM NaCl and 0.25 mM DTT (pH 7.5).

cular mass of $PCuC_{Ct}$ was 13.4 ± 1.2 Da (see Table 5.2 for detailed M_w calculation of each sample) which is close estimate of the theoretical mass of $PCuC_{Ct}$ (17,383 Da), suggesting that $PCuC_{Ct}$ is a monomeric protein in solution which does not aggregate upon Cu^{1+}-binding. The effect of Cu^{2+} was not investigated since the results from section 4.5.3 indicated that $PCuC_{Ct}$ does not bind Cu^{2+}.

The oligomeric state of $PCuC_{Ct}$ was also determined by analytical gel filtration chromatography. Addition of Cu^{1+} to apo-$PCuC_{Ct}$ was performed in an anaerobic glove box and thoroughly degassed buffers were used for the chromatography. Due to the very low extinction coefficient of $PCuC_{Ct}$ samples of 100 μM concentration were loaded into the column in order to be able to detect a significant peak. Figure 5.6 shows the elution chromatograms of apo-$PCuC_{Ct}$ and Cu^{1+}-$PCuC_{Ct}$. In both cases, a single main peak was detected after 17.0 mL which is characteristic of a globular protein of 22.2 kDa. The experimental M_w obtained is ∼ 5 kDa higher than the theoretical molecular weight (17.4 Da) and 12 kDa less than the M_w of a dimer, indicating that $PCuC_{Ct}$ is more likely to be monomeric protein in solution and Cu^{1+}-binding does not affect the oligomerization state of the protein. Therefore, the ASEC of $PCuC_{Ct}$ is in agreement with the AUC results presented in figure 5.5

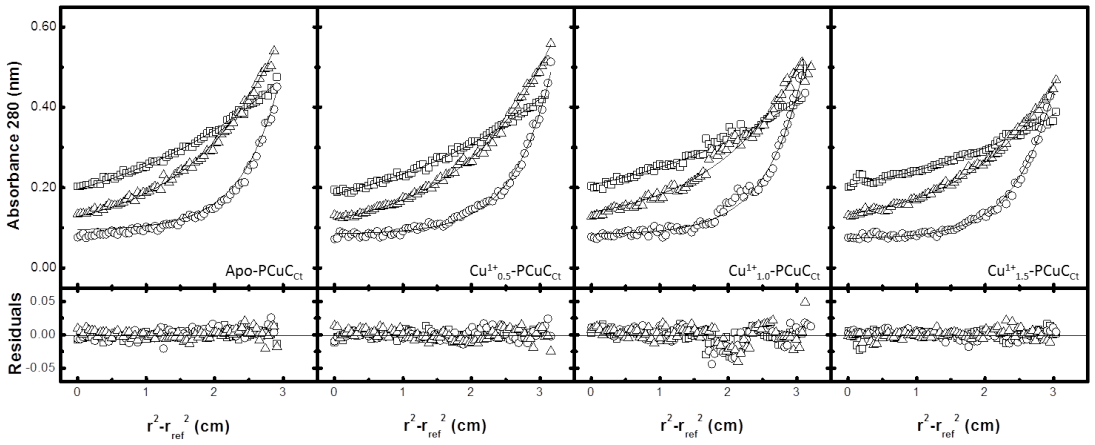

FIGURE 5.5: Effect of Cu^{1+} on the sedimentation equilibrium of $PCuC_{Ct}$. The top graph represent the absorbance profiles of $PCuC_{Ct}$ (110 μM) at 20,000 (□), 30,000 (△) and 50,000 (○) rpm at 20 °C and the lines the fits to a single-component model. The lower panel shows the residual differences between the experimental data and the fitted curves.

Sample	M_w (kDa)	Std
Apo-PCuC$_{Ct}$	13.4	6.2
Cu$^{1+}_{0.5}$-PCuC$_{Ct}$	11.7	1.2
Cu$^{1+}_{1.0}$-PCuC$_{Ct}$	13.6	7.9
Cu$^{1+}_{1.5}$-PCuC$_{Ct}$	14.5	8.5

TABLE 5.2: Calculated M_w of PCuC$_{Ct}$ by sedimentation equilibrium analytical ultracentrifugation. Standard errors of the mean of three technical replicates ($n = 3$).

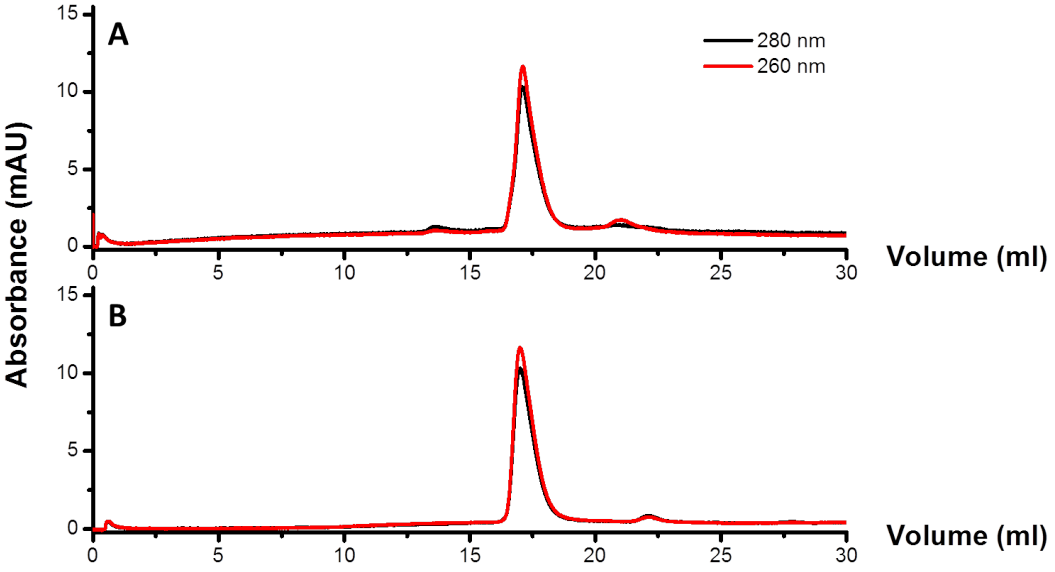

FIGURE 5.6: Analytical size exclusion chromatography of PCuC$_{Ct}$. Plots of absorbance at 280 nm (black line) and 260 nm (red line) as a function of the elution volume for a 100 μM sample of **(A)** apo-PCuC$_{Ct}$ and **(B)** Cu^{1+}-PCuC$_{Ct}$ in 20 mM HEPES, 150 mM NaCl and 0.25 mM DTT (pH 7.5). Sample volume: 150 μL; flow rate: 0.15 mL min^{-1}

5.2.3 Investigating the solution state of $PCuC_{WT}$

The molecular mass and solution state of the native full-length PCuC protein was studied by AUC and ASEC. Equilibrium concentration gradients at lower centrifugal fields (10,000, 18,000 and 25,000 rpm) of reduced apo-$PCuC_{WT}$ containing 0 to 3.0 Cu^{1+} equivalents in 0.5 increments of Cu^{1+}, and 0.0 to 1.5 of Cu^{2+} with 0.5 increments were fit to a single-component model (Figure 5.7 A and B). In graph 5.7, the experimental data has been represented with symbols and the theoretical as solid lines, the residual difference between both data sets is shown in the lower panel. The calculated molecular mass of $PCuC_{WT}$ was 85.3 ± 2.8 kDa (see Table 5.3 for detailed M_w calculation of each sample) which is nearly three times the theoretical mass of $PCuC_{WT}$ (32.2 kDa) and indicates that the protein forms trimers in solution and copper does not affect the oligomeric state adopted by the protein.

The oligomeric state of $PCuC_{WT}$ was also determined by analytical size exclusion chromatography. Addition of Cu^{2+} to apo-$PCuC_{WT}$ was performed under anaerobic conditions in the glove box and buffers were thoroughly degassed with nitrogen before to the chromatography. Figure 5.8 A and B shows the elution chromatograms of apo- and Cu^{2+}-$PCuC_{WT}$. In both cases, a single main peak was detected after 13 mL which is characteristic of a globular protein of 116.5 kDa. This experimental molecular weight is slightly greater than the theoretical weight of a trimeric $PCuC_{WT}$ but smaller than a tetrameric form, indicating that $PCuC_{WT}$ is more likely to form trimers in solution as previously observed by AUC. In addition, copper binding did not affect the oligomerization state of $PCuC_{WT}$, which is also consistent with the AUC results.

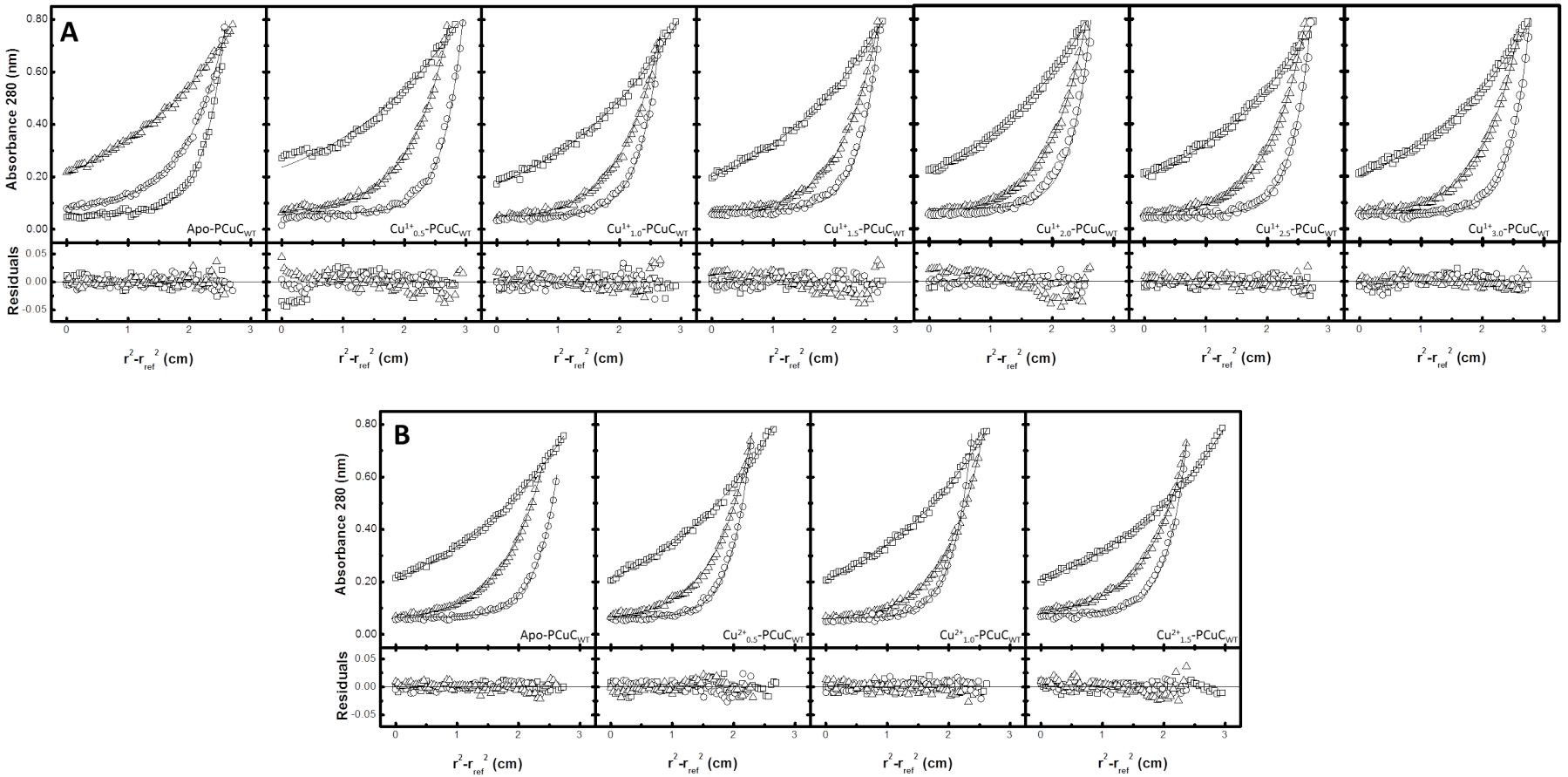

FIGURE 5.7: Effect of **(A)** Cu^{1+} and **(B)** Cu^{2+} on the sedimentation equilibrium of $PCuC_{WT}$. The top graphs represent the absorbance profiles of $PCuC_{WT}$ (15 μM) at 10,000 (□), 18,000 (△) and 25,000 (○) rpm at 20 °C and the lines the fits to a single-component model. The lower panels show the residual differences between the experimental data and the fitted curves.

	Cu^{1+}		Cu^{2+}	
Sample	M_w (kDa)	**Std**	M_w (kDa)	**Std**
Apo-PCuC$_{WT}$	79.3	6.4	88.7	6.2
Cu$_{0.5}$-PCuC$_{WT}$	82.7	8.3	85.7	1.2
Cu$_{1.0}$-PCuC$_{WT}$	81.8	6.0	86.0	7.3
Cu$_{1.5}$-PCuC$_{WT}$	85.4	6.4	84.0	6.9
Cu$_{2.0}$-PCuC$_{WT}$	86.0	6.4	-	-
Cu$_{2.5}$-PCuC$_{WT}$	87.5	6.4	-	-
Cu$_{3.0}$-PCuC$_{WT}$	87.2	6.4	-	-

TABLE 5.3: Calculated M_w of $PCuC_{WT}$ by sedimentation equilibrium analytical ultracentrifugation. Standard errors of the mean of three technical replicates ($n = 3$).

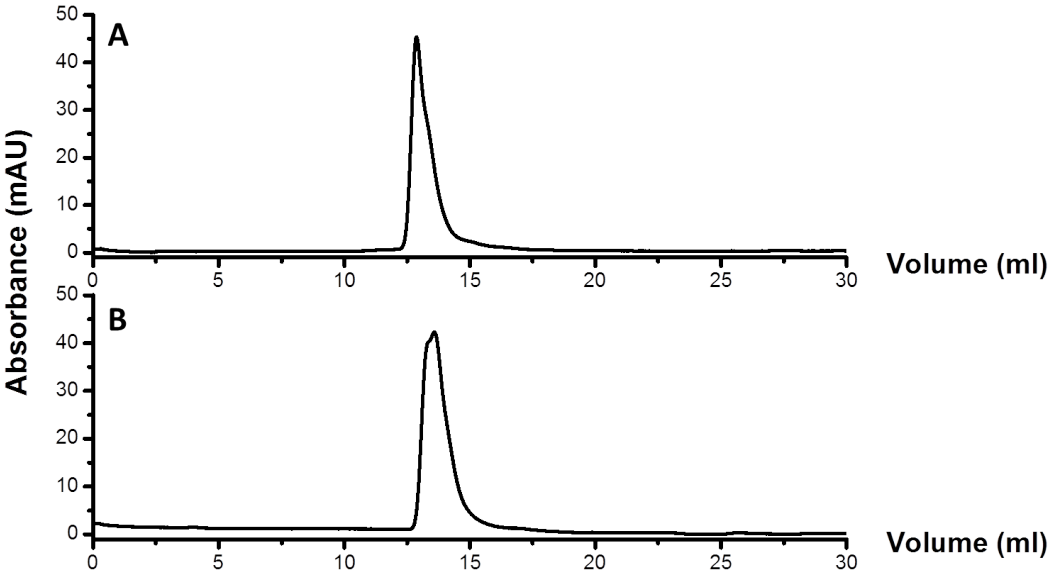

FIGURE 5.8: Analytical size exclusion chromatography of $PCuC_{WT}$. Plots of absorbance at 280 nm as a function of the elution volume for a sample of 60 μM of **(A)** apo-$PCuC_{WT}$ and **(B)** Cu^{2+}-$PCuC_{WT}$ in 20 mM HEPES, 150 mM NaCl and 0.25 mM DTT (pH 7.5). Sample volume: 150 μL; flow rate: 0.15 mL min^{-1}

5.3 Structural determination of PCuC proteins

5.3.1 Crystallographic structure of $PCuC_{Nt}$

With the purpose of trying to solve the crystal structure of PCuC and to understand which of the conserved residues characteristic of YcnI-family proteins (shown in figure 4.9) are involved in copper-binding, samples of 30 mg ml^{-1} of reduced apo-$PCuC_{WT}$ were titrated with $CuSO_4$ (as described in section 2.14) and screened using the sitting drop vapour diffusion method with different commercially available sparse matrix screening kits. After ∼7 days of incubation at 16 °C crystal growth was observed in the conditions listed below in table 5.4. The best diffraction was achieved with the protein crystals that appeared in the condition that contained 20 % PEG8000, 200 mM $MgCl_2$ and 0.1 M Tris-HCl at pH 7.5 and hence this condition was further investigated by varying the concentration of salt, precipitant and the pH range of solutions (see Figure 5.9). During the data acquisition process from PCuC polygonal crystals, it seemed reasonable to use the anomalous scattering of copper for determining the structure, since we had previous evidence that $PCuC_{Nt}$ could bind copper and the protein had been treated with $CuSO_4$. The images collected for the (single-wavelength anomalous dispersion) SAD and native dataset were scaled and merged using the software XIA2 [168] with a resolution of 2.0 and 1.5 Å for the SAD and native dataset, respectively. This software also provides a series of indicators for assessing the quality of the diffraction data (see table 5.5). XIA2 determined the space group of the SAD and native datasets as P63 and their unit cell dimensions as a=68.74, b=68.74 and c=128.71 Å and a=68.58,

Condition	Diffraction
20 % PEG8000, 200 mM $MgCl_2$, 0.1 M Tris-Cl, pH 7.5	∼ 2 Å
2.0 M $(NH_4)_2SO_4$, 0.2 M NaCl, 0.1 M sodium cacodylate, pH 6.5	∼ 8 Å
25 % PEG3350, 0.2 M ammonium acetate, 0.1 M HEPES, pH 7.5	-
25 % PEG1500, 0.1 M PCB buffer	-
25 % PEG4000, 0.1 M sodium cacodylate, pH 6.5	-

TABLE 5.4: Crystallisation conditions where PCuC crystals were produced. The symbol (-) indicates that the crystals were not suitable for data collection.

b=68.58 and c=128.52 Å, respectively. The precision-indicating merging R factor ($R_{p.i.m}$), which ideally should be lower than 0.5 [259], had a value of 0.018 and 0.165 for the inner and outer shell of the SAD dataset, and 0.014 and 0.135 for the native dataset, respectively. The relevance of the measured intensities is estimated with the parameter I/σ(I) which can also be used to determine the cut-off level of the highest resolution shell. Typical values of I/σ(I) should be greater than 2.0 [260] as found for the SAD (outer shell=40.0, inner shell=7.5) and native (outer shell=27.1, inner shell=4.9) dataset. Another parameter that can be used for selecting high-resolution cut-off for data processing and estimates the effective signal-to-noise of the data is the Pearson's correlation coefficient $CC_{1/2}$, which ranges from 0 to 1 and has preferable values above 0.5 [260]. For the SAD dataset, $CC_{1/2}$ of outer and inner shell was 1.000 and 0.979, respectively; and for the native dataset, outer shell=0.995 and inner shell=0.966. The completeness of the SAD dataset was 99.8 for both the outer and inner shell, while for the native dataset had a value of 98.8 and 100, respectively. The redundancy is an indicator of the average number of observations of each reflection and we attempted to satisfy a multiplicity of at least 3 measurements per reflection for the SAD (outer shell=19.4, inner shell=36.9) and native dataset (outer shell=9.8, inner shell=9.9).

The SAD dataset was used to determine the phases and to build a first model with the software Crank2 [170], then this SAD model was feed into the software PHASER [170] in order to solved the $PCuC_{Nt}$ native dataset. Initially PHASER

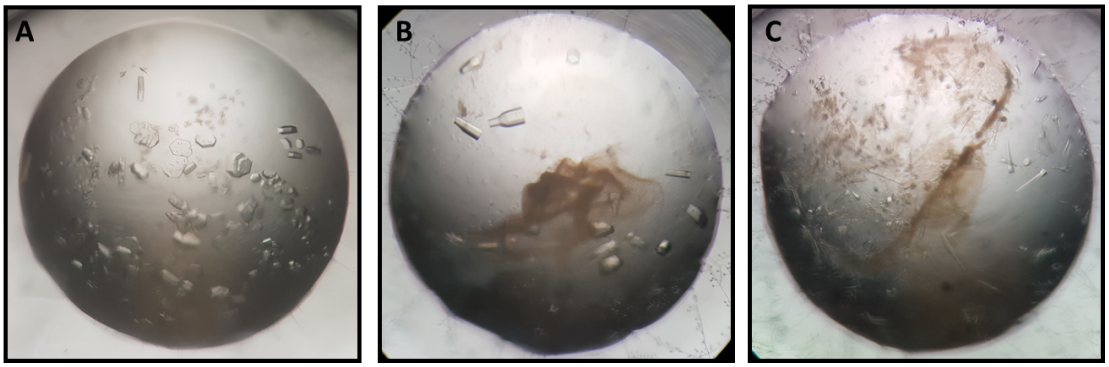

FIGURE 5.9: Protein crystals of $PCuC_{Nt}$ grown at 16 °C in optimised conditions containing PEG8000, $MgCl_2$ and Tris-HCl. Morphology: **(A)** polygonal crystals, **(B)** funnel shaped crystals **(C)** and needle shaped crystals

	$PCuC_{Nt}$ (SAD)	**$PCuC_{Nt}$ (Native)**
Data collection		
Space group	$P6_3$	$P6_3$
Cell dimensions		
a, b, c (Å)	68.74, 68.74, 128.71	68.58, 68.58, 128.52
α, β, γ (°)	90, 90, 120	90, 90, 120
Wavelength (Å)	1.378	0.979
Resolution (Å)	59.53 - 2.00 (2.05 - 2.00)	64.26 - 1.52 (1.56 - 1.52)
$R_{p.i.m}$	0.018 (0.165)	0.014 (0.135)
$I/\sigma(I)$	40.0 (7.5)	27.1 (4.9)
$CC_{1/2}$	1.000 (0.979)	0.995 (0.966)
Completeness (%)	99.8 (98.8)	100 (100)
No. of reflections	10553 (23435)	35609 (23202)
No. of unique reflections	299 (1707)	3578 (3457)
Redundancy	35.3 (13.7)	10.0 (6.7)
Anomalous completeness	97.9 (83.1)	98.8 (4.3)
Anomalous multiplicity	18.2 (6.8)	5.1 (3.6)
Refinement		
Resolution (Å)		1.52
R_{work}/R_{free}		0.168 / 0.193
No of atoms		
Protein		2302
Ligand/ion		2
Water		331
B-factor (Å^2)		
Protein		25.72
Ligand/ion		23.36
Water		47.82
R.m.s. deviations		
Bond lengths (Å)		0.026
Bond angles (°)		2.368

TABLE 5.5: Data collection and structure refinement statistics for $PCuC_{Nt}$. Values indicated in parentheses for outer shell

built two protein chains with 145 residues each and after manual inspection in COOT, an extra residue could be modelled at the C-terminus of each protein molecule. Continuous and defined electron density was observed from residue His^{28} to Asn^{94} and from Thr^{97} to Gly^{173}, residues 95 and 96 were modelled from the calculated non-crystallographic symmetry (NCS) electron density maps. N-terminal sequencing by Edman degradation and ISD MALDI-TOF of $PCuC_{WT}$ (Uniprot ref. A1BAG4) confirmed His^{28} as the first residue of the mature protein after removal of the signal peptide by the Sec apparatus *in vivo*. Conversely since the last residue at the C-terminus was Gly^{173}, this means that although $PCuC_{WT}$ samples were put into crystallisation only the N-terminal domain of the protein managed to crystallise in the pursued condition. Examination of the diffraction data showed that the asymmetric unit contained two protein chains while the biological assembly was in fact a trimer as it had been previously observed for $PCuC_{Nt}$ by AUC and ASEC in section 5.2.1. The standard parameters used to validate refined structural models are indicated in table 5.5. R-factors are indicators of the overall relative disagreement between the experimental and the calculated amplitudes. R_{free} unlike R_{factor} is calculated for only a subset of randomly selected reflections excluded from refinement itself and it helps to highlight when model bias has taken place since the difference between R_{factor} and R_{free} increases drastically. The values obtained for $PCuC_{Nt}$ model were ($R_{factor} = 0.168$ and $R_{free} = 0.193$) within the range for typical structures with a resolution of 1.52 Å as calculated with the software PHENIX ($R_{factor} = 0.102 - 0.232$ and $R_{free} = 0.130 - 0.239$). Root-mean-square deviation (RMSD) parameters measure how well the model fits the expected values for bond length and angles. Typical range of values for RMSD bond length is 0.004 - 0.028 and for angles 0.710 - 2.270, the final model had values of 0.026 and 2.368, respectively. Although, RMSD bond angle value is close to the upper limit, this parameter became less important at high-resolution since the experimental data plays a more relevant role during refinements [261]. Another way of model validation came from the Ramachandran plot, which is a form of visualizing energetically allowed regions for backbone dihedral angles (i.e., angles between two intersecting planes) ϕ (phi) against ψ (psi) of amino acid residues in

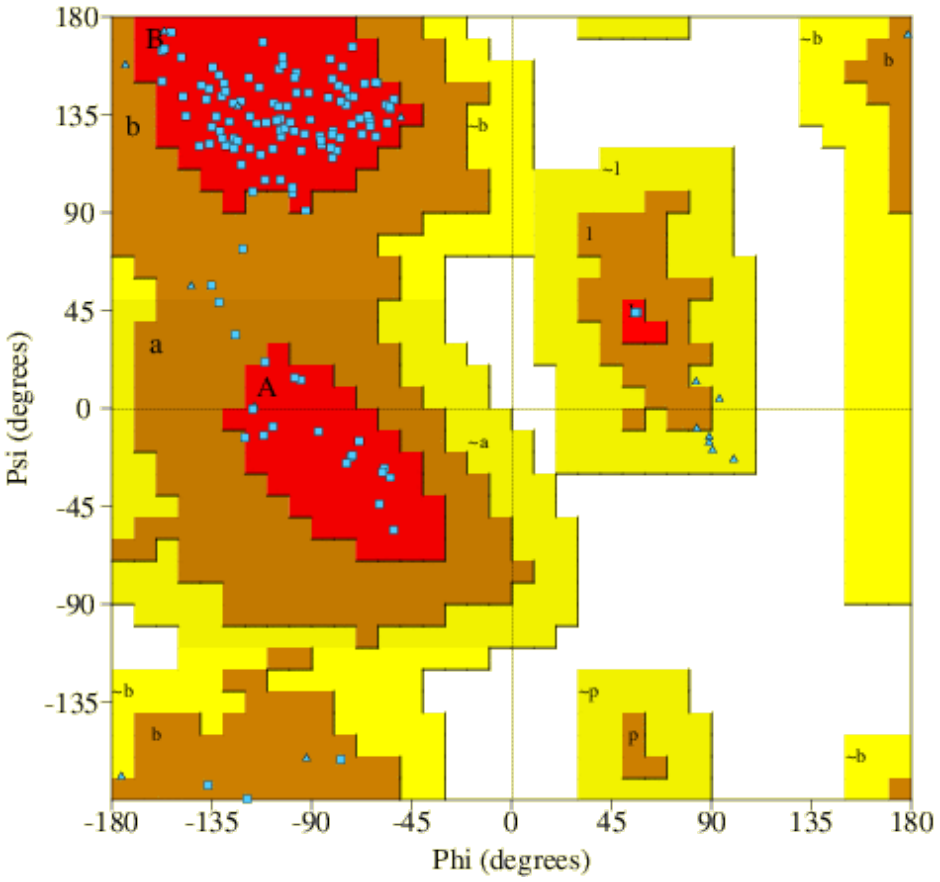

FIGURE 5.10: Ramachandran plot generated from a $PCuC_{Nt}$ monomer. The red, brown and yellow regions represent the favoured, allowed and generously allowed regions, respectively. A total of 143 were plotted, 27 glycines and prolines as triangles (△) and the remaining 116 residues as squares (□).

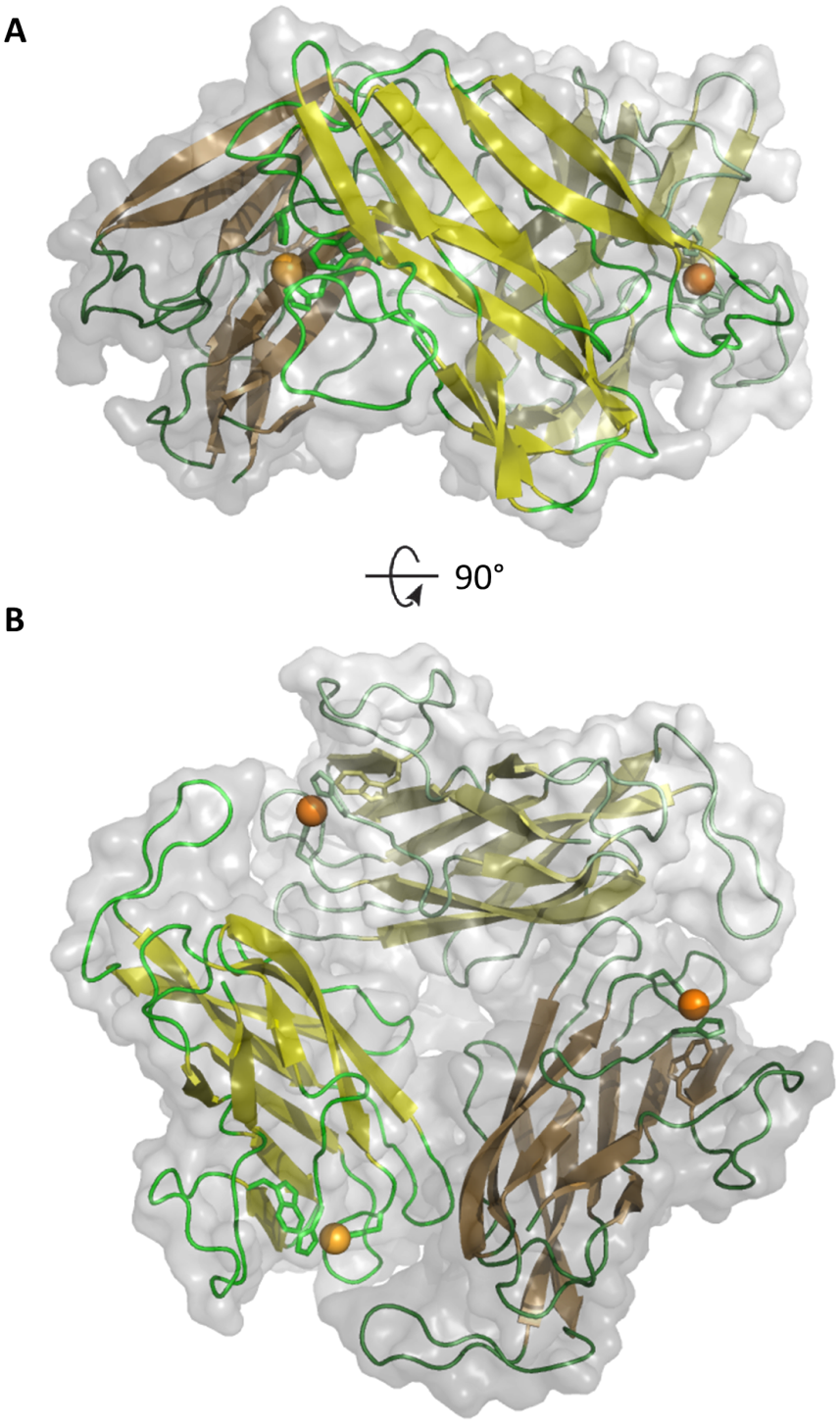

FIGURE 5.11: Cartoon and transparent surface representation of the crystallographic structure of a Cu-bound $PCuC_{Nt}$ trimer. **(A)** Side and **(B)** top view of $PCuC_{Nt}$ trimeric complex. Cu ions have been drawn as ochre spheres.

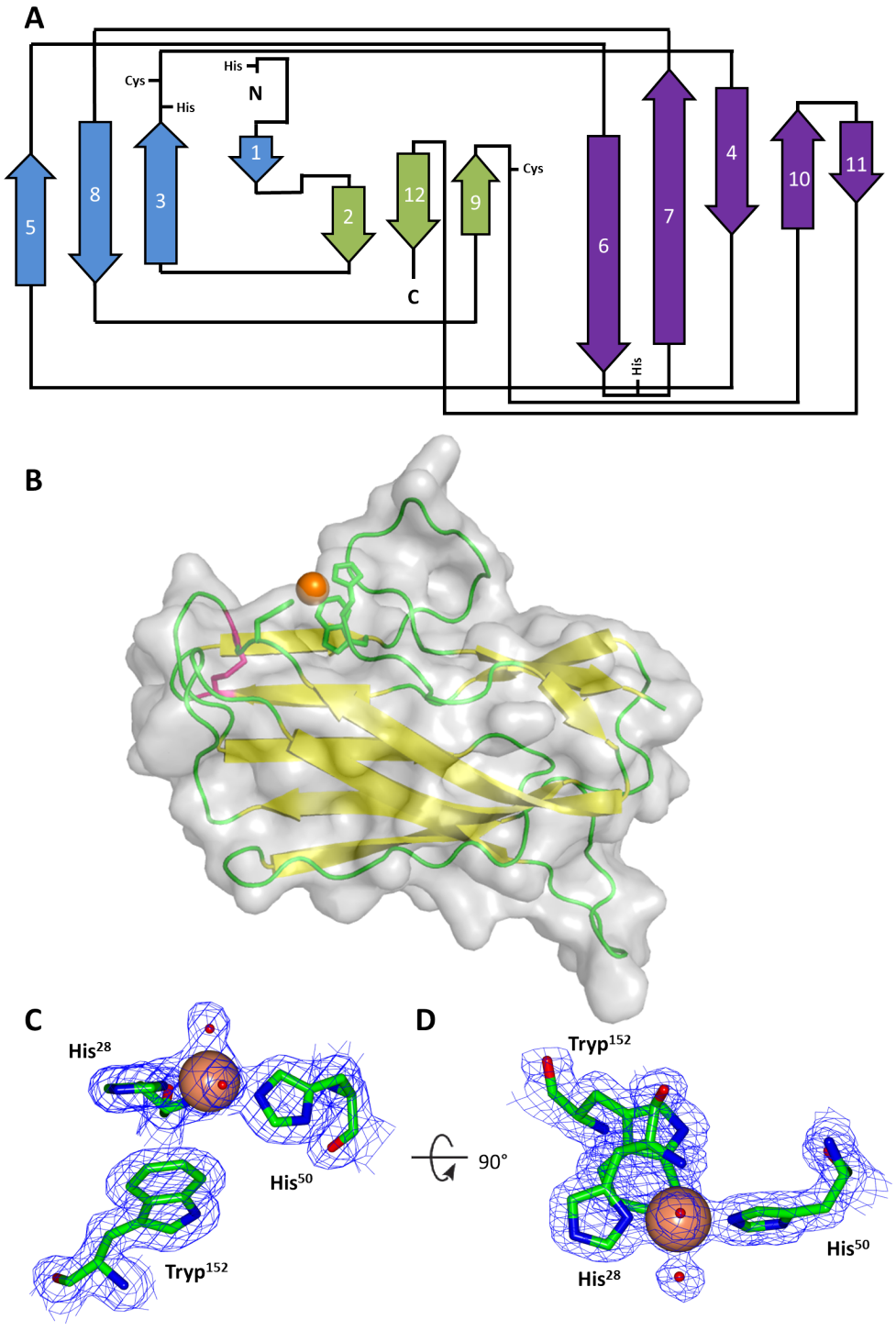

FIGURE 5.12: Crystallographic structure of $PCuC_{Nt}$. **(A)** 2D topology diagram representation of $PCuC_{Nt}$, the 3 β-sheets are coloured in blue, green and purple and the cysteines and histidines residues have also been represented. **(B)** Cartoon and transparent surface representation of a $PCuC_{Nt}$ monomer. Cysteine residues have been coloured in pink to denote the location of the disulphide bond. **(C)** Side and **(D)** top view of the copper binding site and the $2F_0 - F_c$ electron density map contoured at 1.2 σ. Cu ions have been drawn as ochre spheres and water molecules as small red spheres.

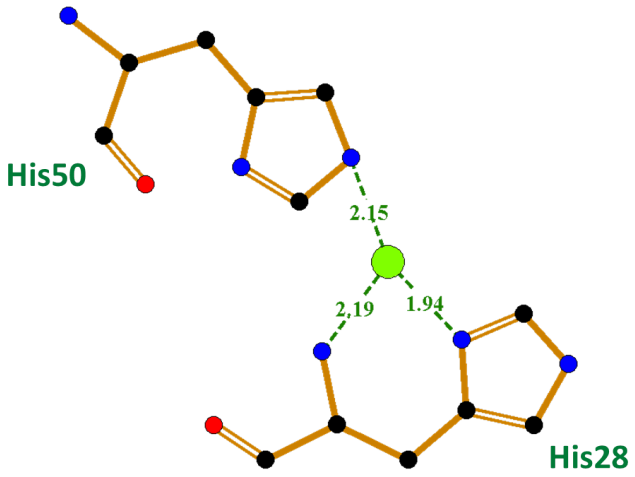

FIGURE 5.13: Schematic diagram of $PCuC_{Nt}$ *histidine brace* using the software LigPlot [94]

Bond	**Length/angle (Å, °)**
His^{28} N1	2.19
His^{28} Nδ1	1.94
His^{50} Nε2	2.15
H_2O 1	2.22
H_2O 2	2.22
His^{28} N1 - Cu - His^{28} Nδ1	89.6
His^{28} N1 - Cu - His^{50} Nε2	84.5
His^{28} Nδ1 - Cu - His^{50} Nε2	159.0
H_2O 1 - Cu - H_2O 2	105.7
H_2O 1 - Cu - His^{28} N1	94.0
H_2O 1 - Cu - His^{28} Nδ1	97.0
H_2O 1 - Cu - His^{50} Nε2	103.6
H_2O 2 - Cu - His^{28} N1	159.8
H_2O 2 - Cu - His^{28} Nδ1	92.6
H_2O 2 - Cu - His^{50} Nε2	86.6

TABLE 5.6: Bond lengths and angles of the Cu-binding site of $PCuC_{Nt}$

protein structures. A total of 146 residues were plotted of which 119 were analysed (excluding 16 glycines and 11 prolines). From the 119 residues, 109 were found in most favoured regions, 10 in additional allowed regions and none in generously allowed or disallowed regions (Figure 5.10).

$PCuC_{Nt}$ trimer was reconstituted by applying crystallographic symmetry (see figure 5.11). Analysis of the trimeric model using the on-line software PISA [262] for the exploration of macromolecular interfaces showed that the oligomerization interface between each monomeric unit has an area of $\sim$ 466 Å^2. At least fourteen residues intervene in the oligomerization forming a total of five hydrogen bonds and four salt bridges between each monomer. The structure of monomeric $PCuC_{Nt}$ is composed of a total of twelve β-strands distributed in a topology that resembles an inmunoglobuline-like fold [263] according to the protein structure classification database CATH [257]. The β-strands are organised in three β-sheets, two antiparallel β-sheets and one mixed, and together they are structured in an overall β-sandwich framework within a classical Greek-key topology (Figure 5.12 A). However, perhaps the most interesting feature is the presence of a copper atom coordinated within a rectangular pyramid geometry at the N-terminus of $PCuC_{Nt}$ by two histidine residues and two water molecules. The copper assignment to the metal site was also validated using the server CheckMyMetal [264] which uses a combination of several well-established concepts that have been frequently used in structural biology such as bond valence [265], vector sum of bond valences (VECSUM) [266], metal binding sites [267], coordination geometries [268], metal binding environment [269], etc. The base of the rectangular pyramid is formed by solvent exposed ligands, two nitrogens (Nδ1 and N1) in a T-shaped arrangement from His^{28}, one nitrogen from the imidazole ring (Nε2) of His^{50} and a water molecule (see figure 5.12 C and D). A fifth water molecule completes the square pyramidal geometry in an axial position while the protein-facing position is occluded by Cη2 from the indole group of Trp^{153} (at a distance of 3.57 Å). The close proximity of Trp^{153} to the Cu-binding site could be the reason for the fluorescence quench observed in section 4.5.1 and 4.5.2. The particular geometry of His^{28} that contributes as a bidentate ligand has previously been termed as *histidine brace* [270]. Two cysteine

residues are present within $PCuC_{Nt}$, the first cysteine residue (Cys^{53}) is located downstream His^{50} in a loop region at the end of β_3 while the second cysteine residue (Cys^{146}) is also found in a loop region at the end of β_9. Cys^{53} and Cys^{146} form a disulfide bond in $PCuC_{Nt}$ model.

5.3.2 Crystallographic structure of $PCuC_{Ct}$

Based on the assumption that the holo form of $PCuC_{Ct}$ would be more likely to crystallise. We reconstituted samples of 20 $mg\,ml^{-1}$ of apo-protein with one equivalent of Cu^{1+} in the glove box. Cu^{1+}-$PCuC_{Ct}$ samples were screened aerobically with hundreds of crystallisation solutions using commercially available sparse matrix screening kits by the sitting drop vapour diffusion method. After more than 30 days of incubation at 16 °C crystals of polygonal morphology were observed in a solution of 100 mM trisodium citrate, 200 mM potassium sodium tartrate and 2.0 M ammonium sulphate pH 5.6 (see figure 5.14). The crystallographic structure of Cu^{1+}-$PCuC_{Ct}$ was solved to a resolution of 1.6 Å by molecular replacement (MR). The software MoRDa [172] used the coordinates of the extracytoplasmic copper chaperone-like protein (ECuC) from *S. lividans* (PDB accession codes: 3ZJA) as a search template, as described in Chapter 2 section 2.19.2.2. The indicators used to assess the quality of the diffraction data and refined model are listed below in table 5.7. Analysis of the 127 residues built within the model by the Ramachandran representation (excluding 19 glycines and 11 prolines) showed that 87 residues were found in most favoured region, 10 in additional allowed regions and none in generously allowed of disallowed regions (see figure 5.16).

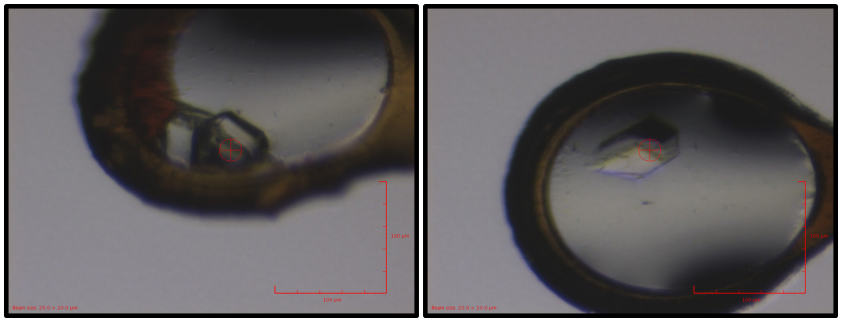

FIGURE 5.14: Example of polygonal crystals obtained for $PCuC_{Ct}$.

	$PCuC_{Ct}$ (Native)
Data collection	
Space group	$P2_1$
Cell dimensions	
a, b, c (Å)	73.8, 43.5, 41.6
α, β, γ (°)	90.0, 111.3, 90.0
Wavelength (Å)	0.979
Resolution (Å)	4.34 - 36.81 (1.60 - 1.63)
$R_{p.i.m}$	0.014 (0.135)
$I/\sigma(I)$	13.7 (1.0)
$CC_{1/2}$	1.0 (0.7)
Completeness (%)	100 (99.9)
No. of reflections	5320 (5300)
No. of unique reflections	1673 (1583)
Redundancy	3.2 (3.3)
Anomalous completeness	88.9 (92.5)
Anomalous multiplicity	1.8 (1.8)
Refinement	
Resolution (Å)	1.60
R_{work}/R_{free}	0.179 / 0.240
No of atoms	
Protein	956
Ligand/ion	7
Water	65
B-factor (Å^2)	
Protein	26.64
Ligand/ion	19.16
Water	34.39
R.m.s. deviations	
Bond lengths (Å)	0.019
Bond angles (°)	1.974

TABLE 5.7: Data collection and structure refinement statistics for $PCuC_{Ct}$. Values indicated in parentheses for outer shell

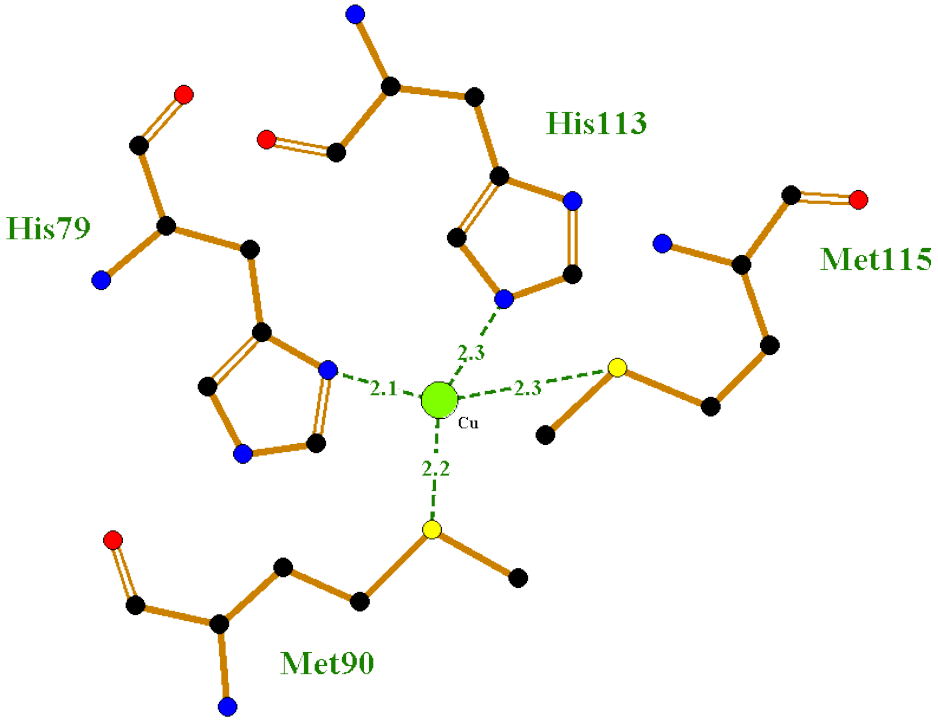

FIGURE 5.15: Schematic diagram of $PCuC_{Ct}$ Cu^{1+} binding site using the software LigPlot [94]

Bond	**Length/angle (Å, °)**
His^{79} Nδ1	2.1
Met^{90} Sσ	2.2
His^{113} Nϵ2	2.3
Met^{115} Sσ	2.3
His^{79} Nδ1 – Cu – Met^{90} Sσ	106.4
His^{79} Nδ1 – Cu – His^{113} Nϵ2	114.1
His^{79} Nδ1 – Cu – Met^{115} Sσ	108.5
Met^{90} Sσ – Cu – His^{113} Nϵ2	110.1
Met^{90} Sσ – Cu – Met^{115} Sσ	111.1
His^{113} Nϵ2 – Cu – Met^{115} Sσ	106.7

TABLE 5.8: Bond lengths and angles of the Cu-binding site of $PCuC_{Ct}$

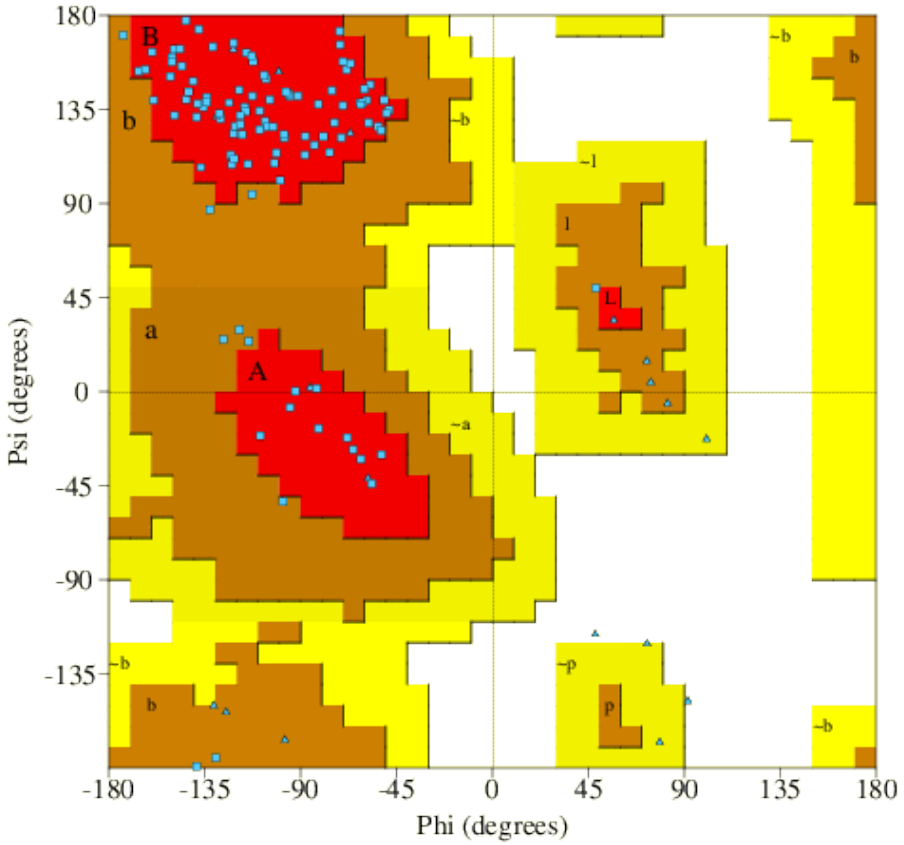

FIGURE 5.16: Ramachandran plot generated for a $PCuC_{Ct}$ monomer. The red, brown and yellow regions represent the favoured, allowed and generously allowed regions, respectively. A total of 127 were plotted, 30 glycines and prolines as triangles (△) and the remaining 97 residues as squares (□).

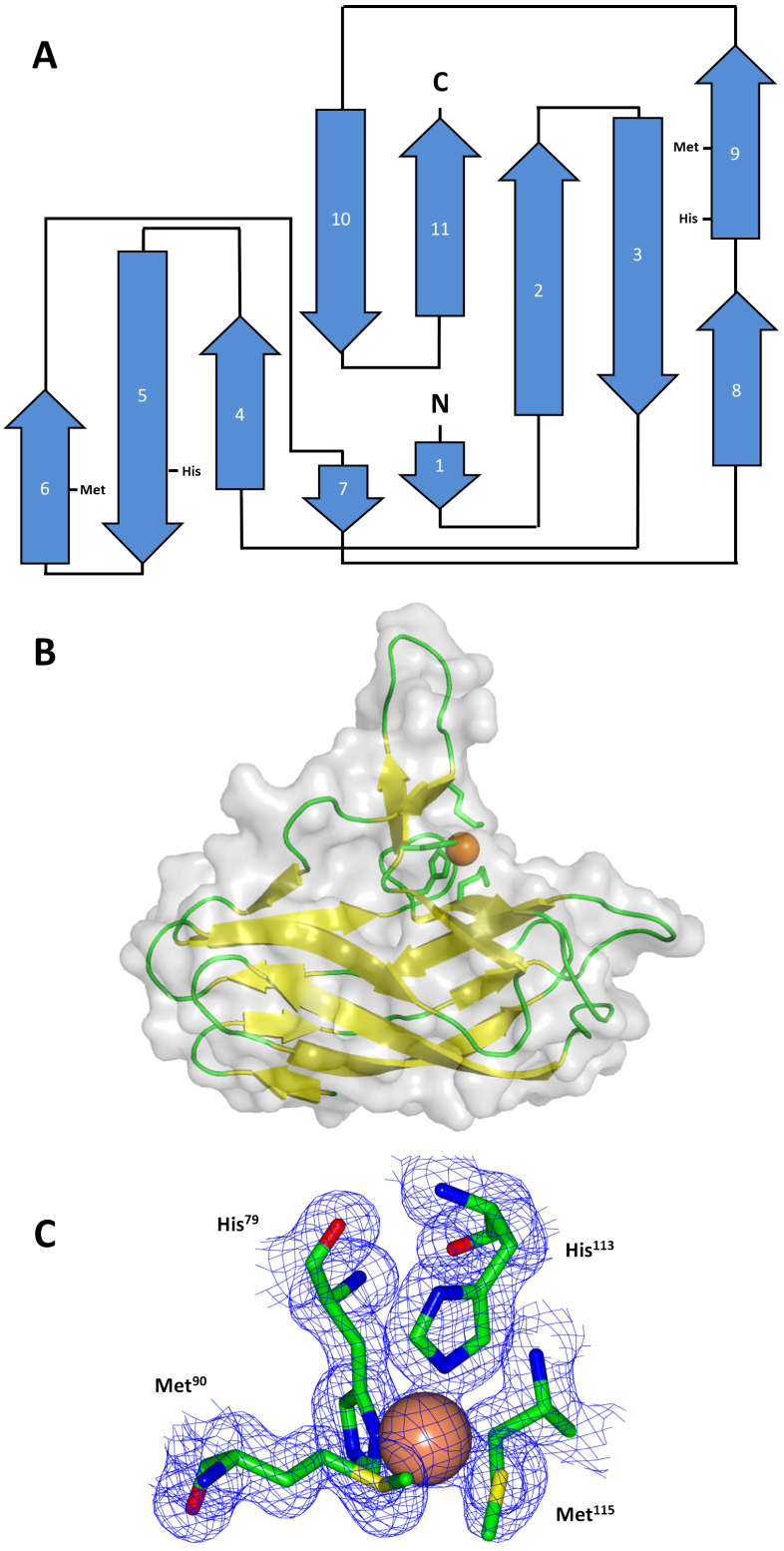

FIGURE 5.17: Crystallographic structure of $PCuC_{Ct}$. **(A)** 2D topology diagram representation of $PCuC_{Ct}$, the β-sheet is coloured in blue, the methionine and histidine residues involved in copper binding have also been represented. **(B)** Cartoon and transparent surface representation of a $PCuC_{Ct}$ monomer. **(C)** Copper binding site and the $2F_0 - F_c$ electron density map contoured at 1.2 σ. Cu ions have been drawn as ochre spheres.

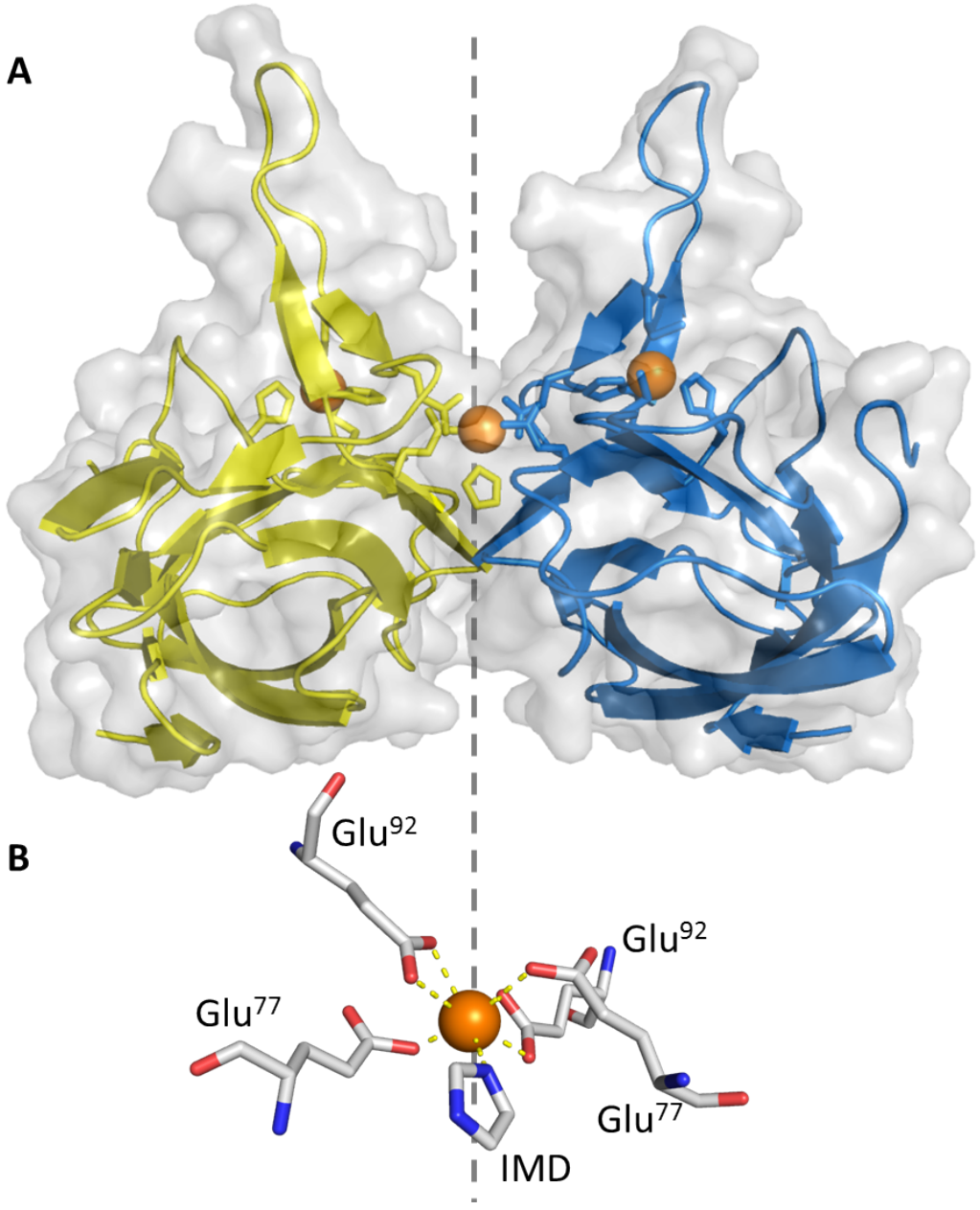

FIGURE 5.18: Symmetry axis of $PCuC_{Ct}$. **(A)** Cartoon and transparent surface representation of two monomers of $PCuC_{Ct}$ facing the symmetry axis. **(B)** Copper ion on special position. Cu ions have been drawn as ochre spheres.

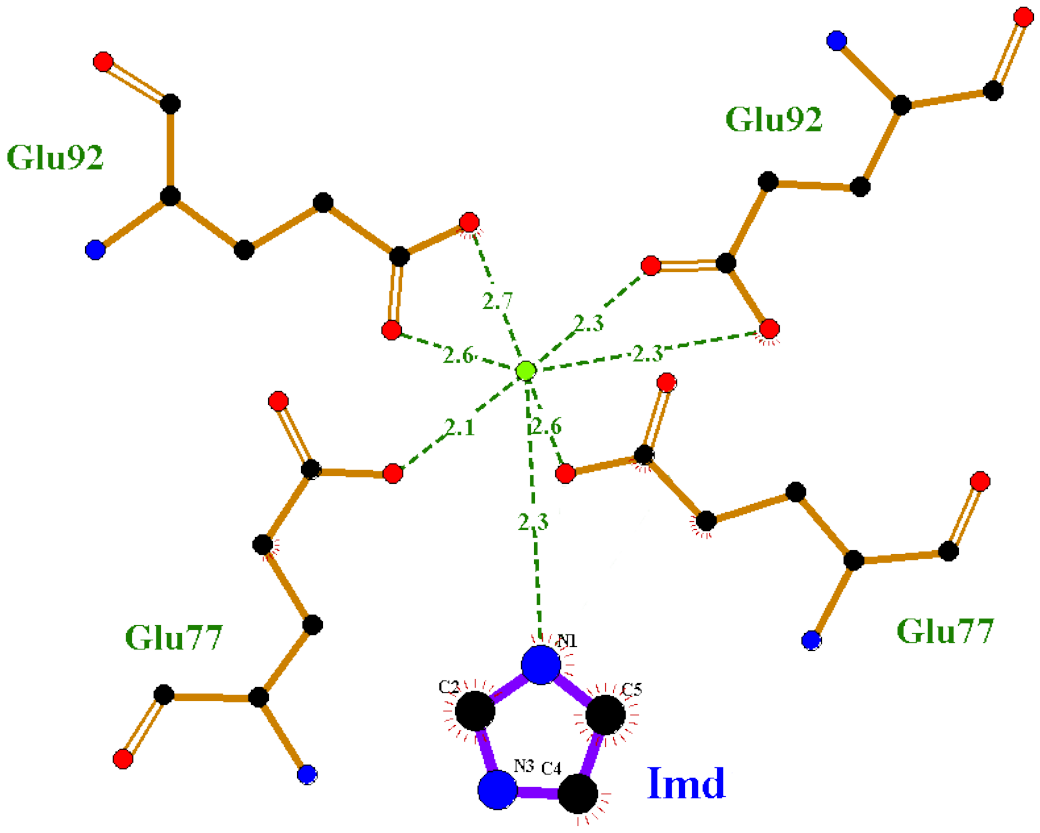

FIGURE 5.19: Schematic diagram of the residues involved in the coordination of the special position Cu ion of $PCuC_{Ct}$ using the software LigPlot [94]

Bond	**Length/angle (Å, °)**
Glu^{77} Oϵ2 chain A	2.6
Glu^{92} Oϵ1 chain A	2.3
Glu^{92} Oϵ2 chain A	2.3
Glu^{77} Oϵ2 chain B	2.1
Glu^{92} Oϵ1 chain B	2.6
Glu^{92} Oϵ2 chain B	2.7
Imidazole N1	2.3
Glu^{77} Oϵ2 chain A – Cu – Glu^{92} Oϵ1 chain A	82.9
Glu^{77} Oϵ2 chain A – Cu – Glu^{92} Oϵ2 chain A	85.9
Glu^{77} Oϵ2 chain A – Cu – Glu^{77} Oϵ2 chain B	167.4
Glu^{77} Oϵ2 chain A – Cu – Glu^{92} Oϵ1 chain B	79.8
Glu^{77} Oϵ2 chain A – Cu – Glu^{92} Oϵ2 chain B	82.3
Glu^{77} Oϵ2 chain A – Cu – Imidazole N1	81.7
Glu^{92} Oϵ1 chain A – Cu – Glu^{92} Oϵ2 chain A	57.5
Glu^{92} Oϵ1 chain A – Cu – Glu^{77} Oϵ2 chain B	98.0
Glu^{92} Oϵ1 chain A – Cu – Glu^{92} Oϵ1 chain B	81.6
Glu^{92} Oϵ1 chain A – Cu – Glu^{92} Oϵ2 chain B	130.7
Glu^{92} Oϵ1 chain A – Cu – Imidazole N1	139.8
Glu^{92} Oϵ2 chain A – Cu – Glu^{77} Oϵ2 chain B	105.2
Glu^{92} Oϵ2 chain A – Cu – Glu^{92} Oϵ1 chain B	138.0
Glu^{92} Oϵ2 chain A – Cu – Glu^{92} Oϵ2 chain B	164.2
Glu^{92} Oϵ2 chain A – Cu – Imidazole N1	84.5
Glu^{77} Oϵ2 chain B – Cu – Glu^{92} Oϵ1 chain B	87.9
Glu^{77} Oϵ2 chain B – Cu – Glu^{92} Oϵ2 chain B	87.8
Glu^{77} Oϵ2 chain B – Cu – Imidazole N1	104.9
Glu^{92} Oϵ1 chain B – Cu – Glu^{92} Oϵ2 chain B	49.6
Glu^{92} Oϵ1 chain B – Cu – Imidazole N1	131.1
Glu^{92} Oϵ2 chain B – Cu – Imidazole N1	83.3

TABLE 5.9: Bond lengths and angles of the special position copper of $PCuC_{Ct}$

$PCuC_{Ct}$ is a soluble monomeric protein and is made up of a total of eleven β-strands. These β-strands are arranged in a single β-sheet within a Greek key β-barrel motif. Peculiarly striking is the presence of a flexible and solvent exposed β-hairpin that involves β_6 and β_7 and protrudes from the β-barrel. However and more importantly, a single Cu^{1+} atom was modelled within the soluble domain of $PCuC_{Ct}$ coordinated by residues His^{79}, Met^{90}, His^{113} and Met^{115} forming the highly conserved $H(M)X_{10}MX_{21}HXM$ copper binding motif (see figure 5.17). The two methionine Cu-ligands are solvent-exposed with their Cγ atoms located at the protein surface, while the histidine Cu-ligands are further away from the protein surface. The bond length and angles between the ligands and Cu^{1+} suggest that the copper atom is coordinated within a distorted tetrahedral geometry (see table 5.8).

A second copper atom has been modelled within the crystallographic unit. Curiously, this copper is located at the surface of the protein on a symmetry axis and is probably a crystal artefact as a result of the crystallisation process of the protein. This Cu is coordinated by an imidazole ring (also located across the symmetry axis), two glutamic acid residues from one protein molecule and another two glutamic acid from a symmetry-related molecule (see figure 5.18). In this case the bond length and angles between the ligands and the copper atom suggest of a pentagonal bipyramidal molecular geometry (see table 5.9).

5.3.3 Small-Angle X-ray scattering, SAXS

Despite extensive screening, we were unable to obtain protein crystals of full length PCuC protein. This is likely due to the presence of a disordered region that links both N- and C-terminal domains together, such flexibility may be incompatible with protein crystal formation. Therefore, we tried to elucidate the structural arrangement of $PCuC_{Nt}$ and $PCuC_{Ct}$ within the two-domain protein by small-angle X-ray scattering (SAXS). This technique provides valuable information about the size and shape of macromolecules in solution and is a commonly used in the study

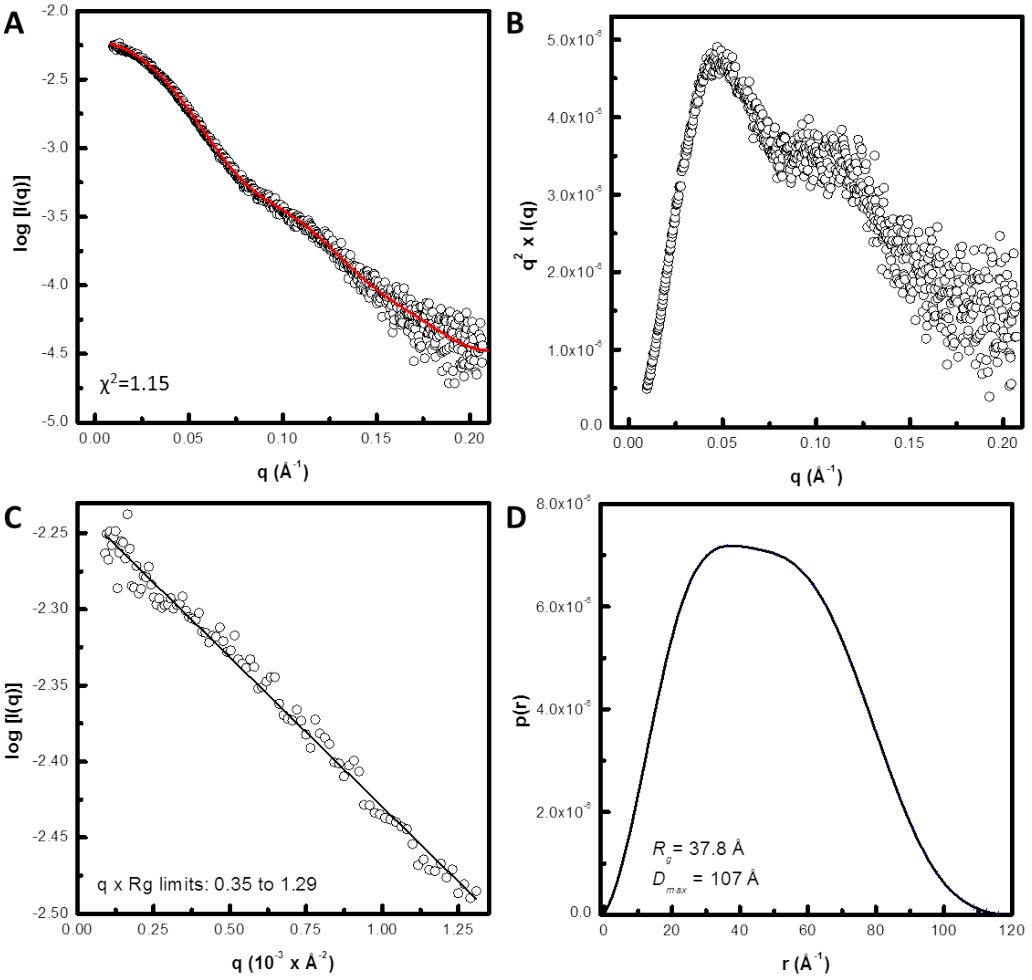

FIGURE 5.20: Solution characterisation of native full-length PCuC by SAXS. **(A)** Scattering curve of PCuC and fitting of the protein envelope generated with the software GASBOR [165] (red line); **(B)** Kratky plot showing that PCuC is a multidomain protein with signs of flexibility; **(C)** Guinier plot and calculated R_g value; **(D)** P(r) distribution function of PCuC, R_g and D_{max} values are indicated.

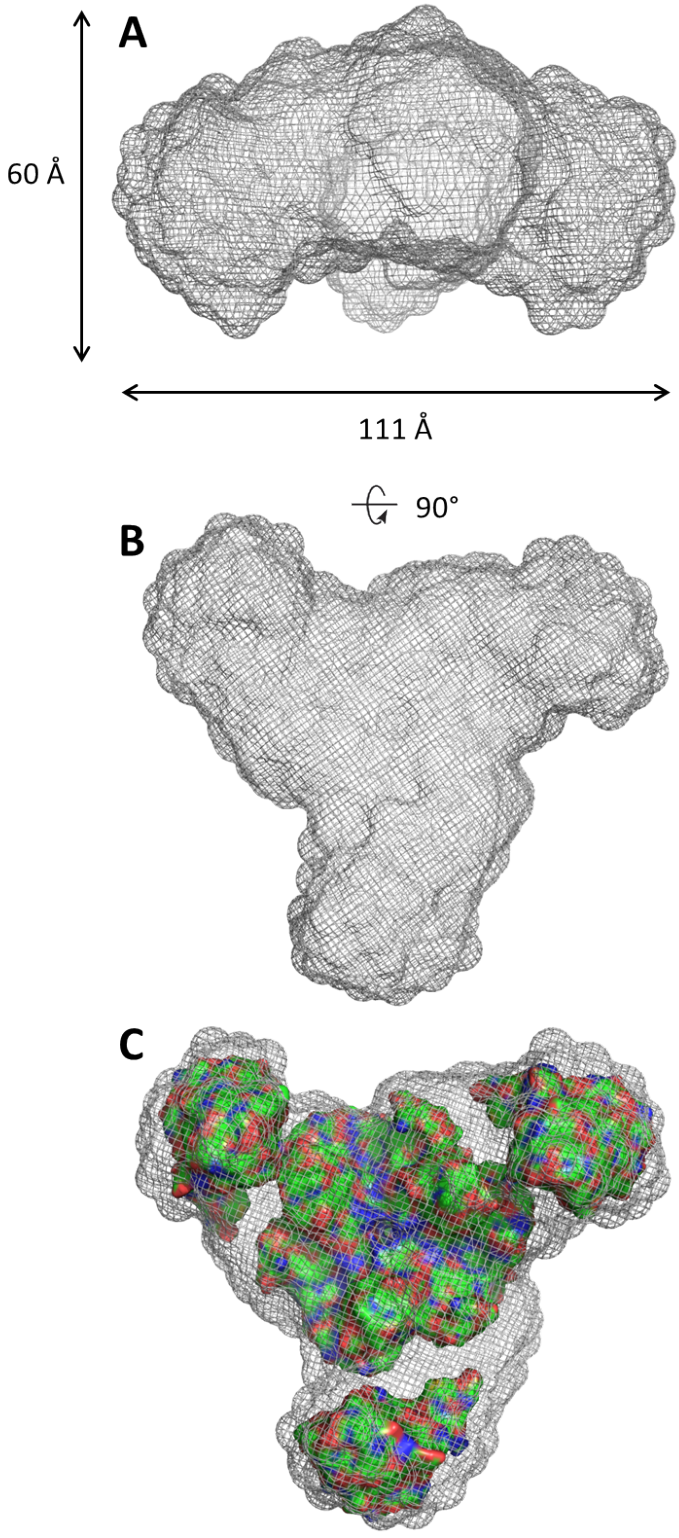

FIGURE 5.21: PCuC full length structural model. (Side view and **(B)** top view. The monomers of the trimer have been coloured in green magenta and blue. Copper atoms are represented as spherical atoms and coloured in orange.)

of flexible proteins. Samples of $PCuC_{WT}$ were analysed at Diamond Light Source beamline B21 by ASEC-SAXS as described in section 2.18.

Throughout the analysis of the scattering curves, features of protein flexibility and signs of the presence of a multidomain protein were observed. For instance, the Kratky plot analysis (see figure 5.20 B) presented a double peak bell-shaped curve at low q and a rise to a plateau at high q, which is typical of a multidomain protein with disordered regions. From the Guinier plot (see figure 5.20 C) we could infer a radius of gyration (R_g) of 36.82 Å^3 and a forward scattered intensity (I(0)) of 5.80 x 10^{-3}. In addition, the pair-wise distance distribution function was estimated by Fourier inversion of the experimental intensities using Scatter [156]. The real space representation of the scattering data generated a bell-shaped profile with a D_{max} of 107 Å and two humps or shoulders, also typical of multidomain proteins. The real space R_g from the P(r) function was calculated to be 37.8 Å^3 and is consistent with the reciprocal R_g obtained from the Guinier Plot.

The software GASBOR from the ATSAS suite was used for *ab initio* shape-determination in order to generate a surface envelope of native full-length PCuC protein. Instead of using *dummy atoms* as DAMMIF or DAMMIN [159, 210], GASBOR attempts to reconstruct a protein structure based on chain-like ensemble of *dummy residues* [165]. The program was set up to model 310 residues in slow mode and P3 symmetry (due to our previous knowledge of the solution properties of $PCuC_{WT}$). The fitting of the surface enveloped model (see figure 5.21) is shown as a red line along the scattering curve in figure 5.20 A. The crystallographic structures of $PCuC_{Nt}$ and $PCuC_{Ct}$ were superposed manually on Pymol [146] into the surface envelope of $PCuC_{WT}$ (see Figure 5.21 C). The best fit indicated that $PCuC_{Nt}$ and $PCuC_{Ct}$ are more likely to be arranged forming a trimeric protein in which the N-terminal domain of each monomer is forming a central core, i.e. contain the majority of protein-protein interactions (as observed with the X-ray structure of the $PCuC_{Nt}$) leaving the C-terminal domain at the outer side of the protein exposed towards surrounding solution through a flexible linker region (see Figure 5.21 C). This structural model is therefore in agreement with the AUC and ASEC data of PCuC, and the fact that the affinity-tagged N-terminal domain

can pull down native full-length PCuC when purified from *P. denitrificans* WT by affinity chromatography.

5.4 Discussion

PCuC from *P. denitrificans* is an interesting protein made up of a YcnI N-terminal domain and a PCu_AC C-terminal domain. Importantly, PCuC is a metal binding protein with an affinity for copper below the femtomolar level and is required for N_2OR respiration when copper is a scarce resource in the bacterial media. Here we have identified and characterised the solution properties $PCuC_{Nt}$, $PCuC_{Ct}$ and $PCuC_{WT}$. In addition, we have resolved the crystallographic structure of $PCuC_{Nt}$ and $PCuC_{Ct}$. By performing SAXS on $PCUC_{WT}$ we have built a structural model for full length PCuC protein.

Investigation of the oligomeric state of $PCuC_{Nt}$ and $PCuC_{WT}$ by analytical ultracentrifugation and size exclusion chromatography showed that both proteins behave as trimers (of $\sim$ 56.4 and 100.7 kDa, respectively) while $PCuC_{Ct}$ behaved as a monomer under all conditions studied (of $\sim$ 17.6 kDa). In addition, a common feature of the three proteins is that complex formation preceded independently of copper binding indicating that the protein may oligomerise prior to copper loading. Similar oligomeric features have been reported for YcnI from *N. farcinica* that forms homodimers within its biological assembly [253] and for monomeric PCu_AC from *D. radiodurans* [5] and *S. lividans* [216]. The fact that $PCuC_{Nt}$ trimerises and that two histidines of each monomer are involved in metal coordination may explain why $PCuC_{WT}$ binds naturally to a Ni^{2+}-IMAC column. This is something that we have repeatedly observed, for instance during the purification of $ScoB_{sol}$ (see figure 3.7 A) or especially during the isolation of $PCuC_{Nt}$ (see figure 5.22), where in both cases the identity of the 35 kDa band has been confirmed by MALDI-TOF as $PCuC_{WT}$. This is also the reason why after the initial exploratory experiment from section 4.2 we decided to purify all PCuC proteins from a *pcuC*$^-$ mutant ba-

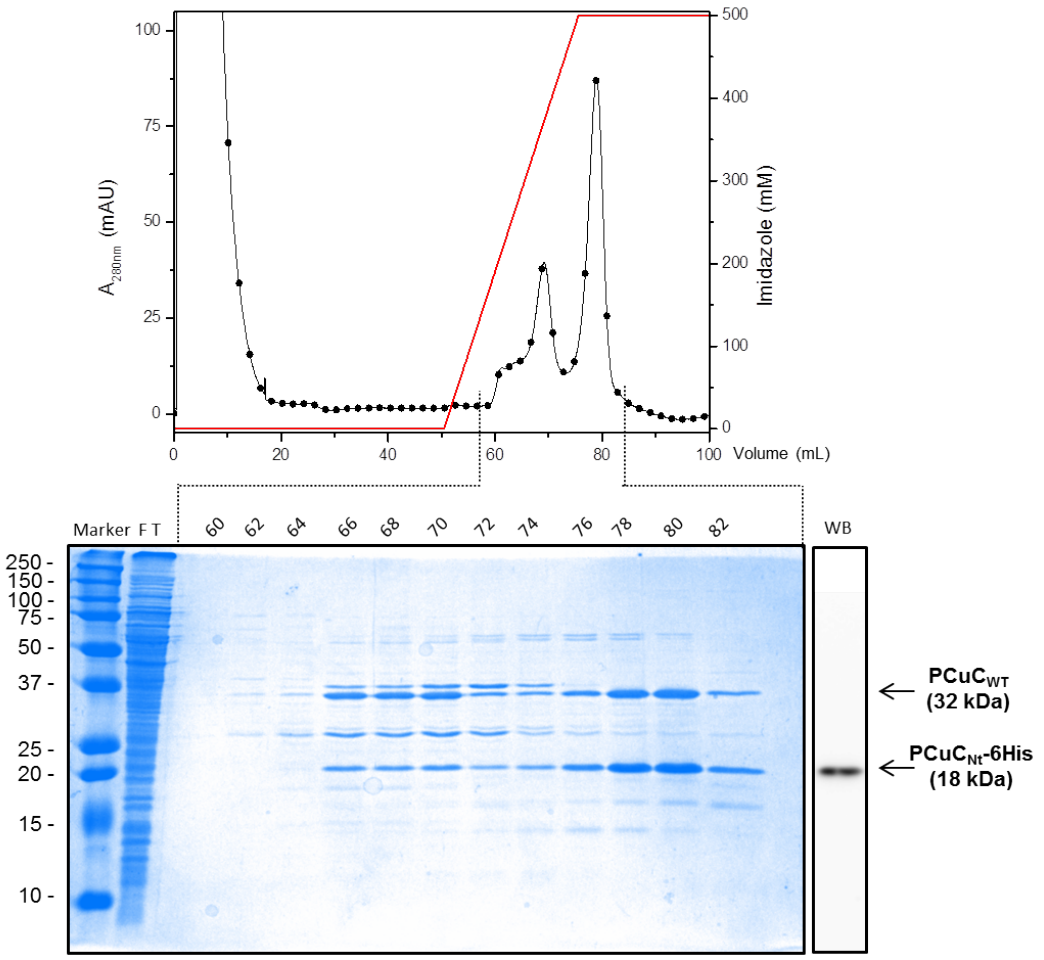

FIGURE 5.22: Purification of $PCuC_{Nt}$-6His from wild-type *P. denitrificans*. Top graph is the elution chromatogram and the bottom graph is the coomassie SDS-PAGE gels of the corresponding fraction along with a Western-Blot from pooled eluted fractions. FT: flow through

ckground since it was not possible to break the strong interaction of $PCuC_{WT}$ and $PCuC_{Nt}$ and separate them using chromatographic techniques.

The crystal structure of Cu^{2+}-$PCuC_{Nt}$ represents the first copper-bound structural determination of a YcnI-type protein. Overall, $PCuC_{Nt}$ is a trimeric protein and each monomer is solely composed of β-strands that are distributed within a topology that resembles an immunoglobulin-like fold [263]. The software DALI [271] was used to search the Protein Data Bank (PDB) [272] for proteins that share a similar fold to $PCuC_{Nt}$. The closest match found was YcnI (PDB accession code: 3ESM) from *N. farcinica* (Z-score: 15.2 %, Id: 25%) and the rest of the structures identified had Z-score values and sequence identity below 9 and 15 %, respectively. Superposition of Cu^{2+}-$PCuC_{Nt}$ and YcnI structures showed a similar overall structure, with the major difference being the presence of an extended disorder loop region between β_6 and β_6 in $PCuC_{Nt}$ that is not present in YcnI. However, the most interesting remark about $PCuC_{Nt}$ structure is the presence of a single copper ion per monomer that is coordinated by the first residue of $PCuC_{Nt}$. The first N-terminal residue in the mature protein, once it has been processed by the Sec apparatus and exported to the periplasm, is His^{28} (which has been confirmed by Edman degradation and ISD MALDI-TOF) and acts as a bidentate ligand to the copper arranged in a T-shaped manner. This special disposition has been previously observed in other copper-binding proteins, such as the copper resistance protein CopC [69] and in lytic polysaccharide monooxygenases (LPMO) proteins [273] and has received the generic name of *histidine brace* (see figure 5.23) [270]. The high Cu^{1+} affinity of $PCuC_{Nt}$ is similar to other histidine-brace copper-binding proteins (see table 5.10). However, it is relevant to notice that the values reported in table 5.10 are only relative to Cu^{2+} based on the assumption that CopC and LPMO are Cu^{2+}-binding proteins although the literature is not clear about whether these proteins can also bind Cu^{1+}. Moreover, almost all K_D determinations of LPMO proteins have been performed by direct titration of Cu^{2+} by ITC, a technique that is not sensitive enough to accurately calculate such a low binding affinities [154, 274].

This manner of protein maturation has important implications, for instance during experimental design identifying the first residue of the mature protein is crucial if a

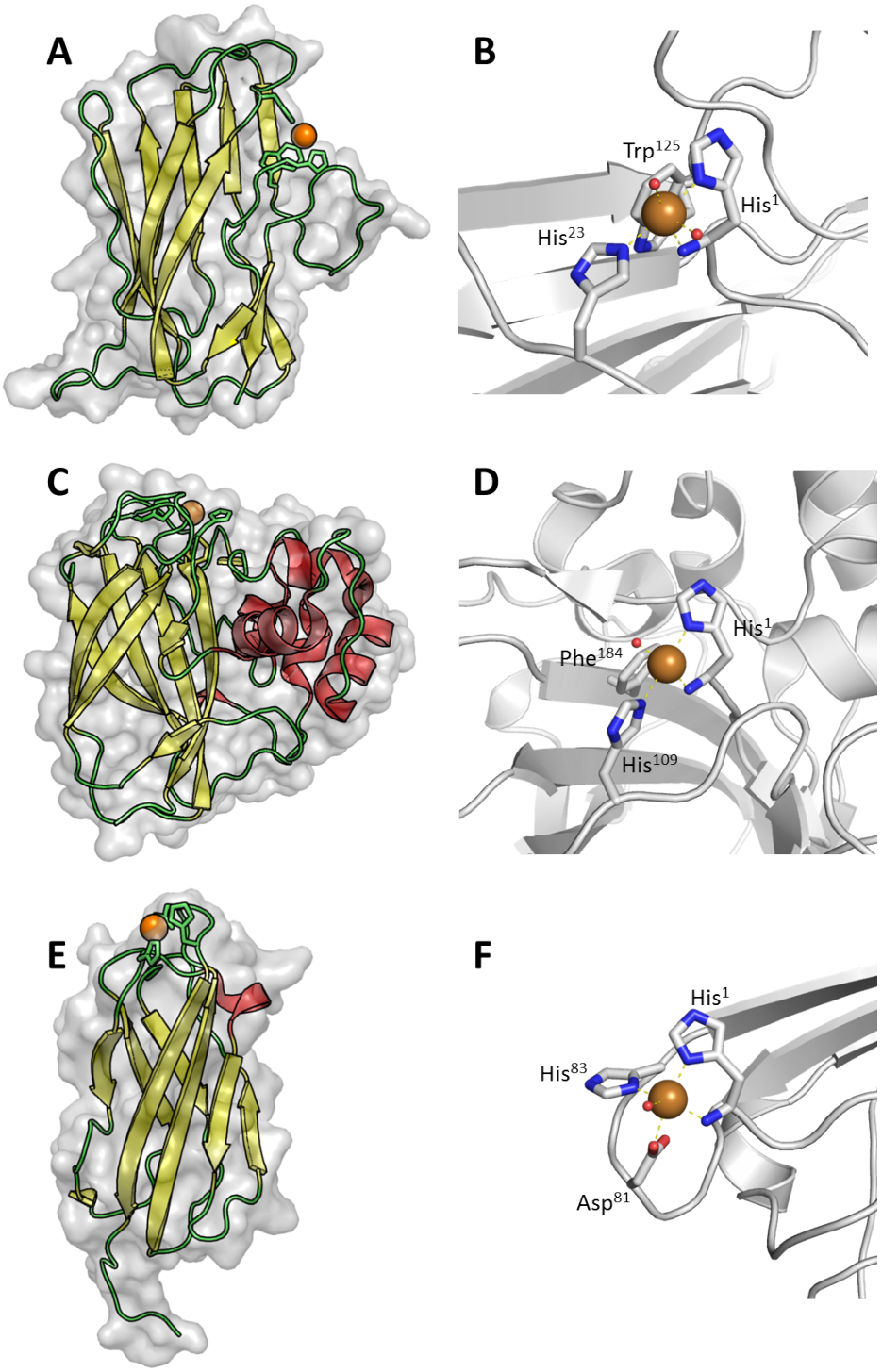

FIGURE 5.23: Structural aspects of *histidine brace* copper-binding proteins. Cartoon and transparent surface representation and active-site architectures of **(A)** and **(B)** $PCuC_{Nt}$ from *P. denitrificans*, **(C)** and **(D)** LPMO (PDB: 4OY7) and **(E)** and **(F)** CopC (PDB: OB3B). The overall structures are coloured according to secondary structure, with α-helices in red, β-strands in yellow and disordered regions in green. Active-site residues are shown as sticks and coloured by atom type. Cu ions have been drawn as ochre spheres and water molecules as small red spheres.

Organism	Protein (Cu-binding residues)	K_D (M)
CopC proteins		
Escherichia coli	Ec-PcoC (H^1, H^{90})	3.2 x 10^{-14} (competition) [275]
Pseudomonas fluorescens	Pf-CopC (H^1, H^3, H^{85})	3.2 x 10^{-16} (competition) [276]
Pseudomonas syringae	Ps-CopC (H^1, H^{90})	2.0 x 10^{-14} (competition) [275]
LPMO proteins		
Aspergillus oryzae	AoAA11 (H^1, H^{60})	$< 10^{-9}$ (ITC) [277]
Aspergillus oryzae	AoAA11 (H^1, H^{60})	7.9 x 10^{-10} (displacement ITC) [277]
Aspergillus oryzae	AoAA13 (M-H^1, H^{91})	1.3 x 10^{-8} (ITC) [278]
Bacillus amyloliquefaciens	BaAA10 (H^1, H^{97})	6.0 x 10^{-9} (ITC) [279]
Serratia marcescens	SmAA10_A (H^1, H^{86})	5.5 x 10^{-8} (ITC) [280]
Streptomyces coelicolor	ScLPMO10C (H^1, H^{109})	3.1 x 10^{-8}(ITC) [281]
Streptomyces coelicolor	ScLPMO10B (H^1, H^{107})	1.2 x 10^{-8} (ITC) [281]
Streptomyces lividans	SliLPMO10E (H^1, H^{90})	2 x 10^{-9} (ITC) [282]
Thermoascus aurantiacus	TaAA9_A (H^1, H^{86})	$< 10^{-9}$ (ITC) [282]

TABLE 5.10: Cu^{2+} binding properties of CopC and LPMO proteins

functional truncated cytoplasmic protein is the desired final product. Alternatively, if the full length protein is overexpress special attention has to be paid to the choice of host organism, otherwise the use of an inappropriate heterologous host would fail to produce functional periplasmic polypeptide. For example, Wijekoon and co-workers introduced point substitutions in Ps-CopC and in PcoC to substitute His^1 for Phe^1 they observed a drastic decrease in the binding capabilities of the proteins [276]. Another example may be YcnI from *N. farcinica*, which undoubtedly contains an unprocessed signal peptide with the most likely cleavage site at position 26 or 28 (see table A.3). However the seven initial residues of the deposited structure are NH_2-SLHVTA, which may mean that the signal peptide have not been taken into account in the genetic construct and the whole sequence of *N. farcinica* was expressed in *Escherichia coli*, an organism with a Sec system perhaps too distant to the one from *N. farcinica* to process the polypeptide to form the complete metal binding site. Another option is that the signal peptide could have been predicted inaccurately since slightly different result can be obtained depending on the software used (see table A.3). In summary, the reason why *N. farcinica* YcnI is found in its apo-form could be due to the election of an inappropriate heterologous host, perhaps incapable of processing the signal peptide of the protein. This has as a direct consequence a drastic decrease in the metal binding affinity of the protein due to the disruption of the *histidine brace*.

An intriguing detail that we observed after solving the structure of $PCuC_{Nt}$ is that His^{50} was actually not a conserved residue in a multiple sequence alignment of YcnI proteins (see figure 4.9) despite being part of the copper binding site of Cu^{2+}-$PCuC_{Nt}$. However, when we tried to compare the copper sites of $PCuC_{Nt}$ and YcnI from *N. farcinica* we quickly realised that in reality under the domain of unknown function 1775 there are two distinct families of proteins grouped together as one (see figure 5.24). Conceding that the first residue of mature YcnI is a histidine as predicted bioinformatically (see table A.3), both proteins would share an N-terminal histidine and a highly conserved tryptophan. Whereas in $PCuC_{Nt}$

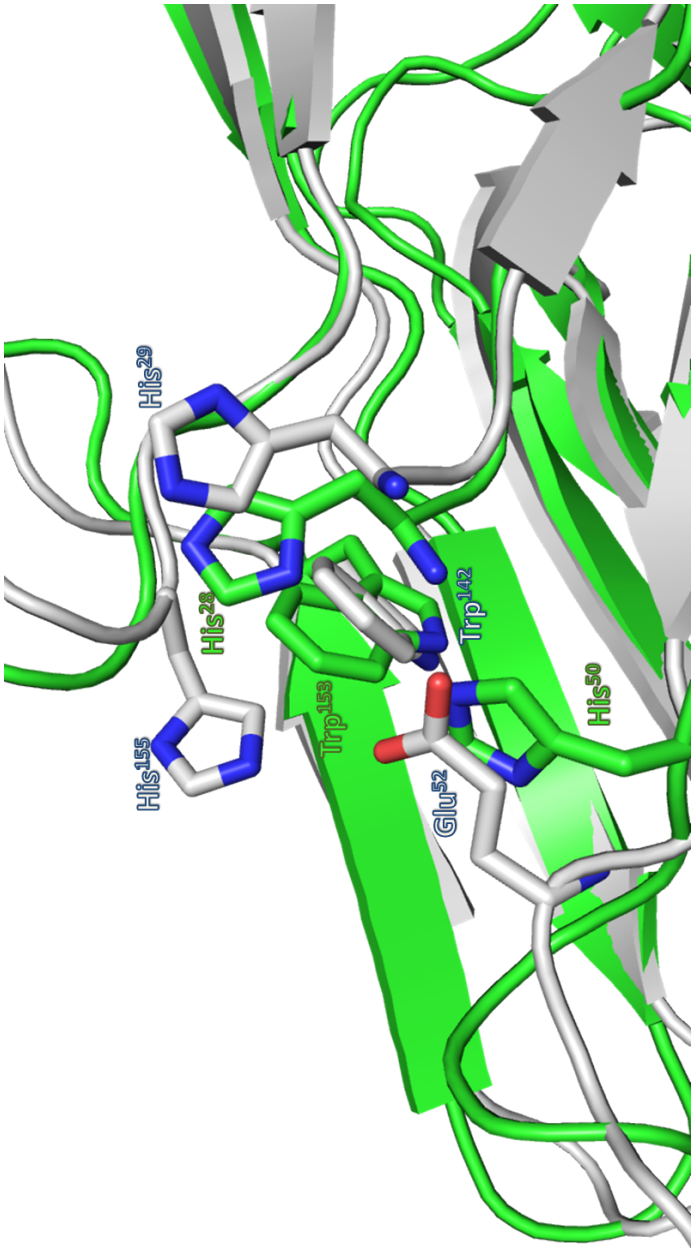

FIGURE 5.24: Superposition of $PCuC_{Nt}$ from *P. denitrificans* and YcnI from *N. farcinica*. The cartoon representation of $PCuC_{Nt}$ is coloured in green and YcnI in white.

YcnI-type proteins (named family-A) the third Cu-ligand arises from a second histidine residue located ∼22 amino acids apart from the first one, in *N. farcinica* YcnI-type of proteins (named family-B), the second histidine has been substituted by a glutamic acid also located ∼22 amino acids from the first histidine. Even more interesting is the presence of a potential second histidine ligand, that may act as a fourth ligand to the copper located 126 residues apart from the initial amino acid of the mature protein. The presence of this third histidine in family B of YcnI proteins could have a direct influence on the binding affinity of this proteins for copper. A similar effect has been observed in *Pseudomonas fluorescens* CopC (Pf-CopC) that presents an extra histidine and has a Cu^{2+} affinity 2 orders of magnitude higher than that of *Pseudomonas syringae* CopC (Ps-CopC) [275, 276]. In order to test this hypothesis, we manually selected a subset of protein sequences of YcnI families A and B, generated multiple sequence alignments using the software Jalview [193]. These MSA were then used as queries in the HMMER web server [244] to search for protein sequences matching each YcnI family. We identified about 280 protein sequences belonging to family A and nearly 500 to family B. The majority of the microorganisms from family A belonged to alphaproteobacteria and in a lesser extend to a few actinobacteria. Within alphaproteobacteria the three most abundant groups were rhizobiaceae, phyllobacteriaceae and bradyrhizobiaceae. By contrast, family B YcnI-type proteins were mainly characteristic of actinobacteria and firmicutes. Within actinobacteria, the actinomycetales, corynebacteriales and pseudonocardiales were the three main groups. This distribution correlates with the overall phylogenetic tree constructed with the sequences deposited in Pfam (accession date: July 30, 2018) (see figures 5.26, 5.27 and 5.25).

The structure of Cu^{1+}-$PCuC_{Ct}$ showed to have an overall β-barrel motif that resembled the one observed for PCu_AC from *D. radiodurans*, *T. thermophilus* and *S. lividans* (see figure 5.28). Remarkably, within the structure two copper atoms were modelled, one present at what in structural biology is referred as a special position and therefore we consider that this copper may be involved in the crystallisation process of the protein. The other copper atom however is located

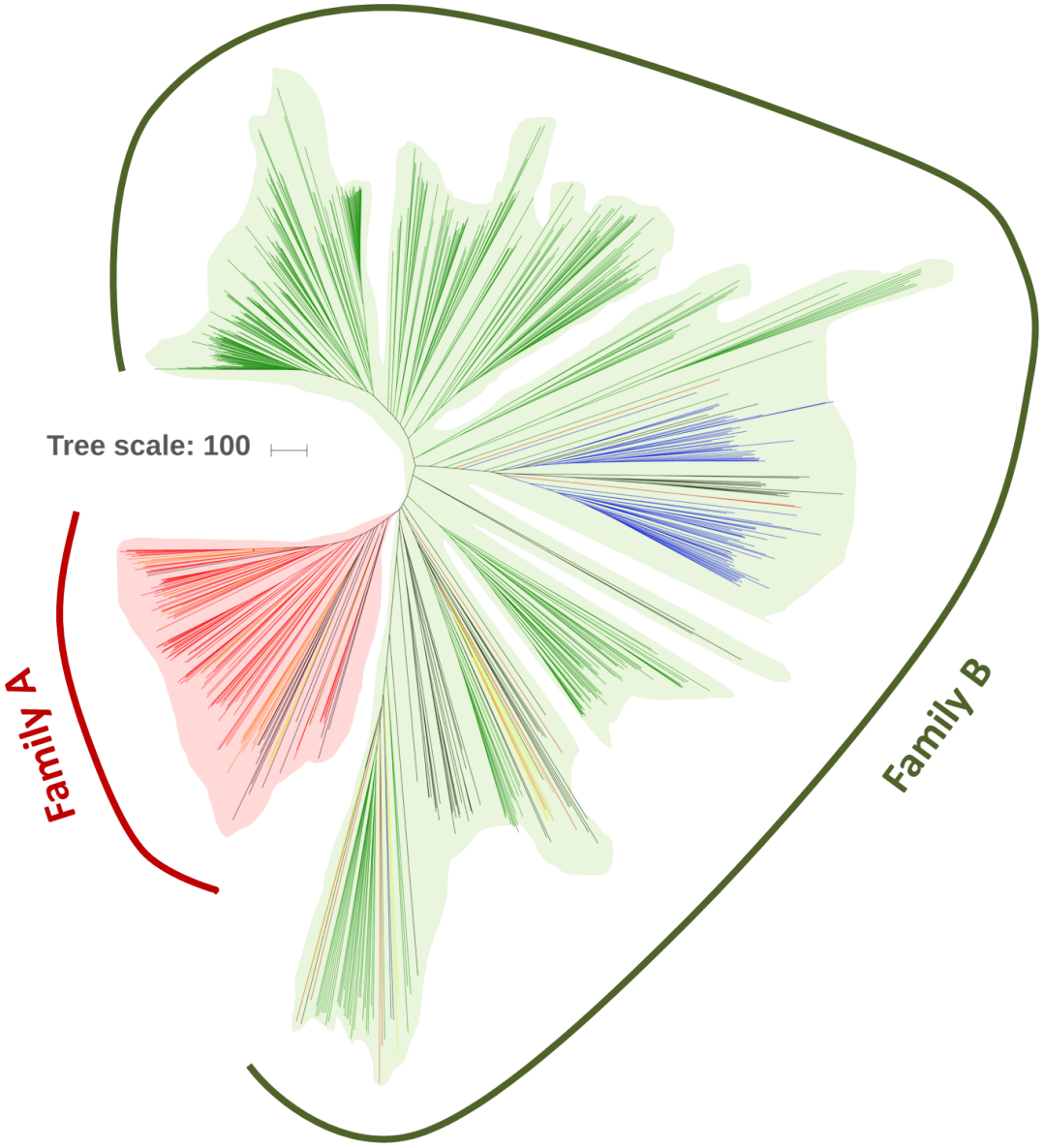

FIGURE 5.25: Phylogenetic tree of YcnI proteins. Member of each family A and B are showed in red and green, respectively. The colours of the branches respond to the following pattern: Rhizobiales (red), Rhodobacterales (orange), Burkoderiales (yellow), Actinobacteria (green), Bacillales (blue). The parameters for the maximum likelihood tree were calculated with the software Jalview [193] and the tree was drawn with the on-line program iTOL [231]

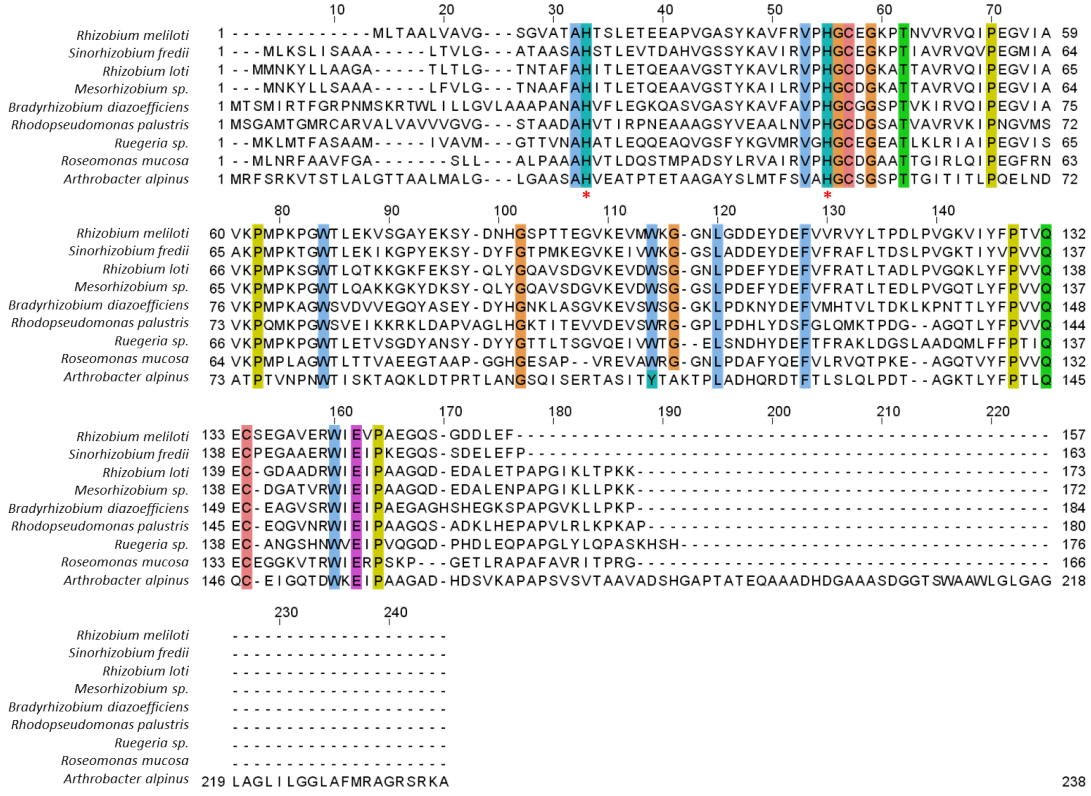

FIGURE 5.26: Multiple sequence alignment of YcnI proteins belonging to family A. The conserved residues of the Cu-binding $HX_{22}HX_{101}W$ motif are highlighted with the symbol ($\star$)

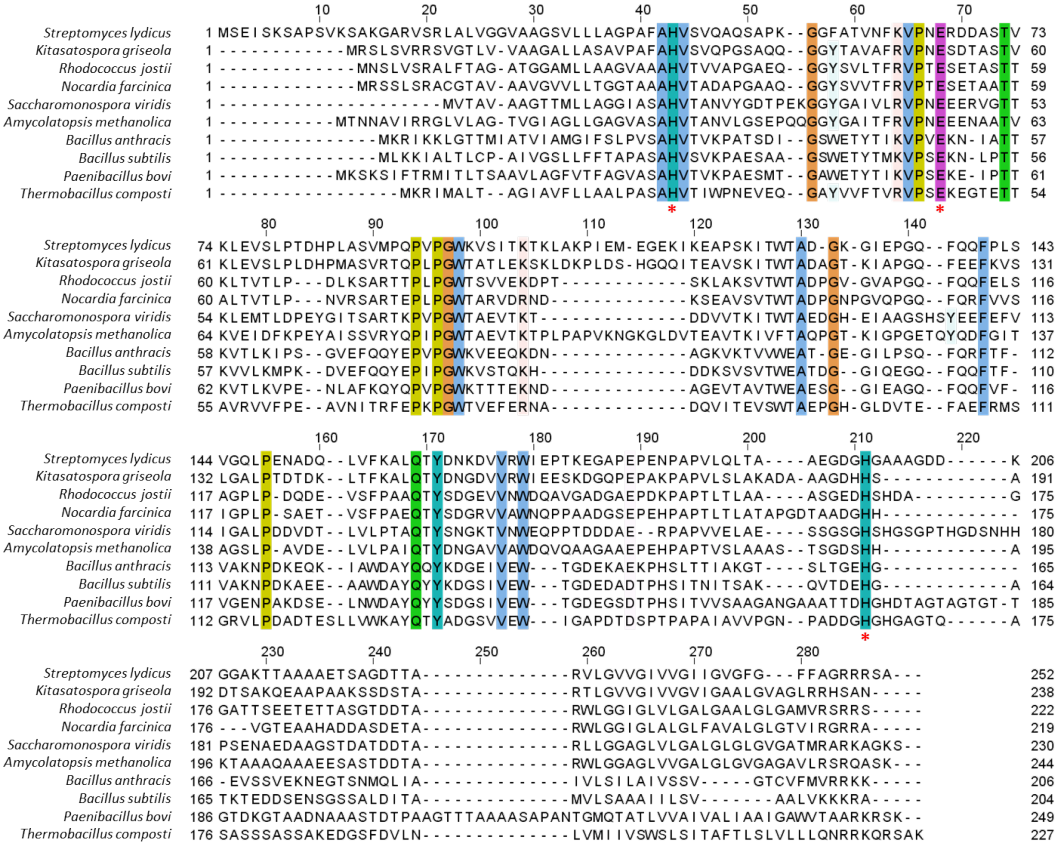

FIGURE 5.27: Multiple sequence alignment of YcnI proteins belonging to family B. The conserved residues of the putative Cu-binding $HX_{22}DX_{90}WX_{13}H$ are highlighted with the symbol ($\star$)

within the well-known H(M)X_{10}MX_{21}HXM Cu^{1+}-binding motif characteristic of PCu_AC proteins [33].

The structure of Cu^{1+}-$PCuC_{Ct}$ presents two solvent exposed β-strands that form a hairpin which protrudes from the β-barrel structure. This hairpin is similar but less accentuated than the one found in PCu_AC from *T. thermophilus* but slightly more obvious than the one present in PCu_AC from*S. lividans* (see figure 5.28).

The collective study of the solution properties of $PCuC_{Nt}$, $PCuC_{Ct}$ and $PCuC_{WT}$, crystallographic resolution of $PCuC_{Nt}$ and $PCuC_{Ct}$, and the analysis of the solution structure of $PCuC_{WT}$ have led to the proposal of a structural model for PCuC. In this model, $PCuC_{Nt}$ is responsible for creating a central core that drives the oligomerization of the protein, a flexible linker region joins the N-terminal domain to $PCuC_{Ct}$ that remains monomeric and has certain freedom of movement within the protein, this may be responsible for the inability to crystallographically resolve the full length protein. Copper binding motifs are present in both domains, at the N-terminal domain a novel type of *histidine brace* within the characteristic $H_{22}H_{101}W$ motif has been described, and at the C-terminal domain a classical H(M)X_{10}MX_{21}HXM motif is present. The calculated K_D points $PCuC_{WT}$ as a high-affinity copper scavenger capable of binding both Cu^{1+} and Cu^{2+} and of storing up to 6 copper atoms per trimer within the periplasm of the cell, ready to deliver them to protein partner(s).

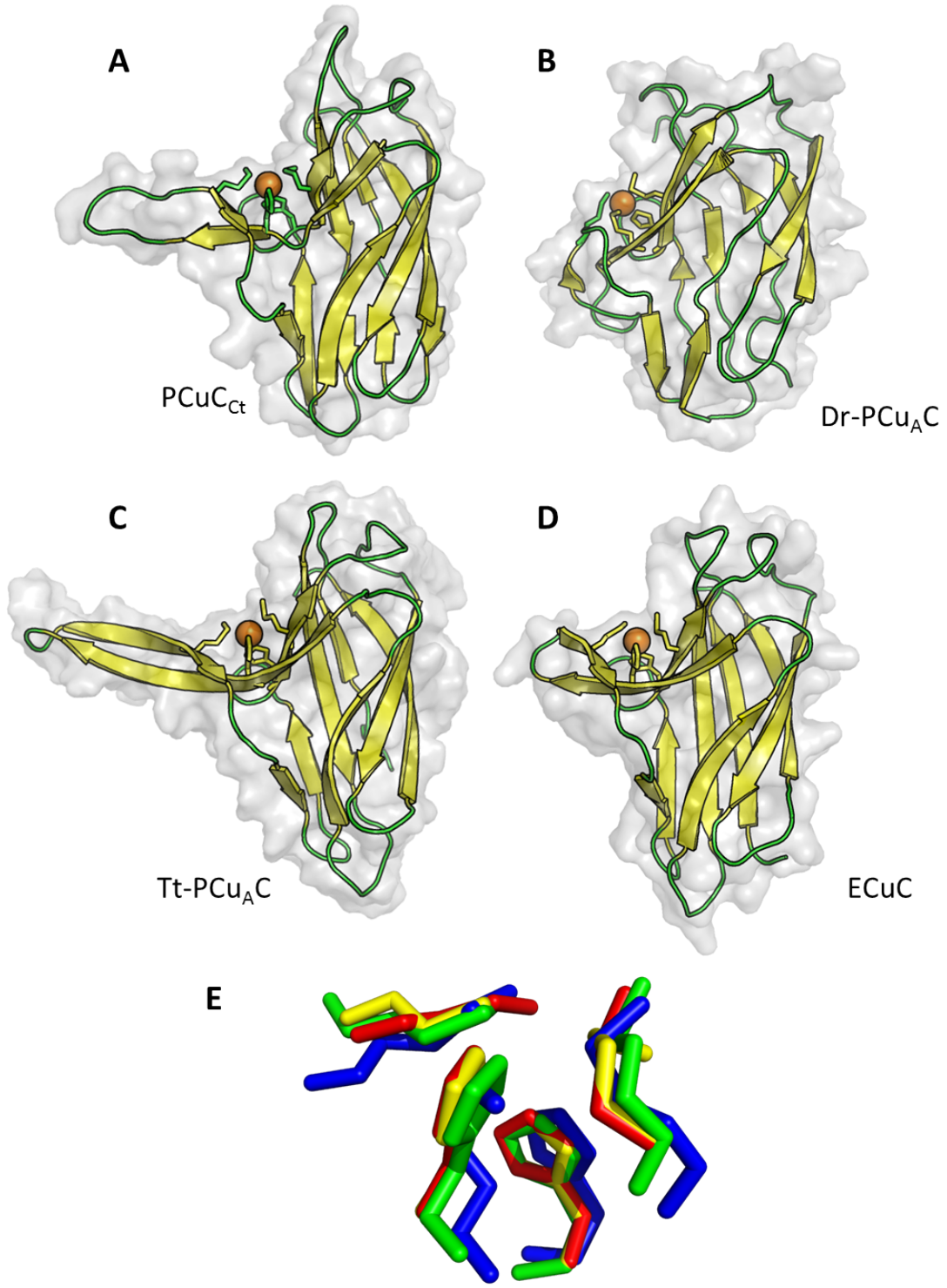

FIGURE 5.28: Structural aspects of PCu$_A$C proteins. Cartoon and transparent surface representation of **(A)** PCuC$_{Ct}$ from *P. denitrificans*, **(B)** PCu$_A$C from *D. radiodurans* (PDB: 1X9L), **(C)** PCu$_A$C from *T. thermophilus* (PDB: 2K6Z) and **(D)** ECuC from *S. lividans* (PDB: 3ZJA). **(E)** Superposition of the copper-binding site of PCuC$_{Ct}$ (yellow), Dr-PCu$_A$C (blue), Tt-PCu$_A$C (green) and ECuC (red). Cu ions have been drawn as ochre spheres.

6

Purification and characterisation of N_2OR from *pcuC* and *scoB* deficient strains

6.1 Introduction

Nitrous oxide reductase (N_2OR) [87], nitrogenase [283, 284] and multicopper oxidase [285] are known metalloenzymes capable of catalysing *in vitro* reaction 6.1. However, of these three proteins only N_2OR is considered to perform the two electron reduction of N_2O *in vivo* [9].

$$N_2O + 2H^+ + 2e^- \longrightarrow N_2 + H_2O;\ \Delta G^{\circ\prime} = -339.5\ \text{kJ mol}^{-1} \tag{6.1}$$

Thermodynamically, N_2O is a stable molecule due to electronic delocalisation and although it is a strong oxidant, an activation energy barrier of 250 kJ mol^{-1} [286] prevents decomposition or reduction of the molecule. This kinetic barrier can be overcome through binding an activation by metal ions and in N_2OR this has been solved by using an unique catalytic copper-sulphur cluster [13].

6.1.1 Assembly of copper centres in N_2OR

Nitrous oxide reductases are generally soluble proteins that are directed to the periplasm through a signal peptide sequence [79]. A bioinformatic analysis by

Jones and co-authors identified that N_2OR proteins group in atypical or typical clades according to the predicted export pathways that the proteins present [287]. Atypical N_2OR proteins are commonly exported through the Sec system, with some exceptions such as the hyperthermophilic archea *Ferroglobus placidus*, *Thermomicrobium roseum* and *Sphaerobacter thermophilum*. Meanwhile, typical N_2OR proteins are predominantly exported to the periplasm by the TAT apparatus [287].

In addition to the export machinery of N_2OR to the periplasm, an array of accessory proteins are required for the assembly of the two copper centres of N_2OR in its final and functional location. However, the exact function and cellular location of these proteins is yet not fully understood. At least three proteins encoded by the genes *nosD, -F*, and *–Y* have been found to be involved in the maturation process of the Cu_Z centre [96]. Meanwhile, despite the similarity of the Cu_A centres of N_2OR and cytochrome *c* oxidase (Cox) [25] and that the maturation process for Cox has been extensively studied [5], the chaperones responsible for Cu_A centre of N_2OR are yet to be defined.

6.1.1.1 Maturation of the Cu_Z centre of N_2OR

The gene product of *nosDFY* have been proposed to form an ABC-type transporter based on structure prediction analysis [96] (see figure 6.1). This system is thought to be involved in the transport of sulphur required for the formation of the Cu_Z of N_2OR [96]. This assumption is primarily based on the fact that the N_2OR protein purified from *nosDFY* mutants present a Cu_A, but lacks Cu_Z centre therefore, copper addition does not seem to be affected [89, 90, 95, 288].

The protein NosF has a molecular weight of 30 kDa, a cytosolic location as deduced from *lacZ* reporter gene fusion experiments [289] and ATPase activity [109]. Based on these characteristics, it has been proposed that NosF could couple energy-dependent transfer of sulphur across the membrane through NosY [96]. NosF differs from other ATP-binding proteins in the presence of an extended C-terminal domain which does not show similarity to any other solved protein structure. NosF is proposed to interact with NosY, a 30 kDa integral membrane protein that

spans the inner membrane five times and is thought to represent the transport protein. NosD is a 45 kDa periplasmic protein containing two predicted CASH (carbohydrate-binding proteins and sugar hydrolases) domains within a β-helical structure [290]. The function of NosD remains unclear as it has yet not been proven that it act as a binding protein.

Another accessory gene broadly distributed among denitrifying organisms and frequently found downstream *nosDFY* is *nosL* [96]. The *nosL* gene codes for a 20 kDa periplasmic protein that is predicted to be exported via the Lol transport system and lipid anchored to the outer-face of the inner-membrane [96, 291] (see figure 6.1). Based on the studies of McGuirl and co-workers using a recombinant form of NosL from the facultative anaerobe *A. cycloclastes*, the researchers deduced that NosL is a metallochaperone that binds one Cu^{1+} atom per monomer and releases the metal upon oxidation or incubation with EDTA [242]. The only known structure available of a NosL protein was generated by Taubner *et al.* and does not present any metal bound [292]. The overall structure consists of two homologous domains that adopt a $\beta\beta\alpha\beta$ topology similar to the one observed in the mercury resistance protein MerB [293]. However, the role of NosL remains elusive since interruption of *nosL* gene [291] or expression *in trans* of *nosZDFY* in a non denitrifying organism [89] result in the synthesis of a functional N_2OR. Therefore, it has been suggested that NosL could be involved in copper transport or assembly of N_2O or other copper containing denitrifying enzymes [96].

6.1.1.2 Maturation of the Cu_A centre of N_2OR

The Cu_A centre of N_2OR is homologue to the electron transport centre of cytochrome *c* oxidase (Cox) [25]. Cytochrome *c* oxidase is the terminal component of the aerobic respiratory chain located in the inner mitochondrial membrane of eukaryotes and in the plasma membrane of many prokaryotes. The enzyme is composed of three highly conserved large subunits (Cox1, Cox2 and Cox3) [25]. Both Cox1 and Cox2 contain metal cofactors necessary for Cox acting, Cox1 contains

the catalytic Cu_B centre while Cox2 binds two copper ions forming the dinuclear Cu_A centre.

Two protein families have been proposed to be involved in Cu_A site assembly in prokaryotes, a process that has been studied in detail by Banci and co-workers in the Gramnegative bacteria *Thermus thermophilus* [5]. The first family consists of the Sco proteins which have been described in chapter 3. These proteins seem to have a main thioredoxin role in prokaryotes, despite of being able to bind both Cu^{1+} and Cu^{2+} ions through a conserved CX_3C motif [180]. The second family of proteins is referred as PCu_AC and have been described in chapter 4. These proteins are able to bind Cu^{1+} through a highly conserved $H(M)X_{10}MX_{21}HXM$ motif [33]. In a recent NMR study, Abriata *et al.* showed that *T. thermophilus* Sco was unable to transfer copper to the Cu_A site of Cox2, but instead it was responsible for maintaining the correct oxidation state of the Cu_A cysteine residues. Copper insertion into Cox2 was carried out by the sequential delivery of Cu^{1+} ions from PCu_AC into apo-Cu_A site giving rise to the holo form of the protein [5].

In the transcriptomic study mentioned in section 1.4.3.4, Sullivan and co-authors identified a gene cluster *hyp-pcuC-scoB* and noted that these genes were essential for N_2O respiration under copper limiting conditions [3]. The hypothetical gene codes for a putative protein with unknown function that has been described in section 4.6. The gene product of *scoB* and *pcuC* have been studied in this thesis and their characteristics are detailed in chapters 4 and 3, respectively. In short, ScoB is a copper binding protein capable of binding both Cu^{1+} and Cu^{2+} forms. PCuC in turn is a two-domain protein, the N-terminal domain is a new type of copper binding protein that can also bind both copper ions while the C-terminal domain is homologue to PCu_AC and chelates only Cu^{1+} with a very high affinity (see figure 6.1). These proteins are expected to be involved in either insertion or maintenance of the Cu-centres of N_2OR. Therefore in this chapter, we explore the effect of these two proteins on N_2OR through the generation of a recombinant N_2OR protein that can be isolated by affinity chromatography for biological analysis and is expressed *in cis* under the control of its native promoter.

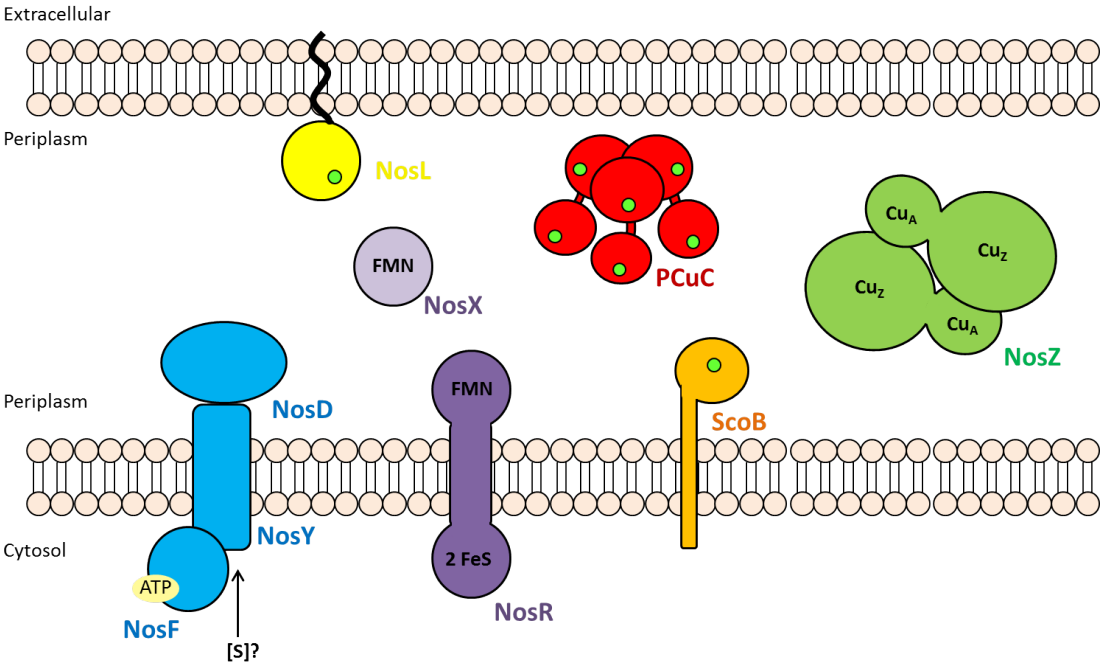

FIGURE 6.1: Schematic illustration of the components involved in N_2OR biogenesis and their cellular location in *P. denitrificans*. The complex NosD-NosF-NosY and NosL are the proposed proteins involved in Cu_Z centre maturation of N_2OR. ScoB and PCuC proteins are the proposed proteins responsible for the assembly of Cu_A centre of N_2OR in *P. denitrificans*. The membrane-bound NosR and NosX are considered to have a redox role during N_2O respiration. [S] is a sulphur species of unknown chemical nature. The small green spheres represent Cu ions.

6.2 Nitrous oxide reductase purification and characterisation

In order to study the *in vivo* role of ScoB and PCuC in the maturation process of N_2OR we knocked-in an affinity tag coding sequence at the 3' end of *nosZ* from *P. denitrificans* before the stop codon as described in section 2.11. Due to the small size and efficient one-step purification that the eight-residues *Strep*-tag II sequence (Trp-Ser-His-Pro-Gln-Phe-Glu-Lys) provides, this sequence was chosen as the preferred affinity tag for the genomic insertions [294]. Initially the *Strep*-tag II sequence was inserted within the *nosZ* gene present in *P. denitrificans* WT ($NosZ_{WT}$), and the growth and N_2O phenotype of *P. denitrificans* WT and $NosZ_{WT}$ variant under anaerobic conditions was examined (see figure 6.2). Overall, no apparent differences in terms of growth and N_2O reduction capabilities were observed under copper sufficient and limited conditions. Then, after the initial phenotypical examination of $NosZ_{WT}$ mutant *Strep*-tag II knock-in strains were generated in *P. denitrificans* $\Delta scoB$ ($NosZ_{\Delta scoB}$) and $pcuC^{-}$ ($NosZ_{pcuC^{-}}$) backgrounds.

The strength of this experimental approach is that these three knock-in mutants ($NosZ_{WT}$, $NosZ_{\Delta scoB}$ and $NosZ_{pcuC^{-}}$) facilitates a framework for the purification of N_2OR produced under the control of the native promoter of the coding gene and therefore is expressed under physiologically relevant conditions. In all cases, N_2OR was purified as a polypeptide of $\sim$ 69 kDa from whole cell soluble extract of *P. denitrificans* (see figures 6.3 and 6.4). The purity of N_2OR was considerably higher when the protein was obtained from copper high cultures as judged from SDS-PAGE gels, while some higher and lower M_w bands than N_2OR could be observed in copper limited conditions. However, this contaminant were present in an small proportion and did not affect significantly downstream applications. Purification of N_2OR from cultures grown under copper sufficient conditions yielded 3.6 ± 0.7 mg of protein per litre of culture. Meanwhile, approximately 25-times less N_2OR (0.1 ± 0.05 mg per litre) was obtained from cultures grown under copper limited conditions.

With the purpose of characterizing spectroscopically N_2OR, the eluted fractions from the purifications shown in figures 6.3 and 6.4 were combined, concentrated and analysed for their spectroscopic purity. Isolated N_2OR from cultures grown in the presence of micromolar amounts of copper displayed as purified a strong 640 nm band (see figure 6.5 A, B and C). These absorbance spectra profile resembled to the one of reduced N_2OR form I or anaerobically purified N_2OR [13, 88], with the difference that $NosZ_{WT}$, $NosZ_{\Delta scoB}$ and $NosZ_{pcuC^-}$ spectra had a minor band at 550 nm that could be indicative of the presence of a subpopulation of air-oxidised protein. By oxidizing N_2OR with ferricyanide the UV-vis features of both Cu_A and

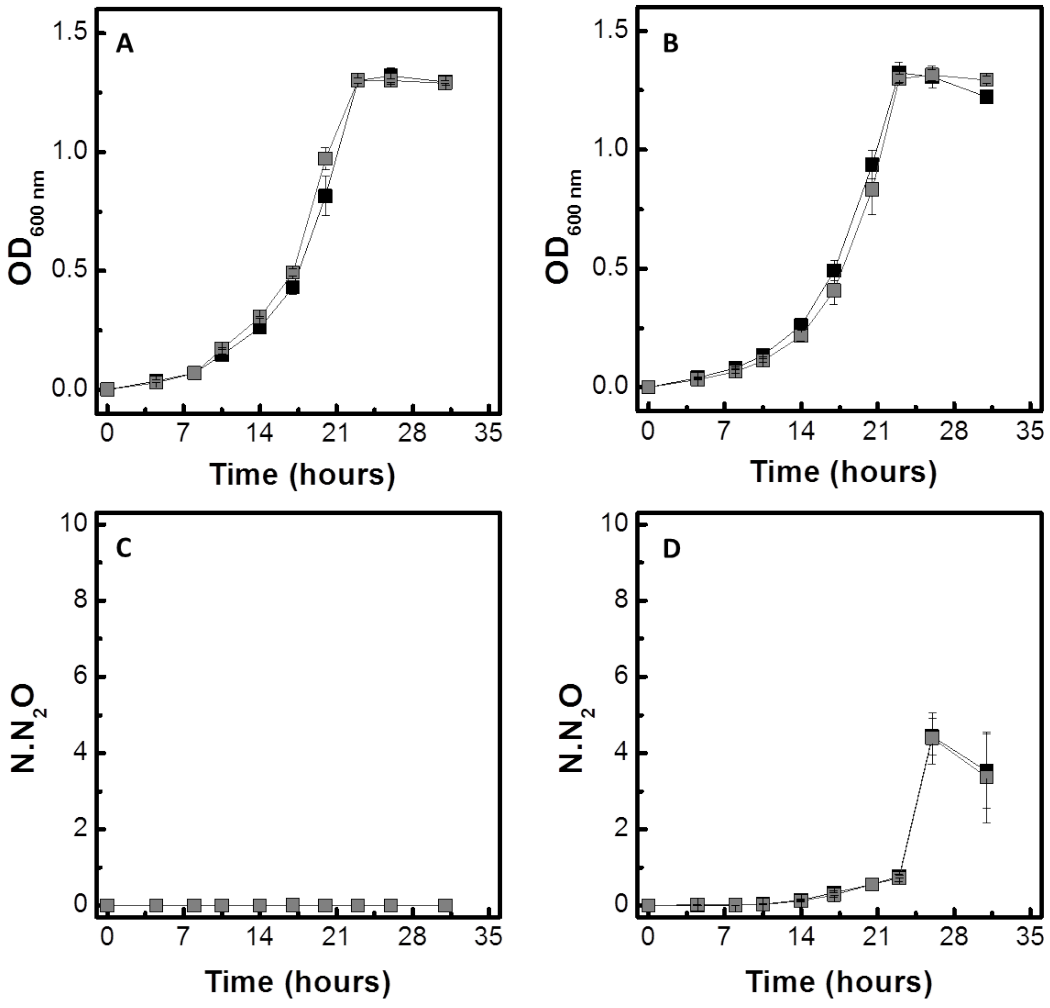

FIGURE 6.2: Anaerobic growth characteristics of *P. denitrificans* WT and $NosZ_{WT}$ mutant in batch culture conditions. **(A)** The anaerobic growth under copper sufficient and **(B)** limited conditions. **(C)** and **(D)** show N_2O production in milimole of N in the form of N_2O. Cultures contained either < 0.5 or 13.5 μM of copper. Standard errors of the mean are indicated by the error bars ($n = 3$)

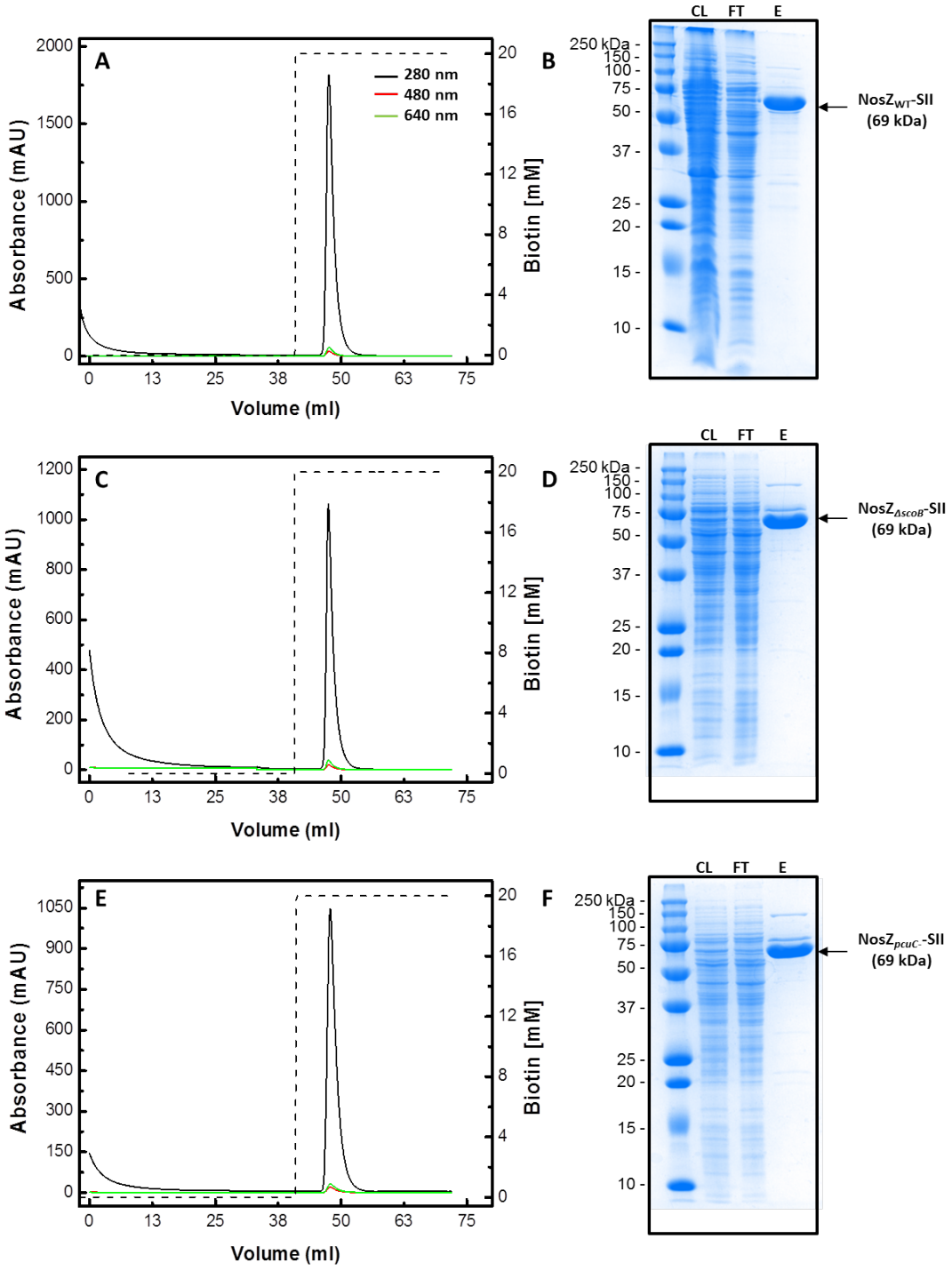

FIGURE 6.3: *Strep*-tag II affinity purification of recombinant N_2OR expressed under copper sufficient conditions. Chromatograms and SDS-PAGE of eluted fractions from **(A)** and **(B)** *P. denitrificans* $NosZ_{WT}$, **(C)** and **(D)** $NosZ_{\Delta scoB}$ and **(E)** and **(F)** $NosZ_{pcuC-}$ mutant strains. Lanes: Whole cell lysate (CL), flow-through (FT).

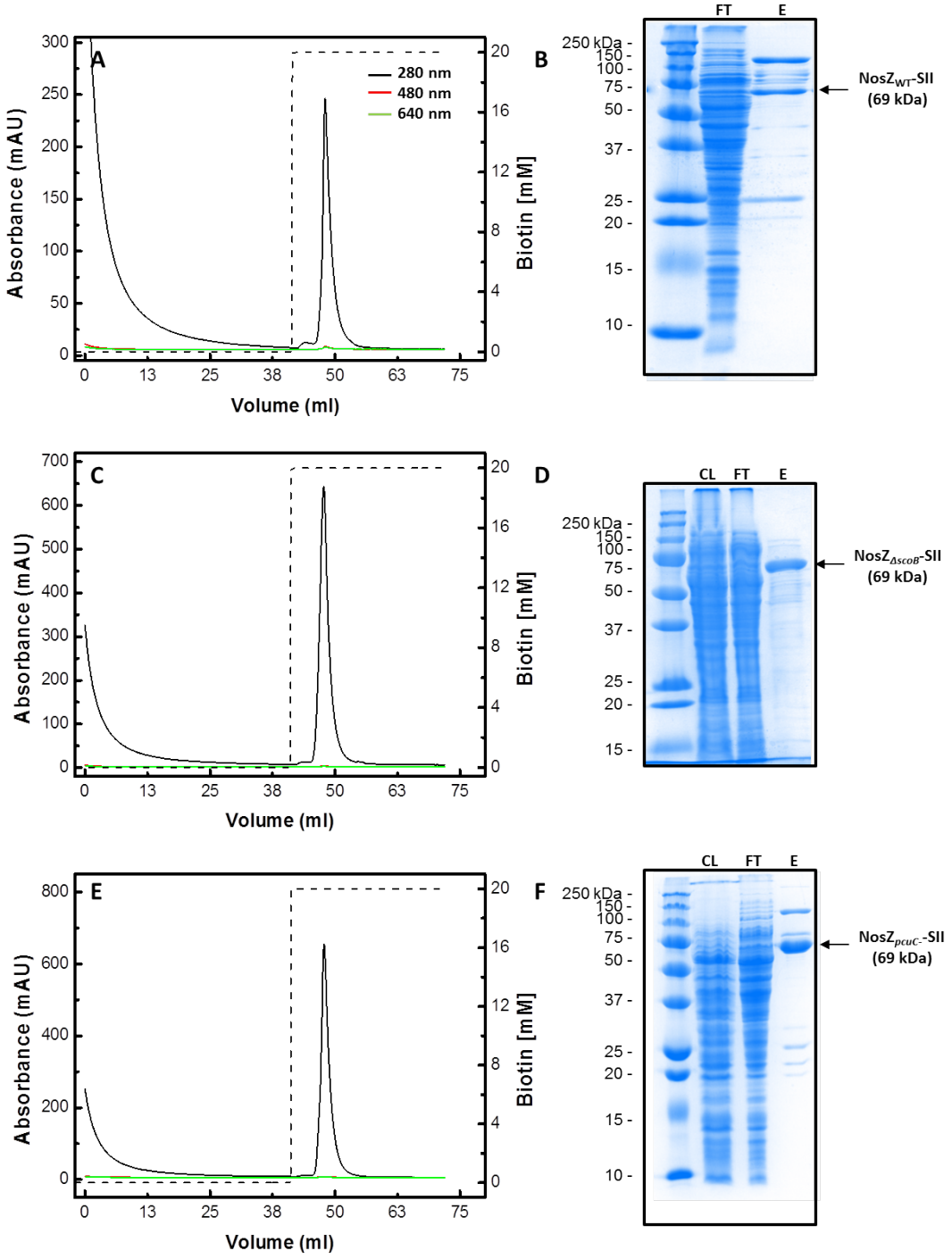

FIGURE 6.4: *Strep*-tag II affinity purification of recombinant N_2OR expressed under copper limited conditions. Chromatograms and SDS-PAGE of eluted fractions from **(A)** and **(B)** *P. denitrificans* $NosZ_{WT}$, **(C)** and **(D)** $NosZ_{\Delta scoB}$ and **(E)** and **(F)** $NosZ_{pcuC-}$ mutant strains. Lanes: Whole cell lysate (CL), flow-through (FT).

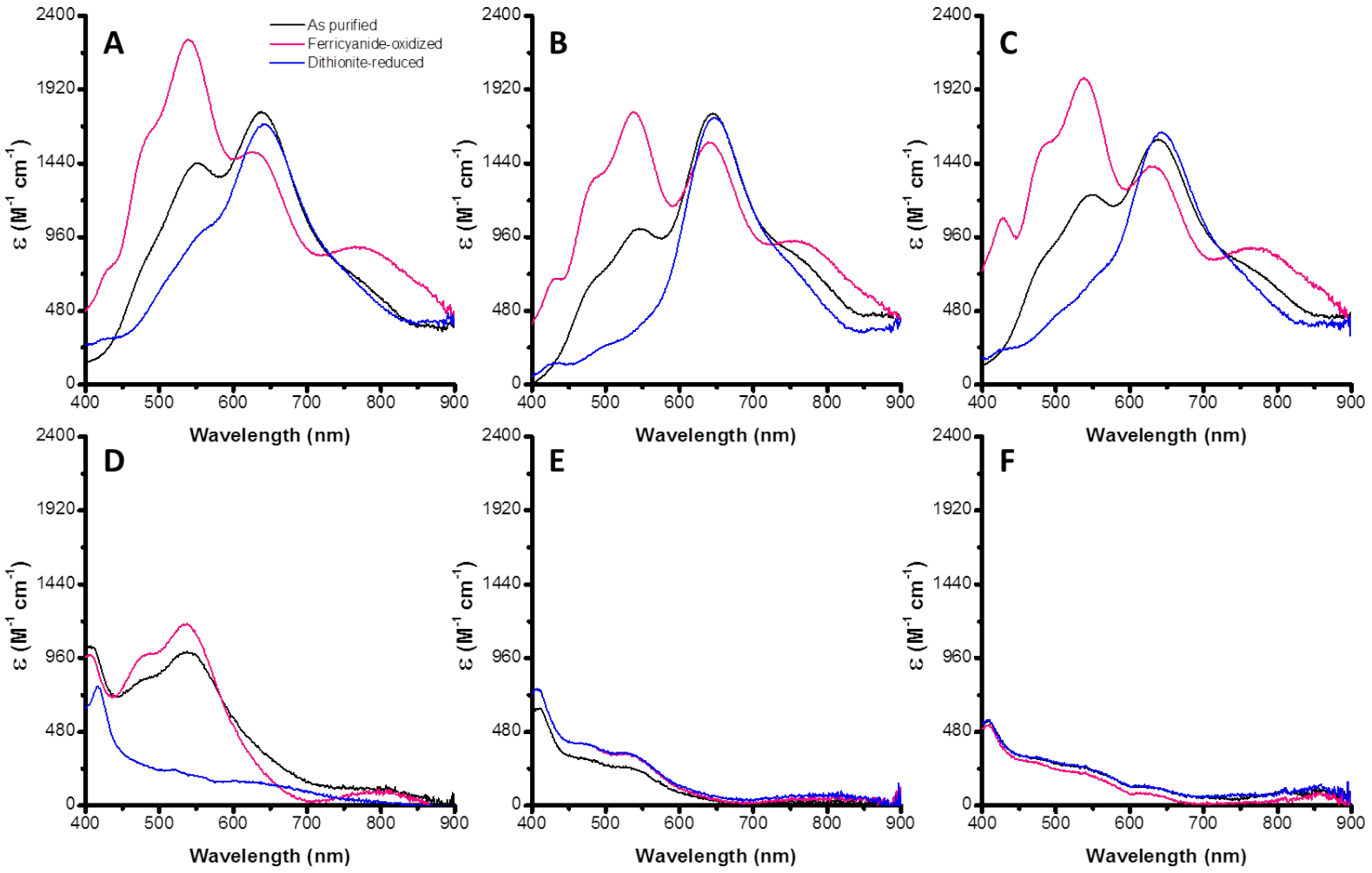

FIGURE 6.5: UV-vis spectra of purified *Strep*-tag II recombinant N_2OR by affinity chromatography. **(A)** As purified, oxidised and reduced spectra of $NosZ_{WT}$, **(B)** $NosZ_{\Delta scoB}$ and **(C)** $NosZ_{pcuC^-}$ purified from copper sufficient conditions. **(D)** $NosZ_{WT}$, **(E)** $NosZ_{\Delta scoB}$ and **(F)** $NosZ_{pcuC^-}$ purified from copper limited conditions

Cu_Z centres are revealed. A shoulder and a peak at 488 and 770 nm, respectively, appeared in the oxidised spectra of $NosZ_{WT}$, $NosZ_{\Delta scoB}$ and $NosZ_{pcuC^-}$ in contrast to the as purified. In addition, an increase in the intensity of the 550 nm band and a reduction of the 640 nm was also noted. Of the three spectra, $NosZ_{\Delta scoB}$ differed the most from the rest. In the spectrum of this particular protein, the intensity of 540 and 640 nm bands were almost the same similarly to ferricyanide-oxidised N_2OR form II [13, 88]. Conversely, reduction of N_2OR with the strong reductant dithionite hides the features of the Cu_A centre and only allows examination of Cu_Z. The spectra of the reduced proteins compared to the as purified flattened the 550 nm band, that in $NosZ_{WT}$ and $NosZ_{pcuC^-}$ stayed as a pronounced shoulder, while the intensity of the 640 nm band remained almost unaltered. When the same N_2OR proteins were purified from copper limited conditions the UV-vis spectrum of as purified $NosZ_{WT}$ showed the presence of two peaks at 476 and 540 nm and no sign of the 640 nm band. By contrast, $NosZ_{\Delta scoB}$ and $NosZ_{pcuC^-}$ presented flat spectra with no apparent recognisable features (see figure 6.5 D, E and F). Oxidation of the proteins with ferricyanide revealed a peak at 800 nm and intensified the bands described for $NosZ_{WT}$, while addition of the oxidizing agent did not affect the UV-vis spectra of $NosZ_{\Delta scoB}$ and $NosZ_{pcuC^-}$. Reduction of the proteins with dithionite under anaerobic conditions in the glove box caused the disappearance of the 476, 540 and 800 nm bands of $NosZ_{WT}$, which resulted in a flat spectrum such us the one displayed by reduced $NosZ_{\Delta scoB}$ and $NosZ_{pcuC^-}$.

Analysis of the difference absorption spectrum of the ferricyanide-oxidised minus dithionite-reduced N_2OR is shown in figure 6.6. $NosZ_{WT}$, $NosZ_{\Delta scoB}$ and $NosZ_{pcuC^-}$ isolated from copper sufficient conditions revealed almost identical profiles to one another and to the absorption spectrum of isolated Cu_A. The absorption spectrum of N_2OR Cu_A was described by Farrar et al. in a mutant form of N_2OR and its characteristic bands at 480, 540 and 800 nm (see figure 6.6 A) [295]. However, when the same proteins where purified under copper limited conditions only N_2OR purified from WT presented Cu_A UV-vis features, while N_2OR purified from a

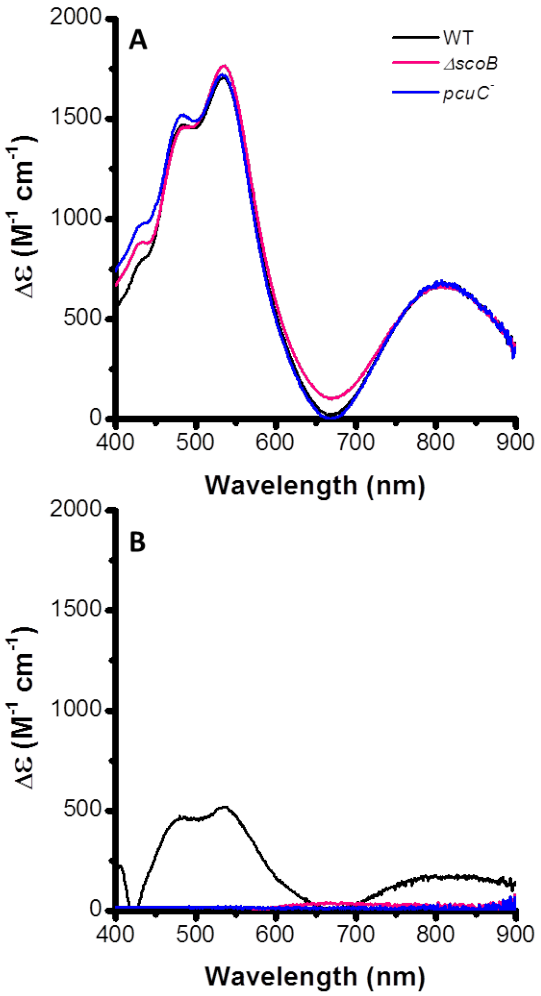

FIGURE 6.6: Ferricyanide-oxidised minus dithionite-reduced UV-vis difference spectra of N_2OR. Purified $NosZ_{WT}$ (−), $NosZ_{\Delta scoB}$ (−)and $NosZ_{pcuC^-}$ (−) from **(A)** Copper sufficient and **(B)** limited conditions.

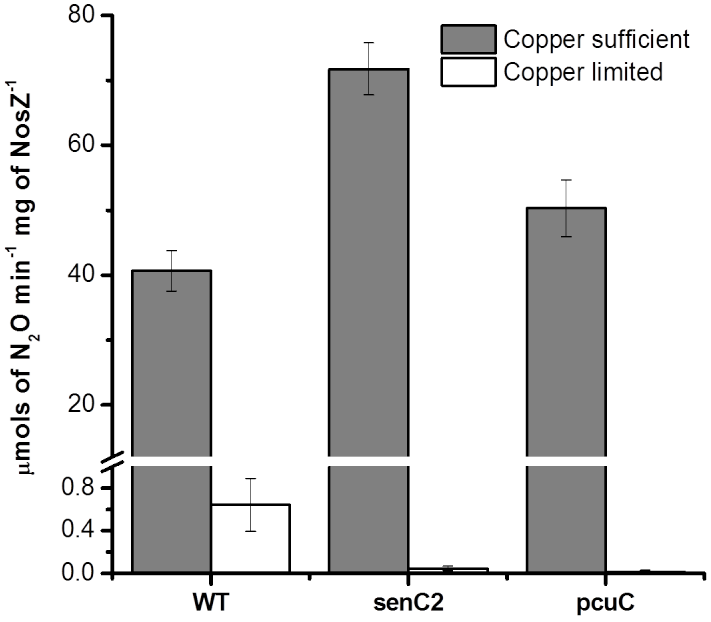

FIGURE 6.7: Methyl viologen activity assay of N_2OR proteins. Dark bars represent N_2OR purified from copper sufficient conditions and empty bars from copper sufficient conditions. Standard errors of the mean are indicated by the error bars ($n = 3$)

Δ*scoB* or a *pcuC*⁻ mutants seemed to lack the absorption bands of such domain (see figure 6.6 B).

The enzymatic activity of N_2OR was also analysed using the methyl viologen method as described in section 2.2.5. When $NosZ_{WT}$, $NosZ_{\Delta scoB}$ and $NosZ_{pcuC^-}$ were purified from *P. denitrificans* grown under anaerobic and copper sufficient conditions an average enzymatic activity of ∼ 53 µmol of N_2O min^{-1} mg of $NosZ^{-1}$ was observed. However, when the same proteins were purified under copper limited conditions only $NosZ_{WT}$ had a detectable activity of ∼ 0.4 µmol of N_2O min^{-1} mg of $NosZ^{-1}$, while $NosZ_{\Delta scoB}$ and $NosZ_{pcuC^-}$ were essentially inactive (see figure 6.7). The UV-vis spectra and enzymatic activity analysis are in agreement with the metal analysis of N_2OR proteins by ICP-AES. When $NosZ_{WT}$, $NosZ_{\Delta scoB}$ and $NosZ_{pcuC^-}$ were purified from copper sufficient conditions an average of 5.6 ± 0.1 copper equivalents per monomer of N_2OR were detected. However, under copper limited conditions $NosZ_{WT}$ contained ∼ 1.5 and, $NosZ_{\Delta scoB}$ and $NosZ_{pcuC^-}$ less than 0.3 ± 0.1 copper equivalents per monomer of N_2OR.

6.3 Discussion

Nitrous oxide reductase (N_2OR) is the only known enzyme in nature capable of conducting the reduction reaction of N_2O into N_2 [80]. The protein is made up to two domains, the active site or Cu_Z centre is located at the N-terminus and, the electron transfer site or Cu_A centre at the C-terminus site. A high copper demand is exerted by this protein on the cell during full denitrification since it requires a total of 12 copper atoms per functional homodimer. The Cu_Z site is a tetranuclear copper centre and there is evidence of the involvement of NosDFY or NosL in the maturation of N_2OR [79]. In contrast to the Cu_Z centre, the Cu_A is a binuclear copper site and it has been long considered that the assembly is this site is carried out by the same proteins that are involved in the maturation of heme-copper oxidases [79]. In this thesis we have studied the role of ScoB and PCuC from *P. denitrificans* in relation to the maturation process of N_2OR based

on the initial work of Sullivan and co-workers where they observed that during copper starvation the coding genes of these two proteins are overexpressed and required for proper N_2OR activity [3].

After having explored the biochemical characteristics of ScoB (see chapter 3) and PCuC (see chapter 4) we examined the role of these two proteins in the maturation process of N_2OR. The experimental approach consisted in the isolation and comparative analysis of the properties of recombinant N_2OR from *P. denitrificans* WT, Δ*scoB* and *pcuC*$^-$ strains from two different copper regimes. At least in two previous occasions recombinant N_2OR proteins have been used in the past, Savelieff *et al.* cloned an N_2OR gene into a pET vector in order to study the link between blue, red and purple copper cupredoxins [296]. Overexpression of this N_2OR protein in *E. coli* resulted in the purification of the apo-form of the protein, which was reconstituted *in vitro* with copper. Earlier on, Fujita and co-workers purified a recombinant N_2OR from *Achromobacter cycloclastes* using the broad host range plasmid pML10 [297]. However, the metal analysis content of the protein revealed a mis-population of N_2OR with considerably different levels of copper. For this reason a more stringent system was put in place that allowed the generation of a recombinant N_2OR that could be purified from *P. denitrificans* under physiologically relevant conditions through a 1-step affinity chromatography. This was achieved by knocking-in a *Strep*-tag II sequence in-frame at the C-terminus of *nosZ* gene. The phenotypical analysis of *P. denitrificans* WT and $NosZ_{WT}$ strains confirmed that there is not any significant difference in terms of growth capacity and N_2O reduction activity between the NosZ-*Strep*-tag II variant and WT. Moreover, the metal content analysis confirm that the purified protein contained approximately 6 copper equivalent per monomer as expected from a fully assembled N_2OR [13].

Recombinant N_2OR, isolated from cultures grown in the presence of micromolar amounts of copper, displayed as purified an UV-vis spectra similar to what has been previously categorised as N_2OR form I or anaerobically purified N_2OR. Some features characteristics of N_2OR form II could also be appreciated, especially in ferricyanide-oxidised $NosZ_{\Delta scoB}$ spectrum. However, the protein purification procedure was carried out in all cases in the presence of oxygen since we were

primarily interested in studying the copper loading properties of N_2OR proteins. The prevalence of form I despite aerobic purification among the purified proteins could be probably explained by the short time that is required to complete the purification procedure (that can be achieved in approximately three hours). Because, the differential spectra analysis of $NosZ_{WT}$, $NosZ_{\Delta scoB}$ and $NosZ_{pcuC^-}$ confirmed the presence of fully metallated Cu_A centres with almost identical profiles, the form II features of $NosZ_{\Delta scoB}$ are probably originated from the air oxidation of the Cu_Z centre. For comparison, the same air oxidised spectrum would also arise in $NosZ_{WT}$ and $NosZ_{pcuC^-}$ over the course of a day (see figure 6.8). This is consistent with purification of form I from anaerobically prepared cells that converts to form II over time as a consequence of prolonged exposure to oxygen

In contrast to N_2OR proteins purified from the variant strains under copper sufficient conditions, when copper was excluded from the formulation of the growth media isolated N_2OR proteins lacked the Cu_Z centre irrespective of the copper chaperoning genetic background of the *P. denitrificans* strain used (see table 6.1). More importantly, only N_2OR from *P. denitrificans* WT showed a metallated Cu_A site while N_2OR proteins isolated from both $\Delta scoB$ and $pcuC^-$ mutant background were in their apo form. In addition, only $NosZ_{WT}$ showed some residual enzymatic activity that was completely absent in $\Delta scoB$ and $pcuC^-$. Since the metal content of $NosZ_{WT}$ indicated the presence of nearly 2 copper equivalents per monomer, the residual activity could be therefore explained by a small subpopulation of fully or partially loaded catalytically capable Cu_Z centre.

Overall, the UV-vis spectroscopy, metal content and enzymatic activity of N_2OR proteins are in agreement with the growth phenotypes of *scoB* and *pcuC* strains studied in sections 3.3 and 4.3. When micromolar amount of copper is added to the growth media, fully metallated and active N_2OR protein is produce and no N_2O phenotype is observed independently of whether *scoB* or *pcuC* genes have been deleted or not (see table 6.1). However, in a copper deficient growth media *P. denitrificans* WT produced an N_2OR protein which is primarily metallated at the Cu_A centre and only retained basal enzymatic activity, nevertheless cells accumulated N_2O transiently and were able to reduce the gas over an extended

time period. When *scoB* or *pcuC* genes were deleted, N_2OR was produced in its apo form and no activity was detected, therefore the cells accumulated all the nitrogen added to the growth media in the form of N_2O (see table 6.1). Wunsch and co-workers studied the effect of the deletion of a *sco* gene (named *scoP*) from *P. putida*, although the authors did not find any significant effect on N_2OR associated with the mutation [89]. However, at the time of this study the genome of *P. putida* was yet not available and inspection of the genome of *P. putida* with contemporaneous bioinformatics tools reveals that *scoP* is encoded within a *surf1-hypothetical-cox15-cox10-scoP* gene cluster. Surf1, Cox15 and Cox10 are proteins that are associated with the maturation and delivery of heme *a* to cytochrome *c* oxidase [298–300]. Moreover, a BLAST search of *P. putida* genome using ScoP as a query identified a second Sco protein with a pairwise identity of 27 %. The gene coding for the second Sco protein is encoded in a binomial *sco-pcu$_A$C* gene cluster such as the classical gene cluster of *D. radiodurans* [33] or *T. thermophilus* [5] that have been found to be involved in cytochrome *c* oxidase Cu_A centre metallation. Gene redundancy is a common feature of *sco* genes as pointed out by Banci *et al.* [177], and it is consider that when the pairwise identity is $\sim$ 24 % the Sco proteins expressed by a given organism might have adapted to play specific roles within the cell, instead of performing redundant functions. Besides, it is not surprising that in *P. denitrificans* N_2OR phenotype of ScoB and PCuC are only apparent when the extracellular concentration of copper drops drastically below micromolar levels since these two types of proteins have been described to hold extremely low copper binding affinities within the order of the femtomolar range [5, 216]. This might account for another reason of why an N_2OR phenotype was not observed since the culture media was supplemented with 5 µM of copper. In a similar manner, as we mentioned in section 3.8, mutation of *sco* in *P. aeruginosa* [211], *R. capsulatus* [212], *S. lividans* [185] and *B. subtilis* [175] entailed a reduction in terminal reductase activity which was only evident in a copper depleted media. Moreover, deletion of *pccA* gene (homologue to *pcu$_A$C*) from *R. capsulatus* resulted in a lower activity of cytochrome *cbb$_3$* in copper limited media [301]. In *R. sphaeroides* deletion of *pcu$_A$C* gene has associated a reduction in the accumulation of both cytochrome *aa$_3$* and

cbb$_3$ and affect the assembly of both Cu_A and Cu_B in a copper depleted media [302]. In *B. japonicum* deletion of the whole gene cluster where *pcuC* (homologue to PCu_AC)and *pcuD* (homologue to YcnI) are encoded resulted in a growth reduction under both oxic and denitrifying conditions only in a copper depleted media [240]. The authors also observed an accumulation of nitrite attributed to the malfunction of the copper dependent nitrite reductase. PCuC was also required for full activation of cytochrome *aa*$_3$ and *cbb*$_3$ during symbiosis [240].

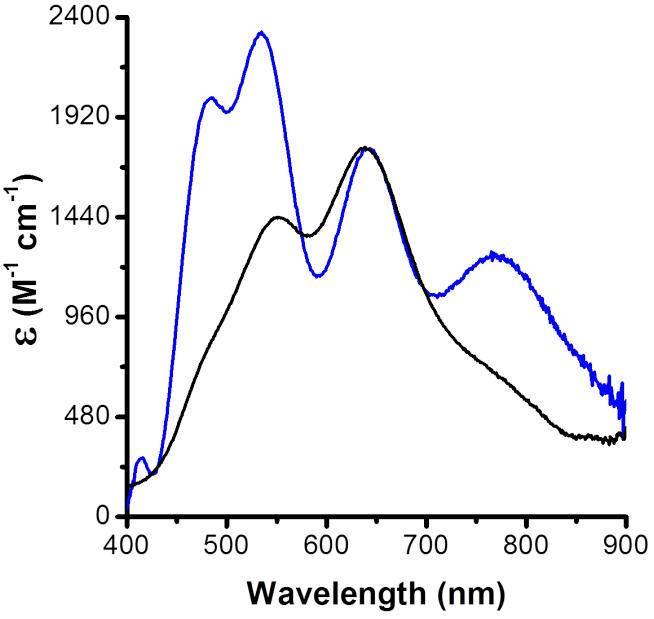

FIGURE 6.8: UV-vis spectrum of recombinant N_2OR. As purified $NosZ_{WT}$ presents a spectrum similar to N_2OR form I (–), during the time course of a day the protein is air oxidised and develops the features typical of a form II protein (–)

	Analysis	$\mathbf{NosZ_{WT}}$	$\mathbf{NosZ_{\Delta scoB}}$	$\mathbf{NosZ_{pcuC^-}}$
Cu sufficient	Phenotype	N_2-genic	N_2-genic	N_2-genic
	UV-vis	Cu_Z, Cu_A	Cu_Z, Cu_A	Cu_Z, Cu_A
	Cu content	5.6	5.7	5.6
	Activity	40.66 ± 3.10	71.7 ± 3.99	50.3 ± 4.37
Cu limited	Phenotype	N_2-genic	N_2O-genic	N_2O-genic
	UV-vis	Cu_A	-	-
	Cu content	1.4	0.3	0.2
	Enzymatic activity	0.6 ± 0.25	0.04 ± 0.02	0.01 ± 0.01

TABLE 6.1: Summary of the characteristics of recombinant N_2OR proteins purified from *P. denitrificans* from growth media supplemented or limited with copper. The results from the phenotypical analysis from sections 3.3 and 4.3 are summarised under the labels N_2-genic/N_2O-genic to refer to whether the cultures produced N_2 or N_2O. UV-vis Cu_Z and Cu_A indicate the presence of the absorbance features distinctive of these Cu centres. The units of the copper content analysis are in equivalents of Cu per monomer of N_2OR and the enzymatic activity in µmol of N_2O min^{-1} mg of $NosZ^{-1}$

7 Conclusions and future perspectives

The process of nitrous oxide reduction imposes a tremendous demand on the copper requirements of the cell: a total of 12 Cu ions are need per functional dimer of N_2OR. It is not surprising that when copper becomes scarce in the extracellular environment (i.e. < 0.5 μM), high affinity systems such as ScoB-PCuC from *Paracoccus denitrificans* turn out to be essential for achieving full enzymatic activity of N_2OR. Although the most plausible role of ScoB from *P. denitrificans* is to function as a Cu binding protein given that titrations of both Cu ions point to a very low K_D. In future investigations it would be interesting to address whether ScoB from *P. denitrificans* also has thioredoxin activity. Nevertheless, at this point we only count with a preliminary competition assay experiment for ScoB from *P. denitrificans* and more conditions and different ligands need to be analysed in order to determine a K_D value within a confident range. Conversely, it would be worth exploring how amenable is ScoB to crystallisation in its apo and holo forms since in bacteria Sco proteins seem to be reluctant to crystallise in the presence of the metal [180]. The only deposited Cu-bound prokaryotic Sco structure up to date is from *Bradyrhizobium japonicum* (pdb: 4WBR) but it lacks a publication associated with it. This could also shed some light in relation to whether a significant conformational change takes place upon Cu^{2+} binding as indicated by Cu^{2+} titration (see 3.5). Alternatively, there is also the possibility that the thioredoxin function could be performed by another specialised protein. For instance, a BLAST search of *P. denitrificans* revealed the presence of four

thioredoxins containing a CX_2C motif which are: Pden_1410, 2023, 2371 and 2793 (see figure 7.2). Among these proteins, Pden_1410 is a CcmG type protein with a periplasmic export sequence, which has been shown to be required for aa_3-type cytochrome biogenesis in *P. denitrificans* [303].

However, the questions of which direction does Cu follows between ScoB and PCuC, and which Cu-chaperone is actually capable of transferring the metal to NosZ still remain to be answered. To test if ScoB and PCuC act together and one pass the metal to the other or whether they individually interact with NosZ. A simple experiment can be set up where the Cu^{1+} or Cu^{2+} bound forms of ScoB or PCuC and the apo form of the other are mixed. Then, ScoB and PCuC can be easily separated by size exclusion or affinity chromatography and analysed for their metal content by ICP-AES. Alternatively, Cu^{2+} changes of the characteristic spectrum of Cu^{2+}-ScoB can be used to tell whether the protein is being metallated or demetallated. Conversely, although a considerably inefficient process due to the low protein yields obtained, apo-NosZ can be isolated from $\Delta scoB$ or $pcuC^{-}$ mutants grown in copper limited cultures and used in Cu transfer studies. Apo-NosZ does not have any spectroscopic feature within the visible region of the electromagnetic spectrum. Therefore, the Cu loaded form of ScoB and/or PCuC can be mixed with reduced apo-NosZ. As a consequence of the Cu transfer from ScoB and/or PCuC the features of a NosZ Cu loaded should reappear within the UV-vis spectra. At the same time, NosZ can also be separated from ScoB and PCuC by affinity chromatography and checked for its metal content.

Nevertheless, it is unclear what pathway follows the metal once it enters the cell, but it has to be bound to a protein until it reaches its final destination [39]. Several scenarios have been contemplated within the context of N_2O respiration, and the two that we consider more probable are shown in figure 7.1. In the first model the main role of ScoB would be to reduce the cysteine residues of the Cu_A centre of N_2OR in a similar manner in which Sco from *T. thermophilus* interacts with cytochrome *c* oxidase [5]. Once the Cu_A centre is ready to receive the redox active cofactor, transfer is performed by a copper loaded PCuC protein. Alternatively,

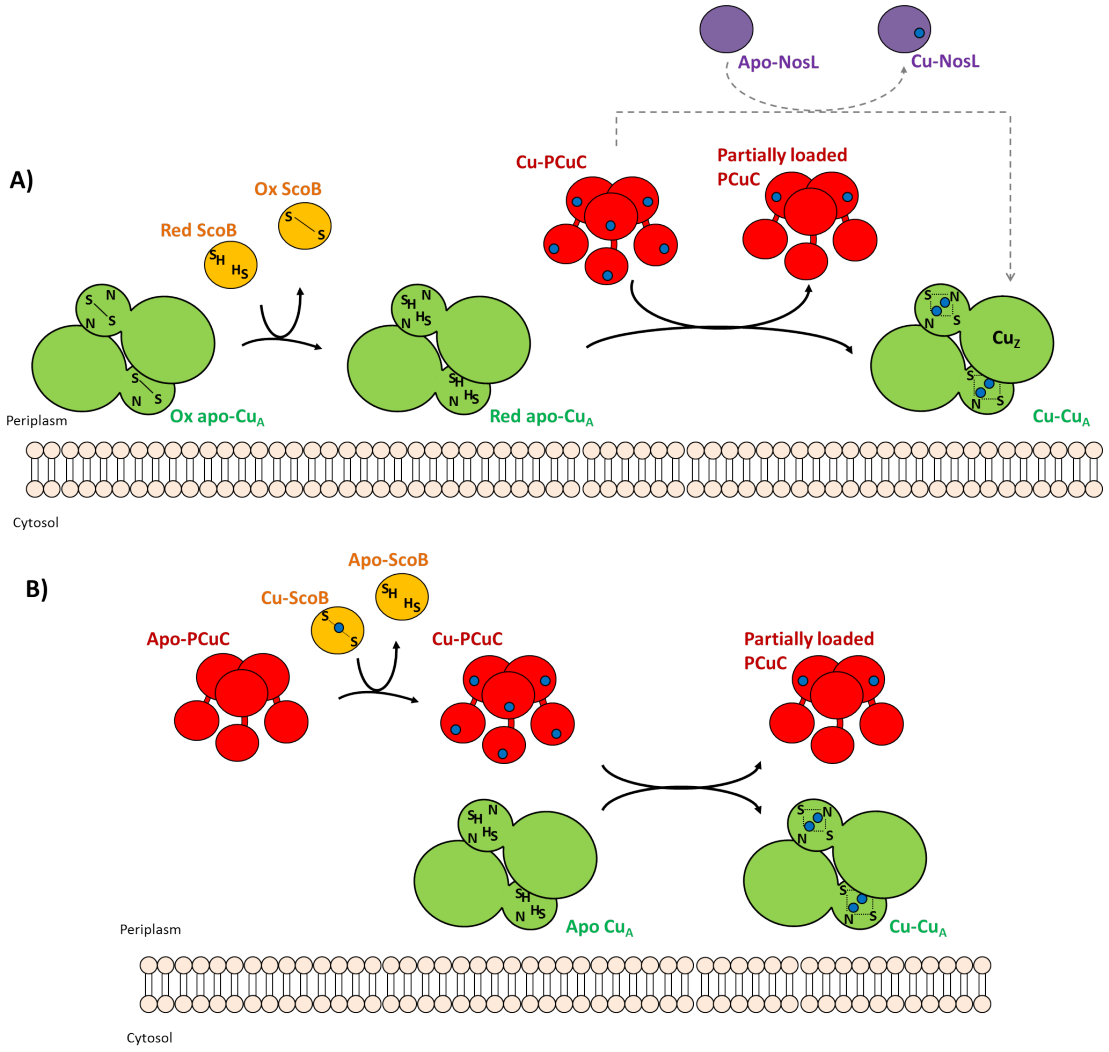

FIGURE 7.1: Proposed mechanisms of maturation of the Cu_A centre of nitrous oxide reductase from *P. denitrificans*. **(A)** In this model ScoB functions primarily as a thiol disulfide isomerase and prepares the Cu_A centre to be metallated by Cu-loaded PCuC. **(B)** In this other model, ScoB acts as a metallochaperone of PCuC, which in turn is responsible for transferring the copper ions to reduced Cu_A centre of nitrous oxide reductase. Alternatively, PCuC could also provide Cu to other metallochaperones such as NosL and be part of the Cu_Z maturation mechanism. For simplification ScoB has been represented as a periplasmic protein although the native protein is bound to the cell membrane.

ScoB could instead be responsible for the metallation of PCuC, which in turn once fully metallated would transfer the Cu ions to reduced N_2OR apo-Cu_A centre.

Either way, since the current understanding is that copper is transferred between proteins following affinity gradients [203]. Based on the K_D values estimates for $ScoB_{sol}$ and PCuC (see Chapters 3 and 4), we consider that the protein responsible for the metallation step of the Cu_A centre of N_2OR would be therefore PCuC as it has an average K_D value at least one order of magnitude higher than the one for ScoB. In addition, the oligomeric nature of PCuC from *P. denitrificans* and the two domain organisation of the protein implies that the protein may indeed be capable of transferring either two Cu^{1+} ions from the Ct-domain to the Cu_A centre, or a Cu^{1+} and a Cu^{2+} ion from both N- and C-domain, giving rise to the production of the mixed valence bimetallic centre present in N_2OR. Likewise, we cannot rule out the possibility that the ScoB/PCuC system may also participate in the maturation process of Cu_Z centre of N_2OR, either through direct Cu-donation to the Cu centre or through metal transfer to other chaperone i.e., NosL (see figure 7.1 A).

ScoB-PCuC system may indeed have a Cu scavenging role in copper limited environments. In Europe, copper deficiency is encountered in many regions due to the prevalence of sandy, calcareous, leached soils enriched in organic matter. Areas dedicated to cereal crops and intensive agricultural practices are also at risk of suffering from Cu-deficiency. For example, Alloway *et al.* estimated that nearly 40 % of arable soils in Ireland and Poland, 30 % in Scotland, 25 % in Germany and Denmark, 20 % in Finland are Cu-deficient or potentially deficient [304] (see figure 7.3). Many aquatic ecosystems are also Cu-deficient and in general Cu is less abundant in seawater than in lakes and soil pore waters (see table 7.1).

However, Cu deficiency is not just determined by the quantity of the trace element present in the environment, but by the bioavailability of the metal. One of the factors that defines the bioavailability of Cu is given by the fluxes of the metal between different pools. According to Alloway's monograph about micronutrient deficiencies in agricultural soils, the total copper of a soils is made up of three di-

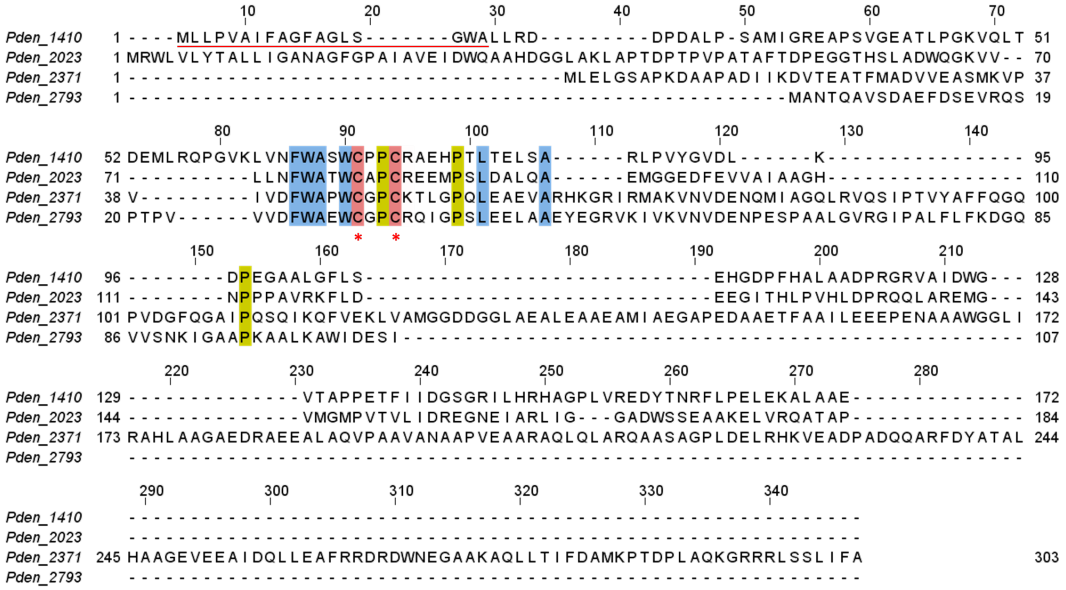

FIGURE 7.2: Multiple sequence alignment of proteins containing a thioredoxin motif encoded in *P. denitrificans*. The CX_2C motif of thioredoxin proteins has been highlighted with the symbol (⋆) below the residues. Pden_1410 is predicted to be exported to the periplasm by the Sec system, the signal peptide is underlined in red.

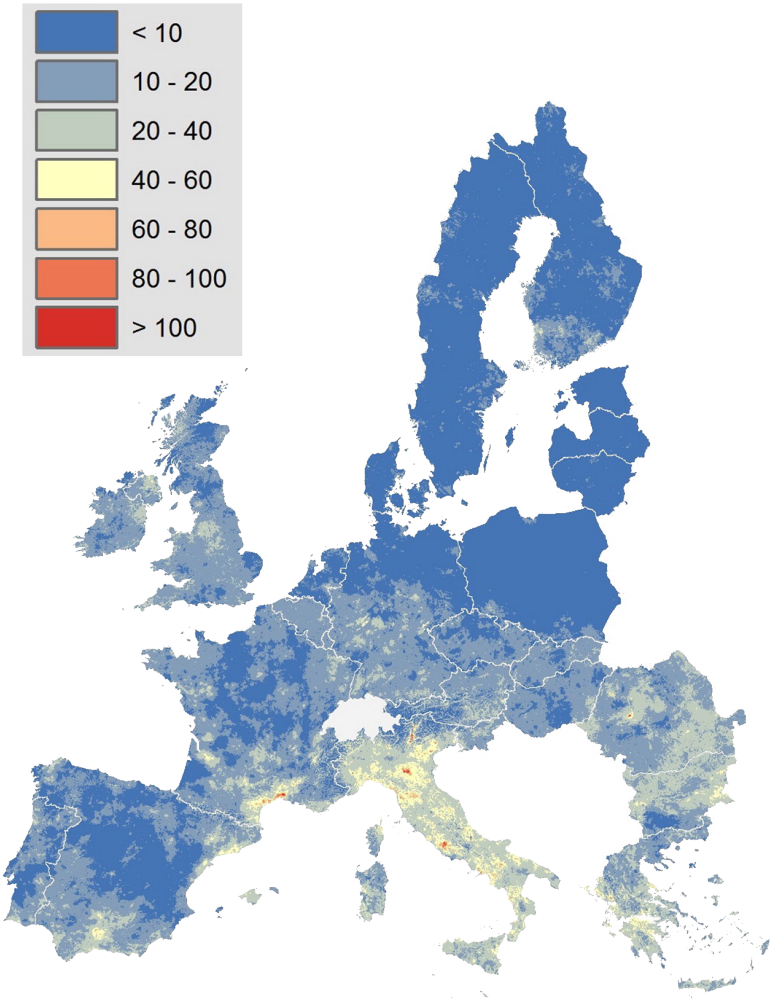

FIGURE 7.3: Concentration of Cu ($mg\,kg^{-1}$) in soil of the European Union. Adapted from [305]

Sample site	Cu	Reference
Representative anoxic waters		
Peat bog waters	0.02–2	[306, 307]
Santa Monica basin sediment pore waters (>5cm depth)	<0.005	[308]
Black Sea sulfidic water column (>200m)	<0.002	[309, 310]
Framvaren Fjord water column (>20m)	<0.001	[309, 310]
Baltic Sea water column (>150m)	<0.007	[311]
Representative oxic waters		
Seawater	<0.001–0.005	[312–314]
Soil pore water	0.1–0.5	[315]
Oxic lake water	0.01–0.8	[316]

TABLE 7.1: Summary of dissolved trace metal concentrations. All concentration units are in micromolar (μM). Adapted from [317]

fferent pools: the soil solution, the labile potentially available pool and the not accessible pool [304]. The soil solution contains free ions and soluble complexes that can be readily uptaken by plant roots and microbes. The labile pool of Cu consists primarily of organo-mineral cation-exchange complexes and hydrous oxides of Mn, Fe, and Al. The fluxes of Cu between the labile and soil solution pools are strongly dominated by the soil pH and in general cationic ions such as copper are more soluble in acidic soils. The unavailable copper pool is mainly compound of primary and secondary mineral crystals and stable organic complexes. These forms of copper are only released by weathering, which can be intensified in low pH soils. Therefore, a soil can potentially be copper deficient even if the total amount of copper is high but the copper soil solution pool is not capable of supplying the microbial needs [304].

Copper availability is also affected by either synergistic or antagonistic interactions between different micronutrients. This process has been known for more than 60 years and initially described by Prevot and Smith within the context of agricultural sciences [318, 319]. The induced Cu-deficiencies are often caused by the presence of relatively high concentrations of other micronutrients such as Zn, Fe and Mn and may occur at different levels: such as ion uptake, translocation or accumulation. Examples have extensively described in medical [320–325] and agricultural sciences [318, 319, 326–328]. Therefore, based on all these factors it would be advisable

to include in future studies the assessment of the N_2O genic capacity of a soil due to potential Cu-deficiencies based on the parameters described above: total Cu content of the soil, soil pH, type of minerals present in the soil, percentage of organic matter and chance of antagonistic reactions from Zn, Fe or Mn.

In conclusion, the sequential reduction of NO_3^- into N_2 under anaerobic conditions is a process highly dependent on copper. When Cu is limiting in the environment bacteria such as *P. denitrificans* express a high affinity system ScoB/PCuC that is fundamental full denitrification. $ScoB_{sol}$ is a monomeric protein that contains a mononuclear copper site, the metal ion can be bound in its Cu^{1+} or Cu^{2+} state and the K_D of the binging lies below the femtomolar range. In contrast to ScoB, the metallochaperone PCuC is a complex trimeric multidomain protein. The formation of the oligomer is driven by the YcnI-like N-terminal domain that forms a central core that is connected through a linker region to the monomeric PCu_AC-like Ct-domain. Two families of YcnI proteins have been identified in this work, family A holds a novel $H_{22}H_{101}W$ motif such as the one found in PCuC Nt-domain from *P. denitrificans*, and family B contains a $H_{22}D_{90}W_{13}H$ motif such as in the canonical YcnI from *B. subtilis* or *N. farcinica*. This new type of histidine brace motif binds a single Cu^{1+} or Cu^{2+} ion with a femtomolar affinity. Furthermore, the PCuC protein contains a recognised Cu^{1+} binding site located within its C-terminal domain that binds the metal with a subfemtomolar affinity. As a result, the full length PCuC protein can potentially harbour up to 6 coper atoms per trimer with a global binding affinity below the subfemtomolar range. Both proteins ScoB and PCuC, were observed to be required for proper Cu_A centre assembly and activity of N_2OR under copper limiting conditions.

A

Supplementary information

A.1 Antibiotics and supplements

Antibiotic	[Stock] (mg mL^{-1})	[Final] (μg mL^{-1})	Storage
Carbenicillin (car)	100	100	4 °C
Gentamicin (gen)	20	20	4 °C
Kanamycin (kan)	50	50	4 °C
Spectinomycin (Spec)	25	25	4 °C
Streptomycin (str)	60	60	4 °C
Taurine (tau)	62.5	1251.5	RT

Table A.1: Antibiotics and supplements

A.2 Sequences of DNA synthesized

```
pLMB510  CATATGCATCATCACCATCATCACATCGAAGGGCGGGGATCCATG    45

pLMB510  AGTAAAGGAGAAGAACTTTTCACTGGAGTTGTCCCAATTCTTGTT    90

pLMB510  GAATTAGATGGTGATGTTAATGGGCACAAATTTTCTGTCAGTGGA   135

pLMB510  GAGGGTGAAGGTGATGCAACATACGGAAAACTTACCCTTAAATTT   180
```

```
pLMB510  ATTTGCACTACTGGAAAACTACCTGTTCCATGGCCAACACTTGTC  225

pLMB510  ACTACTTTGACTTATGGTGTTCAATGCTTTTCAAGATACCCAGAT  270

pLMB510  CACATGAAACGGCATGACTTTTTCAAGAGTGCCATGCCCGAAGGT  315

pLMB510  TATGTACAGGAAAGAACTATATTTTTCAAAGATGACGGGAACTAC  360

pLMB510  AAGACACGTGCTGAAGTCAAGTTTGAAGGTGATACCCTTGTTAAT  405

pLMB510  AGAATCGAGTTAAAAGGTATTGATTTTAAAGAAGATGGAAACATT  450

pLMB510  CTTGGACACAAATTGGAATACAACTATAACTCACACAATGTATAC  495

pLMB510  ATCATGGCAGACAAACAAAAGAATGGAATCAAAGTTAACTTCAAA  540

pLMB510  ATTAGACACAACATTGAAGATGGAAGCGTTCAACTAGCAGACCAT  585

pLMB510  TATCAACAAAATACTCCAATTGGCGATGGCCCTGTCCTTTTACCA  630

pLMB510  GACAACCATTACCTGTCCACACAATCTGCCCTTTCGAAAGATCCC  675

pLMB510  AACGAAAAGAGAGACCACATGGTCCTTCTTGAGTTTGTAACAGCT  720

pLMB510  GCTGGGATTACACATGGCATGGATGAACTATACAAAAGGCCTGCA  765

pLMB510  GCAAACGACGAAAACTACGCTTTAGTAGCTCCCGGGGACGACGAC  810

pLMB510  GACAAGCATCATCACCATCATCACTAAGAATTC   843


pLMB511  CATATGTGGAGCCACCCCCAATTTGAAAAAATCGAAGGGCGGGGA   45

pLMB511  TCCCCCGGGGACGACGACGACAAGTGGAGCCACCCCCAATTTGAA   90

pLMB511  AAATAAGAATTC   102
```

A.3 Clustal X Colour Scheme

Category	Colour	Residue at position
Hydrophobic	BLUE	A,I,L,M,F,W,V
		C
Positive charge	RED	K,R
Negative charge	MAGENTA	E
		D
Polar	GREEN	N
		Q
		S,T
Cysteines	PINK	C
Glycines	ORANGE	G
Prolines	YELLOW	P
Aromatic	CYAN	H,Y
Unconserved	WHITE	any / gap

FIGURE A.1: Clustal X Colour Scheme [329]

A.4 Structures used as templates for homology ScoB model

Protein	PDB ID	Organism
Sco1	2B7K	*Saccharomyces cerevisiae*
Sco1	2K6V	*Thermus Thermophilus*
Sco2	2RLI	*Homo sapiens*
Sco1	2B7K	*Saccharomyces cerevisiae*
Sco1	1WP0	*Homo sapiens*
Sco1	4TXO	*Bradyrhizobium diazoefficiens*

TABLE A.2: Templates used for Phyre2 ScoB model

A.5 Signal peptide prediction

Software	$PCuC_{Nt}$	YcnI
SignalP [200]	1-27	1 - 28
Phobius [199]	1 - 29	1 - 26
Pred-TAT [232]	1 - 29	1 - 28

TABLE A.3: Signal peptide prediction for $PCuC_{Nt}$ from *P. denitrificans* and YcnI from *N. farcinica*

A.6 Dynafit script: Competition with proteins that bind one ligand

```
[task]
task = fit ;
data = equilibria ;
[mechanism]; interaction
M + L + L <==> ML.L : K1 dissociation
P + M <==> PM : K2 dissociation
[constants]
K1 = 6.30957344480194E-18
K2 = 6.1E-19?
[concentrations]
M = 0.00001
[responses]
ML.L=1
[data]
directory C:\DynaFit4\DATA
variable P
file BCA50.txt | concentrations L = 0.00005
[output]
directory C:\DynaFit4\DATA\output


[end]
```

A.7 Dynafit script: Competition with proteins that bind two ligands

```
[task]
task = fit ;
data = equilibria ;
[mechanism]; interaction
M + M + L + L + L + L <==> ML.L + ML.L: K1 dissociation
P + M + M <==> PM.M : K2 dissociation
[constants]
K1 = 6.30957344480194E-18
K2 = 6.1E-19?
[concentrations]
M = 0.00001
[responses]
ML.L=1
[data]
directory C:\DynaFit4\DATA
variable P
file BCA50.txt | concentrations L = 0.00005
[output]
directory C:\DynaFit4\DATA\output
[end]
```

Bibliography

1. Ravishankara, A. R., Daniel, J. S. & Portmann, R. W. Nitrous oxide (N_2O): the dominant ozone-depleting substance emitted in the 21st century. *Science* **326,** 123–125 (2009).

2. *Climate Change 2013 - The Physical Science Basis* (ed Intergovernmental Panel on Climate Change) doi:10.1017/CBO9781107415324. <http://ebooks.cambridge.org/ref/id/CBO9781107415324> (Cambridge University Press, Cambridge, 2014).

3. Sullivan, M. J., Gates, A. J., Appia-Ayme, C., Rowley, G. & Richardson, D. J. Copper control of bacterial nitrous oxide emission and its impact on vitamin B_{12}-dependent metabolism. *Proceedings of the National Academy of Sciences of the United States of America* **110,** 19926–19931 (2013).

4. Chillappagari, S., Miethke, M., Trip, H., Kuipers, O. P. & Marahiel, M. A. Copper acquisition is mediated by YcnJ and regulated by YcnK and CsoR in *Bacillus subtilis*. *Journal of bacteriology* **191,** 2362–2370 (2009).

5. Abriata, L. A., Banci, L, Bertini, I, Ciofi-Baffoni, S, Gkazonis, P, Spyroulias, G. A., Vila, A. J. & Wang, S. Mechanism of CuA assembly. *Nature Chemical Biology* **4,** 599–601 (2008).

6. Nelson, D. L., Cox, M. M. & Lehninger, A. L. *Lehninger principles of biochemistry* 5th, 45 (W. H. Freeman, 2008).

7. Bothe, H., Ferguson, S. J. & Newton, W. E. *Biology of the nitrogen cycle* 427 (Elsevier, 2007).

8. Jetten, M. S. M., Strous, M., Fuerst, J. A., Kramer, E. H. M., Logemann, S., Muyzer, G., van de Pas-Schoonen, K. T., Webb, R. & Kuenen, J. G. Missing lithotroph identified as new planctomycete. *Nature* **400,** 446–449 (1999).

9. Zumft, W. G. Cell biology and molecular basis of denitrification. *Microbiology and Molecular Biology Reviews* **61,** 533–616 (1997).

10. Mosier, A., Kroeze, C., Nevison, C., Oenema, O., Seitzinger, S. & van Cleemput, O. Closing the global N_2O budget: nitrous oxide emissions through the agricultural nitrogen cycle. *Nutrient Cycling in Agroecosystems* **52,** 225–248 (1998).

11. Tolman, W. B. Binding and activation of N_2O at transition-metal centers: recent mechanistic insights. *Angewandte Chemie* **49,** 1018–1024 (2010).

12. Banks, R. G. S., Henderson, R. J. & Pratt, J. M. Reactions of nitrous oxide with some transition-metal complexes. *Chemical Communications* **8,** 387–388 (1967).

13. Pomowski, A., Zumft, W. G., Kroneck, P. M. H. & Einsle, O. N_2O binding at a [4Cu:2S] copper-sulphur cluster in nitrous oxide reductase. *Nature* **477,** 234–237 (2011).

14. Richardson, D., Felgate, H., Watmough, N., Thomson, A. & Baggs, E. Mitigating release of the potent greenhouse gas N_2O from the nitrogen cycle - could enzymic regulation hold the key? *Trends in biotechnology* **27,** 388–397 (2009).

15. Simon, J. & Klotz, M. G. Diversity and evolution of bioenergetic systems involved in microbial nitrogen compound transformations. *Biochimica et Biophysica Acta (BBA) - Bioenergetics* **1827,** 114–135 (2013).

16. Hallin, S., Philippot, L., Löffler, F. E., Sanford, R. A. & Jones, C. M. Genomics and ecology of novel N_2O-reducing microorganisms. *Trends in Microbiology* **69,** 2712–2718 (2017).

17. Beijerinck, M. W. & Minkman, D. C. J. Bildung und Verbrauch von Stickoxydul durch Bakterien. *Zentralblatt für Bakteriologie, Parasitenkunde und Infektionskrankheiten und Hygiene, Abteilung II* **25,** 30–63 (1910).

18. *Paracoccus denitrificans PD1222 complete genome. European Nucleotide Archive* <http://www.ebi.ac.uk/ena/data/view/GCA{_}000203895> (2017).

19. Baker, S. C., Ferguson, S. J., Ludwig, B, Page, M. D., Richter, O. M. & van Spanning, R. J. Molecular genetics of the genus *Paracoccus*: metabolically versatile bacteria with bioenergetic flexibility. *Microbiology and molecular biology reviews* **62,** 1046–1078 (1998).

20. Richardson, D. J. Bacterial respiration: a flexible process for a changing environment. English. *Microbiology* **146,** 551–571 (2000).

21. Garcia-Horsman, J. A., Barquera, B., Rumbley, J., Ma, J. & Gennis, R. B. The superfamily of heme-copper respiratory oxidases. *Journal of Bacteriology* **176,** 5587–5600 (1994).

22. Pitcher, R. S. & Watmough, N. J. The bacterial cytochrome cbb_3 oxidases. *Biochimica et Biophysica Acta (BBA) - Bioenergetics* **1655,** 388–399 (2004).

23. Pereira, M. M., Santana, M. & Teixeira, M. A novel scenario for the evolution of haem–copper oxygen reductases. *Biochimica et Biophysica Acta (BBA) - Bioenergetics* **1505,** 185–208 (2001).

24. Haltia, T, Puustinen, A & Finel, M. The *Paracoccus denitrificans* cytochrome aa_3 has a third subunit. *European journal of biochemistry* **172,** 543–546 (1988).

25. Iwata, S., Ostermeier, C., Ludwig, B. & Michel, H. Structure at 2.8 Å resolution of cytochrome *c* oxidase from *Paracoccus denitrificans*. *Nature* **376,** 660–669 (1995).

26. Denis, M. Structure and function of cytochrome *c* oxidase. *Biochimie* **68,** 459–470 (1986).

27. Ludwig, B. Terminal oxidases in *Paracoccus denitrificans*. *Biochimica et Biophysica Acta (BBA) - Bioenergetics* **1101,** 195–197 (1992).

28. Ekici, S., Pawlik, G., Lohmeyer, E., Koch, H.-G. & Daldal, F. Biogenesis of *cbb_3*-type cytochrome *c* oxidase in *Rhodobacter capsulatus*. *Biochimica et biophysica acta* **1817,** 898–910 (2012).

29. Preisig, O, Anthamatten, D & Hennecke, H. Genes for a microaerobically induced oxidase complex in *Bradyrhizobium japonicum* are essential for a nitrogen-fixing endosymbiosis. *Proceedings of the National Academy of Sciences of the United States of America* **90,** 3309–3313 (1993).

30. Carr, H. S. & Winge, D. R. Assembly of cytochrome *c* oxidase within the mitochondrion. *Accounts of Chemical Research* **36,** 309–316 (2003).

31. Banci, L., Bertini, I., Ciofi-Baffoni, S., Hadjiloi, T., Martinelli, M. & Palumaa, P. Mitochondrial copper(I) transfer from Cox17 to Sco1 is coupled to electron transfer. *Proceedings of the National Academy of Sciences* **105,** 6803–6808 (2008).

32. Banci, L., Bertini, I., Cantini, F. & Ciofi-baffoni, S. Cellular copper distribution: a mechanistic systems biology approach. *Cellular and Molecular Life Sciences* **67,** 2563–2589 (2010).

33. Banci, L., Bertini, I., Ciofi-Baffoni, S., Katsari, E., Katsaros, N., Kubicek, K. & Mangani, S. A copper(I) protein possibly involved in the assembly of Cu_A center of bacterial cytochrome *c* oxidase. *Proceedings of the National Academy of Sciences of the United States of America* **102,** 3994–3999 (2005).

34. Romano, D. & Matteucci, F. Contrasting copper evolution in Centauri and the Milky Way. *Monthly Notices of the Royal Astronomical Society: Letters* **378,** 59–63 (2007).

35. Crichton, R. & Pierre, J.-L. Old iron, young copper: from Mars to Venus. *BioMetals* **14,** 99–112 (2001).

36. Macomber, L. & Imlay, J. A. The iron-sulfur clusters of dehydratases are primary intracellular targets of copper toxicity. *Proceedings of the National Academy of Sciences* **106,** 8344–8349 (2009).

37. Changela, A., Chen, K., Xue, Y., Holschen, J., Outten, C. E., O'Halloran, T. V. & Mondragón, A. Molecular basis of metal-ion selectivity and zeptomolar sensitivity by CueR. *Science* **301,** 1383–1387 (2003).

38. Finney, L. A. & O'Halloran, T. V. Transition metal speciation in the cell: insights from the chemistry of metal ion receptors. *Science* **300,** 931–936 (2003).

39. Rae, T. D., Schmidt, P. J., Pufahl, R. A., Culotta, V. C. & O'Halloran, T. V. Undetectable intracellular free copper: the requirement of a copper chaperone for superoxide dismutase. *Science* **284,** 805–808 (1999).

40. Boal, A. K. & Rosenzweig, A. C. Structural biology of copper trafficking. *Chemical Reviews* **109,** 4760–4779 (2009).

41. Stephen Tottey, Duncan R. Harvie & Robinson, N. J. Understanding how cells allocate metals using metal sensors and metallochaperones. *Accounts of Chemical Research* **38,** 775–783 (2005).

42. Zhang, Y. & Gladyshev, V. N. Comparative genomics of trace elements: emerging dynamic view of trace element utilization and function. *Chemical Reviews* **109,** 4828–4861 (2009).

43. Vita, N., Platsaki, S., Baslé, A., Allen, S. J., Paterson, N. G., Crombie, A. T., Murrell, J. C., Waldron, K. J. & Dennison, C. A four-helix bundle stores copper for methane oxidation. *Nature* **525,** 140–143 (2015).

44. Waldron, K. J. & Robinson, N. J. How do bacterial cells ensure that metalloproteins get the correct metal? *Nature reviews. Microbiology* **7,** 25–35 (2009).

45. Kroll, J. S., Langford, P. R., Wilks, K. E. & Keil, A. D. Bacterial [Cu,Zn]-superoxide dismutase: phylogenetically distinct from the eukaryotic enzyme, and not so rare after all! *Microbiology* **141,** 2271–2279 (1995).

46. Fang, F. C., DeGroote, M. A., Foster, J. W., Bäumler, A. J., Ochsner, U, Testerman, T, Bearson, S, Giárd, J. C., Xu, Y, Campbell, G & Laessig, T. Virulent *Salmonella typhimurium* has two periplasmic Cu, Zn-superoxide dismutases. *Proceedings of the National Academy of Sciences of the United States of America* **96,** 7502–7507 (1999).

47. Krishnakumar, R., Kim, B., Mollo, E. A., Imlay, J. A. & Slauch, J. M. Structural properties of periplasmic SodCI that correlate with virulence in *Salmonella enterica* serovar Typhimurium. *Journal of Bacteriology* **189,** 4343–4352 (2007).

48. Outten, F. W., Outten, C. E., Hale, J. & O'Halloran, T. V. Transcriptional activation of an *Escherichia coli* copper efflux regulon by the chromosomal MerR homologue, CueR. *Journal of Biological Chemistry* **275,** 31024–31029 (2000).

49. Roberts, S. A., Weichsel, A., Grass, G., Thakali, K., Hazzard, J. T., Tollin, G., Rensing, C. & Montfort, W. R. Crystal structure and electron transfer kinetics of CueO, a multicopper oxidase required for copper homeostasis in *Escherichia coli*. *Proceedings of the National Academy of Sciences* **99,** 2766–2771 (2002).

50. Singh, S. K., Grass, G., Rensing, C. & Montfort, W. R. Cuprous oxidase activity of CueO from *Escherichia coli*. *Journal of bacteriology* **186,** 7815–7817 (2004).

51. Lutkenhaus, J. F. Role of a major outer membrane protein in *Escherichia coli*. *Journal of bacteriology* **131,** 631–637 (1977).

52. Egler, M., Grosse, C., Grass, G. & Nies, D. H. Role of the extracytoplasmic function protein family sigma factor RpoE in metal resistance of *Escherichia coli*. *Journal of bacteriology* **187,** 2297–2307 (2005).

53. Kim, H. J., Graham, D. W., DiSpirito, A. A., Alterman, M. A., Galeva, N., Larive, C. K., Asunskis, D. & Sherwood, P. M. A. Methanobactin, a copper-acquisition compound from methane-oxidizing bacteria. *Science* **305,** 1612–1615 (2004).

54. Balasubramanian, R., Kenney, G. E. & Rosenzweig, A. C. Dual pathways for copper uptake by methanotrophic bacteria. *Journal of Biological Chemistry* **286,** 37313–37319 (2011).

55. Anttila, J., Heinonen, P., Nenonen, T., Pino, A., Iwaï, H., Kauppi, E., Soliymani, R., Baumann, M., Saksi, J., Suni, N. & Haltia, T. Is coproporphyrin III a copper-acquisition compound in *Paracoccus denitrificans*? *Biochimica et Biophysica Acta (BBA) - Bioenergetics* **1807,** 311–318 (2011).

56. Ekici, S., Yang, H., Koch, H.-G. & Daldal, F. Novel transporter required for biogenesis of cbb_3-type cytochrome *c* oxidase in *Rhodobacter capsulatus*. *mBio* **3,** 293–304 (2012).

57. Khalfaoui-Hassani, B., Verissimo, A. F., Koch, H.-G. & Daldal, F. Uncovering the transmembrane metal binding site of the novel bacterial major facilitator superfamily-type copper importer CcoA. *mBio* **7,** 1981–1996 (2016).

58. Petersen, C & Møller, L. B. Control of copper homeostasis in *Escherichia coli* by a P-type ATPase, CopA, and a MerR-like transcriptional activator, CopR. *Gene* **261,** 289–298 (2000).

59. Radford, D. S., Kihlken, M. A., Borrelly, G. P., Harwood, C. R., Brun, N. E. & Cavet, J. S. CopZ from *Bacillus subtilis* interacts *in vivo* with a copper exporting CPx-type ATPase CopA. en. *FEMS Microbiology Letters* **220,** 105–112 (2003).

60. Osman, D., Patterson, C. J., Bailey, K., Fisher, K., Robinson, N. J., Rigby, S. E. J. & Cavet, J. S. The copper supply pathway to a *Salmonella* Cu,Zn-superoxide dismutase (SodCII) involves P_{1B} -type ATPase copper efflux and periplasmic CueP. *Molecular Microbiology* **87,** 466–477 (2013).

61. Loftin, I. R., Franke, S., Roberts, S. A., Weichsel, A., Héroux, A., Montfort, W. R., Rensing, C. & McEvoy, M. M. A novel copper-binding fold for the periplasmic copper resistance protein CusF. *Biochemistry* **44,** 10533–10540 (2005).

62. Long, F., Su, C.-C., Zimmermann, M. T., Boyken, S. E., Rajashankar, K. R., Jernigan, R. L. & Yu, E. W. Crystal structures of the CusA efflux pump suggest methionine-mediated metal transport. *Nature* **467,** 484–488 (2010).

63. Su, C.-C., Yang, F., Long, F., Reyon, D., Routh, M. D., Kuo, D. W., Mokhtari, A. K., Van Ornam, J. D., Rabe, K. L., Hoy, J. A., Lee, Y. J., Rajashankar, K. R. & Yu, E. W. Crystal structure of the membrane fusion protein CusB from *Escherichia coli*. *Journal of Molecular Biology* **393,** 342–355 (2009).

64. Franke, S., Grass, G., Rensing, C. & Nies, D. H. Molecular analysis of the copper-transporting efflux system CusCFBA of *Escherichia coli*. *Journal of bacteriology* **185,** 3804–3812 (2003).

65. Rensing, C. & Grass, G. *Escherichia coli* mechanisms of copper homeostasis in a changing environment. *Fems Microbiology Reviews* **27,** 197–213 (2003).

66. Cha, J. S. & Cooksey, D. A. Copper resistance in *Pseudomonas syringae* mediated by periplasmic and outer membrane proteins. *Proceedings of the National Academy of Sciences of the United States of America* **88,** 8915–8919 (1991).

67. Brown, N. L., Barrett, S. R., Camakaris, J, Lee, B. T. & Rouch, D. A. Molecular genetics and transport analysis of the copper-resistance determinant (pco) from *Escherichia coli* plasmid pRJ1004. *Molecular microbiology* **17,** 1153–1166 (1995).

68. Djoko, K. Y., Xiao, Z., Huffman, D. L. & Wedd, A. G. Conserved mechanism of copper binding and transfer. A comparison of the copper-resistance proteins PcoC from *Escherichia coli* and CopC from *Pseudomonas syringae*. *Inorganic Chemistry* **46,** 4560–4568 (2007).

69. Arnesano, F., Banci, L., Bertini, I., Felli, I. C., Luchinat, C. & Thompsett, A. R. A strategy for the NMR characterization of type II copper(II) proteins: the case of the copper trafficking protein CopC from *Pseudomonas Syringae*. *Journal of the American Chemical Society* **125,** 7200 –7208 (2003).

70. Arnesano, F., Banci, L., Bertini, I., Mangani, S. & Thompsett, A. R. A redox switch in CopC: an intriguing copper trafficking protein that binds copper(I) and copper(II) at different sites. *Proceedings of the National Academy of Sciences of the United States of America* **100,** 3814–3819 (2003).

71. Arnesano, F., Banci, L., Bertini, I. & Thompsett, A. R. Solution structure of CopC. *Structure* **10,** 1337–1347 (2002).

72. Cooksey, D. A. Copper uptake and resistance in bacteria. *Molecular Microbiology* **7,** 1–5 (1993).

73. Puig, S., Rees, E. M. & Thiele, D. J. The ABCDs of periplasmic copper trafficking. *Structure* **10,** 1292–1295 (2002).

74. Matsubara, T & Iwasaki, H. A new-type of copper-protein from *Alcaligenes faecalis*. *Journal of biochemistry* **71,** 747–750 (1972).

75. Iwasaki, H., Saigo, T. & Matsubara, T. Copper as a controlling factor of anaerobic growth under N_2O and biosynthesis of N_2O reductase in denitrifying bacteria. *Plant and Cell Physiology* **21,** 1573–1584 (1980).

76. Walter, G, Matsubara, T., Frunzke, K. & Zumft, W. G. Modulation by copper of the products of nitrite respiration in *Pseudomonas perfectomarinus*. *Journal of bacteriology* **149,** 816–823 (1982).

77. Viebrock, A & Zumft, W. G. Molecular cloning, heterologous expression, and primary structure of the structural gene for the copper enzyme nitrous oxide reductase from denitrifying *Pseudomonas stutzeri*. *Journal of bacteriology* **170,** 4658–4668 (1988).

78. Sanford, R. a., Wagner, D. D., Wu, Q., Chee-Sanford, J. C., Thomas, S. H., Cruz-García, C., Rodríguez, G., Massol-Deyá, A., Krishnani, K. K., Ritalahti, K. M., Nissen, S., Konstantinidis, K. T. & Löffler, F. E. Unexpected nondenitrifier nitrous oxide reductase gene diversity and abundance in soils. *Proceedings of the National Academy of Sciences of the United States of America* **109,** 19709–19714 (2012).

79. Zumft, W. G. & Kroneck, P. M. H. Respiratory transformation of nitrous oxide (N_2O) to dinitrogen by *Bacteria* and *Archaea*. *Advances in microbial physiology* **52,** 107–227 (2007).

80. Pauleta, S. R., Dell'Acqua, S. & Moura, I. Nitrous oxide reductase. *Coordination Chemistry Reviews* **257,** 332–349 (2013).

81. Pauleta, S. R., Carreira, C. & Moura, I. in *Metalloenzymes in Denitrification* 141–169 (Royal Society of Chemistry, Cambridge, 2016).

82. Torres, M., Simon, J., Rowley, G., Bedmar, E., Richardson, D., Gates, A. & Delgado, M. in *Advances in microbial physiology* 353–432 (2016).

83. Zumft, W. G. & Matsubara, T. A novel kind of multi-copper protein as terminal oxidoreductase of nitrous oxide respiration in *Pseudomonas perfectomarinus*. *FEBS Letters* **148,** 107–112 (1982).

84. Jeannine M. Chan, John A. Bollinger, Cassidy L. Grewell & Dooley, D. M. Reductively activated nitrous oxide reductase reacts directly with substrate. *Journal of the American Chemical Society* **126,** 3030–3031 (2004).

85. Prudencio, M., Pereira, A. S., Tavares, P., Besson, S., Cabrito, I., Brown, K., Samyn, B., Devreese, B., Van Beeumen, J., Rusnak, F., Fauque, G., Moura, J. J. G., Tegoni, M., Cambillau, C. & Moura, I. Purification, characterization, and preliminary crystallographic study of copper-containing nitrous oxide reductase from *Pseudomonas nautica* 617. *Biochemistry* **39,** 3899–3907 (2000).

86. SooHoo, C. K. & Hollocher, T. C. Purification and characterization of nitrous oxide reductase from *Pseudomonas aeruginosa* strain P2. *The Journal of biological chemistry* **266,** 2203–2209 (1991).

87. Kristjansson, J. K. & Hollocher, T. C. First practical assay for soluble nitrous oxide reductase of denitrifying bacteria and a partial kinetic characterization. *The Journal of biological chemistry* **255,** 704–707 (1980).

88. Rasmussen, T., Berks, B. C., Butt, J. N. & Thomson, A. J. Multiple forms of the catalytic centre, Cu_Z, in the enzyme nitrous oxide reductase from *Paracoccus pantotrophus*. *The Biochemical journal* **364,** 807–815 (2002).

89. Wunsch, P., Herb, M., Wieland, H., Schiek, U. M. & Zumft, W. G. Requirements for Cu_A and Cu-S center assembly of nitrous oxide reductase deduced from complete periplasmic enzyme maturation in the nondenitrifier *Pseudomonas putida*. *Journal of Bacteriology* **185,** 887–896 (2003).

90. Riester, J, Zumft, W. G. & Kroneck, P. M. Nitrous oxide reductase from *Pseudomonas stutzeri*. Redox properties and spectroscopic characterization of different forms of the multicopper enzyme. *European journal of biochemistry* **178,** 751–762 (1989).

91. Kroneck, P. M., Antholine, W. A., Riester, J. & Zumft, W. G. The nature of the cupric site in nitrous oxide reductase and of Cu_A in cytochrome *c* oxidase. *FEBS Letters* **248,** 212–213 (1989).

92. Dell'Acqua, S., Pauleta, S. R., Monzani, E., Pereira, A. S., Casella, L., Moura, J. J. G. & Moura, I. Electron transfer complex between nitrous oxide reductase and cytochrome c_{552} from *Pseudomonas nautica*: cinetic, nuclear magnetic resonance, and docking studies. *Biochemistry* **47,** 10852–10862 (2008).

93. Wüst, A., Schneider, L., Pomowski, A., Zumft, W. G., Kroneck, P. M. H. & Einsle, O. Nature's way of handling a greenhouse gas: the copper-sulfur cluster of purple nitrous oxide reductase. *Biological chemistry* **393,** 1067–1077 (2012).

94. Wallace, A. C., Laskowski, R. A. & Thornton, J. M. LIGPLOT: a program to generate schematic diagrams of protein-ligand interactions. *Protein engineering* **8,** 127–34 (1995).

95. Dooley, D. M., McGuirl, M. A., Rosenzweig, A. C., Landin, J. A., Scott, R. A., Zumft, W. G., Devlin, F. & Stephens, P. J. Spectroscopic studies of the copper sites in wild-type *Pseudomonas stutzeri* N_2O reductase and in an inactive protein isolated from a mutant deficient in copper-site biosynthesis. *Inorganic Chemistry* **30,** 3006–3011 (1991).

96. Zumft, W. G. Biogenesis of the bacterial respiratory Cu_A, Cu-S enzyme nitrous oxide reductase. *Journal of Molecular Microbiology and Biotechnology* **10,** 154–166 (2005).

97. Chan, J. M., Bollinger, J. A., Grewell, C. L. & Dooley, D. M. Reductively activated nitrous oxide reductase reacts directly with substrate. *Journal of the American Chemical Society* **126,** 3030–3031 (2004).

98. Bar-Nahum, I., Gupta, A. K., Huber, S. M., Ertem, M. Z., Cramer, C. J. & Tolman, W. B. Reduction of nitrous oxide to dinitrogen by a mixed valent tricopper-disulfido cluster. *Journal of the American Chemical Society* **131,** 2812–2814 (2009).

99. Lambden, P. R. & Guest, J. R. Mutants of *Escherichia coli* K12 unable to use fumarate as an anaerobic electron acceptor. *Journal of General Microbiology* **97,** 145–160 (1976).

100. Kiley, P. J. & Beinert, H. Oxygen sensing by the global regulator, FNR: the role of the iron-sulfur cluster. *FEMS microbiology reviews* **22,** 341–52 (1998).

101. Hutchings, M. I. & Spiro, S. The nitric oxide regulated *nor* promoter of *Paracoccus denitrificans*. *Microbiology* **146,** 2635–2641 (2000).

102. Hutchings, M. I., Crack, J. C., Shearer, N., Thompson, B. J., Thomson, A. J. & Spiro, S. Transcription factor FnrP from *Paracoccus denitrificans* contains an iron-sulfur cluster and is activated by anoxia: Identification of essential cysteine residues. *Journal of Bacteriology* **184,** 503–508 (2002).

103. Van Spanning, R. J., De Boer, A. P., Reijnders, W. N., Westerhoff, H. V., Stouthamer, A. H. & Van Der Oost, J. FnrP and NNR of *Paracoccus denitrificans* are both members of the FNR family of transcriptional activators but have distinct roles in respiratory adaptation in response to oxygen limitation. *Molecular microbiology* **23,** 893–907 (1997).

104. Wood, N. J., Alizadeh, T, Bennett, S, Pearce, J, Ferguson, S. J., Richardson, D. J. & Moir, J. W. Maximal expression of membrane-bound nitrate reductase in *Paracoccus* is induced by nitrate via a third FNR-like regulator named NarR. *Journal of bacteriology* **183,** 3606–3613 (2001).

105. Bergaust, L, van Spanning, R. J. M., Frostegard, A & Bakken, L. R. Expression of nitrous oxide reductase in *Paracoccus denitrificans* is regulated by oxygen and nitric oxide through FnrP and NNR. *Microbiology-Sgm* **158,** 826–834 (2012).

106. Wunsch, P & Zumft, W. G. Functional domains of NosR, a novel transmembrane iron-sulfur flavoprotein necessary for nitrous oxide respiration. *Journal of Bacteriology* **187,** 1992–2001 (2005).

107. Zhang, L., Trncik, C., Andrade, S. L. & Einsle, O. The flavinyl transferase ApbE of Pseudomonas stutzeri matures the NosR protein required for nitrous oxide reduction. *Biochimica et Biophysica Acta (BBA) - Bioenergetics* **1858,** 95–102 (2017).

108. Brondijk, T. H. C., Nilavongse, A., Filenko, N., Richardson, D. J. & Cole, J. A. NapGH components of the periplasmic nitrate reductase of *Escherichia coli* K-12: location, topology and physiological roles in quinol oxidation and redox balancing. *The Biochemical journal* **379,** 47–55 (2004).

109. Honisch, U. & Zumft, W. G. Operon structure and regulation of the nos gene region of Pseudomonas stutzeri, encoding an ABC-Type ATPase for maturation of nitrous oxide reductase. *Journal of Bacteriology* **185,** 1895–1902 (2003).

110. Vollack, K. U. & Zumft, W. G. Nitric oxide signaling and transcriptional control of denitrification genes in *Pseudomonas stutzeri*. *Journal of Bacteriology* **183,** 2516–2526 (2001).

111. Cuypers, H, Viebrock-Sambale, A & Zumft, W. G. NosR, a membrane-bound regulatory component necessary for expression of nitrous oxide reductase in denitrifying *Pseudomonas stutzeri*. *Journal of Bacteriology* **174,** 5332–5339 (1992).

112. Wunsch, P., Körner, H., Neese, F., van Spanning, R. J., Kroneck, P. M. & Zumft, W. G. NosX function connects to nitrous oxide (N_2O) reduction by affecting the Cu_Z center of NosZ and its activity *in vivo*. *FEBS Letters* **579,** 4605–4609 (2005).

113. Luque-Almagro, V. M., Lyall, V. J., Ferguson, S. J., Roldán, M. D., Richardson, D. J. & Gates, A. J. Nitrogen oxyanion-dependent dissociation of a two-component complex that regulates bacterial nitrate assimilation. *Journal of Biological Chemistry* **288,** 29692–29702 (2013).

114. Sánchez, C., Mitsui, H. & Minamisawa, K. Regulation of nitrous oxide reductase genes by NasT-mediated transcription antitermination in *Bradyrhizobium diazoefficiens*. *Environmental Microbiology Reports* **9,** 389–396 (2017).

115. Koropatkin, N. M., Pakrasi, H. B. & Smith, T. J. Atomic structure of a nitrate-binding protein crucial for photosynthetic productivity. *Proceedings of the National Academy of Sciences* **103,** 9820–9825 (2006).

116. Shu, C. J. & Zhulin, I. B. ANTAR: an RNA-binding domain in transcription antitermination regulatory proteins. *Trends in biochemical sciences* **27,** 3–5 (2002).

117. Sánchez, C., Itakura, M., Okubo, T., Matsumoto, T., Yoshikawa, H., Gotoh, A., Hidaka, M., Uchida, T. & Minamisawa, K. The nitrate-sensing NasST system regulates nitrous oxide reductase and periplasmic nitrate reductase in *Bradyrhizobium japonicum*. *Environmental Microbiology* **16,** 3263–3274 (2014).

118. Minagawa, N. & Zumft, W. G. Cadmium-copper antagonism in the activation of periplasmic nitrous oxide reductase of copper-deficient cells from *Pseudomonas stutzeri*. *Biology of Metals* **1,** 117–122 (1988).

119. Granger, J. & Ward, B. B. Accumulation of nitrogen oxides in copper-limited cultures of denitrifying bacteria. *Limnology and Oceanography* **48,** 313–318 (2003).

120. Moffett, J. W., Tuit, C. B. & Ward, B. B. Chelator-induced inhibition of copper metalloenzymes in denitrifying bacteria. *Limnology and Oceanography* **57,** 272–280 (2012).

121. Jacobson, F., Pistorius, A., Farkas, D., De Grip, W., Hansson, O., Sjölin, L. & Neutze, R. pH dependence of copper geometry, reduction potential, and nitrite affinity in nitrite reductase. *The Journal of biological chemistry* **282,** 6347–6355 (2007).

122. Felgate, H, Giannopoulos, G, Sullivan, M. J., Gates, A. J., Clarke, T. A., Baggs, E, Rowley, G & Richardson, D. J. The impact of copper, nitrate and carbon status on the emission of nitrous oxide by two species of bacteria with biochemically distinct denitrification pathways. *Environmental Microbiology* **14,** 1788–1800 (2012).

123. Bertani, G. Studies on lysogenesis. The mode of phage liberation by lysogenic *Escherichia coli*. *Journal of bacteriology* **62,** 293–300 (1951).

124. Bertani, G. Lysogeny at mid-twentieth century: P1, P2, and other experimental systems. *Journal of bacteriology* **186,** 595–600 (2004).

125. De Vries, G. E., Harms, N., Hoogendijk, J. & Stouthamer, A. H. Isolation and characterization of *Paracoccus denitrificans* mutants with increased conjugation frequencies and pleiotropic loss of a (nGATCn) DNA-modifying property. *Archives of Microbiology* **152,** 52–57 (1989).

126. Wood, W. B. Host specificity of DNA produced by *Escherichia coli*: bacterial mutations affecting the restriction and modification of DNA. *Journal of molecular biology* **16,** 118–133 (1966).

127. Woodcock, D. M., Crowther, P. J., Doherty, J, Jefferson, S, DeCruz, E, Noyer-Weidner, M, Smith, S. S., Michael, M. Z. & Graham, M. W. Quantitative evaluation of *Escherichia coli* host strains for tolerance to cytosine methylation in plasmid and phage recombinants. *Nucleic acids research* **17,** 3469–3478 (1989).

128. Messing, J. A multipurpose cloning system based on the single-stranded DNA bacteriophage M13. *Recombinant DNA technical bulletin* **3,** 43–48 (1979).

129. Yanisch-Perron, C, Vieira, J & Messing, J. Improved M13 phage cloning vectors and host strains: nucleotide sequences of the M13mp18 and pUC19 vectors. *Gene* **33,** 103–119 (1985).

130. Harms, N., de Vries, G. E., Maurer, K., Veltkamp, E. & Stouthamer, A. H. Isolation and characterization of *Paracoccus denitrificans* mutants with defects in the metabolism of one-carbon compounds. *Journal of Bacteriology* **164,** 1064–1070 (1985).

131. Vishniac, W. & Santer, M. The *thiobacilli*. *Bacteriological reviews* **21,** 195–213 (1957).

132. Robertson, L. A. & Kuenen, J. G. *Thiosphaera pantotropha* gen. nov. sp. nov., a facultatively anaerobic, facultatively autotrophic sulphur bacterium. *Microbiology* **129,** 2847–2855 (1983).

133. Bradford, M. M. A rapid and sensitive method for the quantitation of microgram quantities of protein utilizing the principle of protein-dye binding. *Analytical biochemistry* **72,** 248–254 (1976).

134. Untergasser, A., Nijveen, H., Rao, X., Bisseling, T., Geurts, R. & Leunissen, J. A. Primer3Plus, an enhanced web interface to Primer3. *Nucleic Acids Research* **35,** 71–74 (2007).

135. Kalendar, R., Lee, D. & Schulman, A. H. in *Methods in molecular biology* 271–302 (2014).

136. Rutherford, K, Parkhill, J, Crook, J, Horsnell, T, Rice, P, Rajandream, M. A. & Barrell, B. Artemis: sequence visualization and annotation. *Bioinformatics (Oxford, England)* **16,** 944–945 (2000).

137. Cohen, S. N., Chang, A. C. & Hsu, L. Nonchromosomal antibiotic resistance in bacteria: genetic transformation of *Escherichia coli* by R-factor DNA. *Proceedings of the National Academy of Sciences of the United States of America* **69,** 2110–2114 (1972).

138. Figurski, D. H. & Helinski, D. R. Replication of an origin-containing derivative of plasmid RK2 dependent on a plasmid function provided *in trans*. *Proceedings of the National Academy of Sciences of the United States of America* **76,** 1648–1652 (1979).

139. Johnston, A. W. B., Beynon, J. L., Buchanan-Wollaston, A. V., Setchell, S. M., Hirsch, P. R. & Beringer, J. E. High frequency transfer of nodulating ability between strains and species of *Rhizobium*. *Nature* **276,** 634–636 (1978).

140. Beringer, J. E. & Hopwood, D. A. Chromosomal recombination and mapping in *Rhizobium leguminosarum*. *Nature* **264,** 291–293 (1976).

141. Laemmli, U. K. Cleavage of structural proteins during the assembly of the head of bacteriophage T4. *Nature* **227,** 680–685 (1970).

142. Williams, D. E. & Reisfeld, R. A. Disc electrophoresis in polyacrylamide gels: extension to new conditions of pH and buffer. *Annals of the New York Academy of Sciences* **121,** 373–381 (1964).

143. Schafer-Nielsen, C, Svendsen, P. J. & Rose, C. Separation of macromolecules in isotachophoresis systems involving single or multiple counterions. *Journal of biochemical and biophysical methods* **3,** 97–128 (1980).

144. Kyhse-Andersen, J. Electroblotting of multiple gels: a simple apparatus without buffer tank for rapid transfer of proteins from polyacrylamide to nitrocellulose. *Journal of biochemical and biophysical methods* **10,** 203–209 (1984).

145. Kelley, L. A., Mezulis, S., Yates, C. M., Wass, M. N. & Sternberg, M. J. E. The Phyre2 web portal for protein modeling, prediction and analysis. *Nature Protocols* **10,** 845–858 (2015).

146. Schrödinger, L. *The PyMOL Molecular Graphics System, Version 1.8* 2015.

147. Tett, A. J., Rudder, S. J., Bourdes, A., Karunakaran, R. & Poole, P. S. Regulatable vectors for environmental gene expression in *alphaproteobacteria*. *Applied and Environmental Microbiology* **78,** 7137–7140 (2012).

148. Bond, S. R. & Naus, C. C. RF-Cloning.org: an online tool for the design of restriction-free cloning projects. *Nucleic Acids Research* **40,** 209–213 (2012).

149. Schäfer, a, Tauch, A, Jäger, W, Kalinowski, J, Thierbach, G & Pühler, A. Small mobilizable multi-purpose cloning vectors derived from the *Escherichia coli* plasmids pK18 and pK19: selection of defined deletions in the chromosome of *Corynebacterium glutamicum*. *Gene* **145,** 69–73 (1994).

150. Ghose, S., Tao, Y., Conley, L. & Cecchini, D. Purification of monoclonal antibodies by hydrophobic interaction chromatography under no-salt conditions. *mAbs* **5,** 795–800 (2013).

151. Laue TM, Shah BD, R. T.&.P. S. Computer aided interpretation of analytical sedimentation data for proteins. In the analytical ultracentrifuge in biochemistry and polymer science. *Royal Society of Chemistry,* 90–125 (1992).

152. B, D. *Ultrascan* 2003.

153. Magyar, J. S. & Godwin, H. A. Spectropotentiometric analysis of metal binding to structural zinc-binding sites: accounting quantitatively for pH and metal ion buffering effects. *Analytical Biochemistry* **320,** 39–54 (2003).

154. Xiao, Z. & Wedd, A. G. The challenges of determining metal–protein affinities. *Natural Product Reports* **27,** 768 (2010).

155. Kuzmič, P. Program DYNAFIT for the analysis of enzyme kinetic data: application to HIV proteinase. *Analytical Biochemistry* **237,** 260–273 (1996).

156. *Bioisis: scatter* 2017. <http://www.bioisis.net/scatter> (2017).

157. Petoukhov, M. V., Franke, D., Shkumatov, A. V., Tria, G., Kikhney, A. G., Gajda, M., Gorba, C., Mertens, H. D. T., Konarev, P. V. & Svergun, D. I. New developments in the ATSAS program package for small-angle scattering data analysis. *Journal of Applied Crystallography* **45,** 342–350 (2012).

158. Svergun, D. I. Determination of the regularization parameter in indirect-transform methods using perceptual criteria. *Journal of Applied Crystallography* **25,** 495–503 (1992).

159. Franke, D. & Svergun, D. I. DAMMIF, a program for rapid *ab-initio* shape determination in small-angle scattering. *Journal of Applied Crystallography* **42,** 342–346 (2009).

160. Volkov, V. V. & Svergun, D. I. Uniqueness of *ab initio* shape determination in small-angle scattering. *Journal of Applied Crystallography* **36,** 860–864 (2003).

161. Kozin, M. B. & Svergun, D. I. Automated matching of high- and low-resolution structural models. *Journal of Applied Crystallography* **34,** 33–41 (2001).

162. Rambo, R. P. & Tainer, J. A. Accurate assessment of mass, models and resolution by small-angle scattering. *Nature* **496,** 477–481 (2013).

163. Schneidman-Duhovny, D., Hammel, M., Tainer, J. A. & Sali, A. Accurate SAXS profile computation and its assessment by contrast variation experiments. *Biophysical Journal* **105,** 962–974 (2013).

164. Svergun, D., Barberato, C. & Koch, M. H. J. CRYSOL-a program to evaluate X-ray solution scattering of biological macromolecules from atomic coordinates. *Journal of Applied Crystallography* **28,** 768–773 (1995).

165. Svergun, D. I., Petoukhov, M. V. & Koch, M. H. Determination of domain structure of proteins from X-ray solution scattering. *Biophysical journal* **80,** 2946–53 (2001).

166. Battye, T. G. G., Kontogiannis, L., Johnson, O., Powell, H. R. & Leslie, A. G. W. iMOSFLM: a new graphical interface for diffraction-image processing with MOSFLM. *Acta crystallographica. Section D, Biological crystallography* **67,** 271–281 (2011).

167. Incardona, M.-F., Bourenkov, G. P., Levik, K., Pieritz, R. A., Popov, A. N. & Svensson, O. EDNA : a framework for plugin-based applications applied to X-ray experiment online data analysis. *Journal of Synchrotron Radiation* **16,** 872–879 (2009).

168. Winter, G. XIA2: an expert system for macromolecular crystallography data reduction. *Journal of Applied Crystallography* **43,** 186–190 (2010).

169. Winn, M. D., Ballard, C. C., Cowtan, K. D., Dodson, E. J., Emsley, P., Evans, P. R., Keegan, R. M., Krissinel, E. B., Leslie, A. G. W., McCoy, A., McNicholas, S. J., Murshudov, G. N., Pannu, N. S., Potterton, E. A., Powell, H. R., Read, R. J., Vagin, A. & Wilson, K. S. Overview of the CCP4 suite and current developments. *Acta crystallographica. Section D, Biological crystallography* **67,** 235–242 (2011).

170. Pannu, N. S., Waterreus, W.-J., Skubák, P., Sikharulidze, I., Abrahams, J. P. & de Graaff, R. A. G. Recent advances in the CRANK software suite for experimental phasing. *Acta Crystallographica Section D Biological Crystallography* **67,** 331–337 (2011).

171. Murshudov, G. N., Skubák, P., Lebedev, A. A., Pannu, N. S., Steiner, R. A., Nicholls, R. A., Winn, M. D., Long, F. & Vagin, A. A. REFMAC5 for the refinement of macromolecular crystal structures. *Acta crystallographica. Section D, Biological crystallography* **67,** 355–367 (2011).

172. Vagin, A. & Lebedev, A. MoRDa, an automatic molecular replacement pipeline. *Acta Crystallographica Section A Foundations and Advances* **71,** 19 (2015).

173. Buggy, J & Bauer, C. E. Cloning and characterization of *senC*, a gene involved in both aerobic respiration and photosynthesis gene expression in *Rhodobacter capsulatus*. *Journal of bacteriology* **177,** 6958–6965 (1995).

174. Eraso, J. M. & Kaplan, S. Oxygen-insensitive synthesis of the photosynthetic membranes of *Rhodobacter sphaeroides*: a mutant histidine kinase. *Journal of bacteriology* **177,** 2695–2706 (1995).

175. Mattatall, N. R., Jazairi, J & Hill, B. C. Characterization of YpmQ, an accessory protein required for the expression of cytochrome *c* oxidase in *Bacillus subtilis*. *The Journal of biological chemistry* **275,** 28802–28809 (2000).

176. Chinenov, Y. V. Cytochrome *c* oxidase assembly factors with a thioredoxin fold are conserved among prokaryotes and eukaryotes. *Journal of molecular medicine* **78,** 239–242 (2000).

177. Lucia, B., Bertini, I., Cavallaro, G. & Rosato, A. The functions of Sco proteins from genome-based analysis. *Proteome* **6,** 1568–1579 (2007).

178. Arnesano, F., Banci, L., Bertini, I. & Martinelli, M. Ortholog search of proteins involved in copper delivery to cytochrome *c* oxidase and functional analysis of paralogs and gene neighbors by genomic context. *Proteome* **4,** 63–70 (2005).

179. Porcelli, D., Oliva, M., Duchi, S., Latorre, D., Cavaliere, V., Barsanti, P., Villani, G., Gargiulo, G. & Caggese, C. Genetic, functional and evolutionary characterization of *scox*, the *Drosophila melanogaster* ortholog of the human SCO1 gene. *Mitochondrion* **10,** 433–448 (2010).

180. Banci, L, Bertini, I, Cavallaro, G & Ciofi-Baffoni, S. Seeking the determinants of the elusive functions of Sco proteins. *FEBS Journal* **278,** 2244–2262 (2011).

181. Martin, J. L. Thioredoxin: a fold for all reasons. *Structure* **3,** 245–250 (1995).

182. Banci, L., Bertini, I., Ciofi-Baffoni, S., Kozyreva, T., Mori, M. & Wang, S. Sco proteins are involved in electron transfer processes. *Journal of biological inorganic chemistry* **16,** 391–403 (2011).

183. Badrick, A. C., Hamilton, A. J., Bernhardt, P. V., Jones, C. E., Kappler, U., Jennings, M. P. & McEwan, A. G. PrrC, a Sco homologue from *Rhodobacter sphaeroides*, possesses thiol-disulfide oxidoreductase activity. *FEBS Letters* **581,** 4663–4667 (2007).

184. Williams, J. C., Sue, C., Banting, G. S., Yang, H., Glerum, D. M., Hendrickson, W. A. & Schon, E. A. Crystal structure of human SCO1: implications for redox signaling by a mitochondrial cytochrome *c* oxidase "assembly" protein. *The Journal of biological chemistry* **280,** 15202–15211 (2005).

185. Blundell, K. L.I. M., Wilson, M. T., Svistunenko, D. A., Vijgenboom, E. & Worrall, J. A. R. Morphological development and cytochrome *c* oxidase activity in *Streptomyces lividans* are dependent on the action of a copper bound Sco protein. *Open Biology* **3** (2013).

186. Banci, L., Bertini, I., Calderone, V., Ciofi-Baffoni, S., Mangani, S., Martinelli, M., Palumaa, P. & Wang, S. A hint for the function of human Sco1 from different structures. *Proceedings of the National Academy of Sciences of the United States of America* **103,** 8595–8600 (2006).

187. Banci, L., Bertini, I., Ciofi-Baffoni, S., Gerothanassis, I. P., Leontari, I., Martinelli, M., Wang, S., Yaono, R., Yoshikawa, S. & Robinson, B. A structural characterization of human SCO2. *Structure* **15,** 1132–1140 (2007).

188. Edgar, R. C. MUSCLE: multiple sequence alignment with high accuracy and high throughput. *Nucleic acids research* **32,** 1792–1797 (2004).

189. Nittis, T., George, G. N. & Winge, D. R. Yeast Sco1, a protein essential for cytochrome *c* oxidase function is a Cu(I)-binding protein. *Journal of Biological Chemistry* **276,** 42520–42526 (2001).

190. Rentzsch, A, Krummeck-Weiss, G, Hofer, A, Bartuschka, A, Ostermann, K & Rödel, G. Mitochondrial copper metabolism in yeast: mutational analysis of Sco1p involved in the biogenesis of cytochrome *c* oxidase. *Current genetics* **35,** 103–108 (1999).

191. Leary, S. C., Cobine, P. A., Kaufman, B. A., Guercin, G.-H., Mattman, A., Palaty, J., Lockitch, G., Winge, D. R., Rustin, P., Horvath, R. & Shoubridge, E. A. The human cytochrome *c* oxidase assembly factors SCO1 and SCO2 have regulatory roles in the maintenance of cellular copper homeostasis. *Cell metabolism* **5,** 9–20 (2007).

192. Matoba, S., Kang, J.-G., Patino, W. D., Wragg, A., Boehm, M., Gavrilova, O., Hurley, P. J., Bunz, F. & Hwang, P. M. p53 regulates mitochondrial respiration. *Science* **312,** 5780 (2006).

193. Waterhouse, A. M., Procter, J. B., Martin, D. M. A., Clamp, M. & Barton, G. J. Jalview Version 2-a multiple sequence alignment editor and analysis workbench. *Bioinformatics* **25,** 1189–1191 (2009).

194. Pedro Reche. *Sequence Identity And Similarity (SIAS)* <http://imed.med.ucm.es/Tools/sias.html> (2017).

195. Dorman, C. J. H-NS: a universal regulator for a dynamic genome. *Nature Reviews Microbiology* **2,** 391–400 (2004).

196. Elsen, S., Swem, L. R., Swem, D. L. & Bauer, C. E. RegB/RegA, a highly conserved redox-responding global two-component regulatory system. *Microbiology and Molecular Biology Reviews* **68,** 263–279 (2004).

197. Swem, L. R., Kraft, B. J., Swem, D. L., Setterdahl, A. T., Masuda, S., Knaff, D. B., Zaleski, J. M. & Bauer, C. E. Signal transduction by the global regulator RegB is mediated by a redox-active cysteine. *The EMBO journal* **22,** 4699–4708 (2003).

198. Dash, B. P., Alles, M., Bundschuh, F. A., Richter, O.-M. & Ludwig, B. Protein chaperones mediating copper insertion into the Cu_A site of the aa_3-type cytochrome *c* oxidase of *Paracoccus denitrificans*. *Biochimica et Biophysica Acta (BBA) - Bioenergetics* **1847,** 202–211 (2015).

199. Kall, L., Krogh, A. & Sonnhammer, E. L. Advantages of combined transmembrane topology and signal peptide prediction–the Phobius web server. *Nucleic Acids Research* **35,** 429–432 (2007).

200. Petersen, T. N., Brunak, S., von Heijne, G. & Nielsen, H. SignalP 4.0: discriminating signal peptides from transmembrane regions. *Nature Methods* **8,** 785–786 (2011).

201. Andruzzi, L., Nakano, M., Nilges, M. J. & Blackburn, N. J. Spectroscopic studies of metal binding and metal selectivity in *Bacillus subtilis* BSco, a homologue of the yeast mitochondrial protein Sco1p. *Journal of the American Chemical Society,* 16548–16558 (2005).

202. Siluvai, G. S., Nakano, M., Mayfield, M. & Blackburn, N. J. The essential role of the Cu(II) state of Sco in the maturation of the Cu_A center of cytochrome oxidase: evidence from H135Met and H135SeM variants of the *Bacillus subtilis* Sco. *Journal of biological inorganic chemistry* **16,** 285–297 (2011).

203. Banci, L., Bertini, I., Ciofi-Baffoni, S., Kozyreva, T., Zovo, K. & Palumaa, P. Affinity gradients drive copper to cellular destinations. *Nature* **465,** 645–648 (2010).

204. Ford, P. C. & Vogler, A. Photochemical and photophysical properties of tetranuclear and hexanuclear clusters of metals with d^{10} and s^2 electronic configurations. *Accounts of Chemical Research* **26,** 220–226 (1993).

205. Pountney, D. L., Schauwecker, I, Zarn, J & Vasák, M. Formation of mammalian Cu_8-metallothionein in vitro: evidence for the existence of two $Cu(I)_4$-thiolate clusters. *Biochemistry* **33,** 9699–9705 (1994).

206. Lakowicz, J. R. *Principles of fluorescence spectroscopy* 954 (Springer, 2006).

207. Vivian, J. T. & Callis, P. R. Mechanisms of tryptophan fluorescence shifts in proteins. *Biophysical Journal* **80,** 2093–2109 (2001).

208. Mertens, H. D. & Svergun, D. I. Structural characterization of proteins and complexes using small-angle X-ray solution scattering. *Journal of Structural Biology* **172,** 128–141 (2010).

209. Peng, M., Cascio, D. & Egea, P. F. Crystal structure and solution characterization of the thioredoxin-2 from *Plasmodium falciparum*, a constituent of an essential parasitic protein export complex. *Biochemical and Biophysical Research Communications* **456,** 403–409 (2015).

210. Svergun, D. Restoring low resolution structure of biological macromolecules from solution scattering using simulated annealing. *Biophysical Journal* **76,** 2879–2886 (1999).

211. Frangipani, E. & Haas, D. Copper acquisition by the SenC protein regulates aerobic respiration in *Pseudomonas aeruginosa* PAO1. *FEMS Microbiology Letters* **298,** 234–240 (2009).

212. Lohmeyer, E., Schröder, S., Pawlik, G., Trasnea, P.-I., Peters, A., Daldal, F. & Koch, H.-G. The ScoI homologue SenC is a copper binding protein that interacts directly with the *cbb_3* type cytochrome oxidase in *Rhodobacter capsulatus*. *Biochimica et biophysica acta* **1817,** 2005–2015 (2012).

213. Horng, Y.-C., Leary, S. C., Cobine, P. A., Young, F. B. J., George, G. N., Shoubridge, E. A. & Winge, D. R. Human Sco1 and Sco2 function as copper-binding proteins. *The Journal of biological chemistry* **280,** 34113–34122 (2005).

214. Banci, L., Bertini, I., Ciofi-Baffoni, S., Leontari, I., Martinelli, M., Palumaa, P., Sillard, R. & Wang, S. Human Sco1 functional studies and pathological implications of the P174L mutant. *Proceedings of the National Academy of Sciences of the United States of America* **104,** 15–20 (2007).

215. Davidson, D. E. & Hill, B. C. Stability of oxidized, reduced and copper bound forms of *Bacillus subtilis* Sco. *Biochimica et biophysica acta* **1794,** 275–281 (2009).

216. Blundell, K. L.I. M., Hough, M. A., Vijgenboom, E. & Worrall, J. A. R. Structural and mechanistic insights into an extracytoplasmic copper trafficking pathway in *Streptomyces lividans*. *Biochemical Journal* **459,** 525–538 (2014).

217. Rigby, K., Cobine, P. A., Khalimonchuk, O. & Winge, D. R. Mapping the functional interaction of Sco1 and Cox2 in cytochrome oxidase biogenesis. *The Journal of biological chemistry* **283,** 15015–15022 (2008).

218. Bühler, D., Rossmann, R., Landolt, S., Balsiger, S., Fischer, H.-M. & Hennecke, H. Disparate pathways for the biogenesis of cytochrome oxidases in *Bradyrhizobium japonicum*. *The Journal of biological chemistry* **285,** 15704–15713 (2010).

219. Beers, J., Glerum, D. M. & Tzagoloff, A. Purification and characterization of yeast Sco1p, a mitochondrial copper protein. *The Journal of biological chemistry* **277,** 22185–22190 (2002).

220. Siluvai, G. S., Mayfield, M., Nilges, M. J., DeBeer George, S. & Blackburn, N. J. Anatomy of a red copper center: spectroscopic identification and reactivity of the copper centers of *Bacillus subtilis* Sco and its cys-to-ala variants. *Journal of the American Chemical Society* **132,** 5215–5226 (2010).

221. Holm, R. H., Kennepohl, P. & Solomon, E. I. Structural and functional aspects of metal sites in biology. *Chemical reviews* **96,** 2239–2314 (1996).

222. Lieberman, R. L., Arciero, D. M., Hooper, A. B. & Rosenzweig, A. C. Crystal structure of a novel red copper protein from *Nitrosomonas europaea*. *Biochemistry* **40,** 5674–5681 (2001).

223. Ye, Q., Imriskova-Sosova, I., Bruce C. Hill & Jia, Z. Identification of a disulfide switch in BsSco, a member of the Sco family of cytochrome *c* oxidase assembly proteins. *Biochemistry* **44,** 2934–2942 (2005).

224. Balatri, E., Banci, L., Bertini, I., Cantini, F. & Ciofi-Baffoni, S. Solution structure of Sco1: a thioredoxin-like protein involved in cytochrome *c* oxidase assembly. *Structure,* 1431–1443 (2003).

225. McEwan, A. G., Lewin, A., Davy, S. L., Boetzel, R., Leech, A., Walker, D., Wood, T. & Moore, G. R. PrrC from *Rhodobacter sphaeroides*, a homologue of eukaryotic Sco proteins, is a copper-binding protein and may have a thiol-disulfide oxidoreductase activity. *FEBS Letters* **518,** 10–16 (2002).

226. Singleton, C., Banci, L., Ciofi-Baffoni, S., Tenori, L., Kihlken, M. A., Boetzel, R. & Le Brun, N. E. Structure and Cu(I)-binding properties of the N-terminal soluble domains of *Bacillus subtilis* CopA. *The Biochemical journal* **411,** 571–579 (2008).

227. Kihlken, M. A., Leech, A. P. & Le Brun, N. E. Copper-mediated dimerization of CopZ, a predicted copper chaperone from *Bacillus subtilis. The Biochemical journal* **368,** 729–739 (2002).

228. Lode, A., Kuschel, M., Paret, C. & Rödel, G. Mitochondrial copper metabolism in yeast: interaction between Sco1p and Cox2p. *FEBS Letters* **485,** 19–24 (2000).

229. Leary, S. C., Kaufman, B. A., Pellecchia, G., Guercin, G.-H., Mattman, A., Jaksch, M. & Shoubridge, E. A. Human SCO1 and SCO2 have independent, cooperative functions in copper delivery to cytochrome *c* oxidase. *Human Molecular Genetics* **13,** 1839–1848 (2004).

230. Imriskova-Sosova, I., Diann Andrews, Katherine Yam, David Davidson, Yachnin, B. & Hill, B. C. Characterization of the redox and metal binding activity of BsSco, a protein implicated in the assembly of cytochrome *c* oxidase. *Biochemistry,* 16949–16956 (2005).

231. Letunic, I. & Bork, P. Interactive Tree Of Life (iTOL): an online tool for phylogenetic tree display and annotation. *Bioinformatics* **23,** 127–128 (2007).

232. Bagos, P. G., Nikolaou, E. P., Liakopoulos, T. D. & Tsirigos, K. D. Combined prediction of Tat and Sec signal peptides with hidden Markov models. *Bioinformatics* **26,** 2811–2817 (2010).

233. Cha, J. S. & Cooksey, D. A. Copper hypersensitivity and uptake in *Pseudomonas syringae* containing cloned components of the copper resistance operon. *Applied and environmental microbiology* **59,** 1671–1674 (1993).

234. Knapp, S., Kardinahl, S., Hellgren, N., Tibbelin, G., Schafer, G. & Ladenstein, R. Refined crystal structure of a superoxide dismutase from the hyperthermophilic archaeon *Sulfolobus acidocaldarius* at 2.2 Å resolution. *Journal of Molecular Biology* **285,** 689–702 (1999).

235. Lo, Y.-C., Lin, S.-C., Shaw, J.-F. & Liaw, Y.-C. Crystal structure of *Escherichia coli* thioesterase I/protease I/lysophospholipase L1: consensus sequence blocks constitute the catalytic center of SGNH-hydrolases through a conserved hydrogen bond network. *Journal of molecular biology* **330,** 539–551 (2003).

236. Allen, G. S., Wu, C.-C., Cardozo, T. & Stokes, D. L. The architecture of CopA from *Archeaoglobus fulgidus* studied by cryo-electron microscopy and computational docking. *Structure* **19,** 1219–1232 (2011).

237. Hirooka, K., Edahiro, T., Kimura, K. & Fujita, Y. Direct and indirect regulation of the *ycnKJI* operon involved in copper uptake through two transcriptional repressors, YcnK and CsoR, in *Bacillus subtilis*. *Journal of bacteriology* **194,** 5675–5687 (2012).

238. Karlsen, O. A., Lillehaug, J. R. & Jensen, H. B. The presence of multiple *c*-type cytochromes at the surface of the methanotrophic bacterium *Methylococcus capsulatus* (Bath) is regulated by copper. *Molecular Microbiology* **70,** 15–26 (2008).

239. Karlsen, O. A., Larsen, Ø. & Jensen, H. B. The copper responding surfaceome of Methylococccus capsulatus Bath. *FEMS Microbiology Letters* **323,** 97–104 (2011).

240. Serventi, F., Youard, Z. A., Murset, V., Huwiler, S., Bühler, D., Richter, M., Luchsinger, R., Fischer, H.-M., Brogioli, R., Niederer, M. & Hennecke, H. Copper starvation-inducible protein for cytochrome oxidase biogenesis in *Bradyrhizobium japonicum*. *The Journal of biological chemistry* **287,** 38812–38823 (2012).

241. Akanuma, G., Nanamiya, H., Mouri, Y., Ishizuka, M. & Ohnishi, Y. Proteomic analysis of the *Streptomyces griseus* ribosomal fraction. *Bioscience, Biotechnology, and Biochemistry* **76,** 2267–2274 (2012).

242. McGuirl, M. A., Bollinger, J. A., Cosper, N., Scott, R. A. & Dooley, D. M. Expression, purification, and characterization of NosL, a novel Cu(I) protein of the nitrous oxide reductase (*nos*) gene cluster. *Journal of biological inorganic chemistry* **6,** 189–195 (2001).

243. Eddy, S. R. Profile hidden Markov models. *Bioinformatics* **14,** 755–763 (1998).

244. Finn, R. D., Clements, J., Arndt, W., Miller, B. L., Wheeler, T. J., Schreiber, F., Bateman, A. & Eddy, S. R. HMMER web server: 2015 update. *Nucleic Acids Research* **43,** 30–38 (2015).

245. Broberg, A., Menkis, A. & Vasiliauskas, R. Kutznerides 1-4, depsipeptides from the actinomycete *Kutzneria sp.* 744 inhabiting mycorrhizal roots of *Picea abies* seedlings. *Journal of Natural Products* **69,** 97–102 (2006).

246. Von Mering, C., Jensen, L. J., Snel, B., Hooper, S. D., Krupp, M., Foglierini, M., Jouffre, N., Huynen, M. A. & Bork, P. STRING: known and predicted protein-protein associations, integrated and transferred across organisms. *Nucleic Acids Research* **33,** 433–437 (2004).

247. Robinson, N. J. & Winge, D. R. Copper metallochaperones. *Annual review of biochemistry* **79,** 537–562 (2010).

248. Lawton, T. J., Kenney, G. E., Hurley, J. D. & Rosenzweig, A. C. The CopC family: structural and bioinformatic insights into a diverse group of periplasmic copper binding proteins. *Biochemistry* **55,** 2278–2290 (2016).

249. Zhang, L., Koay, M., Maher, M. J., Xiao, Z. & Wedd, A. G. Intermolecular transfer of copper ions from the CopC protein of *Pseudomonas syringae*. Crystal structures of fully loaded $Cu^{I}Cu^{II}$ forms. *Journal of the American Chemical Society* **128,** 5834–5850 (2006).

250. Casella, L. & Gullotti, M. Coordination modes of histidine. *Journal of Inorganic Biochemistry* **18,** 19–31 (1983).

251. Sarkar, B & Wigfield, Y. The structure of copper(II)-histidine chelate. The question of the involvement of the imidazole group. *The Journal of biological chemistry* **242,** 5572–5577 (1967).

252. Velázquez Campoy, A. & Freire, E. ITC in the post-genomic era. . . ? Priceless. *Biophysical Chemistry* **115,** 115–124 (2005).

253. Bonanno, J., Freeman, J, Bain, K., Hu, S, Romero, R, Wasserman, S, Sauder, J., Burley, S. & Almo, S. Crystal structure of an uncharacterized protein from *Nocardia farcinica* reveals an immunoglobulin-like fold. *To be Published.*

254. Badarau, A. & Dennison, C. Copper trafficking mechanism of CXXC-containing domains: insight from the pH-dependence of their Cu(I) affinities. *Journal of the American Chemical Society* **133,** 2983–2988 (2011).

255. Changela, A., Chen, K., Xue, Y., Holschen, J., Outten, C. E., O'Halloran, T. V. & Mondragón, A. Molecular basis of metal-ion selectivity and zeptomolar sensitivity by CueR. *Science (New York, N.Y.)* **301,** 1383–1387 (2003).

256. *Protein Structure Initiative (program ended 7/1/2015) - National Institute of General Medical Sciences* <https://www.nigms.nih.gov/Research/specificareas/PSI/Pages/default.aspx> (2017).

257. Sillitoe, I., Lewis, T. E., Cuff, A., Das, S., Ashford, P., Dawson, N. L., Furnham, N., Laskowski, R. A., Lee, D., Lees, J. G., Lehtinen, S., Studer, R. A., Thornton, J. & Orengo, C. A. CATH: comprehensive structural and functional annotations for genome sequences. *Nucleic Acids Research* **43,** 376–381 (2015).

258. De Beer, T. A. P., Berka, K., Thornton, J. M. & Laskowski, R. A. PDBsum additions. *Nucleic Acids Research* **42,** 292–296 (2014).

259. Weiss, M. S. Global indicators of X-ray data quality. *Journal of Applied Crystallography* **34,** 130–135 (2001).

260. Karplus, P. A. & Diederichs, K. Linking crystallographic model and data quality. *Science* **336,** 1030–1033 (2012).

261. Wlodawer, A., Minor, W., Dauter, Z. & Jaskolski, M. Protein crystallography for non-crystallographers, or how to get the best (but not more) from published macromolecular structures. *FEBS Journal* **275,** 1–21 (2008).

262. Krissinel, E. & Henrick, K. Inference of macromolecular assemblies from crystalline state. *Journal of Molecular Biology* **372,** 774–797 (2007).

263. Bork, P., Holm, L. & Sander, C. The immunoglobulin fold. *Journal of Molecular Biology* **242,** 309–320 (1994).

264. Zheng, H., Chordia, M. D., Cooper, D. R., Chruszcz, M., Muller, P., Sheldrick, G. M. & Minor, W. Validation of metal-binding sites in macromolecular structures with the CheckMyMetal web server. *Nature Protocols* **9,** 156–170 (2013).

265. Brown, I. D. Recent developments in the methods and applications of the bond valence model. *Chemical reviews* **109,** 6858–6919 (2009).

266. Müller, P., Köpke, S. & Sheldrick, G. M. Is the bond-valence method able to identify metal atoms in protein structures? *Acta crystallographica. Section D, Biological crystallography* **59,** 32–37 (2003).

267. Harding, M. M., Nowicki, M. W. & Walkinshaw, M. D. Metals in protein structures: a review of their principal features. *Crystallography Reviews* **16,** 247–302 (2010).

268. Kuppuraj, G., Dudev, M. & Lim, C. Factors governing metal-ligand distances and coordination geometries of metal complexes. *The Journal of Physical Chemistry B* **113,** 2952–2960 (2009).

269. Zheng, H., Chruszcz, M., Lasota, P., Lebioda, L. & Minor, W. Data mining of metal ion environments present in protein structures. *Journal of inorganic biochemistry* **102,** 1765–1776 (2008).

270. Quinlan, R. J., Sweeney, M. D., Lo Leggio, L., Otten, H., Poulsen, J.-C. N., Johansen, K. S., Krogh, K. B.R. M., Jørgensen, C. I., Tovborg, M., Anthonsen, A., Tryfona, T., Walter, C. P., Dupree, P., Xu, F., Davies, G. J. & Walton, P. H. Insights into the oxidative degradation of cellulose by a copper metalloenzyme that exploits biomass components. *Proceedings of the National Academy of Sciences of the United States of America* **108,** 15079–15084 (2011).

271. Holm, L. & Rosenström, P. Dali server: conservation mapping in 3D. *Nucleic Acids Research* **38,** 545–549 (2010).

272. Berman, H. M., Westbrook, J., Feng, Z., Gilliland, G., Bhat, T. N., Weissig, H., Shindyalov, I. N. & Bourne, P. E. The Protein Data Bank. *Nucleic Acids Research* **28,** 235–242 (2000).

273. Frandsen, K. E. H. & Lo Leggio, L. Lytic polysaccharide monooxygenases: a crystallographer's view on a new class of biomass-degrading enzymes. *IUCrJ* **3,** 448–467 (2016).

274. Velazquez-Campoy, A. & Freire, E. Isothermal titration calorimetry to determine association constants for high-affinity ligands. *Nature Protocols* **1,** 186–191 (2006).

275. Young, T. R., Wijekoon, C. J. K., Spyrou, B., Donnelly, P. S., Wedd, A. G., Xiao, Z., O'Halloran, T. V., Faller, P., Dorlet, P., Foster, A. W. & Robinson, N. J. A set of robust fluorescent peptide probes for quantification of Cu(II) binding affinities in the micromolar to femtomolar range. *Metallomics* **7,** 567–578 (2015).

276. Wijekoon, C. J. K., Young, T. R., Wedd, A. G. & Xiao, Z. CopC protein from *Pseudomonas fluorescens* SBW25 features a conserved novel high-affinity Cu(II) binding site. *Inorganic Chemistry* **54,** 2950–2959 (2015).

277. Hemsworth, G. R., Henrissat, B., Davies, G. J. & Walton, P. H. Discovery and characterization of a new family of lytic polysaccharide monooxygenases. *Nature Chemical Biology* **10,** 122–126 (2013).

278. Lo Leggio, L., Simmons, T. J., Poulsen, J.-C. N., Frandsen, K. E. H., Hemsworth, G. R., Stringer, M. A., von Freiesleben, P., Tovborg, M., Johansen, K. S., De Maria, L., Harris, P. V., Soong, C.-L., Dupree, P., Tryfona, T., Lenfant, N., Henrissat, B., Davies, G. J. & Walton, P. H. Structure and boosting activity of a starch-degrading lytic polysaccharide monooxygenase. *Nature Communications* **6,** 5961 (2015).

279. Hemsworth, G. R., Taylor, E. J., Kim, R. Q., Gregory, R. C., Lewis, S. J., Turkenburg, J. P., Parkin, A., Davies, G. J. & Walton, P. H. The copper active site of CBM33 polysaccharide oxygenases. *Journal of the American Chemical Society* **135,** 6069–6077 (2013).

280. Aachmann, F. L., Sorlie, M., Skjak-Braek, G., Eijsink, V. G. H. & Vaaje-Kolstad, G. NMR structure of a lytic polysaccharide monooxygenase provides insight into copper binding, protein dynamics, and substrate interactions. *Proceedings of the National Academy of Sciences* **109,** 18779–18784 (2012).

281. Forsberg, Z., Mackenzie, A. K., Sorlie, M., Rohr, A. K., Helland, R., Arvai, A. S., Vaaje-Kolstad, G. & Eijsink, V. G. H. Structural and functional characterization of a conserved pair of bacterial cellulose-oxidizing lytic polysaccharide monooxygenases. *Proceedings of the National Academy of Sciences* **111,** 8446–8451 (2014).

282. Chaplin, A. K., Wilson, M. T., Hough, M. A., Svistunenko, D. A., Hemsworth, G. R., Walton, P. H., Vijgenboom, E. & Worrall, J. A. R. Heterogeneity in the histidine-brace copper coordination sphere in auxiliary activity family 10 (AA10) lytic polysaccharide monooxygenases. *The Journal of biological chemistry* **291,** 12838–12850 (2016).

283. Jensen, B. B. & Burris, R. H. N_2O as a substrate and as a competitive inhibitor of nitrogenase. *Biochemistry* **25,** 1083–1088 (1986).

284. Christiansen, J., Seefeldt, L. C. & Dean, D. R. Competitive substrate and inhibitor interactions at the physiologically relevant active site of nitrogenase. *Journal of Biological Chemistry* **275,** 36104–36107 (2000).

285. Fernandes, A. T., Damas, J. M., Todorovic, S., Huber, R., Baratto, M. C., Pogni, R., Soares, C. M. & Martins, L. O. The multicopper oxidase from the archaeon *Pyrobaculum aerophilum* shows nitrous oxide reductase activity. *FEBS Journal* **277,** 3176–3189 (2010).

286. Tolman, W. B. Binding and activation of N_2O at transition-metal centers: recent mechanistic insights. *Angewandte Chemie International Edition* **49,** 1018–1024 (2010).

287. Jones, C. M., Graf, D. R., Bru, D., Philippot, L. & Hallin, S. The unaccounted yet abundant nitrous oxide-reducing microbial community: a potential nitrous oxide sink. *The ISME Journal* **7,** 417–426 (2013).

288. Arai, H., Mizutani, M. & Igarashi, Y. Transcriptional regulation of the *nos* genes for nitrous oxide reductase in *Pseudomonas aeruginosa*. *Microbiology (Reading, England)* **149,** 29–36 (2003).

289. Cuypers, H., Jürgen, B. & Zumft, W. G. Multiple *nosZ* promoters and anaerobic expression of nos genes necessary for *Pseudomonas stutzeri* nitrous oxide reductase and assembly of its copper centers. *Biochimica et Biophysica Acta (BBA) - Gene Structure and Expression* **1264,** 183–190 (1995).

290. Ciccarelli, F. D., Copley, R. R., Doerks, T., Russell, R. B. & Bork, P. CASH–a beta-helix domain widespread among carbohydrate-binding proteins. *Trends in Biochemical Sciences* **27,** 59–62 (2002).

291. Dreusch, A, Riester, J, Kroneck, P. M. & Zumft, W. G. Mutation of the conserved Cys165 outside of the Cu_A domain destabilizes nitrous oxide reductase but maintains its catalytic activity. Evidence for disulfide bridges and a putative protein disulfide isomerase gene. *European Journal of Biochemistry* **237,** 447–453 (1996).

292. Taubner, L. M., McGuirl, M. A., Dooley, D. M. & Copié, V. Structural studies of apo NosL, an accessory protein of the nitrous oxide reductase system: insights from structural homology with MerB, a mercury resistance protein. *Biochemistry* **45,** 12240–12252 (2006).

293. Lello, P. D., Benison, G. C., Valafar, H., Pitts, K. E., Summers, A. O., Legault, P. & Omichinski, J. G. NMR structural studies reveal a novel protein fold for MerB, the organomercurial lyase involved in the bacterial mercury resistance system. *Biochemistry* **43,** 8322–8332 (2004).

294. Schmidt, T. G. & Skerra, A. The Strep-tag system for one-step purification and high-affinity detection or capturing of proteins. *Nature Protocols* **2,** 1528–1535 (2007).

295. Farrar, J. A., Neese, F., Lappalainen, P., Kroneck, P. M. H., Saraste, M., Zumft, W. G. & Thomson, A. J. The electronic structure of Cu_A: a novel mixed-valence dinuclear copper electron-transfer center. *Journal of the American Chemical Society* **118,** 11501–11514 (1996).

296. Savelieff, M. G., Wilson, T. D., Elias, Y., Nilges, M. J., Garner, D. K. & Lu, Y. Experimental evidence for a link among cupredoxins: red, blue, and purple copper transformations in nitrous oxide reductase. *Proceedings of the National Academy of Sciences of the United States of America* **105,** 7919–7924 (2008).

297. Fujita, K., Chan, J. M., Bollinger, J. A., Alvarez, M. L. & Dooley, D. M. Anaerobic purification, characterization and preliminary mechanistic study of recombinant nitrous oxide reductase from *Achromobacter cycloclastes*. *Journal of Inorganic Biochemistry* **101,** 1836–1844 (2007).

298. Tzagoloff, A, Nobrega, M, Gorman, N & Sinclair, P. On the functions of the yeast COX10 and COX11 gene products. *Biochemistry and molecular biology international* **31,** 593–598 (1993).

299. Bundschuh, F. A., Hannappel, A., Anderka, O. & Ludwig, B. Surf1, associated with Leigh syndrome in humans, is a heme-binding protein in bacterial

oxidase biogenesis. *The Journal of biological chemistry* **284,** 25735–25741 (2009).

300. Bareth, B., Dennerlein, S., Mick, D. U., Nikolov, M., Urlaub, H. & Rehling, P. The heme *a* synthase Cox15 associates with cytochrome *c* oxidase assembly intermediates during Cox1 maturation. *Molecular and cellular biology* **33,** 4128–4137 (2013).

301. Trasnea, P.-I., Utz, M., Khalfaoui-Hassani, B., Lagies, S., Daldal, F. & Koch, H.-G. Cooperation between two periplasmic copper chaperones is required for full activity of the cbb_3-type cytochrome *c* oxidase and copper homeostasis in *Rhodobacter capsulatus*. *Molecular Microbiology* **100,** 345–361 (2016).

302. Thompson, A. K., Gray, J., Liu, A. & Hosler, J. P. The roles of Rhodobacter sphaeroides copper chaperones PCu_AC and Sco (PrrC) in the assembly of the copper centers of the aa_3-type and the cbb_3-type cytochrome *c* oxidases. *Biochimica et Biophysica Acta - Bioenergetics* **1817,** 955–964 (2012).

303. Page, M. D. & Ferguson, S. J. Paracoccus denitrificans CcmG is a periplasmic protein-disulphide oxidoreductase required for c- and aa3-type cytochrome biogenesis; evidence for a reductase role in vivo. *Molecular microbiology* **24,** 977–990 (1997).

304. Alloway, B. J. *Micronutrient deficiencies in global crop production* (ed Alloway, B. J.) 369 (Springer Netherlands, Dordrecht, 2008).

305. Tóth, G., Hermann, T., Szatmári, G. & Pásztor, L. Maps of heavy metals in the soils of the European Union and proposed priority areas for detailed assessment. *Science of The Total Environment* **565,** 1054–1062 (2016).

306. Basiliko, N. & Yavitt, J. B. Influence of Ni, Co, Fe, and Na additions on methane production in Sphagnum-dominated Northern American peatlands. *Biogeochemistry* **52,** 133–153 (2001).

307. Bragazza, L. Heavy metals in bog waters: An alternative way to assess atmospheric precipitation quality? *Global and Planetary Change* **53,** 290–298 (2006).

308. Shaw, T. J., Gieskes, J. M. & Jahnke, R. A. Early diagenesis in differing depositional environments: The response of transition metals in pore water. *Geochimica et Cosmochimica Acta* **54,** 1233–1246 (1990).

309. Haraldsson, C. & Westerlund, S. Trace metals in the water columns of the Black Sea and Framvaren Fjord. *Marine Chemistry* **23,** 417–424 (1988).

310. Emerson, S. R. & Huested, S. S. Ocean anoxia and the concentrations of molybdenum and vanadium in seawater. *Marine Chemistry* **34,** 177–196 (1991).

311. Kremling, K. The behavior of Zn, Cd, Cu, Ni, Co, Fe, and Mn in anoxic baltic waters. *Marine Chemistry* **13,** 87–108 (1983).

312. Bruland, K. W. Oceanographic distributions of cadmium, zinc, nickel, and copper in the North Pacific. *Earth and Planetary Science Letters* **47,** 176–198 (1980).

313. Collier, R. W. Molybdenum in the Northeast Pacific Ocean. *Limnology and Oceanography* **30,** 1351–1354 (1985).

314. Johnson, K. S., Gordon, R. M. & Coale, K. H. What controls dissolved iron concentrations in the world ocean? *Marine Chemistry* **57,** 137–161 (1997).

315. Kinniburgh, D. G. & Miles, D. L. Extraction and chemical analysis of interstitial water from soils and rocks. *Environmental Science & Technology* **17,** 362–368 (1983).

316. Wetzel, R. G. *Limnology : lake and river ecosystems* 1006 (Academic Press, 2001).

317. Glass, J. B. & Orphan, V. J. Trace metal requirements for microbial enzymes involved in the production and consumption of methane and nitrous oxide. *Frontiers in Microbiology* **3,** 61 (2012).

318. P., P. & M., O. *Law of the minimum and balanced mineral nutrition.* Reuther W (Am Inst BioI Sci, Washington DC, 1961).

319. Smith, P. F. Mineral analysis of plant tissues. *Annual Review of Plant Physiology* **13,** 81–108 (1962).

320. *Copper Bioavailability and Metabolism* (ed Kies, C.) 308 (Springer US, Boston, MA, 1989).

321. Grace, N., Wilson, P. & Quinn, A. Impact of molybdenum on the copper status of red deer (Cervus elaphus). *New Zealand Veterinary Journal* **53,** 137–141 (2005).

322. Shen, X.-y., Du, G.-z., Chen, Y.-m. & Fan, B.-l. Copper deficiency in yaks on pasture in western China. *The Canadian veterinary journal = La revue veterinaire canadienne* **47,** 902–906 (2006).

323. Xiao-yun, S., Guo-zhen, D. & Hong, L. Studies of a naturally occurring molybdenum-induced copper deficiency in the yak. *The Veterinary Journal* **171,** 352–357 (2006).

324. Zhou, L., Long, R., Pu, X., Qi, J. & Zhang, W. Studies of a naturally occurring sulfur-induced copper deficiency in Przewalski's gazelles. *The Canadian veterinary journal* **50,** 1269–1272 (2009).

325. Ha, J.-H., Doguer, C., Wang, X., Flores, S. R. & Collins, J. F. High-iron consumption impairs growth and causes copper-deficiency anemia in Weanling Sprague-Dawley rats. *PLOS ONE* **11** (ed Pantopoulos, K.) 161033 (2016).

326. *Inorganic plant nutrition* (eds Läuchli, A. & Bieleski, R. L.) (Springer Berlin Heidelberg, Berlin, Heidelberg, 1983).

327. Marques, A. P. L., Botteon, R. d.C.C. M., de Amorim, E. B., Botteon, P. D.T. L. & Botteon, P. d.T. L. Copper deficiency conditioned by high levels of zinc, manganese and iron in the Middle Paraíba, RJ, Brazil. *Semina: Ciências Agrárias* **34,** 1293–1300 (2013).

328. Gielen, H., Vangronsveld, J. & Cuypers, A. Cd-induced Cu deficiency responses in *Arabidopsis thaliana*: are phytochelatins involved? *Plant, Cell & Environment* **40,** 390–400 (2017).

329. *Clustal X Colour Scheme* <http://www.jalview.org> (2017).